Amyloid Disease: Are the oligomeric species a good therapeutic target?

Amy Irvine

A thesis submitted for the degree of Doctor of Philosophy

Department of Molecular Biology and Biotechnology

University of Sheffield

Abstract

It is believed that in many amyloid diseases, including Alzheimer's, the primary toxic species responsible for neurodegeneration are small oligomers of the causative protein, rather than the fibres that often define the disease. Oligomers of our model protein cystatin B have, therefore, been prepared in order to characterise them.

Conversion of these oligomers into non-toxic aggregates could be a good therapeutic strategy. I have, therefore, been looking at agents that facilitate oligomer detoxification as this therapeutic approach would address the underlying mechanism of disease, not just alleviate the symptoms.

One example is the sage plant, *Salvia sclareoides. Salvia* species have been used in folk medicine as a treatment for memory loss and insomnia, as well as an antiseptic.

Extracts from *S. sclareoides* (partitioned according to their hydrophobicity) can stop amyloid formation by converting amyloidogenic forms of cystatin B, α-synuclein and Amyloid β into non- amyloidogenic aggregates. However, compounds within the Salvia extracts do not stabilise soluble oligomeric forms of these proteins directly. The extracts remodel amyloid fibrils into amorphous aggregates. The extracts are also effective in Creutzfeld-Jakob Disease, where they reduce levels of infectious PrP^{Sc} in scrapie-infected mouse neuronal cells. The extracts, themselves, show no toxicity towards human neuronal cells.

Acknowledgments

My mum once told me that doing a PhD is like belonging to a secret club…only those who have also done one know what it's like!

I must, firstly, thank the members of the Staniforth lab who have been wonderful throughout my PhD. Firstly, thank you to my wonderful PhD supervisor, Dr Rosie Staniforth for all her support, enthusiasm for biochemistry, words of encouragement and help in getting this thesis finally finished! Thank you to Pete who was brilliantly helpful when I first started and Abi who passed on all her wonderful lab knowledge. Thank you also to Liam, Sirwan and Alex for being brilliant, helpful and fun lab friends. I must also thank Jin Yi, Gus, Clare and Nicki and the rest of the NMR group for being brilliant friends and cake-bakers! Thank you also to Professor Mike Blackburn, Professor Mike Williamson and Professor Jon Waltho for all their help and guidance.

I would also like to thank Svet Tzokov for all his help in making my EM pictures look so good and Andrea Hounslow for all her NMR assistance.

Thank you to all my music friends who have kept things in perspective and reminded me that there is a life outside of the lab!

Thank you and all my love to Johann for looking after me, wine-ing me and believing in me.

Lastly, but not least, thank you to my brilliant family. Thank you to my Dad and Allliott for all your kind words and my fantastic Mum who encouraged me start out on this journey.

Table of Contents

Abbreviations

$A\beta$ Amyloid β

$A\beta_{1-49}$ 40 residue Amyloid β protein fragment

$A\beta_{1-42}$ 42 residue Amyloid β protein fragment

ALS   Amyloid lateral sclerosis

AFM   Atomic force microscopy

$\beta2m$ $\beta2$-microglobulin

C-terminal   Carboxylate end protein region

CD Circular dichroism spectroscopy

Cryo-EM Cryogenic Electron Microscopy

DOSY-NMR Diffusion Ordered Spectroscopy Nuclear Magnetic Resonance

EDTA   Ethylenediaminetetraacetic acid

EGCG   Epigallocatechin-gallate

EM   Electron microscopy

EPM1 Myoclonus epilepsy of type I (Unverricht-Lundborg Disease)

ESI-MS   Electrospray-ionisation mass spectroscopy

FAP   Familial amyloidotic polyneuropathy

FLM   Fluourescence light microscopy

FTIR   Fourier transform infrared spectroscopy

hCC   Cystatin C

H/D   Exchange Hydrogen/deuterium exchange of protein backbone amides

HPLC   High Pressure Liquid Chromatography

HPLC-MS Reverse-phase high-Pressure-liquid-chromatography coupled with electrospray-ionisation mass spectroscopy

HSQC Heteronuclear single quantum coherence NMR spectroscopy

LP Limited proteolysis

MALS Multi Angle Light Scattering

Mg-ATP   Magnesium adenosine triphosphate

MPL Mass per unit length

MS   Mass spectroscopy

MWCO   Molecular weight cut-off

N-terminal   Amide end protein region

NMR Nuclear magnetic resonance

NOESY Nuclear Overhauser effect spectroscopy

OD Optical density

PES Polyethersulfone

PMSF Phenylmethanesulfonyl fluoride

RP-HPLC Reverse-phase high-pressure-liquid-chromatography

SDM Site-directed mutagenesis

SDS-PAGE Sodium dodecyl sulphate polyacrylamide gel electrophoresis

SEC HPLC Size exclusion chromatography high-pressure-liquid-chromatography

SSNMR Solid state nuclear magnetic resonance spectroscopy

STEM   Scanning transmission electron microscopy

TEM   Transmission electron microscopy

TFE   2,2,2, trifluoroethanol

ThT   Thioflavin-T

TROSY Transverse relaxation optimised NMR spectroscopy

TTR   Transthyretin

UV   Ultraviolet

Chapter 1: Introduction

1.1 <u>Amyloid</u>

How and why normally soluble, functional proteins are converted into amyloid deposits are now questions of fundamental importance. Such conversion of misfolded proteins into the amyloid state is generally avoided in living organisms through a variety of mechanisms such as molecular chaperones to assist with folding, and protein degradation pathways to destroy proteins which are not folded into their correct native structure (Nelson & Cox, 2013).

However, changes in the cellular environment can drastically affect the cell's ability to deal with misfolded proteins and therefore protect the organism from damage and disease. Oxidative stress, ageing and changes in the proteins being produced, such as mutations, are all thought to be key factors in this process.

There are now thought to be over 50 diseases and disorders associated with misfolded proteins forming amyloid aggregates, the amyloid fibrils being the hallmark of these diseases (Knowles et al. 2014). Many of these disorders or amyloidoses are now some of the most common and debilitating medical conditions facing the world's population as they are often associated with ageing and modern lifestyles e.g. Alzheimer's Disease and Type II Diabetes. Indeed, the UN has declared, "the global burden and threat of non-communicable diseases constitutes one of the major challenges for development in the twenty-first century" (WHO, 2012).

Disease	Aggregating protein	Number of residues	Native structure of protein
Neurodegenerative diseases			
Alzheimer's Disease	Amyloid β peptide	40-42•	Unfolded
Spongiform encephalo-pathies	Prion	253	Unfolded(1-120), α-helical (121-230)
Parkinson's disease	α-Synuclein	140	unfolded
Dementia with lewy bodies	α-Synuclein	140	unfolded
Huntington's disease	Huntington with poly-q expansion	3144+	Largely unfolded
Amyotrophic lateral sclerosis	Superoxide dismutase 1	153	All β-sheet
Systemic amyloidoses			
Hemodialysis-related amyloidosis	β2-microglobulin	99	All β-sheet
Icelandic hereditary cerebral amyloid angiopathy	Mutant of Cystatin C	120	α-helix and β-sheet
Senile systemic amyloidosis	Transthyretin	127	All β-sheet
Familial amyloidotic polyneuropathy	Mutant Transthyretin	127	All β-sheet
Type II diabetes	Amylin	37	Unfolded
Hereditary cerebral hemorrhage with amyloidosis	Mutants of Aβ peptide	40-42•	Unfolded

Table 1.1: Human amyloid diseases associated with formation of extracellular amyloid deposits or intracellular inclusions
Other fragments of various lengths have also been shown to be present in amyloid fibrils (Table adapted from Chiti & Dobson, 2006).

1.2 Classification of Amyloids

Amyloid diseases can be split into two broad categories-neurodegenerative diseases in which the aggregation occurs in the brain, and systemic amyloidoses in which aggregation occurs in tissues other than the brain.

A well-studied example of a systemic amyloidosis is Haemodialysis related amyloidosis which is caused by β_2-Microglobulin (β_2m) -a component of the class I major histocompatibility complex (MHC). β_2m is normally broken down and excreted by the kidney. However, in patients suffering from renal failure β_2m is not degraded and the concentration of β_2m in the serum can increase by up to 60-fold. This leads to association of freely circulating β_2m into insoluble amyloid fibrils, which often accumulate in the musculoskeletal system, particularly at synovial joints (Morten et al. 2007).

However, it is neurodegenerative disease which has really made amyloid a key area of research in the biochemistry field (Selkoe, 2003). Alzheimer's disease is the most prevalent neurodegenerative disease (Caughey & Landsbury, 2003). The pathology of Alzheimer's was first decribed by Alois Alzheimer who described plaques and tangles in the cerebral cortex of the brain. The plaques are extracellular and are composed of a protein called Amyloid β. The tangles are located inside neurons, axons and dendrites and are composed of Tau (Wolfe, 2006). Such plaques and tangles in brain sections can be stained using silver (the Bielschowsky technique) as shown in Figure 1.1 below.
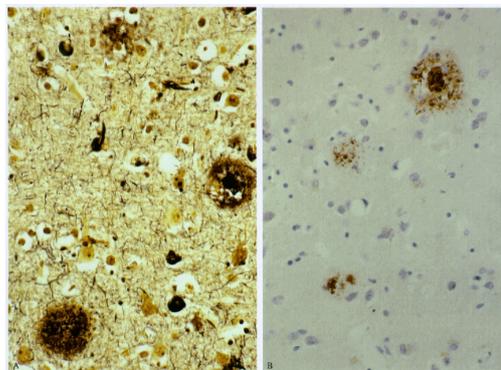
Figure 1.1: Neuritic plaques in a section of the temporal cortex from an AD patient stained with the Bielschowsky technique (left). Neurofibrillary tangles can also be seen. (Right) Section of AD cortex immunostained with an antibody to Aβ42. (Figure taken with permission from Cummings et al. 1998)

It should also be noted that there are functional Amyloids, not associated with disease. A well-characterised example is the protein curlin used by *Escherichia coli* to colonise inert surfaces (biofilm production) and initiate binding to host proteins (Chiti & Dobson, 2006).

Proteins which form amyloids can also be categorized into three groups:

1. Non Structured proteins:

Many of the peptides and proteins involved in amyloid diseases are intrinsically disordered under normal physiological conditions, such as amyloid-β (Aβ) peptide in Alzheimer's disease. Aβ is a short peptide of between 39-43 amino acid residues (Serpell, 2000). The longer the Aβ variant the more prone to aggregation it is (Schnabel, 2011). The peptide is produced from the proteolysis of amyloid β precursor protein (APP) by γ and β secretase. Figure 1.2 shows the cleavage sites for proteolysis of APP. Mutations which increase Aβ production (e.g. Swedish) or change its aggregation properties (e.g. arctic), and, therefore, are linked to early onset Alzheimer's disease, are also shown. The exact physiological role of APP or its Aβ fragments in healthy individuals has not been clearly defined but APP has been linked to the regulation of synapse structure and function (Tyan, 2012). Neurons from APP deficient mice have deficient survival and growth suggesting that APP plays a role in neuron viability, axonogenesis and dendritic branching (Perez et al. 1997, De Stooper and Annaert, 2000)
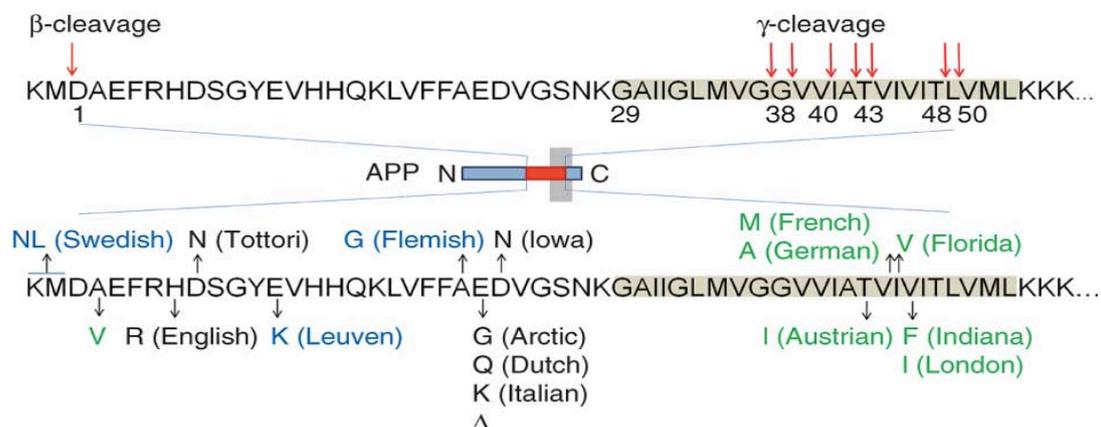
Figure 1.2: β- and γ-secretase cleave APP. *The transmembrane domain of APP is highlighted in grey. γ-cleavage produces Aβ fragments that vary in length and hydrophobicity. Mutations in APP can increase the total Aβ production (blue) or alter the Aβ aggregation properties (black and green) Taken from Benilova et al. (2012) with permission*

Another key example of an intrinsically disordered protein responsible for an amyloid disease is α-synuclein. α-synuclein is the major fibrillar component of the Lewy bodies found in the substantia nigra of Parkinson's disease patients (Caughey & Landsbury, 2003). Such Lewy bodies can be seen in Figure 1.3. α-synuclein is a 140 residue protein and is predominantly expressed in the brain. It is still unclear what the main role of α-synclein is although there are many proposed functions; signal transduction, vesicular trafficking, synaptic plasticity, oxidative stress regulation and mitochondrial behaviour. Early onset Parkinson's disease is caused by mutations in the α-synuclein gene, the most common being A53T and A30P.
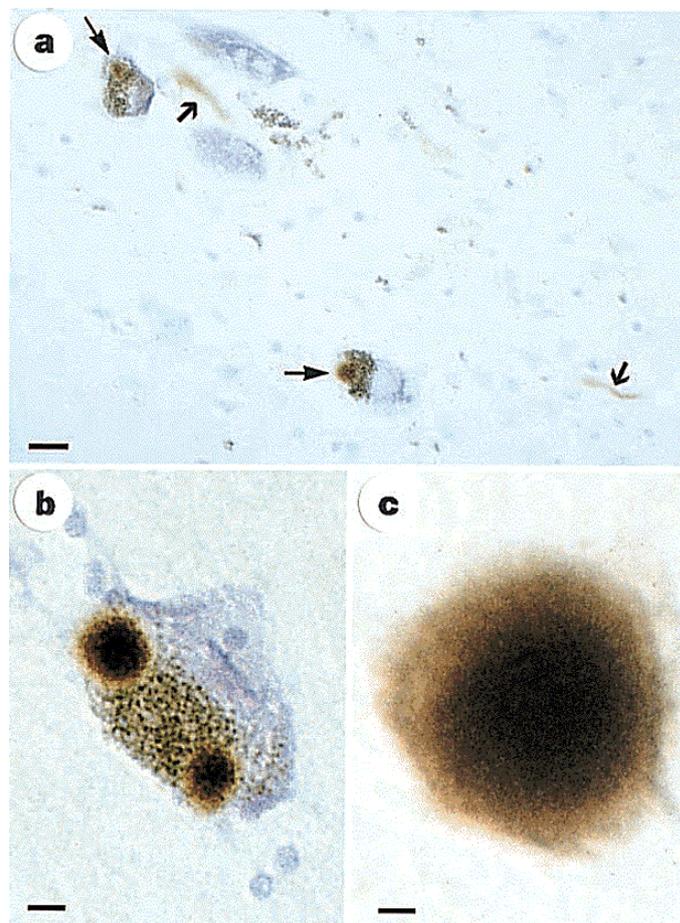
Figure 1.3: Immunostained lewy bodies containing α-synuclein. a, Nerve cells and neuritis containg lewy bodies. b, Nerve cell with two lewy bodies. c, extracellular lewy body. Taken with permission from Spillantini et al. 1997.

2. *Partially folded proteins:*

Prion diseases such as Creutzfeldt-Jakob disease in humans and bovine spongiform encephalopathy in animals are caused by the accumulation of aggregates of the disease-associated scrapie isoform of prion, PrP^{Sc}, in the brain. PrP^{Sc} is derived from the host-encoded glycoprotein PrP$^{c.}$ The NMR structure of the cellular prion isoform (PrP^{C}) consists of an unstructured N-terminal region of about 100 amino acids and a structured C-terminal of a similar length (three α-helices and a short β-sheet). The role of PrP^{C} *in vivo* is unknown but PrP^{C} is associated with prion pathogenesis as mutations in the human prion protein gene result in inherited prion diseases. Prion propagation requires conformational change of PrP^{C}, primarily an α-helical structure, to a β-sheet rich structure (PrP^{Sc}) (Trevitt & Collinge, 2006). PrP^{Sc} can then act as a template which promotes further conversion of PrP^{C} to PrP^{Sc}.

The exact link between the different prion disease pathologies and the kinetics of prion propagation is still to be determined. However, the Collinge group has shown the prion strain type (the dominant PrP^{Sc} polymer) to be important in this process. An intermediate species between PrP^{c} and PrP^{Sc} which they call PrP^{L} is thought to mediate neurotoxicty.

3. Structured proteins:

Our group for many years has been studying cystatins, a superfamily of cysteine proteinase inhibitors. Cystatins are a useful tool in the study of amyloid at a molecular level; NMR and crystal structures have been determined for many of the cystatins and their folding pathways are well-defined.

Animal cystatins can be categorized into three groups: type 1 which are intracellular (cystatin A and B), extracellular type 2 cystatins (C, D, E, F, S, SN, SA) and type 3 also known as the high and low molecular weight kininogens (Turk & Bode, 1991). Structurally, type 1 and type 2 cystatins (the most characterized) are highly homologous. They all have a five stranded β-sheet overlaid by an α-helix-"the hot dog fold" (Zerovnik et al. 2002). Type 2 cystatins e.g. cystatin c (hCC) can be distinguished from type 1 by the presence of two disulphide bonds and an unstructured region of ~ 20 residues between strands 3 and 4.

Interest in the amyloidogenic properties of cystatins came with the discovery that hCC, cystatin B and cystatin A form inactive dimers (Ekiel and Abrahamson, 1996; Jerala and Zerovnik, 1999; Zerovnik et al. 1997). NMR chemical shift changes revealed that this dimerization involved no major structural rearrangement apart from changes to the active site region between strands 2 and 3. The high kinetic barrier of this reaction led to the realisation that cystatins form domain swapped dimers (Ekiel et al. 1997; Jerala and Zerovnik, 1999). NMR and crystallographic studies of cystatin A and cystatin C provided further evidence of this (Staniforth et al. 2001; Janowski et al. 2001).

This domain swapped dimer is intriguing to those working on amyloid fibril structures as it is an attractive candidate for the individual units which make up the highly extended β-sheet structure (see 1.3). Domain swapping requires extension of β-strands 2 and 3, meaning the β-sheets of the two cystatin molecules can hydrogen bond.

A mutant form of hCC (L68Q) causes the amyloidogenic disease, hereditary cystatin C amyloid angiopathy. Deposits of hCC in the cerebral blood vessels cause repeated hemorrhaging, dementia, paralysis and eventually death (Abrahamson, 1996).

Amyloid studies of hCC, especially the mutant form, are hampered by difficulties in purification and manipulation (Ekiel et al. 1997). However, due to structural homology, cystatin B is a useful model for the study of cystatin amyloids. Cystatin B is expressed in most human tissues and is localized to both the nucleus and cytoplasm where it inhibits cysteine cathepsins. Cystatin B is a protein of 98 amino acids and its 3D structure has been determined (Figure 5). Mutations in cystatin B are linked to a hereditary form of myoclonus epilepsy called Unverricht-Lundborg disease also known as EPM1 (Genton, 2010). Although an uncommon autosomal recessive disease, it is devastating for sufferers. Patients suffer from frequent tonic-clonic seizures, myoclonic jerks and progressive cognitive decline. In most EPM1 cases (90%) the mutation is an unstable dodecamer repeat expansion in the promotor region of the gene which causes decreased expression of cystatin B. This expansion can be repeated up to 75 times. The gene also usually carries one of these mutations: G4R, Q17P, three splice site mutations which alter the positions of introns and exons, a stop codon at position 68, or a frameshift at position 72 followed by a stop codon at position 75 (Lafreniere et al. 1997, Virtaneva et al. 1997).

Cystatin B is now also thought to play a far more important physiological role. As well as a protease inhibitor, it is has now been linked to indirect regulation of the cell cycle through binding to histones and inhibiting cathepsin L in the nucleus (Ceru et al. 2010). Its important role in cell homeostasis has been further highlighted by studies showing it binds Aβ (Skerget et al. 2009), reduces oxidative stress through binding to SOD1 (Ulbrich et al. 2013) and prevents apoptosis. Cystatin B has also been linked to induction of autophagy, an intracellular quality control mechanism that disposes of protein aggregates and damaged organelles (Poljanar & Zerovnik, 2011). Further

evidence for these multiple functions have come from studies showing its involvement in cancer, immunity, inflammation and neurodegenerative amyloid diseases. Indeed, cystatins A, B and C are found in the plaques of Alzheimer's and Parkinson's disease patients (Li et al. 1993).

Cystatin B is a useful model for looking at amyloid as it forms fibres readily *in vitro* over about 2 weeks (pH 4.7, 100mM NaCl, 37°C). (Zerovnik et al, 2002). Cystatin B can also form domain swapped dimers (figure 1.4) and higher order oligomers.
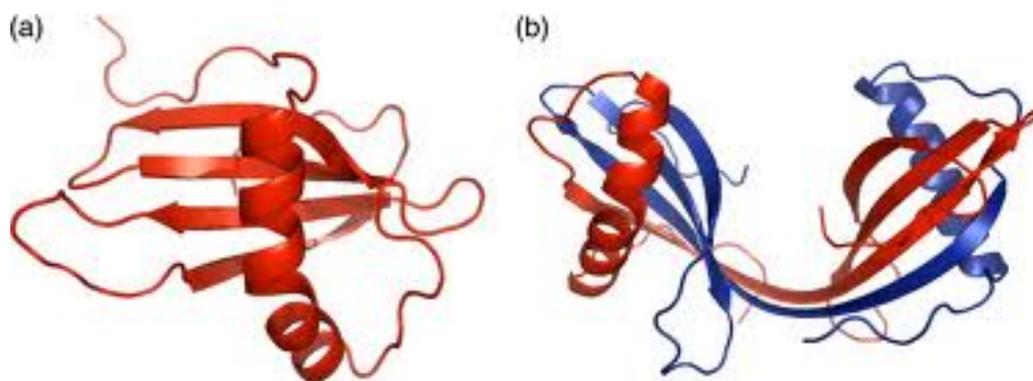
Figure 1.4: Cystatins form domain swapped dimers. *Cystatin b monomer **(a)** and dimer **(b)**. A non-covalent interaction within the monomer is broken and the corresponding region on another monomer takes its place (Sanders et al, 2004).*

It is interesting to note that the ability of a polypeptide to form amyloid fibres is not restricted to those associated with disease. It is now clear that this is a generic feature of all proteins given the correct conditions *in vitro.* Myoglobin can form amyloid fibres in 50mM sodium borate, pH 9.0 at 65ºC (Fändrich et al. 2001). This has led many researchers to the conclusion that amyloid formation is a natural alternative conformation for proteins and that strategies such as chaperones are important evolutionary adaptions to suppress amyloid formation *in vivo* (Fändrich et al. 2001).

1.3 Structure of Amyloid Fibrils

Although each amyloid is formed by the misfolding of a specific protein, the fibrillar aggregates they form are remarkably similar. They all form highly ordered fibrils which have a diameter of 7-10nm and are rich in β-sheet structure. The β-sheet strands run perpendicular to the axis of the fibril (Sunde & Blake, 1997).

One of the major research challenges in the amyloid field is to move beyond these initial observations and develop a high-resolution structure of the amyloid fibrils and indeed other aggregated states (Wetzel, 2002). Due to the insoluble nature of amyloid fibrils, traditional methods of structural determination such as x-ray crystallography and solution state NMR cannot be used. It has therefore been necessary to exploit and develop other techniques such as solid state NMR, circular dichroism, x-ray fibre diffraction, electron microscopy and fourier transform infrared spectroscopy to examine amyloid fibre structure (Serpell et al. 1999).
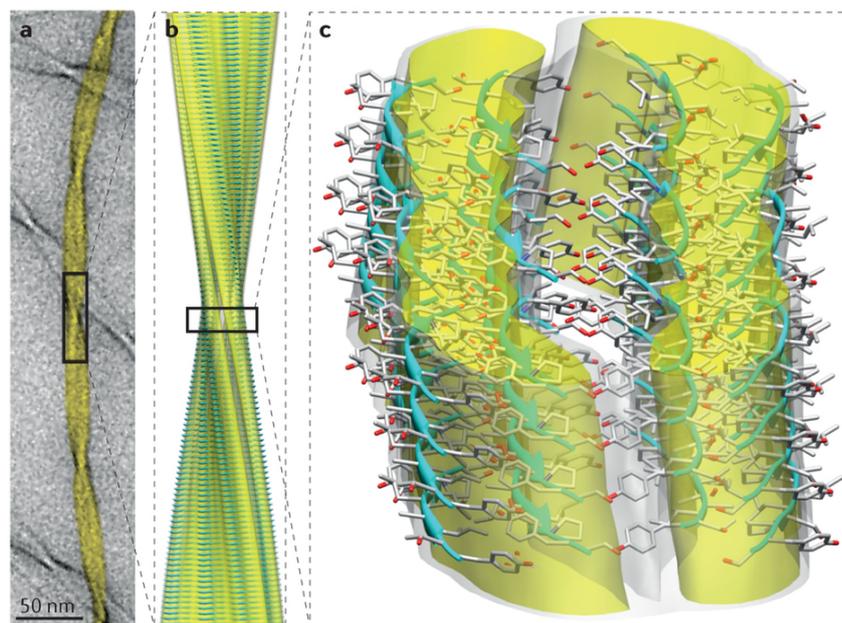
Figure 1.5: The structure of amyloid fibrils formed from an 11-residue fragment of transthyretin*. A combination of cryo-electron microscopy (**a**) with solid-state NMR has enabled a detailed atomic-level structure to be detrmined (**b**). A more detailed view (**c**) shows the three filaments that form the mature fibril formed by pairs of cross-β protofilaments, which are composed of pairs of β-sheets.The fibril surfaces are shown as electron density maps, and β-sheet areas as ribbons; Oxygen (red), carbon (grey) and nitrogen (blue) atoms are also shown. Figure taken with permission from Knowles et al. 2014.*

1.3.1 Amyloid β Fibrils

One of the most useful techniques by which Aβ fibrils have been studied is by electron microsopy. When viewed by negative stain transmission EM, Aβ filbrils are shown as smooth, regularly twisting fibres (Figure 1.6 A). EM analysis of Aβ fibrils has also highlighted the importance of the fibril assembly conditions. pH and the presence of other additives such as cholesterol and liposomes have been shown to affect fibril morphology (Stromer & Serpell, 2005).

Direct visualization of β-strands is now possible by Cryo-EM. The Serpell group have visualized fibrils of a synthetic Aβ peptide (residues 11-25 of Aβ$_{1-42}$). They showed that the fibrils are composed of in register β-sheets that form a tube (Serpell & Makin, 2002).

Cryo EM along with mass-per-length (MPL) measurements and 3D image reconstruction has revealed even more about the exact morphology of Aβ fibrils-they are composed of smaller protofilaments. Aβ$_{1-42}$ fibrils are composed of only one protofilament. However, Aβ$_{1-40}$ fibrils are composed of two protofilaments (Figure 1.7). A fibril structure was resolved at 8 Å resolution and it showed pairs of β-sheets within the two protofilaments. Comparison of Aβ$_{1-42}$ and Aβ$_{1-40}$ fibril structures revealed that they have very similar axial twofold symmetry and similar protofilament structure. The MPL data showed that the protofilaments of Aβ$_{1-40}$ and Aβ$_{1-42}$ fibrils have the same number of Aβ molecules per cross-β repeat. They also observed two different Aβ$_{1-40}$ morphologies; fibrils with a 20nm distance between protofilament cross-overs and fibrils where this distance was 30nm. However, MPL data showed that these fibrils are structurally very similar and the difference observed could be due to the packing of the protofilaments, or different packing of the Aβ peptide within them (Schmidt et al. 2009).
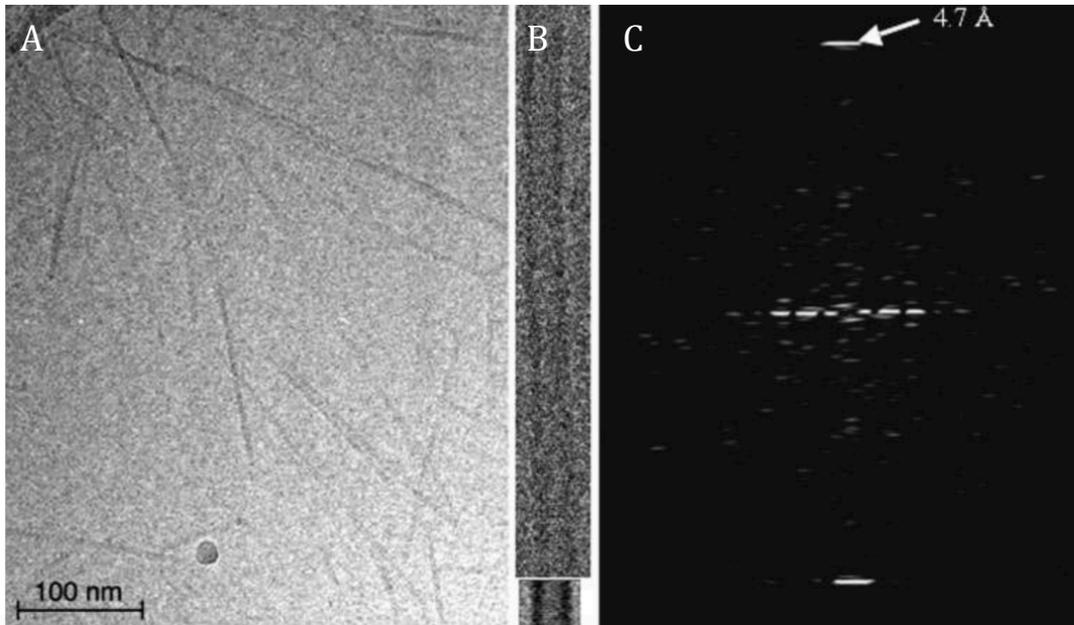
Figure 1.6: Cryo-EM of Aβ₁₁₋₂₅ fibrils. *A: Unstained fibrils in vitreous ice. B: A single fibril showing striations across the fibril with a distance between them of 4.7 Å. Box below is an enhanced image which shows striations more clearly. C: A Fourier transform from fibril shown in B shows a strong central reflection at 4.7 Å (from Stromer & Serpel, 2005).*
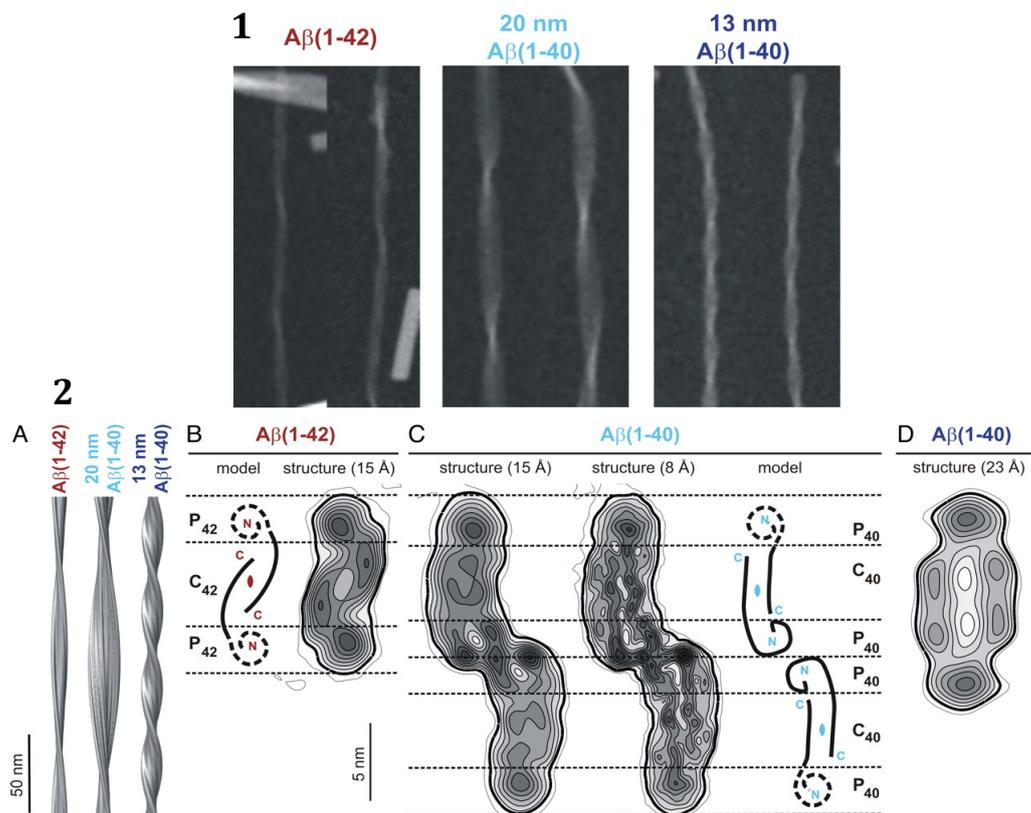
Figure 1.7: STEM images and density maps of Aβ fibrils. *1: STEM images of Aβ₁₋₄₂, 20-nm Aβ₁₋₄₀ and 13-nm Aβ₁₋₄₀ fibrils. 2: Density reconstructions of Aβ₁₋₄₀ and Aβ₁₋₄₂ fibrils. 2: (A) Side views of Aβ₁₋₄₂ and Aβ₁₋₄₀ fibrils. (B) Mapped densities of Aβ₁₋₄₂ fibril cross-sections (cross-sectional area is ≈44 nm²) (C) Cross-section through the 20-nm Aβ₁₋₄₀ fibril density map (left) 15 Å and (center) 8 Å resolution (The cross-sectional area is ≈90 nm²). (D) Cross-section through the 13-nm Aβ₁₋₄₀ fibril density map. The cross-sectional area is ≈77 nm² (Schmidt et al. 2009).*

However, it is solid state NMR which has so far been the most powerful tool for determining the structure of Aβ fibrils. The Tycko group recently published an important structural model of Aβ$^{1-40}$ fibrils seeded from Alzheimer's brain extract. *In vitro* studies have shown that Aβ fibrils grown from seeds (sonicated, short fragments of mature fibrils) keep the structure of their seeds. This enabled them to study the fibril structures from the brains of two Alzheimer's disease patients as shown in Figure 1.8 (Lu et al. 2013).

Solid state NMR and EM of the seeded fibrils showed that each patient had a single predominant fibril structure and that the morphologies were different for each patient. This structural specificity of the brain seeded fibrils has exciting possible implications for the disease process; fibrils could spread from a single nucleation site and different clearance mechanisms in patients' brains may promote different nucleation events.

From one of the patients they were able to build a full molecular structure of the fibrils. From the chemical shift data it appears that the whole Aβ sequence is part of the highly ordered, rigid fibril structure.

Importantly, they compared their structure to previous *in vitro* work done by themselves and others. Their fibres had a three fold symmetry consistent with some *in vitro* fibril structures with twisted morphologies. However, other *in vitro* studies have shown fibrils with a 2-fold symmetry (Perkova, 2005). There were also novel conformation features in fibrils seeded from the Alzheimer's brain. These included a twist in residues 19-23 that allows the burying of sidechains F20 or E22, a kink at G33 and bend at G37-38. In vitro fibrils have not shown such complexity (Lu et al. 2013).
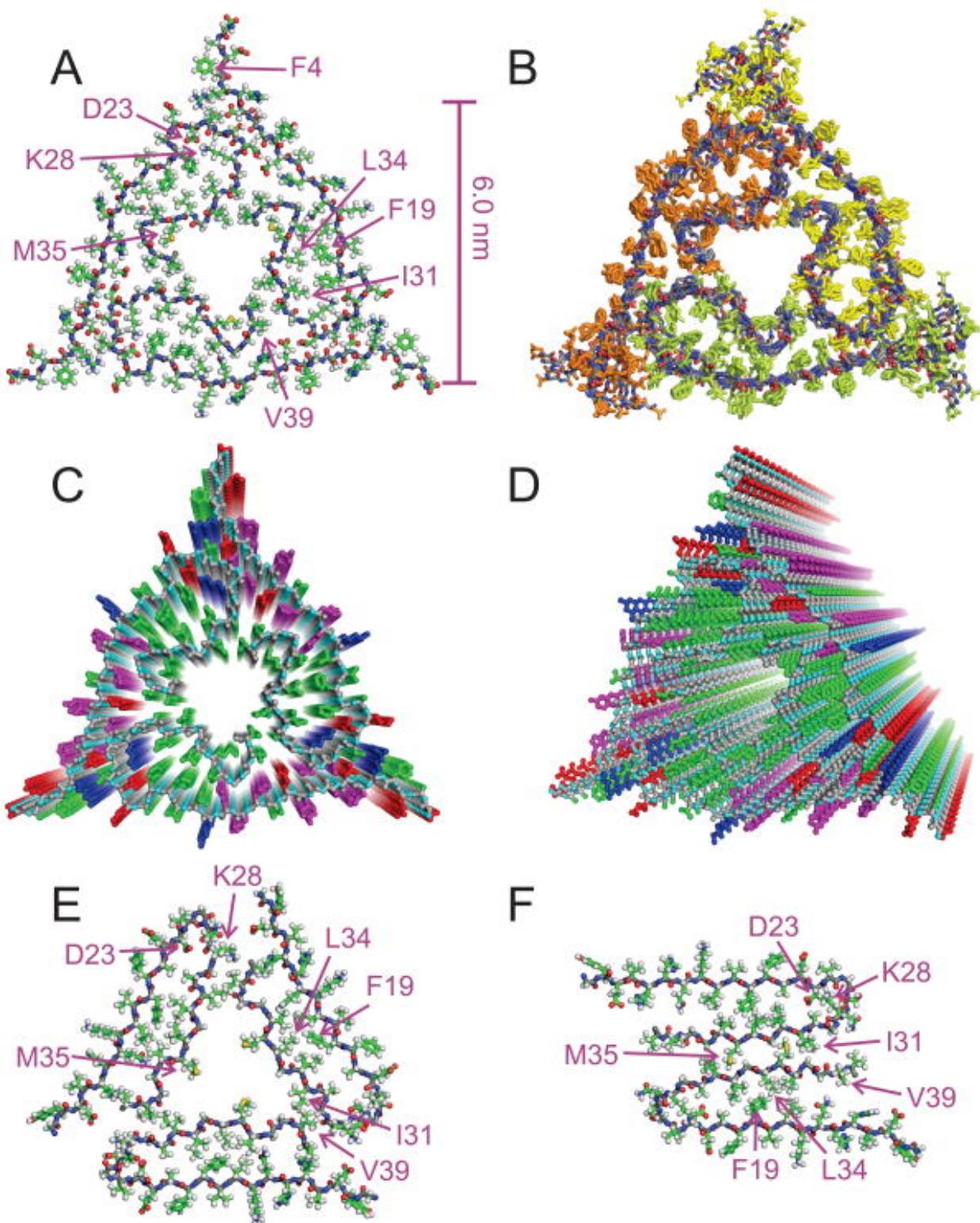
Figure 1.8: Molecular structure of Aβ40 fibrils from an AD patient A) Structural model with the lowest total experimental restraint energy in Xplor-NIH calculations. The three-fold-symmetric repeat unit can be seen, including the backbone (grey) and sidechain (green) carbon. (B) A model structure created from the superposition of structures which fit within experimental restraints (PDB 2M4J). The sidechains of three $A\beta_{1-40}$ molecules are shown in yellow, green, or orange. (C, D) Two views of a fibril structure, created by repeating the three molecule $A\beta_{1-40}$ unit 18 times with 0.48 nm spacing along the fibril axis. (E) Possible structural polymorph of $A\beta_{1-40}$ fibrils with three-fold and (F) two-fold symmetry, developed from SSNMR and EM of fibrils grown in vitro (Lu et al. 2013).

Whilst the structure of $A\beta_{1-40}$ fibrils has been well studied by the Tycko group and others, the structure of $A\beta_{1-42}$ fibrils has proved more elusive. This is largely to do with difficulties in the production of a large homogeneous sample of $A\beta^{1-42}$ fibrils.

Some recent interesting EM data along with previous H/D data has now furthered our understanding of the molecular architecture of these fibrils.

3D reconstructions of Cryo-images have shown that the layers within the fibril are formed from dimers of the $A\beta_{1-42}$. The two peptides, which form the dimer, have identical conformations; the C-terminal has β-sheet structure, whereas the N-terminal has a much more flexible structure (Schmidt et al. 2015). A density map reconstruction (figure 1.9) showed a central core domain along the main axis of the fibre with two peripheral domains. The Grigorieff group were able to image fibrils decorated with fragments antigen binding (Fab) from the 2H4 antibody. 2H4 recognises the N-terminal of $A\beta_{1-42}$, indicating the N-terminal of the $A\beta_{1-42}$ peptides form the peripheral domains. The C-terminal segments, therefore, form the β-sheet core structural domain of the fibrils (Schmidt et al. 2015). This agrees with previous H/D exchange data, which showed that the $A\beta_{1-42}$ N-terminal residues 18-42 exchanged very slowly, meaning they must be part of the core structure (Lührs et al, 2005)

However, how exactly the C-terminal domains of the Aβ peptides stack to form this extended β-sheet is still not entirely clear. Some groups have assumed a U-shaped conformation in the fibril core (Lührs et al, 2005). This is similar to what has been proposed for $A\beta_{1-40}$. EM density map data, however, suggests packing of the dimer units by back-to-back interactions along the longest uncharged β-sheet face of the $A\beta_{1-42}$ peptide-like a zip.

In reality, all these models could exist since small differences in fibril production protocols could result in different fibril morphologies being enhanced under different conditions.
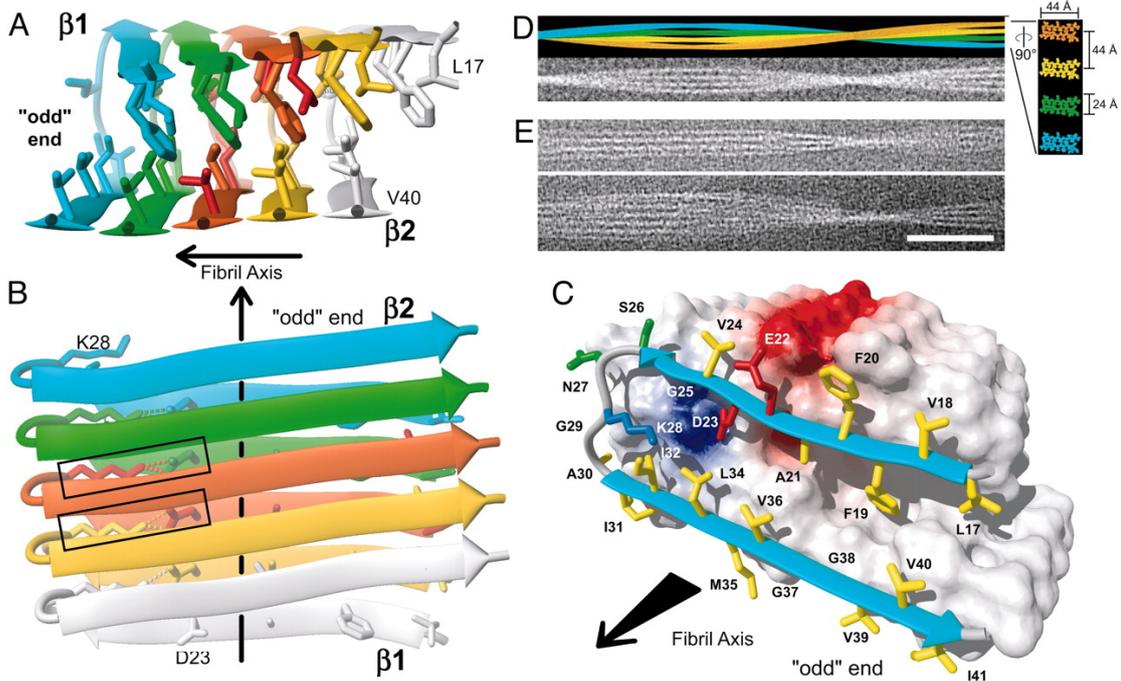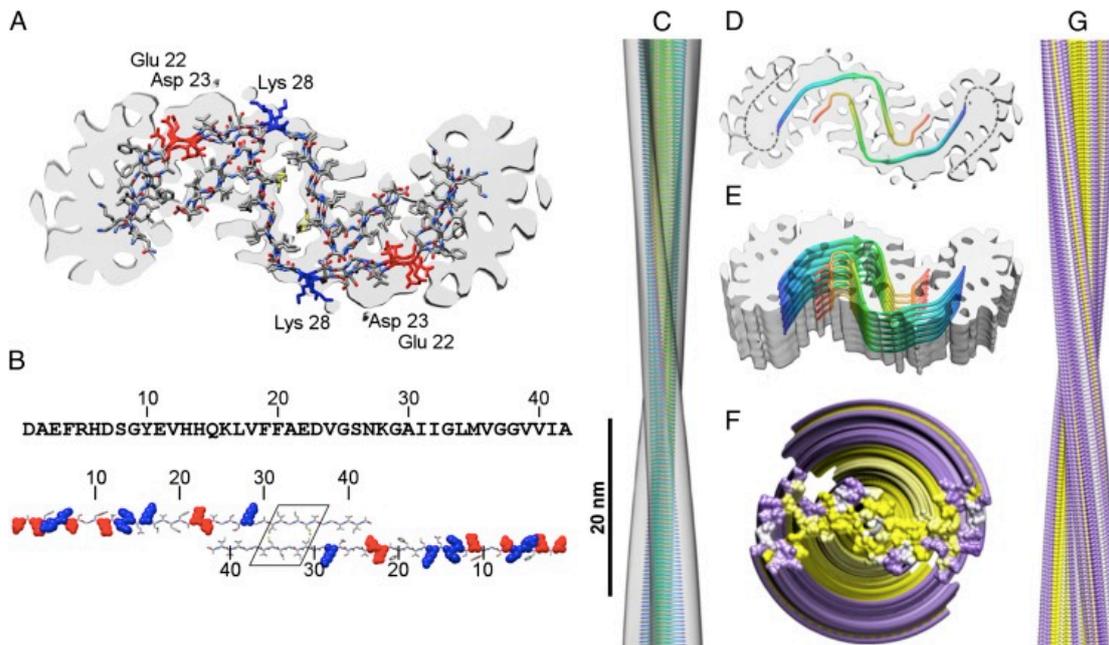
Figure 1.9: Two models for the 3D structure of an Aβ₁₋₄₂ fibril. *1: (A and B) Ribbon models of the structural core formed by residues 17–42 showing intermolecular interactions between β-strands. (B) Salt bridge between residues D23 and K28 (dotted lines) and two other important salt bridges formed by the central Aβ₁₋₄₂ molecule (boxed) are shown. (C) Diagram of the odd end of 35MoxAβ₁₋₄₂. Hydrophobic (yellow), polar (green), negatively charged (red), and positively charged (blue) side chains are shown. (D) Simulation of a 35MoxAβ₁₋₄₂ fibril that consists of four protofilaments. Lower diagram is a noisy gray-scale image of the fibrils which has been blurred to give a resolution of 2 nm. A ×5-magnified cross section perpendicular to the fibril axis is also shown. The twist angle is 0.45° per molecule. (E) Cryo EM of single 35MoxAβ₁₋₄₂ fibrils (Scale bar: 50 nm.) (Figure from L Lührs et al, 2005)*
2: (A) Models of fibrils by this group overlayed (B) Aβ₁₋₄₂ diagram showing two Aβ₁₋₄₂ peptides with zipper-like region (boxed). Positively charged (blue) and negatively charged residues (red) are shown. (C) Side view of the fibril superimposed with a backbone model of the fibril core. (D) Cross-section through the fibril showing dimer arrangement (E) Cros section through a stack of seven dimers. (F and G) A space filled model showing arrangement of charged (purple) and uncharged (yellow) residues (figure from Schmidt et. al 2015).

1.3.2 Cystatin B Fibrils

As mentioned in section 1.2, cystatin B can form fibrils *in vitro* and due to its structural homology to other amyloid proteins e.g. cystatin c it is a useful model when studying amyloid fibril structure. In conditions favourable to fibrillisation, like the other cystatins, cystatin B initially forms a 3D domain swapped dimer using the central 2 and 3 β-strands. It has been hypothesized that this type of dimerization could be the mechanism for fibril propagation, i.e. molecule 1 domain swaps with molecule 2, molecule 2 swaps with molecule 3 and so on. The extended β-strand is, therefore, formed from interactions within adjacent dimers (strand 1 forms an interface with strands 5 of the next dimer in cystatins). This propagated 3D domain swapped model of amyloidogenesis would explain why amyloid fibrils of mixed proteins or even protein isomers do not exist.

Conservation of this central β-strand in mature fibrils of cystatin B was shown by hydrogen deuterium exchange. It was also discovered that that N-terminal region of the protein, an α-helix in the monomer, becomes unstructured during fibril assembly (Morgan et al. 2008).

The evidence, however, for whether cystatin B forms fibrils through propagated domain swapping is unclear. For such domain swapping to occur over a whole fibril length, not just two molecules, a degree of conformational freedom is required in the hinge loop which exchanges with the rest of the structure. However, the domain which exchanges in cystatin B is not a flexible loop; it instead forms part of the hydrogen bonded β-sheet in the dimer and fibril. A different fibril model has therefore been proposed by our group with evidential data from limited proteolysis. This model shows that 3D domain swapping is maintained between dimers in the fibril chain but is not propagated. Protection of β-sheet strand five suggests that this forms part of the extended fibril β-sheet, not an edge strand as in the original model. This model, therefore, proposes that dimers are stacked on top of each other to create an interface between strand 5 of one molecule and strands 2 of the next (Davis et al. 2016).
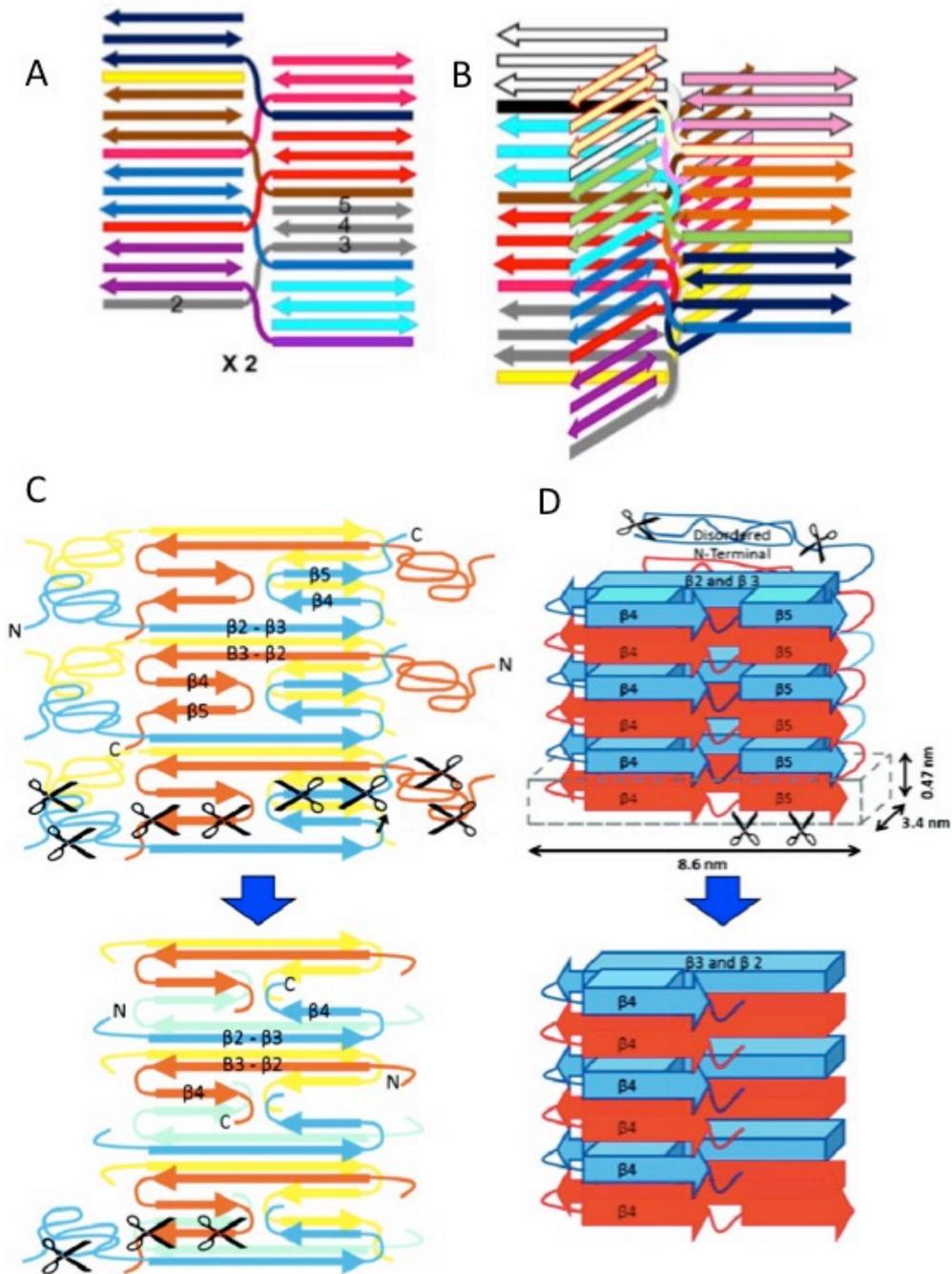
Figure 1.10: Two different structural models of cystatin B fibrils. *A and B are proposed models for the propagated 3D domain swapped fibril. The N terminal strand and α-helix are removed from the models as data shows these domains are disordered in the fibril. B shows how the swapping interface or loop could be shortened by having four molecules of cystatin B, in plane, side by side. However, the loop would still have to be flexible and electron microscopy dimensions do not match up to this model. C is a model based on H/D exchange NMR data. The dimer units stack on top of each other forming contacts between strand 5 and 2 (blue and orange). The removal of the helix from the β-sheet surface creates a hydrophobic surface for another protofilament to form a hydrophobic sandwich so the hydrophobic side chains are shielded from the solvent (yellow). D shows the current working model taking into account limited proteolysis data. Strand 5 needs to be accessible to proteases without large scale structural remodeling. Both models C and D fit EM size restrictions (indicated by the dotted line).*

1.3.3 α-synuclein Fibrils

Like other amyloid proteins, fibrils of α-synuclein are composed of several protofilaments which contain a cross β-structure in which the individual strands run perpendicular to the fibre axis. EPR, limited proteolysis and SSNMR have shown that residues 31-109 are folded in the fibril. The N-terminus can have a number of different conformations, whilst the C-terminus remains unstructured.

Clever hydrogen/deuterium studies have been used to determine secondary structure elements of the fibrils. Del Mar et al. proposed a model whereby the main chain bends back on itself in order to fulfill the width constraint of ≤10nm observed by EM. Their model showed tight hairpin bends running perpendicular to the fibril axis so that side chain amides could H-bond with β-sheet amides (Del Mar et al. 2005).

A more recent study (figures 1.11 and 1.12), which combined H/D exchange data together with the SSNMR data, showed five possible β-sheets in the fibril core. The first three β-strands are 6-8 amino acids long, whereas the other two are 9-13 amino acids in length. These strands stack to form a 5-layer β-sandwich with β1 next to β2, β2 adjacent to β3 and so on with hairpin loops between each β-strand (Vilar et al. 2008).

In straight α-synuclein fibrils, two protofilaments align with one another to form a fibril. Twisted fibrils also consist of two protofilaments but they are twisted around one another. The packing of straight and twisted fibrils requires different protofilament interactions. β4 and β5 interact in straight filaments, whereas in the twisted fibrils residues 22-30, which are not in the fibril core, are thought to interact.
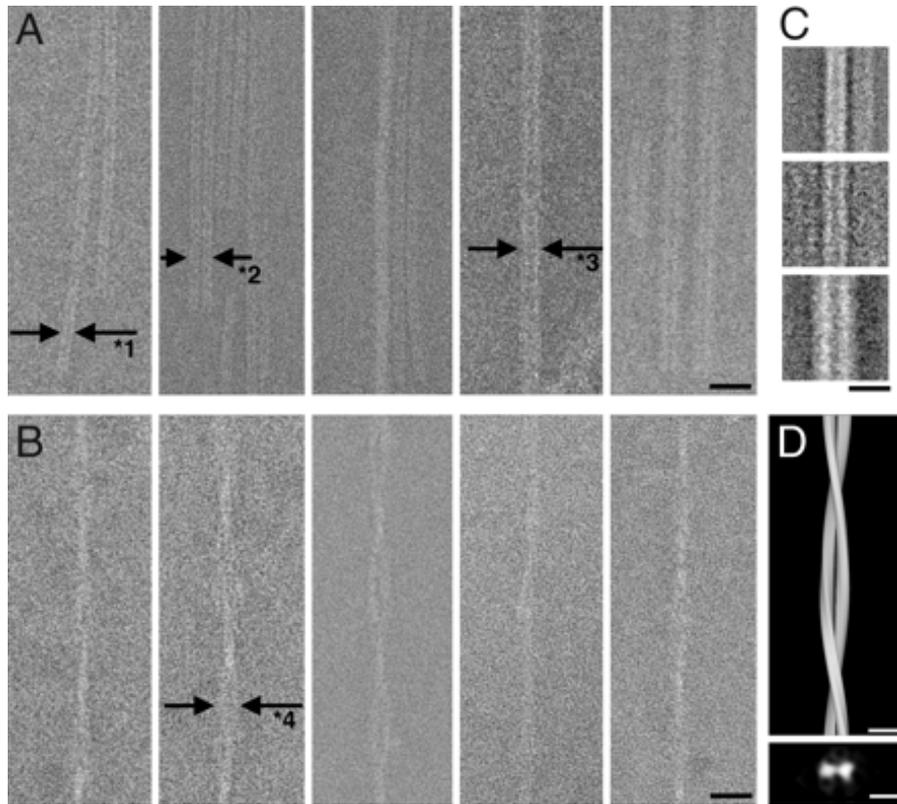
Figure 1.11: Cryo-EM images of straight and twisted α-synclein fibrils. *In both cases two dense lines 2nm wide form a thicker filament. Scale bars: A and B, 20nm; C and D, 10nm (from Vilar et al. 2008)*
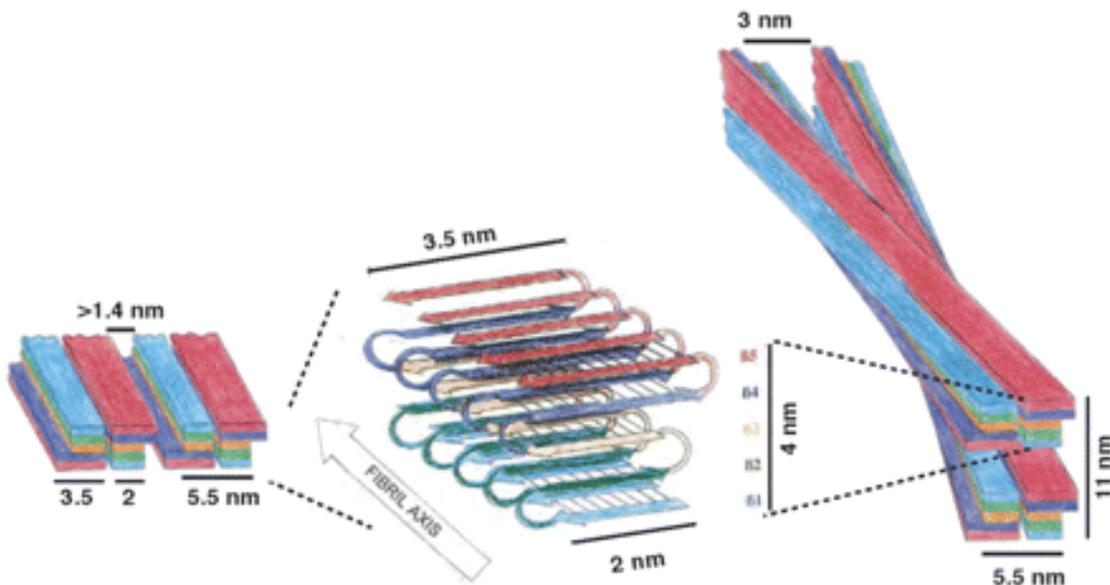
Figure 1.12: Structural model of α-synuclein fibrils from all published data. *Center: Model of folding in a molecule of α-synuclein within a protofilament. Left: The packing of a straight protofilament. Right: Packing in a twisted filament. (from Vilar et al. 2008)*

1.4 Structure of Intermediate Species

Although it has been known for many years that there is a close relationship between the appearance of amyloid deposits and pathology in protein misfolding diseases, there is still much to be understood about how this aggregation causes these pathological events.

In the case of systemic amyloidoses it is thought that simply the presence of large amounts, in some cases kilograms, of amyloid deposits in vital tissues and organs is the cause of disease (Knowles et al. 2014).

However, the mechanism of disease in the case of neurodegenerative disorders is obviously much more complicated. In many patients there is no detectable correlation between the quantity of fibrillogenic aggregates (amyloid plaques) in post mortem brain sections and the extent of cognitive decline pre-mortem (Haas & Selkoe, 2007).

There is now substantial evidence that soluble pre-fibrillar (oligomeric and protofibrillar) species are the primary toxic agents in neurodegenerative disease (Härd, 2011). The study of these fibrillar precursors and early oligomeric assemblies is challenging due to their transient, heterogeneous and unstable nature. However, new experimental approaches have started to provide useful information about these structures and their mechanism of toxicity (Stefani, 2012).

It is important to note here that the large insoluble aggregates are often surrounded by the smaller, soluble species both *in vitro* and *in vivo*. It is, therefore, difficult to say which species is directly inducing neuronal loss and dysfunction. Caughey and Lansbery warned researchers "not to throw the baby out with the bathwater" in their 2003 review. It is now considered more likely that there is continuous exchange between the fibrils and oligomeric species (Haas & Selkoe, 2007).

1.4.1 Amyloid β Oligomers

There is now a plethora of confusing literature describing the many small intermediate assemblies of Aβ. These different classes include protofibrils, annular assemblies, Aβ derived diffusible ligands (ADDLs) and globulomers (Haas & Selkoe, 2007). It also unclear which of these intermediates are on or off pathway to amyloid fibril production.

Protofibrillar Aβ was the first of these intermediates to be studied as they are directly observed during the fibrillisation of Aβ *in vitro*. Typically, protofibrils can be up to 200nm long and 5-6nm wide (mature amyloid fibrils are usually ~10nm). They can continue to polymerise *in vitro* to form amyloid fibrils and can also dissociate to form smaller aggregates (Figure 1.13). Electron microscopy and Atomic Force Microscopy have shown that they are more flexible than mature fibrils as they exist as both curved and straight assemblies (Härd, 2011). Aβ protofibrils interact weakly with the amyloid staining dyes Congo red and Thioflavin T indicating that they contain high levels of the β-sheet structure observed in mature fibrils. Circular dichroism, infrared spectroscopy, x-ray diffraction and SSNMR have been used to reveal a secondary structure of two β-strands (Fändrich, 2012).
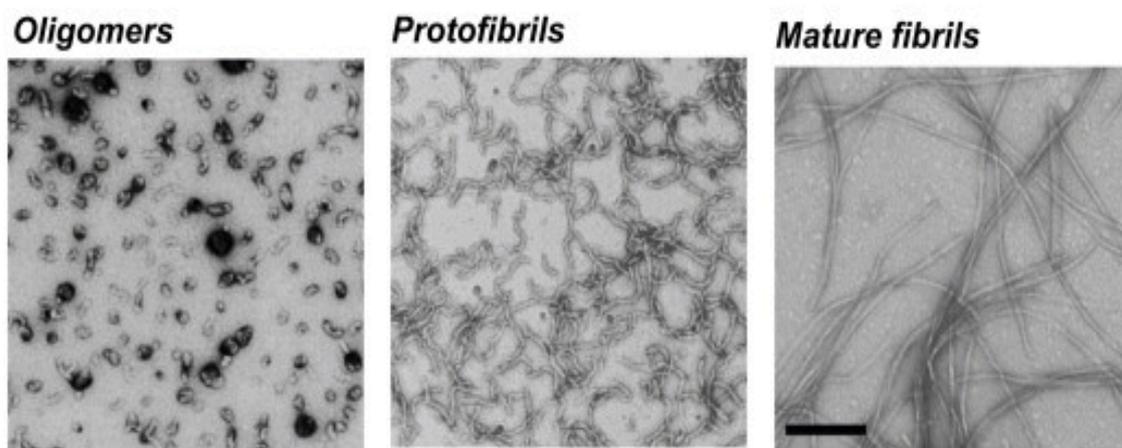
Figure 1.13: Structure of Aβ$_{1-40}$ oligomers, protofibrils and mature fibrils.
Negative stain EM images from Fändrich, 2012.

Annular assemblies of Aβ *in vitro* are doughnut shaped structures with an outer diameter of 8-12nm. They are believed to enclose a water filled channel and have some structural similarity to pore forming toxins (Lashuel et al. 2002). Little is known about their molecular structure due to the heterogeneity of preparations but it has been hypothesized that their pore forming nature enables them to perturb the cell membrane, ultimately causing cell death.

There have been smaller oligomeric species (4-6nm in diameter) observed in preparations of Aβ *in vitro.* These are termed Aβ-derived diffusible ligands or ADDLs. Ultracentrifugation has been used to identify ADDL-like assemblies from post mortem AD brains. How structurally analogous these species are is still unclear. There is evidence that both synthetic Aβ ADDLs and natural soluble ADDL-like oligomers can inhibit hippocampal long-term potentiation (Walsh & Selkoe, 2007, Haas & Selkoe, 2007).

Globulomers of Aβ have also been well characterized using protein engineering. Globulomers are the spherical oligomers seen in SDS or fatty acid containing preparations. Solution NMR was initially used to identify dimeric Aβ units within globulomers of Aβ$_{1-42}$. These dimers were created by residues 18-23 and 28-33 forming a two stranded anti-parallel β-sheet connected by a hairpin at residues 24-27. Intramolecular interactions between the two 34-39 fragments formed the final dimer structure in a two stranded parallel β-sheet. By introducing a Cysteine at position 17 and 34 they were able to stabilize the hairpin with a disulphide bond. This β hairpin structure is similar to the cross β conformation of Aβ observed in mature fibrils. However, the hydrogen bonding in these hairpins is intramolecular resulting in antiparallel β-strands. In mature fibrils the β-strands are parallel due to intermolecular hydrogen bonds (Yu et al. 2009, Hard, 2011).

1.4.2 Cystatin B Oligomers

There are two important reasons for studying cystatin B oligomers:

1) Cell metabolism and viability assays have shown that oligomers show similar effects on cells even if the oligomers are prepared from a protein not implicated in an amyloid disease. This suggests that there is a generic mechanism by which oligomers are causing cellular dysfunction (Fandrich, 2012). Due to the difficulties in working with Aβ oligomers it is useful to be able to produce "model oligomers" of an alternative, well characterized protein which can still be used to study toxicity.

2) As mentioned earlier, mutants of cystatin B are responsible for a form of progressive myoclonus epilepsy called Unvericht-lundborg disease or EPM1. Loss of function of cystatin B is observed in most patients as EPM1 mutations usually result in lower expression of cystatin B. However, gain of toxic function of some EPM1 cystatin B mutants may also play a role in the disease, since cystatin B can behave as an amyloidogenic protein (see 1.3.2). Indeed, intracellular inclusions have been found in the brain of an EPM1 patient (Polajnar et al. 2014). Wild type and mutant cystatin B have been shown to aggregate upon overexpression in cells (Cipollini et al. 2007). It has also been shown that the small aggregates are toxic to cells and increase oxidative stress. It has, therefore, been hypothesized that these oligomers are responsible for some of the pathology seen in EPM1 including loss of the Purkinje layer of the cerebellum, cerebral atrophy, reduced cortical thickness and white mass loss throughout the brain (Polajnar et al. 2014).

Purifying large quantities of overexpressed wild type cystatin B oligomers from *E. coli* had not yet been achieved prior to this project. However, oligomers of the G4R mutant cystatin B have been purified from *E. coli*, in previous work by our group and visualized by EM (figure 1.14). Whilst, the yield of these oligomers was low (less than 1.5mg/L of LB) the oligomers are stable for months at 4°C, meaning further structural analysis could take place.

G4R cystatin B produces oligomers of at least 5 different classes. The diameter of these oligomers ranges from 8-88nm as determined by electron microscopy. The G4R cystatin B oligomers do not bind Thioflavin T indicating that they do not share the large extended β-sheet structure observed in the amyloid fibrils. The oligomers are also resistant to denaturants such as guanidine hydrochloride and SDS. They are also resistant to digestion by the strong proteinase K enzyme indicating a strong, dense and compact structure (Davis, 2016).
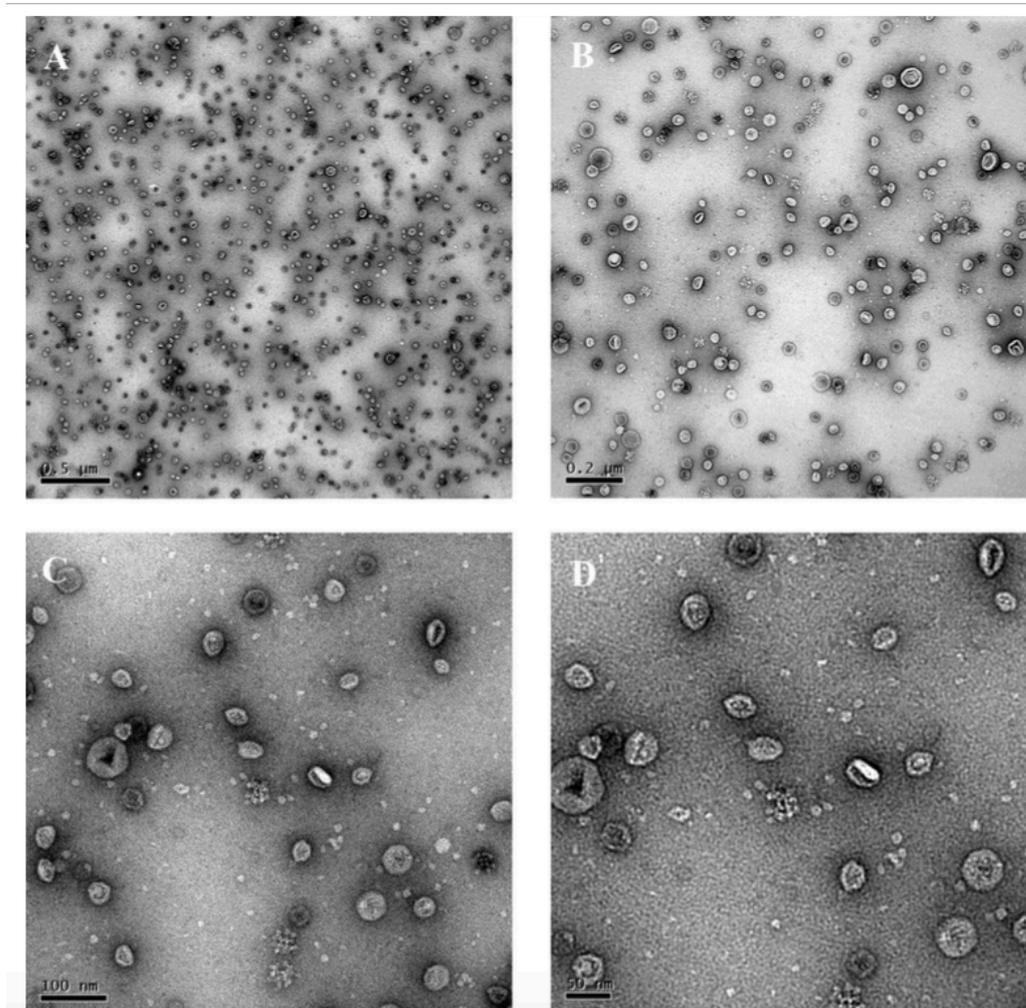
Figure 1.14 TEM of purified cystatin B G4R oligomeric species *(taken with permission from Davis, 2013.*

1.4.3 α-synuclein oligomers

Similar to Aβ, during *in vitro* fibrilisation of α-synuclein, a number of spherical oligomers and protofibrils are observed prior to production of mature fibrils (Figure 1.15). A number of genetic mutations linked to Parkinson's disease, e.g. the A30P mutation, promote the production of spherical oligomers and slow their conversion to fibrils. The protofibrillar form is also able to create pores in synthetic vesicles (Lashuel et al. 2002).
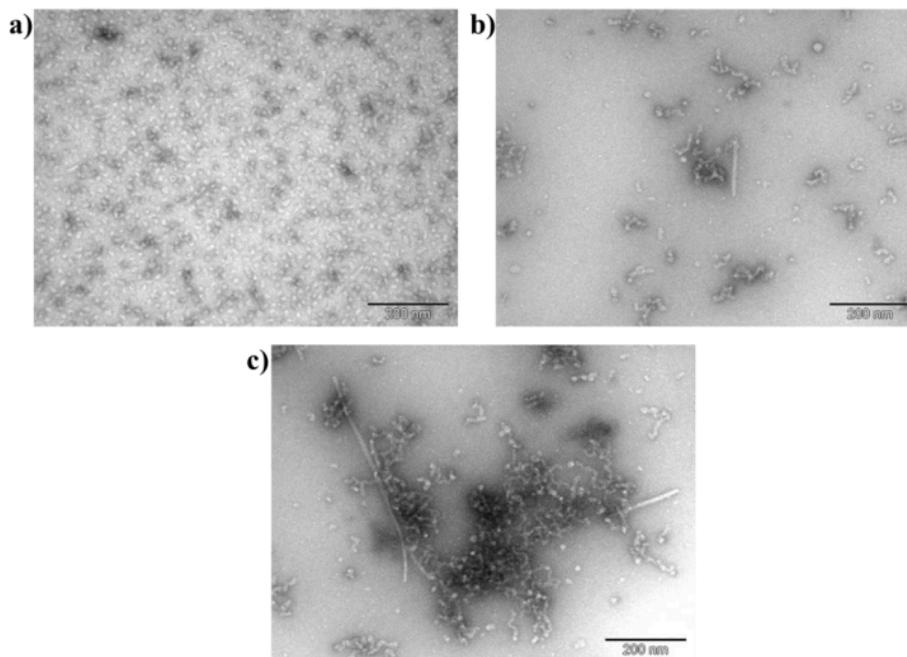
***Figure 1.15: TEM analysis of oligomeric samples of α-synuclein** (a) before incubation (b) after incubation for 3 days. Notice the appearance of small straight fibrils and worm like structures. (c) after 1 week (Paslawski et al. 2014)*

Single molecule FRET (intermolecular fluorescence resonance energy transfer) data has been used to characterize two distinct species of α-synuclein oligomer-small oligomer (A) with medium FRET values and large oligomers (B) with higher FRET values. Some structural insight of these oligomers was gained by measuring susceptibility to proteinase K digestion compared to monomer and fibrillar forms. The type A oligomers were as sensitive to proteinase K digestion as monomers, whereas the type B

oligomers were substantially more resistant to digestion. This indicates that the larger oligomers are more strongly structured and contain more β-sheet structure, reminiscent of the mature amyloid fibrils. Kinetic data showed that the smaller type A oligomer could grow through monomer addition into mature fibrils. The type B oligomers, however, are formed though conversion of type A oligomers or the disaggregation of fibrils. The larger oligomers are also able to convert into the smaller oligomers (Cremades et al. 2012).

A further H/D exchange study further refined this oligomerisation model (Paslawski et al. 2014). Oligomer type A was the most protected. The population of Oligomer type A also decreased with prolonged labeling. This type of exchange kinetics is related to slow refolding or dissociation during labeling. Oligomer type B was stable over the labeling timescale (100min). EM analysis revealed that if the oligomer preparation is incubated at 37°C for 3 days two distinct structures appear-worm like clusters and straight fibrils (Figure 1.16). This data all leads to a model whereby Type A oligomers are on pathway aggregates to fibril formation and due to their equilibrium with monomers, they can form fibrils that are elongated by monomers. Oligomer type B is more abundant and appears to cluster to form worm like structures. This makes oligomer type B the likely cytotoxic, membrane permeabilising species.

1.5 Kinetics of Amyloid Formation

Understanding the kinetic factors involved in the conversion of soluble proteins into amyloid assemblies is of high importance if one is to understand the circumstances which cause this conversion in amyloid disease in humans. However, researching this self-assembly of soluble proteins into ordered insoluble aggregates is extremely challenging. Most agree that proteins need to unfold from their native structure in order to form amyloid fibrils *in vitro* and *in vivo.* Delineating the mechanisms of folding and aggregation requires the identification of the key species involved in the aggregation pathway by detailed kinetic analysis (Jahn et al. 2006).

Producing reproducible aggregation data is often difficult and the non-linear nature of this aggregation makes the theoretical mathematics difficult to elucidate. However, analysis of the typical sigmoidal Thioflavin T reaction time course has revealed that aggregation is a nucleated polymerization reaction. An initial lag phase is normally observed before an exponential growth phase until a plateau is reached as all soluble species have been converted into fibrils. When pre-formed aggregates are added to a solution of soluble protein the lag phase can be completely removed and rapid flibril formation can take place due to seeding (Knowles et al. 2014).

However, the relationship between the duration of the lag phase and processes taking place at the molecular level is in reality very complex (as shown in Figure 1.17). Primary nucleation is thought to be responsible for the initial formation of aggregates from soluble species but in the case of amyloid formation, especially the well studied examples such as $A\beta_{1-42,}$ secondary processes are thought to be more important in the production of new fibrils. Whilst initially, in the absence of fibrils, early aggregates and oligomers are formed by primary nucleation, once a critical aggregate concentration has been reached secondary processes will be the major source of fibril production (Cohen et al. 2012 and Xue, 2015). Fragmentation is thought to be the most critical secondary process as each fragmentation event increases the number of fibril ends to which soluble species can attach. Secondary

nucleation, where the fibrils themselves act as surfaces for nucleation may also contribute to the observed lag phase and exponential growth processes (Knowles et al. 2014).
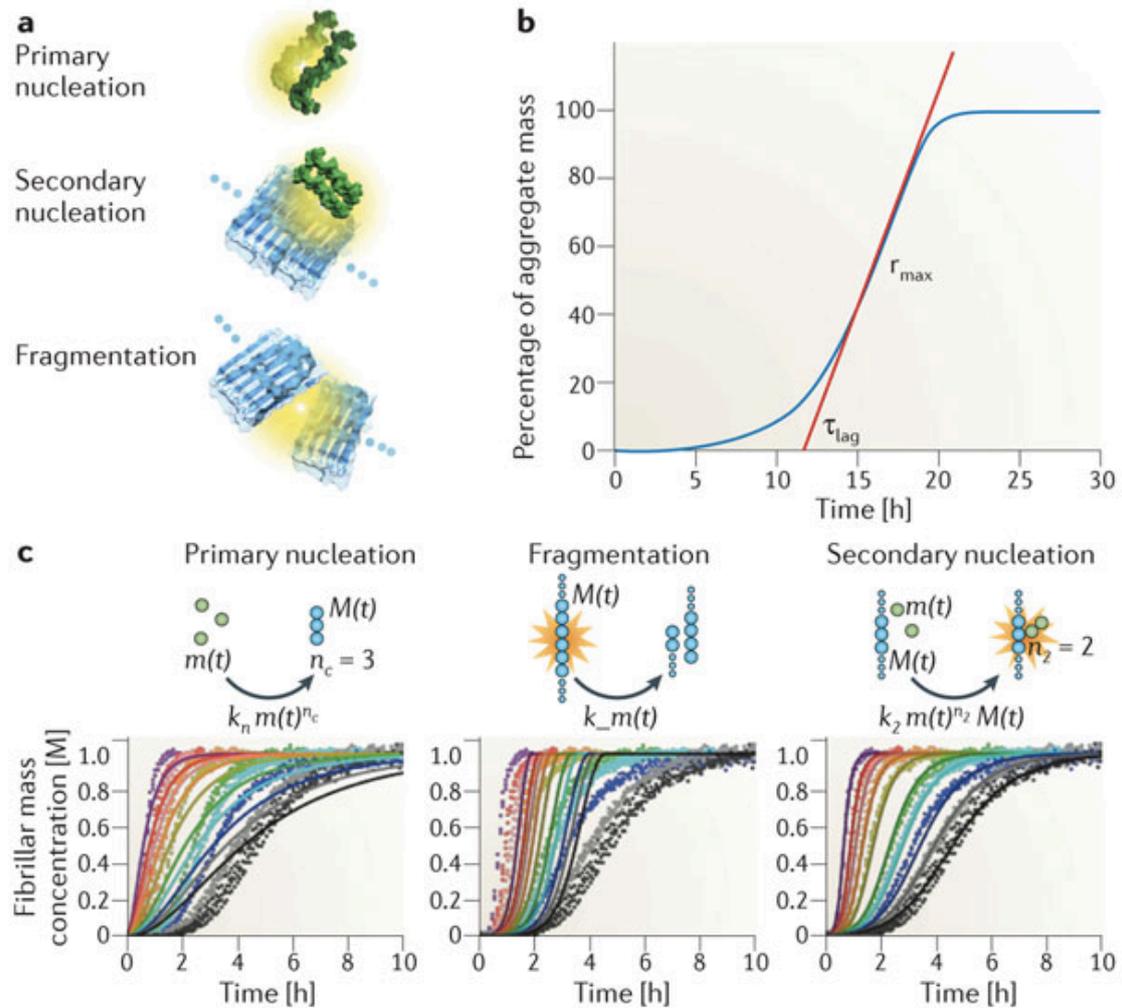
Nature Reviews | Molecular Cell Biology

Figure 1.16 Kinetics of amyloid formation. (a) Amyloid formation occurs via the monomer (green) through primary nucleation or from existing fibrils through both monomeric and aggregated species by secondary nucleation. (b) Integrated rate laws from filament growth show that they have sigmoidal functions which are characterized by a lag time (τlag) and a maximal growth rate (rmax; red line). (c) Comparison of these integrated rate laws with experimental measurements. From Knowles et al. 2014.

1.6 Other types of oligomers or inclusions

In chapter 4 of this thesis I present a study of the polymerization of cystatin B into "oligomers" *in vitro*. However, the pathological nature of these cystatin B oligomers is unclear and, indeed, others such as the Melli group have found them to be "physiological and functional" *in vivo* (Rispoli et al, 2013). I have, therefore, presented here a review of other protein inclusions which show similar characteristics to those of cystatin B.

1.6.1 Marinesco Bodies

Marinesco bodies (MBs) are eosin positive, ubiquitinated, intranuclear inclusion bodies and were first described by Georges Marinesco in 1902. They are found in the substantia nigra and locus coeruleus of the human brain. The bodies are small (2-10μm) homogeneous, droplet shaped structures (Figure 1.17). Their formation is thought to be a response to cell stress and ageing as they are found more frequently in adult cells but whether they have a role in neurodegenerative disease is unclear. Work on MBs in the 1960s showed that they were found as frequently in patients killed in accidents as those suffering from terminal illness. They also found that there are no more or larger MBs in PD patients than those found in patients of a comparable age not suffering from the disease (Yuen & Baxter, 1963).

However, later studies on intranuclear ubiquitin inclusions in trinucleotide repeat diseases such as Huntington's disease (Alves-Rodrigues et al. 1998) and the discovery of higher numbers of MBs in those suffering from myotonic dystrophy has led to research into a possible pathogenic role for these bodies. More recent work has shown an increase in the number of MBs in dementia with Lewy body patients and that MB frequency correlates inversely with markers of striatal dopamine in healthy elderly people. It has, therefore, been hypothesised that MBs are involved in the age-related loss of nigral dopaminergic neurons (Beach et al. 2004).

There are other intranuclear inclusions such as intranuclear rodlets (INRs) which are thought to be both structurally and functionally related to MBs. They

are both formed from amorphous granular material, interspersed with regular parallel or lattice-like fibrillar arrangements. INRs and MBs have also both been shown to contain pro-myelocytic leukemia (PML) protein (Kumada et al. 2002; Woulfe et al. 2004). PML nuclear bodies (another type of inclusion body which are scattered throughout cell nuclei) are thought to have a number of functions including protein storage, degradation, and sequestration, and regulation of transcription. However, it is still not clear whether all these bodies, which are all found in healthy brains, are part of normal brain functionality or are abnormal structures, detrimental to neurons. However, their ubiquitination and the fact that they are analogous structures to those seen in trinucleotide repeat diseases indicates that they are an important regulatory mechanism for controlling the concentration of nuclear proteins (Woulfe et al. 2004).
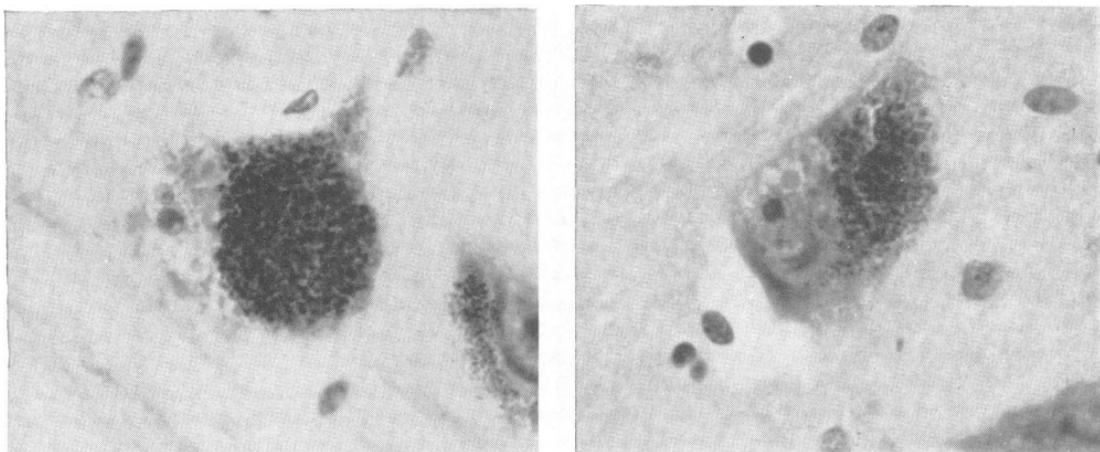
Figure 1.17: Marinesco Bodies in the nucleus of substantia nigra cells. They are small droplet like structures 2µm-10µm in diameter (from Yuen & Baxter, 1963).

1.6.2 Bunina Bodies

Bunina bodies (BBs) are small eosinophilic intraneuronal cystoplasmic inclusions. They are one of the pathological hallmarks of amyotrophic lateral sclerosis (ALS) and are found in the remaining lower motor neurons (LMNs) of the spinal chord and brain stem of ALS patients. They were first described by Bunina in 1962 in two familial cases of ALS. Since then their morphology has been well studied. Electron microscopy shows that they consist of amorphous, electron dense material, showing clear areas in the centre which contain filaments and vesicles (Figure 1.18). They often form chain-like clusters and do not have a limiting membrane (Okamoto et al. 2007).

However, their exact function still remains unclear. There have been many immunohistochemical studies on BBs using a huge number of antibodies against a variety of proteins e.g. tau, APP, α-synuclein, actin, myosin, neurofilament, α/β-tubulins and microtubule associated proteins (Sasaki et al, 2006). However, only two proteins have been found in BBs: cystatin C (Okamoto et al. 1993) and transferrin (an iron binding protein which transports ferric iron into tissues) (Mizuno et al. 2006).

Interestingly, cystatin C immunoreactivity is significantly lower in the LMNs of ALS patients and the formation of TDP-43 inclusions (another hallmark of ALS) may be linked to this. There is a positive correlation between the occurrence of BBs and TDP-43 inclusions in spinal and brainstem LMNs (Mori et al. 2009, 2010, 2014). However, a recent case report (Kimura et al. 2014) showed that BBs can be present elsewhere in the brain such as in the cerebellar dentate nucleus where TDP-43 inclusions are rarely found indicating that the mechanism of BB formation is separate from that of TDP-43 inclusions.
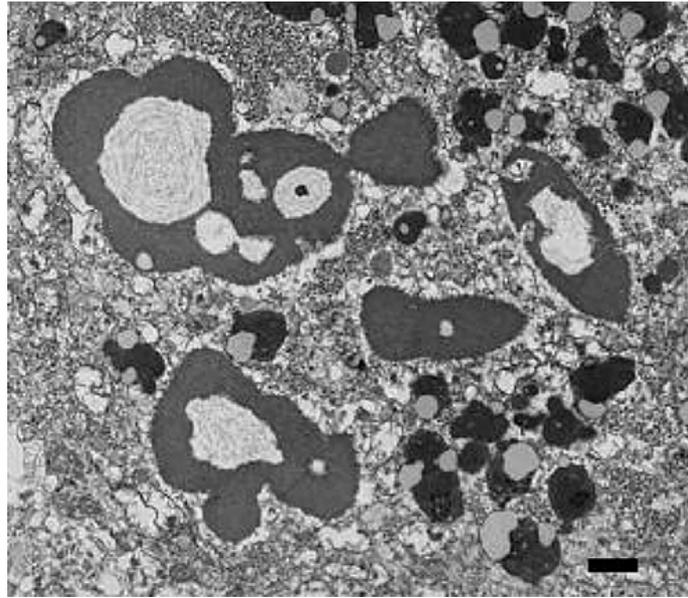
Figure 1.18: Electron microscopy of Bunina Bodies. One can see two main features-amorphous material and other tubular and vesicular structures. Typically Bunina bodies consist of densely packed amorphous material surrounded by some tubular and vesicular structures, sometimes with a central clear are containing 10 filaments of about 10nm (from Okamoto et al. 2007).

1.6.3 Cystatin B

As mentioned in section 1.4.2 of this introduction, cystatin B is able to form oligomers. The Melli group have studied whether such polymerisation occurs *in vivo* and what functions these oligomers or inclusions may have. They showed that cystatin B does indeed form oligomeric structures in human and rat cells when overexpressed. They hypothesise that this may be an important regulatory mechanism as regulation and expression of protease inhibitors such as cystatin B must be tightly controlled in order to prevent neural degeneration (Cipollini et al. 2007). Further discussion of the importance of such cystatin B inclusions can be found in chapter 4.

1.7 Chaperones and Amyloid Disease

1.7.1 Chaperones: An Introduction

A chaperone protein assists proteins to obtain their correct three-dimensional, functional conformation. In English, a human chaperone is "a person, usually a married or elderly woman who, for the sake of propriety, accompanies a young unmarried lady in public as guide and protector". Chaperone is therefore an apt name in biochemistry for these important proteins which inhibit incorrect interactions between molecules but do not give steric information or form part of final protein functional structures (Ellis, 1991).

Chaperones have evolved for a number of important reasons, stemming from the fact that proteins are stabilized by many non-covalent, and therefore weak, interactions. These include ionic interactions, hydrogen bonding, van der Waals forces and hydrophobic effects. In the cellular environment, where overall protein concentration can be over 200mg/ml in eukaryotes, there is potential for these weak interactions to form non-specifically, leading to incorrect protein interactions, protein misfolding and, therefore, aggregation. Cell stresses such as heat stress and reactive oxygen species can also increase the propensity for proteins to misfold and aggregate, and indeed chaperone expression levels are increased during these events. Chaperones are also required during normal cellular events including the emergence of proteins from the ribosome. The N-terminus of proteins is synthesized before the C-terminus, meaning the partially synthesized protein, when still attached to the ribosome, is exposed in a partially unfolded and aggregation prone state. Chaperones, especially those from the Hsp70 family, have also been linked to protein transport across membranes. Proteins have to unfold in order to pass across membranes and so are particularly vulnerable to inappropriate interactions and aggregation during this process (Zimmermann, 1998). It should also be noted that many proteins are multimeric and/or need further components in order to be fully functional. Chaperones are required for different polypeptide chains to meet and form complete, stable complexes. They also allow the correct addition of post-translational modifications such as

glycosylation and phosphorylation and the binding of other components such as DNA and haem groups.

There are four large families of ATP-dependent molecular chaperones: Hsp100 proteins (also called Clps), Hsp90 proteins, Hsp70 proteins and Hsp60 proteins. There are also ATP-independent chaperones including small Hsps (sHsps). Enzymatically active chaperones such as peptidyl proline isomerases and protein disulphide isomerases are important in the correct remodeling of peptide bonds and disulphide bridges (Doyle et al. 2013).

How chaperones actually work is an area of huge scientific interest and many of the mechanisms are still to be fully established. One of the most characterised chaperone systems are those involving Hsp70 also know as DnaK in *E. coli.* Hsp70 proteins are essential, highly conserved and are involved in many cellular processes including nascent protein folding and the remodeling of protein complexes. Hsp70 proteins have an N-terminal binding domain (NBD) and a substrate-binding domain (SBD) (Meimaridou et al, 2009). The SBD has two sub-domains; a β-sheet substrate binding pocket and an α-helical lid domain. NMR has been used to show the structure of the ADP-bound closed form of DnaK. The SBD and NBD are joined by a short flexible linker region, meaning conformational changes can occur during the chaperone cycle. A triple mutant of DnaK (E47C, T199A and F529C) was used to mimic the ATP-bound open conformation. The crystal structure showed interactions between the lid and β-sheets of the SBD with the NBD.

The nucleotide present at the NBD is known to allosterically regulate binding at the SBD of DnaK. When ADP is present, DnaK has high affinity for substrates. The ATP-bound state has low affinity for substrates. This substrate binding and ATP hydrolysis by Hsp70 proteins is regulated by two co-chaperones, Hsp40 (DnaJ) and NEF (GrpE).

Hsp60s have also been well studied due their "unfoldase" activity. For proteins which fold slowly, Hsp60s bind to hydrophobic regions in the

misfolded state and induce local unfolding that helps overcome the kinetic barrier to correct protein folding. The bacterial Hsp60, GroEL, is the best-characterised example of this type of chaperone. It is composed of 14 subunits of 60 kDa which are arranged into 2 rings, making it 840 kDa in total (Zahn et al. 1996). Like Hsp70, nucleotide binding and a co-chaperone called Hsp10 (GroES in bacteria) are required for its activity.

The Hsp100s are members of the AAA+ superfamily of ATPases. Most members of the family bind a substrate protein and use energy from ATP to unfold and translocate the protein to an associated protease to be degraded. However, the bacterial Hsp100, ClpB, and its yeast (Hsp104) and mitochondrial (Hsp78) homologues are able to resolubilise protein aggregates without the need for an associated protease. This disaggregation activity is mediated by interaction between ClpB (and its homologues) with the Hsp70 chaperone system (Glover & Lindquist, 1998, Hodson et al. 2012).

Hsp104 is one of the most well studied of this type of chaperone due to its role in yeast prion propagation. Yeast prions can adopt a β-sheet rich amyloid fibril conformation similar to the mammalian prions. It has been shown that Hsp104 is involved in Sup35p fibril formation as deletion of Hsp104 results in a loss of the yeast prion phenotype (Chernoff et al. 1995). This is thought to be because Hsp104 is not acting to break up the amyloid fibrils. This results in less fibril seeds, meaning the process of seeding further amyloidosis cannot take place (Wegrzyn etl. 2001).

1.7.2 Hsp70/DnaK and amyloid disease

There is a strong link between chaperone regulation and the onset of amyloidogenic diseases (Dobson, 2003). Hsp70 has been shown to have a broad range of anti-aggregation functions. Indeed, as mentioned earlier Hsp70 works alongside Hsp104 and ClpB to dissolve large aggregates.

However, Hsp70/DnaK itself has also been shown to be important in a number of neurodegenerative diseases and has been studied for its therapeutic potential, particularly in Parkinsons disease. Hsp70 is found in AD plaques, polyglutamine aggregates in HD patients and in Lewy bodies of PD patients (Muchowski & Wacker, 2005). There has been much *in vivo* work showing the effect of Hsp70 on α-syn aggregation. Over-expression of Hsp70 along with WT α-syn rescued PD flies from neuronal loss. Interestingly, Lewy bodies were still present when the neurons were examined under the microscope. This indicates that Hsp70 protects neurons from soluble toxic forms of α-syn and may even stabilize the fibrils present in Lewy bodies (Auluck et al. 2002, Witt, 2009).

There are also some interesting *in vitro* experiments showing the anti-amyloid activity of Hsp70. Hsp70 has been shown to be one of the key proteins involved in chaperone mediated autophagy (CMA). Along with co-chaperones (Hsp40, Hsp90, Hip and Hop) it is believed to associate with proteins such as α-synuclein on the cytosolic side of lysosome membrane. The exact details of how this chaperone machinery unfolds the protein substrate before translocation into the lysosome are unknown. However, by keeping α-synuclein soluble and shunting it into this lysosomal sink it is unable to form toxic aggregates (Agarraberes & Dice, 2001).

Thioflavin T experiments have shown that Hsp70 inhibits α-synuclein amyloid formation *in vitro* without the need for co-chaperones or ATP. However, Hsp70 is only able to influence aggregation at the "early stages" of the process and has no effect on the fibrils. Addition of Hsp70 at time points

during the course of an aggregation reaction resulted in a premature levelling off of the fluorescence intensity. However, Hsp70 did not alter the ThT fluorescence in a reaction that has already reached its maximum. This indicates that Hsp70 does not cause the dissociation of α-synuclein fibrils, and is not acting as a disaggregase chaperone like Hsp104. NMR showed that Hsp70 does not bind to monomeric α-synuclein but instead binds to a range of prefibrillar species, including very early aggregates or even non-native monomeric species. It is thought that Hsp70 is "capping" these hydrophobic species, therefore, halting their maturation into amyloid fibrils and keeping them in a more soluble state so that they can be degraded (Dedmon et al. 2005). Figure 1.19 shows binding of prefibrillar α-synuclein to Hsp70 by gel filtration.
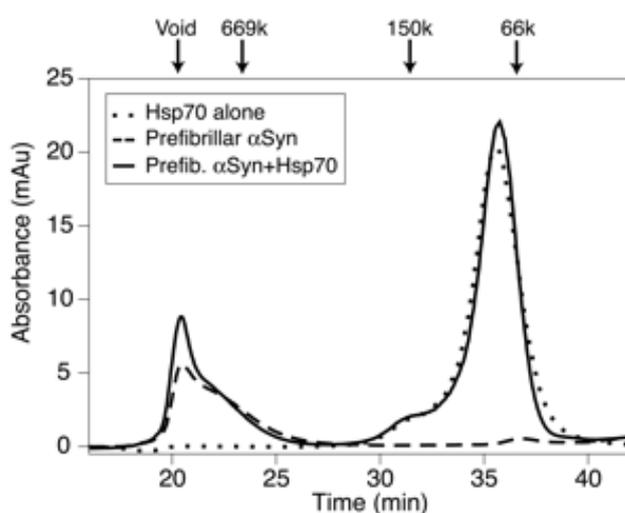
Figure 1.29: Gel filtration chromatography data showing Hsp70 binds prefibrillar α-synuclein. *Binding is shown by an increase in the area of the void volume peak by nearly 25% accompanied by a 5% decrease in the area of the Hsp70 peak when pre-fibrillar α-synuclein and Hsp70 are co-incubated. (Dedmon et al. 2005).*

Very recent work by the Radford group has shown a further role for Hsp70. They observed that Hsp70 inhibits β-2-microglobulin fibril mediated cellular dysfunction by preventing molecular shedding. Using ThT fluorescence, they showed that Hsp70 enhances the kinetic stability of the fibrils and that no depolymerisation of the fibrils occurs after 3hrs in conditions when this normally occurs (pH 6.4). Hsp70 also reduced membrane disruption by β2m fibrils and rescued SH-SY5Y cells from fibril-mediated inhibition of MTT reduction (Tipping et al, 2015).

1.7.3 DnaK and Cystatin B

As further detailed in Chapter 4, DnaK (along with copper) has been shown to be the "polymerizing factor" responsible for cystatin B oligomerisation in *E. coli.* When DnaK is added to CysB in stoichiometric amounts no ATP or co-chaperones are required for these oligomers to form. Even at sub-stoichiometric amounts only Magnesium and ATP are required.

1.8 Amyloid disease therapeutics

Therapeutics for amyloid diseases such as Alzheimer's and Parkinsons remain elusive. Researchers are still searching for "wonder neuroprotective drugs" that would both delay the onset of disease and slow their progression. There have been many unsuccessful clinical trials which have highlighted the many obstacles in the way of developing therapies for neurodegenerative diseases. There are still vast gaps in our knowledge of the complex molecular mechanisms underlying neurodegenerative disease and it is thought that any successful treatment would have to work on multiple targets. The lack of a good biomarker for these neurodegenerative diseases also makes recruiting patients for clinical trials difficult. However, the *in vitro* and *in vivo* studies discussed in the first half of this introduction have provided researchers with some key therapeutic strategies: inhibition of amyloid protein production, inhibition of protein aggregation and clearance of aggregated protein. Anti-inflammatories and anti-oxidative therapies may also play their part as potential therapeutics for amyloid disease.

There are a huge range of therapeutics being researched. Discussed below are a few examples of promising approaches.

1.8.1 Inhibition of amyloidogenic protein production

As mentioned in 1.2, Aβ is produced from the cleavage of APP by β and γ secretase. Inhibitors of these two enzymes are therefore thought to be promising targets for an AD therapeutic. Indeed, protease inhibitors have proved effective therapies for other diseases such as HIV and hypertension (Wolfe, 2006).

β-Secretase has been well studied; its cleavage mechanism and the inhibitory pathways which could reduce Aβ production are well characterised. Structural studies of β-secretase suggest that a large inhibitor molecule would be needed to fit into its relatively large active site (Ghosh et al. 2012). However, such molecules with large molecular weights do not have good blood brain

barrier (BBB) permeability, making these types of β-secretase inhibitors poor drugs for AD (Gravitz, 2011). One β-secretase inhibitor which has been trialed is LY2886721. This drug was initially promising as it could be taken orally, reduced Aβ production and rescued transgenic AD mice from cognitive decline. Unfortunately, a phase II trial of this promising β-secretase inhibitor was suspended in June 2013 by Eli Lilly and Co. due to liver toxicity in patients (Lahiri et al. 2014).

γ-secretase, the second enzyme involved in APP cleavage, is a membrane embedded protease complex which has a heterogeneous site preference for APP and therefore cleaves APP at multiple sites. This is the reason for the variable lengths of Aβ peptide, with the $A\beta^{1-42}$ isoform being the most aggregation prone. Modifiers of γ-secretase activity such as some non-steroidal anti-inflammatory drugs (NSAIDs) and their analogs do not stop γ-secretase cleavage of APP but shift its cleavage site from residue 42 to 38 meaning the Aβ variant produced is less likely to aggregate. Secretase inhibitors would also decrease oligomer formation (Haas & Selkoe, 2007).

Eli Lilly had to halt the Phase III clinical trial of their γ-secretase inhibitor, Semegacestat, as it was found to be accelerating disease progression. The reasons for this are unclear but could be due to an as yet unknown activity of γ-secretase in the brain. γ-secretase is known to have several other physiological substrates, including Notch which is involved in cell fate decisions, hence a degree of caution in the use of such inhibitors as they may lead to very serious side effects.

1.8.2 Immunotherapy

There are several types of immunotherapy which could be used in Amyloid disease. Direct active immunotherapy with synthetic intact $A\beta^{1-42}$ provided the first vaccine against Alzheimer's disease, called AN-1792. However, the Phase IIa trial had to be halted due to 18 out of 298 (6%) of patients developing meningoencephalitis. The reason for this pathogenicity has not

been fully established, although most evidence points to Aβ specific T-cells (Delrieu et al. 2012).

The second type of immunotherapy which has been trialed is passive immunisation using monoclonal anti Aβ antibodies. However, the efficacy of such a vaccine has also been called into question. A Phase II clinical trial for the passive vaccine containing the monoclonal anti Aβ antibody Bapineuzumab showed the effects of the vaccine were almost non-existent and 12 out of 124 patients developed vasogenic cerebral edema.

The reasons for the failure of these vaccines are unclear but some theories suggest that the vaccine only concentrates on Aβ and not tau. It is also likely that the antibodies do not clear the oligomeric species of aggregated Aβ. However, it is thought that vaccines would work in patients who have less advanced forms of the disease or are presymptomatic as the vaccine would keep amyloid β aggregates within manageable levels (Schnabel, 2011).

1.8.3 Natural compounds

Epidemiological studies have moved attention away from traditional drug discovery techniques towards therapeutic approaches stemming from diet and natural remedies. Much epidemiological evidence points to a lower risk of Alzheimer's disease in populations with diets rich in polyphenols. Polyphenols are naturally occurring small molecules, found in fruits, vegetables and plants. More than 8,000 natural polyphenols have been identified. These range from simple small molecules to highly polymerized compounds. The number of phenol rings and the types of chemical groups attached to these rings is used to classify such compounds. Generally, they consist of two aromatic rings with hydroxyl groups which are joined by a three-carbon bridge. The two main groups are the flavonoids and the non-flavanoids (Beecher, 2003). Importantly, for their therapeutic use, they absorbed efficiently in the small intestine and do not usually show adverse side effects (Thapa & Chi, 2015).

It should be noted here that there are huge challenges involved in conducting these types of epidemiological studies. In order to analyse the independent effects of any dietary supplement there is a long list of other lifestyle variants linked to amyloid disease which must be accounted for including: gender, age, history of hypertension, diabetes, hyperlipidemia, formal education, ApoE status, smoking, alcohol consumption and physical activity (Yamada et al. 2015).

The Mediterranean diet has garnered much attention due to its already strong associations with a reduced risk of cardiovascular diseases, type II diabetes and cancer (Diez-Espino et al. 2011). The Mediterranean diet is characterised by high intake of extra virgin olive oil, plant-based foods and fish, low intake of meat, moderate intake of dairy products and regular but moderate intake of red wine. There have been a number of trials which have reported that such a diet is associated with a reduction in risk of dementia, mild cognitive impairment (MCI) and AD.

A recent randomized trial with the PREDIMED (PREvención DIeta MEDiterránea)- Navarra cohort showed that intervention with a Mediterranean diet high in extra virgin olive oil (1L/week) improved cognitive performances in fluency and memory tasks and reduced MCI compared to controls. This cohort of 268 subjects (74.1 ± 5.7 years old, 44.8% men with no cardiovascular disease but at high risk of cardiovascular disease due to type II diabetes or other vascular risk factors) were randomly put into three groups for a period of 6.5 years. Each received either a low fat diet, a typical Mediterranean diet containing 1L per week of extra virgin olive oil or the same diet but with mixed nuts (30g/day). The trial confirmed that it was the phenolic content of the olive oil and not the unsaturated lipid content which was responsible for the beneficial effect. Those on the Mediterranean diet high in extra virgin olive oil had significantly better performances on both visual and verbal memory tasks than those who received the nut supplementation (Jacomelli et al. 2010; Valls-Pedret et al. 2012).

Whilst olive oil is mainly composed of glycerides (98%), the remaining 2% consists of several phenolic compounds including phenolic acids (caffeic, vanillic, syringic), phenolic alcohols (tyrosol and hyrdroxytyrosol), lignans (acetoxypinoresinol and pinoresinol), flavones (apigenin and luteolin) and secoiridoids (oleuropein, aglycone, oleohcantal). Total phenols in olive oil usually range from 130-350mg/kg.

One of the most widely studied polyphenols present in extra virgin olive oil is oleuropein aglycone (OLE) (figure 1.20). Like many of the polyphenols I will cover in this thesis it has been shown to have many beneficial effects: anti-cancer, anti-hypertensive, anti-mircobial and anti-inflammatory. Recently, however, it has been studied due to promising anti-amyloid and neuroprotective activity (Rigacci et al 2010).
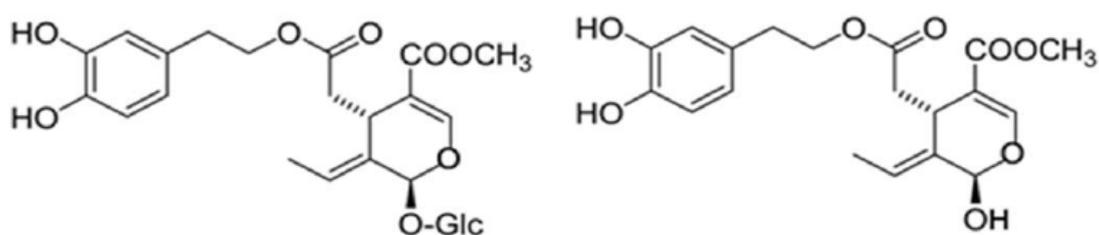
Figure 1.20: Oleuropein (left) and oleuropein aglycone (OLE) (right) structures (from Stefani & Rigacci, 2013).

Preliminary mass spectrometry and NMR work showed that OLE associates with monomeric $A\beta_{1-40}$ (Bazoti et al. 2008, Galanakis et al. 2011, Kallberg et al. 2001). Interestingly, the OLE-binding region overlaps with the $A\beta$ peptide sequence critical for fibrillisation indicating that binding of OLE interferes with aggregation. Further evidence for this was demonstrated with $A\beta_{1-42}$ and human islet amyloid polypeptide (hIAPP). Thioflavin T (ThT), ANS binding, circular diochromism, AFM and TEM showed that OLE redirects the aggregation pathway away from toxic oligomers and fibrils towards non-toxic amorphous aggregates (Rigacci et al. 2010). *In vivo* work also corroborated the idea that OLE inhibits toxic amyloid aggregation. When OLE was administered to CL2600 *Caenorhabditis elegans* (*C. elegans* strain constitutively expressing $A\beta_{3-42}$) it resulted in a significantly lower number of

plaques and toxic oligomers meaning a reduction in worm paralysis and an increase in survival (Diomede et al. 2013). The anti-amyloid activity of OLE has been most recently studied by using the TgCRND8 transgenic AD mouse model (encodes a double-mutant form of APP and shows amyloid plaque deposition and cognitive decline from the age of 3 months). Mice fed with an OLE supplemented diet for 8 weeks had a significantly lower $A\beta$ plaque load and performed much better on memory tasks than control mice (Grossi et al. 2013).

Traditional Asian diets have also been associated with a reduction in risk of amyloid disease. Indeed, frequency of AD in India is about one quarter of that in the USA (0.7% in India compared to 3.1% in the USA among 70-79 year olds) (Ganguli et al. 2000). The curry spice turmeric has been linked to this trend and has long history as a traditional medicine in Asia. Curcumin (figure 1.21) is thought to be the main active ingredient in turmeric. Curcumin has been reported to be a potent antioxidant and anti-inflammatory. Some of the highest profile research and clinical trials have been studying the anti-cancer properties of Curcumin (Hatcher et al. 2008; Aggarwal et al. 2007; Jobin et al.1999; Chan et al. 1998). It is for its anti-amyloid properties, however, that Curcumin has come to the forefront of much recent therapeutic work.
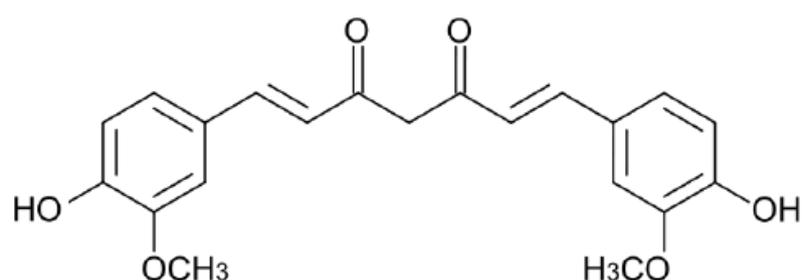
*Figure 1.21: Curcumin Structure (from Stefani & Rigacci, 2013).*

The Yamada and Cole groups have shown that Curcumin inhibits aggregation of $A\beta_{1-40}$ and $A\beta_{1-42}$ as well as disaggregating preformed fibrils. Curcumin also prevented the formation of $A\beta$ oligomers shown using an antibody specific to $A\beta$ oligomers. It should also be noted that the Cole group found

Curcumin to be the strongest inhibitor of fibril formation out of a library of 214 compounds. Curcumin, due to its slight structural similarity to Congo red, can stain amyloid plaques in hippocampus sections from the Tg2576 mouse brain (a mouse model expressing a 695 residue splice from human APP with the Swedish double mutation-K670N/M671L). Using the same mouse model they were also able to show that Curcumin is able to cross the BBB and stain plaques after oral feeding (Yang et al. 2004, Ono et al. 2004).

Green tea, which is the unfermented (non-oxidised) form of black tea, is also a large part of the Asian diet, being mainly consumed in China, Japan and India (Caruana and Vessallo, 2015). Green teas contain many simple flavonoids (catechins or flavon-3-ols). The most abundant of these is epigallocatechin-3-gallate (EGCG) (figure 1.22); 10% of the dry weight of tea leaves is EGCG (Graham, 1992).
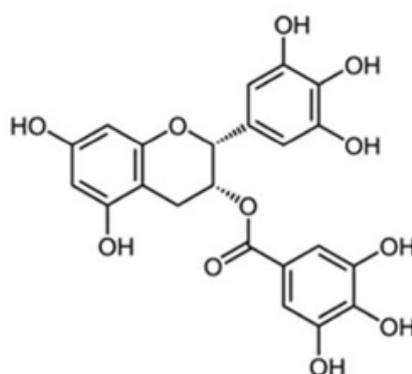
Figure 1.22 EGCG structure (from Palhano et al. 2013).

EGCG is one of the most widely studied polyphenols in terms of its neuroprotective properties having been studied for use on 14 amyloidogenic proteins (Andrich & Bieschke, 2015). The earliest studies with EGCG identified that it reduced cytotoxicity of Aβ in cellular models (Choi et al. 2001, Levites et al, 2003), reduced amyloid deposition in APP-transgenic mice (Rezai-Zadeh et al, 2005) and reduced aggregate formation in *Drosophila* and yeast models of Huntingtin aggregation (Ehrnhoefer et al. 2006).

There are many hypotheses for the mechanism of EGCG neuroprotection in amyloid disease. Much early work pointed to its antioxidant and iron-chelating activity (Mandel et al. 2008). EGCG has a 3', 4'-dyhdroxyl group on the B-ring as well as a gallate group which can reduce Fe^{2+} to form redox inactive iron and, therefore, protect cells against oxidative damage. The OH groups mean that it is a potent chelator of transition metals such as copper. In terms of amyloid disease, the anti oxidant and metal chelating properties of EGCG are significant since oxidative stress and the accumulation of transition metals have been clearly linked to neurodegeneration (Zecca et al. 2004).

However, the radical scavenging and metal chelating properties of EGCG are only part of the story. Much evidence suggests that EGCG prevents the formation of fibrils and other toxic aggregates by binding to amyloidogenic proteins. NMR of EGCG with monomeric α-synuclein showed that 30% of amino acid resonances were lost suggesting hydrophobic interactions or hydrogen bonding of EGCG with the peptide backbone or hydrophobic residues within the polypeptide chain (Ehrnhoefer et al, 2008). EGCG has also been shown to interact with Aβ at hydrophobic sequences important for β-sheet formation (residues 14-24, 27-37) (Lopez del Amo et al. 2012; Grelle et al. 2011)

Aggregation of amyloid proteins in the presence of EGCG has demonstrated that EGCG inhibits the formation of Thioflavin T and Congo red positive fibrils. In the case of Huntingtin (Ehrnhoefer et al. 2006), Aβ (Ehrnhorfer et al. 2008; Lopez del Amo et al. 2012) α-syn (Bieschke et al. 2010), IAPP (Meng et al. 2010) and Insulin (Wang et al. 2012) EGCG redirects the fibril formation pathway to the production of spherical aggregates-named amorphous aggregates. These amorphous aggregates are considered off-pathway to amyloid formation as they do not act as fibril seeds when added to monomeric Aβ or α-syn, they do not contain much β-sheet content compared to fibrils and they are not cytotoxic (Ehrnhorfer et al. 2008; Lopez del Amo et al. 2012).
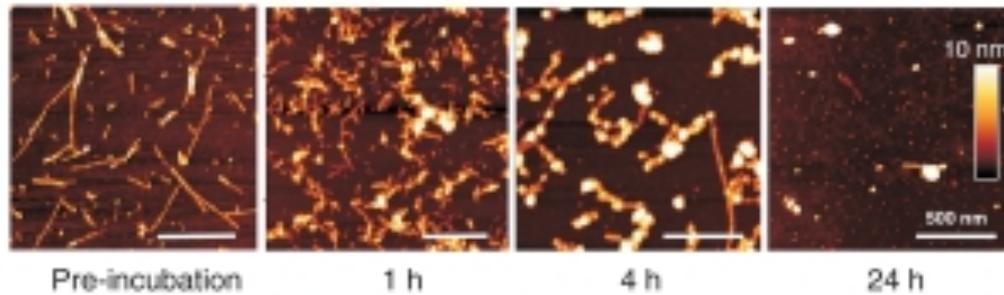
Figure 1.23: AFM showing EGCG remodeling Aβ₄₂ fibrils and oligomers into amorphous aggregates. Fibrillar Aβ₄₂ (15 µM) was incubated with EGCG (15 µM) for 24 h in PBS at 37 °C (from Bieschke et al. 2010).

Even more interestingly, EGCG has also been shown to remodel preformed amyloid fibrils into amorphous aggregates (Figure 1.23). EGCG was added to preformed α-syn and Aβ fibrils and after incubation for 24hrs amorphous aggregates, instead of the long fibrils, are detected by EM and AFM. CD and seeding experiments confirmed that these amorphous aggregates have similar properties to those formed with monomeric α-syn and Aβ in the presence of EGCG-a lack of β sheet structure and off pathway to amyloid fibril formation. Neuronal cell models (SYSY5Y and PC12) were used to show that these remodeled amorphous aggregates are not cytotoxic (Bieschke et al. 2010).

The mechanism of this remodeling has also been studied using red (Cy5) and green (Alexa 488) fluorescently labeled α-syn fibrils. The labeled fibrils were mixed and incubated with EGCG. Immunofluorescence (IF) microscopy was then used to visualize the fibrils. It was hypothesized that the fibrils are dissociated by EGCG, which allows for re-aggregation into amorphous aggregates, meaning the aggregates would be a mix of red and green fluorescence (yellow). However, the amorphous aggregates seen by IF in this experiment were uniformly red or green. This result confirmed a different hypothesis whereby EGCG directly converts the fibrils into amorphous aggregates without the need for fibril dissociation into monomers or small oligomers (Bieschke et al. 2009). The Kelly group has elucidated the nature of EGCG binding to amyloid fibrils and how this may remodel the fibrils. They

propose that oxidized EGCG (EGCG based quinones) are able to covalently modify amyloid fibrils through Schiff base formation using free amines or thiols present at the EGCG hydrophobic binding sites. This covalent modification of the fibrils causes cross-linking meaning that they cannot dissociate or fragment to form toxic oligomers (Palhano et al. 2013).

As one can see from the example of small molecule therapeutics in this chapter, the exact molecular detail of how these molecules may be acting on the amyloid are still to be fully understood.

1.9 Overview of Thesis

The title of this thesis "Amyloid Disease: Are the oligomeric species a good therapeutic target?" was chosen because of the two original aims of this thesis; to isolate and characterise oligomers of cystatin B and to identify small molecule therapeutics that could be used to detoxify such species.

In Chapter 3 and 4, the preparation and characterisation of cystatin B oligomers is presented. This project investigated the role of DnaK and copper in this process.

Chapter 5 presents work on identifying a novel therapeutic for amyloid disease from *Salvia sclareoides* (a species of Sage plant) using NMR and mass spectrometry.

Chapter 2: Materials and Methods

2.1 Buffers and Reagents

All reagents were analar grade and obtained from Fisher Scientific (UK) or Sigma-Aldrich, except where indicated. Deionised water (18.2Ω) from an Elga Purelab 611 Classic UVF was used in all experiments. Buffers were filtered through a 0.2 μm filter and 1 mM sodium azide (NaN_3) was added to all buffers, except bacterial growth media.

2.1.1 Luria-Bertani Media:

For 1l: 10 g bacto-tryptone (Oxoid ltd, UK)

5 g yeast extract (Oxoid)

10 g NaCl (Melford)

The solution was made up in deionised water and sterilised by autoclaving. Antibiotic was added after cooling. LB-agar was made by adding 2.8 g Nutrient agar in 100ml of deionised water and autoclaved. Around 20ml is used to pour 1 plate.

2.1.2 M9 Minimal Media

This is used for growing labeled protein for NMR experiments.

For 1l: 6 g Na_2HPO_4

3 g KH_2PO_4

0.5 g NaCl

The solution was made up in deionized water. The pH was adjusted to 7.4 before autoclaving. The following were added to the media after autoclaving:

For 1l: 650 μl trace elements (autoclaved)-see below

1.5 g glucose

1 ml 1 mg/ml thiamine

2 ml 0.5 g/ml ($15NH_4)_2SO_4$

1 ml 1 M $MgSO_4$

0.1 ml 1 M $CaCl_2$

Trace elements

Per 100 ml dH$_2$O:

> 550 mg CaCl$_2$.2H$_2$O
>
> 140 mg MnSO$_4$.H$_2$O
>
> 40 mg CuSO$_4$.5H$_2$O
>
> 220 mg ZnSO$_4$.H$_2$O
>
> 45 mg CoCl$_2$.6H$_2$O
>
> 26 mg Na$_2$MoO$_4$.2H$_2$O
>
> 40 mg H$_3$BO$_4$
>
> 26 mg KI

The above were added to 70ml of water and the pH adjusted to 8 before 500 mg EDTA was added. The pH was readjusted to 8.0 and then 375 mg FeSO$_4$.7H$_2$O was added. The solution was made up to 100ml and autoclaved.

2.1.3 SDS-PAGE gels and buffer

4 x Upper Buffer: 0.5 M Tris/HCl pH 6.8, 0.4% w/v SDS
4 x Lower Buffer: 1.5 M Tris/HCl pH 8.8, 0.4% w/v SDS

Running Gel (16% acrylamide, tris-HCl pH 8.8):
4 ml 40% acrylamide (37.5 : 1 acrylamide : bis-acrylamide; Bio-Rad), 2.5ml lower buffer, 3.5 ml H$_2$O, 100 µl 10% w/v ammonium persulphate and 10 µl N,N,N'N-tetramethylethylenediamine (TEMED).

Stacking Gel (4.5% acylamide tris-HCl pH 6.8):
1.1 ml 40% acrylamide (37.5 : 1 acrylamide : bis-acrylamide Bio-Rad), 2.5 ml Upper Buffer, 6.4 ml water, 110µl 10% w/v ammonium persulphate and 11 µl TEMED.

Running Buffer: 25 mM Tris/HCl pH 8.3, 190 mM glycine, 0.1% w/v SDS
2 x Loading Buffer: 100 mM Tris/HCl pH 6.8, 200 mM DTT, 4% w/v SDS, 0.2 % w/v bromophenol blue, 30 % v/v glycerol. 200µl aliquots were stored at -20°C and defrosted as required.

Stain: 450 ml methanol, 450 ml d.H$_2$O, 100 ml glacial acetic acid, 2.5 g coomassie brilliant blue R250.

Destain: 450 ml methanol, 450 ml d.H$_2$O, 100 ml glacial acetic acid.

2.1.4 Sodium Phosphate Buffers

Two 1l stock solutions of the following were made:

1) 0.1 M Di-sodium hydrogen orthophosphate (Na$_2$HPO$_4$)
2) 0.1 M Sodium dihydrogen orthophosphate (NaH$_2$PO$_4$)

These stocks were combined to the relevant final concentrations to make the required buffer. For example, for 1l of 10mM sodium phosphate buffer pH 6.0, 12ml Na$_2$HPO$_4$ and 88ml NaH$_2$PO$_4$ were added together and made up to 1L with dH$_2$O.

2.1.5 Buffers for making competent cells

RF1: 30mM KCH$_3$CO$_2$, 100mM RbCl, 10mM CaCl$_2$, 50mM MnCl$_4$, 15% glycerol

RF2: 10 mM MOPS, 10 mM RbCl, 75 mM CaCl$_2$, 15% glycerol

2.1.6 IPTG

A 0.5M stock solution of isopropyl-β-D-galactosidase was prepared. The solution was added to growth media to a final concentration of 0.5 mM to induce protein over-expression.

2.1.7 Antibiotics

Ampicillin: A stock solution of 100 mg/ml ampicillin sodium salt (Melford) was made up in sterile water. Aliquots were stored at –20°C and thawed on ice before being added to growth media at a final concentration of 100µg/ml.

Kanamycin: A stock solution of 15mg/ml was made up in sterile water. This was added to growth media to a final concentration of 15µg/ml.

Chloramphenicol: A stock solution of 25mg/ml was made up in absolute ethanol. This was added to growth media to give a final concentration of 25µg/ml.

2.1.8 Cystatin B Fibrillisation Buffer

For fibrillisation of Cystatin B, 15mM sodium acetate 150mM NaCl buffer pH4.7 was used. 10% TFE was added to trigger the reaction.

2.2 Protein production

2.2.1 Expression and Purification of Cystatin B

Making competent cell stocks

The *E. coli* strain BL21 Gold (DE3) was used for protein expression. XL10 Blue cells were used for production of plasmid stocks.

LB Agar plates were streaked using non-competent frozen glycerol cell stocks of the desired strains. The plates were incubated overnight at 37ºC. A single colony from the plate was used to inoculate 5ml of LB growth media. This 5ml culture was grown overnight at 37ºC in a shaking incubator (200rpm). 200µl was taken from this starter culture and used to inoculate 10ml of LB. This was grown at 37ºC, 200rpm until the OD_{600} was ~0.6. The cells were then incubated on ice for 5 minutes. The cells were centrifuged for 10 minutes at 3500 xg4000 rpm and the cell pellet re-suspended in 3.3ml of RF1 buffer. The cells were incubated on ice for 30 minutes. After centrifuging again the pellet was re-suspended in 1ml RF2 buffer and incubated on ice for 30 minutes. The cells were aliquoted into 200µl fractions and stored at -80ºC.

Plasmid preparation

Plasmid pET11a DNA containing the cystatin B construct was provided by Peter Davis. The plasmid DNA was extracted and purified from 5 ml overnight

cultures of competent *E. coli* XL1-Blue using the QIAprep Spin Miniprep Kit (Qiagen), following the manufacturer's instructions.

Transformations

A 200µl aliquot of competent cells was thawed on ice. 180µl was placed in a thin walled falcon tube and the remaining 20µl left in the cryo-tube to be used as a no plasmid control. 1µl of plasmid DNA was added to the 180µl aliquot and incubated on ice for 30 minutes. The cells were heat shocked at 42ºC for 90 seconds and then incubated on ice for 2 minutes. 800µl of LB media was added to the falcon tube and 80µl of LB media was added to the cryo-tube. The cells were incubated at 37ºC, 200 rpm for an hour. The cells from the falcon tube were serially diluted in fresh LB (undiluted, 10x and 100x) and 100µl was plated onto selective LB agar (containing 100mg/ml Ampicillin). 100µl of the no plasmid control cells were also plated. The plates were grown overnight at 37ºC.

Expression of Cystatin B

A single colony was selected from a suitable plate and used to inoculate 50ml of LB or M9 media (containing 100 mg/ml ampicillin). This starter culture was incubated overnight at 37ºC, 200rpm. 10ml of this starter culture was used to inoculate 1l of LB media containing 100mg/ml ampicillin. 4l of culture were grown as this generally gives a good yield of protein. Flasks were incubated at 37ºC, 200rpm until the OD_{600} reached 0.6. Isopropyl-β-D-thiogalactopyranoside (IPTG) was then added to each flask at a final a concentration of 0.5mM to induce the cells. The cells were then grown for a further four hours at 37ºC, 200rpm. The cells were centrifuged at 17700 xg10,000rpm for 15 minutes at 4ºC. The cell pellets were re-suspended in ~50ml of 10mM Sodium phosphate buffer (pH6) and frozen at -80ºC.

Cell Lysis

Cells were thawed on ice and transferred to a 200ml beaker. The following were added to the cell suspension: EDTA-free protease inhibitor (1 tablet per 50ml; Roche Life Science, UK), 0.1 mg/ml DNase1 and 20 mM $MgCl_2$. The

cell suspension was sonicated on ice for 6 cycles (30 seconds of sonication, 1 minute cooling) at 12 microns using a Soniprep 1500. The suspension was then centrifuged at 28174 xg15000 rpm for 10 minutes at 4°C to pellet the cell debris. The supernatant was retained and filtered using a 0.45µm filter. This solution was then dialysed overnight against 1l of 10mM sodium phosphate pH6 at 4°C.

Ion-Exchange Chromatography

The dialysed solution was loaded onto a 50ml SP-sepharose fast-flow column (GE Healthcare) which had been equilibrated with 10mM sodium phosphate buffer, pH6. The column was washed with the same buffer until the OD_{280} was reduced to the baseline value. The protein was then eluted over a 160ml 0-500mM NaCl gradient in 10mM sodium phosphate buffer. 4ml fractions of eluent were collected and the presence of cystatin B checked by SDS-PAGE. All fractions containing cystatin B were pooled and concentrated to a volume of ~10ml using an Amicon ultrafiltration cell (Millipore, UK). The solution was filtered using a 0.2µm filter.

Gel Filtration Chromatography

The 10ml protein solution was loaded onto a 350ml preparative Superdex-75 gel filtration column which had been equilibrated with 10mM phosphate buffer, pH6, 100mM NaCl (filtered and degassed). The protein was then eluted with the same buffer and 6ml fractions collected. The OD_{280} of the fractions was monitored and fractions containing cystatin B were pooled and stored at 4°C. 4l of bacterial growth yielded 100 mgs of cystatin B.

2.2.2 Expression and Purification of α-synuclein

The α-synuclein plasmid construct was kindly provided by Dr Diane Hanger from Kings College, London. The WT α-synuclein insert was cloned into the NdeI/HindIII sites of pRK172 (AmpR). This plasmid was amplified in XL-10 Blue cells, transformed into BL21 Gold (DE3) and cell cultures were grown as detailed for cystatin B (2.2.1). The bacterial cell pellets were re-suspended in

100ml high salt buffer (50mM Tris, 0.75M NaCl, 1mM EDTA, pH 7.4) containing 2 protease inhibitor tablets (Roche Life Sciences, UK). The suspension was incubated at 100ºC for 10 minutes and then centrifuged at 17700 xg10,000 rpm for 20 minutes. The supernatant was dialysed against a salt free buffer (10mM Tris, pH.7.5) and then applied on to a 50ml Q-sepharose fast-flow column and eluted using a 160ml 0-0.5M NaCl gradient. Fractions containing the protein were pooled, concentrated to 10ml and run down a preparative Superdex 75 SEC column (GE Healthcare). A 4L growth yielded about 70mg of purified α-synuclein protein. An extinction coefficient at 280nm of 5800 $cm^{-1} M^{-1}$ was used to calculate protein concentration.

2.2.3 Aβ preparation

Lyophilised HFIP treated A$\beta_{1-42 \text{ or } 1-40}$ was purchased from rPeptide (Georgia, USA) as 1mg aliquots. Before re-suspension the aliquot was allowed to equilibrate to room temperature for 10 minutes. 1ml of cold HFIP was added to the vial to produce a 1mg/ml solution of Aβ peptide. The vial was sonicated in a sonicator bath (DECON Ultrasonics, Sussex UK) for 10 minutes at room temperature to allow for complete dissolution. 0.1mg aliquots of the resulting peptide solution were transferred to sterile eppendorfs. The HFIP was removed by evaporation under a stream of N_2 and any further traces were removed by lyophilisation of the aliquots. The eppendorfs were stored at -20ºC.

2.3 Protein Analysis

2.3.1 Gel Electrophoresis

Tris-glycine SDS-Polyacrylamide Gel Electrophoresis (SDS-PAGE) was used to determine presence of protein during protein purifications. The BioRad Protean 3 apparatus was used. A running gel was first cast (16%acrylamide) and a stacking gel (4.5% acrylamide) cast above this. The gel was run in tris-glycine buffer, 0.1%SDS, pH8.6. 10µl of each protein sample was added to 10µl of loading buffer and 10µl of this was loaded into a well. 5µl of Precision

Plus Protein Dual Xtra Standards (Bio-Rad) were loaded into one well on the gel. The gel was run at 180kV for around 45 minutes or until the dye front neared the bottom of the gel. After removing the gel from its casing, it was stained using Coomassie Blue on a gel shaker for 1 hour. The gel was then destained overnight. Pictures of gels were taken using a Hewlett Packard scanner.

2.3.2 Protein concentration

Protein concentration was determined using the UV absorption of the protein at 280nm. The absorption spectra of the proteins from 250-350nm was recorded using a Cary 50 spectrophotometer. The concentration of protein can then be determined using the Beer-Lambert Law:

Concentration $= \dfrac{A}{\varepsilon t}$

where A is the absorbance, ε is the extinction coefficient and t is the path length. The extinction coefficients for the proteins used in this thesis were 4470 $M^{-1}cm^{-1}$ for cystatin B, 5120 $M^{-1}cm^{-1}$ for α-synuclein and 1490 $M^{-1}cm^{-1}$ for amyloid β samples.

2.4 Amyloid Fibrils

2.4.1 Cystatin B Fibril production

The cystatin B protein sample was concentrated to 30µM using a rinsed vivaspin (Sartorius, UK) with a 3500MW cut off. The protein sample was then buffer exchanged also using a vivaspin (with a difiltration cup) into the fibrilisation buffer (15mM sodium acetate). The protein concentration was checked by UV absorbance. 10% Trifluoroethanol (TFE) was added to the solution last. The solution was incubated at 37ºC for 2 weeks, over which time fibrils formed.

2.4.2 A$\beta_{1\text{-}40}$ fibrils production

A 0.1mg aliquot of HFIP treated Aβ was allowed to equilibrate to room temperature before addition of 20µl DMSO (giving a peptide concentration of 10mM). The sample was sonicated for 10 minutes before the addition of 1 ml of fibrillisation buffer (50mM sodium phosphate, 150mM NaCl, pH 7.4). The sample was left at 37ºC for 48hrs.

2.4.3 α-synuclein fibril production

Soluble α-synuclein protein was buffer exchanged into a fibrilsation buffer (20 mM Tris, 150 mM NaCl, pH 7.2) and concentrated to 100µM using a 10 KDa MWCO vivaspin. To produce fibrils, the protein solution was transferred to microcentrifuge tubes and placed in a rotating mixer (20 rpm) for 7 days at 37 °C. Each tube contained a small glass bead (approximately 2 mm diameter) to increase agitation. Production of fibrils was checked using EM.

2.5 Electron Microscopy

2µl of sample was applied to a carbon coated copper grid which had been glow discharged at low pressure using a Cressington 208 glow-discharge unit. The sample was left to adsorb onto the grid for 1 minute and then blotted. The grid was then washed in two drops of water and blotted before being stained in 0.75% uranyl formate (a negative stain). Excess stain is blotted and the grid dried using vacuum suction. Grids were viewed using a Philips CM-100 microscope at 100kV. Micrographs were recorded using a 1024x1024 pixel Gatan CCD camera.

Chapter 3: Cystatin B Mutation and Characterisation

3.1 Introduction

Previous studies on cystatin B by the Staniforth group have been completed using a cystatin B variant originally used for crystallographic studies. This meant it did not contain the cysteine residue present at position 3 in the true wild type protein. This had been mutated to a serine to prevent potential disulphide bridges forming so that the protein would produce good crystals. Recent studies, however, have shown that this cysteine residue is important in the oligomerisation of cystatin B (Rispoli et al., 2013).

The serine was therefore mutated back to a cysteine in both the WT and G4R variants of cystatin B. As mentioned in Chapter 1, G4R is an EPM1-associated mutation. Although overexpression of the cystatin B (S3C) WT should produce oligomers, it is believed that the G4R (S3C) mutation will promote increased oligomerisation as previous work in our lab has shown that the G4R mutant can oligomerise even without a cysteine residue at position 3 (Davis, 2013).

To avoid confusion, in this thesis cystatin B used previously will be called cystatin B C3S so other references to cystatin B will be to the true WT or G4R construct with a cysteine in position 3.

3.2 Materials and Methods

3.2.1 Mutagenesis

Mutant constructs were produced using the pet11a plasmid which already contained the cystatin B C3S sequence. The following primers were used to mutate the serine to a cysteine at position 3:

WT Forward: 5' – GATATACATATGATG`TGT`GGTGCTCCGTCTGCTACTC – 3'
WT Reverse: 5' – GAGTAGCAGACGGAGCAC`CAC`ACATCATATGTATATC – 3'
G4R Forward: 5 '– GATATACATATGATG`TGT``CGT`GCTCCGTCTGCTACTC – 3'
WT Reverse: 5' – GAGTAGCAGACGGAGC`ACGACA`CATCATATGTATATC – 3'

Primers were diluted to a concentration of 125 ng/µl with distilled water. A QuikChange Site-Directed Mutagenesis Kit (Qiagen, UK) was used along with the diluted primers to produce the desired mutation.

The PCR reaction mixture was set up as follows:

1 µl pET11a plasmid template
1 µl Forward primer
1 µl Reverse primer
1 µl dNTPs
5 µl 10x reaction buffer
41 µl dH$_2$O
1 µl *PfuTurbo* DNA polymerase

PCR was carried out using the following cycling parameters:

Segment	No. Cycles	Temp /°C	Time
1	1	95	30 seconds
2	18	95	30 seconds
		55	1 minute
		68	1 minute per kb of plasmid (pET11a plasmid = 6 mins) plus an extra 2 mins, therefore 8 mins

After PCR, the reaction was placed on ice for 2 minutes, after which 1 µl of Dpn1 restriction enzyme was added. This degrades methylated (non-mutant DNA) but leaves the unmethylated newly mutated DNA intact.

The mutant plasmid was amplified using transformation into XL-10 Blue cells. The plasmid was then transformed into BL21 GOLD (DE3) cells as described in Chapter 2.

The mutant proteins were purified as described in Chapter 2.

3.2.2 ThT fibrillisation

100µl samples of 30 µM cystatin B (prepared as in 2.4.1) in 15mM sodium acetate, 150 mM NaCl, 10% TFE, pH 4.7 containing 10 µM Thioflavin T were added to 96 black half-well plates (Corning). These were incubated in a

Biotech Omega Fluorescence plate reader (BMG Labtech, UK) at 37°C with double orbital shaking at 100 r.p.m. for 10 seconds before each reading. There were 5 replicates for each mutant and the mean of these replicates was plotted along with the standard error of the mean. The excitation wavelength was 440 nm and the fluorescence emission was measured at 485 nm every 5 minutes.

3.3 Results

3.3.1 Cystatin B mutants were successfully purified

The results of the final stage of the cystatin B purification involving size-exclusion can be seen in Figure 3.1. SDS-PAGE analysis shows clear bands at ~ 11 KDa suggesting that cystatin B was purified successfully. This purified cystatin B was pooled and kept at 4°C. The gels only show monomeric cystatin B and there are no larger species or oligomers due to the presence of SDS, a denaturant, and DTT, a reducing agent. A clue to the oligomeric nature of the cystatin B species can be gathered from the elution time from a superdex 75 preparative size-exclusion column.

As can be seen in Figure 3.1, WT cystatin B shows a tetramer peak (A) and an unresolved dimer and monomer peak (B). The cystatin B G4R size-exclusion chromatogram showed an additional peak between fractions 16 and 18. The fractions were pooled separately and analysed on the discontinuous SDS- PAGE gel to check for potential oligomers. No band corresponding to 11 kDa cystatin B can be seen which suggests little if any monomeric cystatin B is in those fractions. This may suggest that the protein present in those samples is of a large molecular weight which cannot enter the 16% gel; if similar to oligomers produced by Davis (2013), these species may be resistant to dissolution in a variety of solvents including SDS. These fractions were analysed further using an analytical Superdex 200 HR 10/30 (bottom panel of Fig 3.1). There is no peak for monomer or dimer cystatin B (elute at 32 and 30 minutes respectively). Instead, peaks can be seen at 15 and 50 minutes, which could be oligomeric species since 15 minutes is the void volume and 50 minutes would correspond to a very retarded peak, typical of

hydrophobic species.

The oligomer fractions shown in Figure 3.1 were also examined by electron microscopy (EM). No oligomers were seen by EM from the WT preparation, however, oligomers were seen in the G4R preparation (Figure 3.2). Both WT and G4R oligomers were visualized by EM when cystatin B was purified from *E. coli* grown in minimal media as described in chapter 4.

Figure 3.3 shows chromatograms for cystatin B C3S and G4R/C3S from previous constructs with serine in position 3 for comparison to the chromatograms in Figure 3.1.
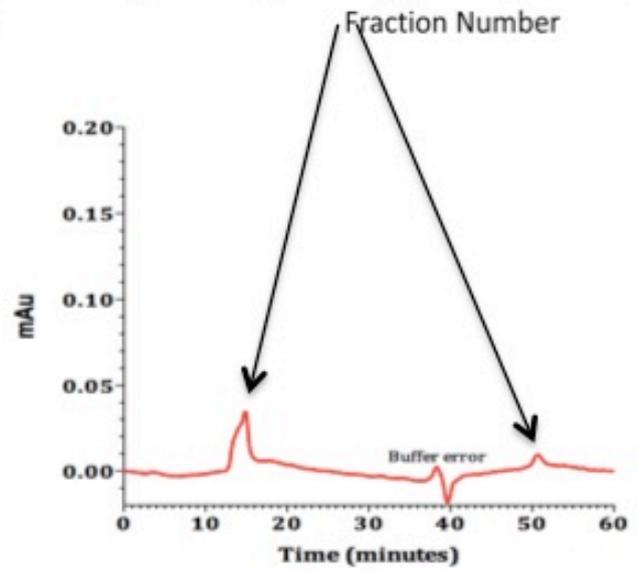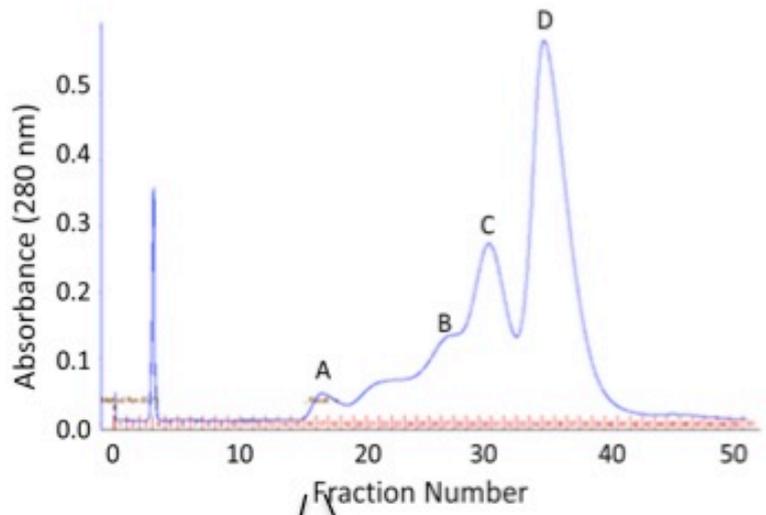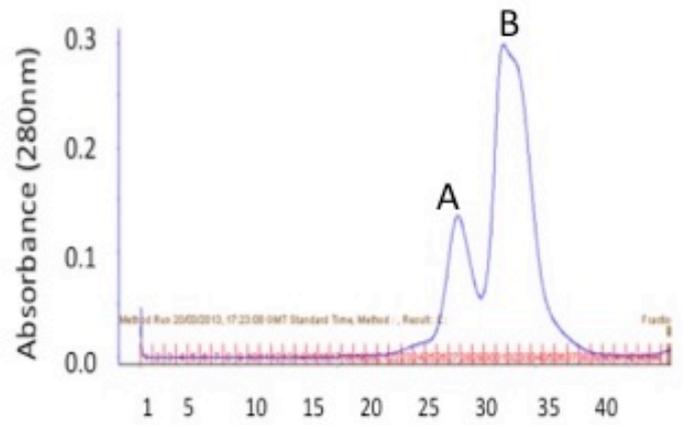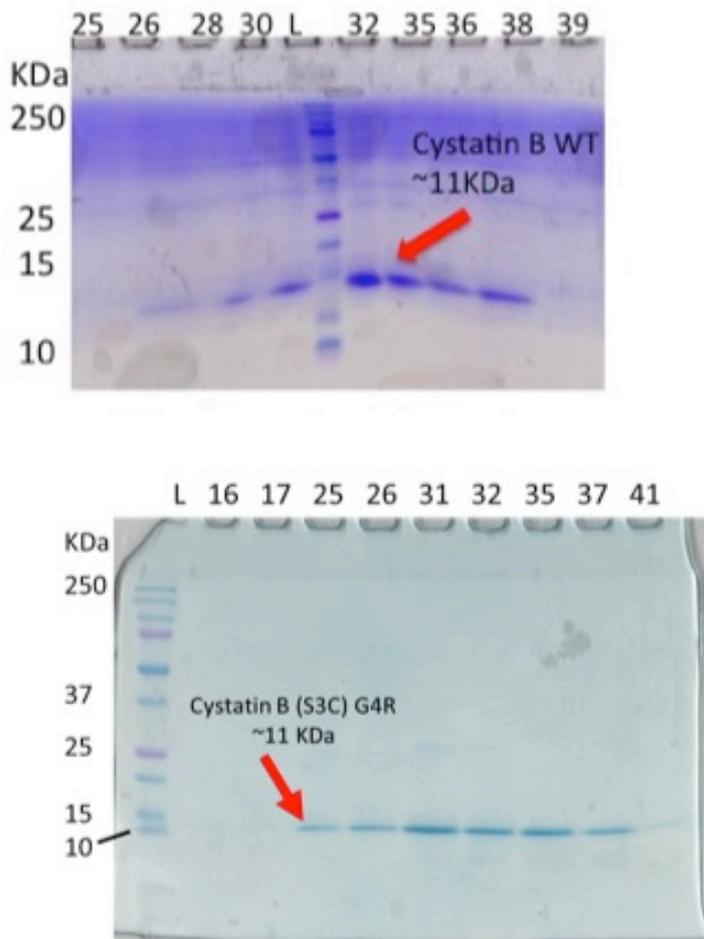
Figure 3.1: Cystatin B WT and G4R purification. Top left: SDS-PAGE gel of fractions from SEC of Cystatin B (S3C) WT. Top Right: Chromatogram from SEC of Cystatin B (S3C) WT. The peaks are labelled (A) tetramer, (B) dimer/monomer peak. Monomer can be seen as a shoulder on this peak. Middle left: SDS-PAGE gel of fractions from SEC of Cystatin B (S3C) G4R. Protein containing fractions were 24-41. Middle right: Chromatogram from SEC of Cystatin B (S3C) G4R. (A) is an oligomer peak corresponding to fractions 16-18 which were pooled seperately. (B) is a tetramer peak, (C) is dimer and (D) is monomer. Bottom right: SEC-HPLC analysis of fractions 16-18. Small peaks at 15 and 50 mins could correspond to oligomers.
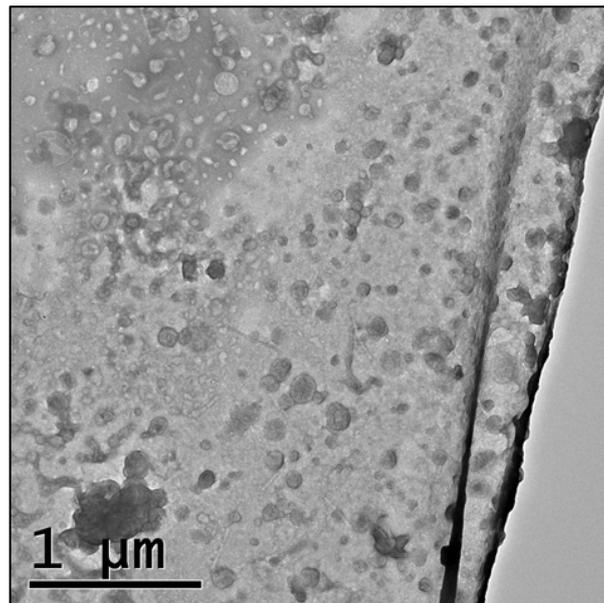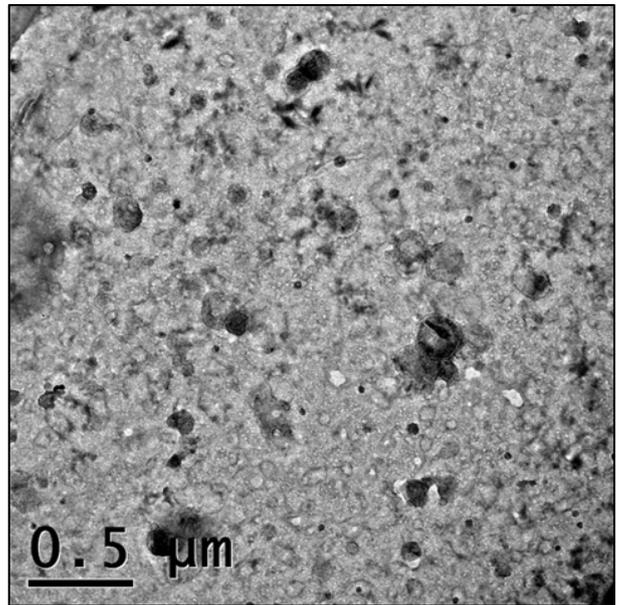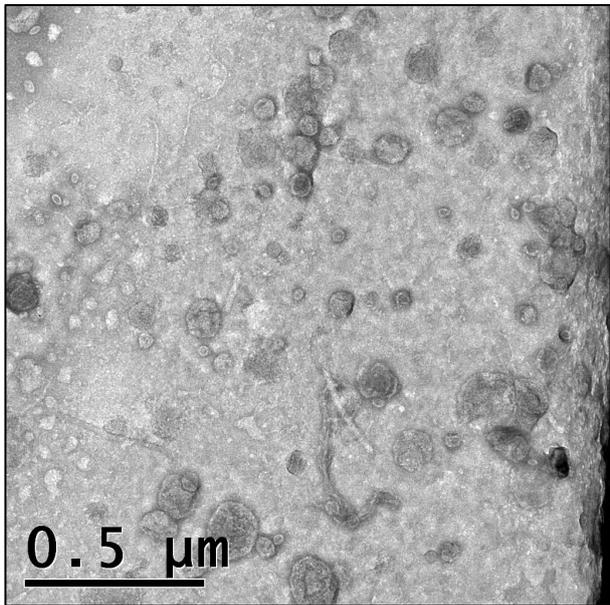
Figure 3.2: Electron microscopy images of cystatin B G4R oligomers observed in the oligomer fraction from purification by the SEC shown in figure 3.1.
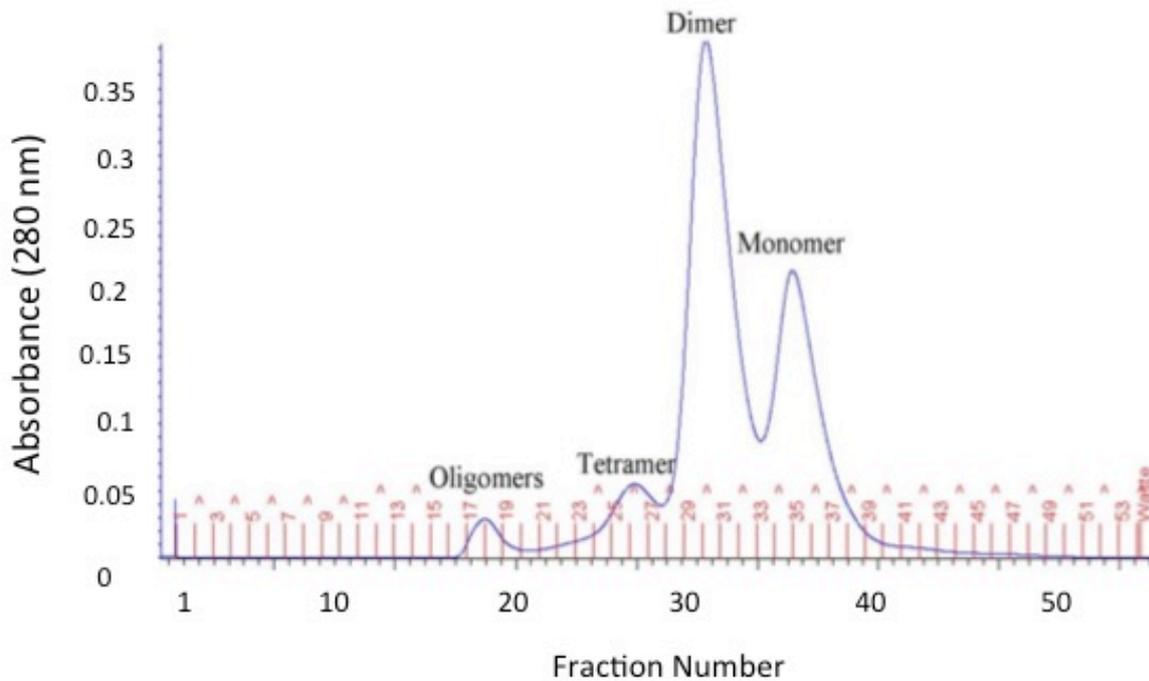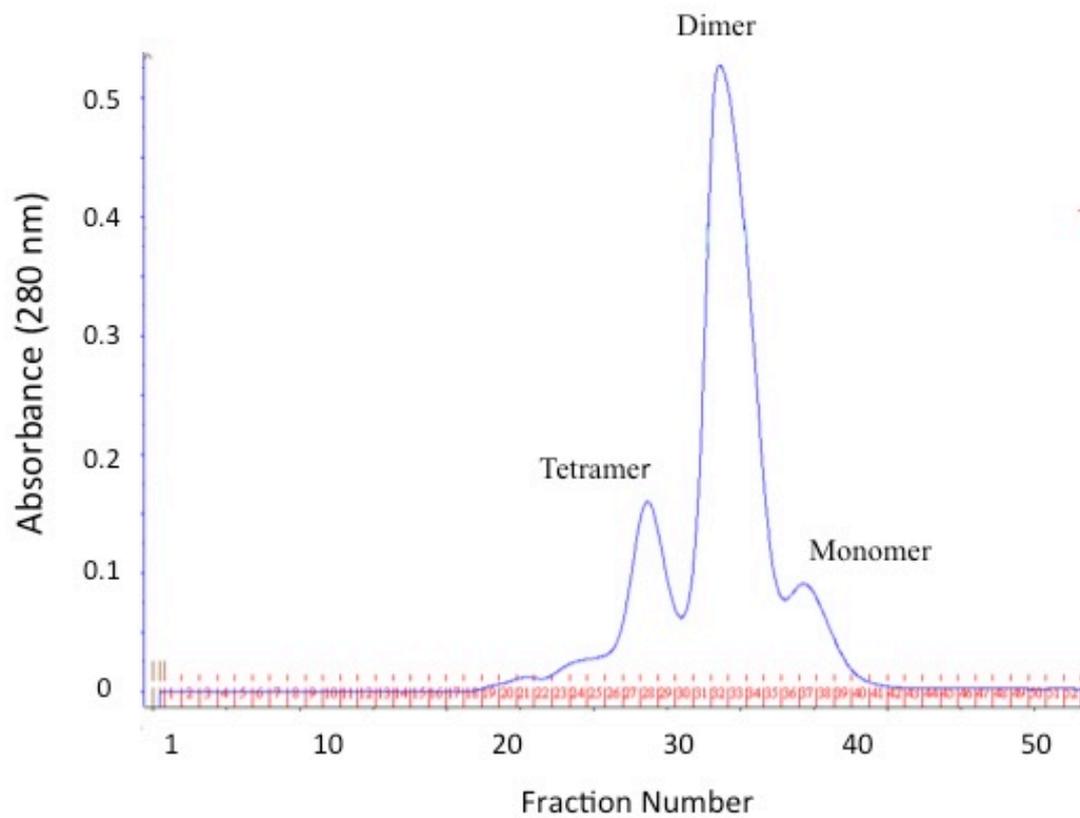
Figure 3.3: SEC profiles of the original (C3S) Cystatin B constructs. *Top: Cystatin B C3S. The tetramer and dimer peak and monomer peaks are labelled. Bottom: Cystatin B C3S/G4R . There is a small oligomer peak covering fractions 16-19. The amount of dimer exceeds the amount of monomer significantly in both proteins.*

Samples of the mutated proteins after gel filtration were analysed by electrospray ionisation (ESI) mass spectrometry. Figure 3.4 shows the mass spectrometry data for a sample of cystatin B WT. The mass peak at 11110.25 Da corresponds to cystatin B WT monomer. The mass peak at 22,277 Da corresponds to cystatin B WT dimer. ExPASy Protparam (Gasteiger et al. 2005) was used to calculate the expected molecular weight and this was 11,139.5 Da. This difference of 29.25 Da on the purified monomer could correspond to a common mass lost associated with de-amidation (Keller et al. 2008). The dimer peak has no adducts.

Figure 3.5 shows the analysis of cystatin B G4R. The mass peak at 11,239.34 Da corresponds to the cystatin B G4R monomer. A mass peak at 22476.74 Da corresponds to cystatin B G4R dimer. These masses are both within error of the ESI mass spectrometry method (S. Thorpe personal communication) as ExPASy Protparam calculated the molecular weight of the cystatin B G4R monomer to be 11,238.7 Da.

The masses corresponding to the dimer for both proteins are very close to the masses calculated by ExPASy and are within error of the ESI-MS equipment available (0.5 Da for WT, 1.3 Da for G4R). In an instance where disulphide bonding was occurring there would be a concurrent loss of 2 protons (2 Da). This was not observed in this experiment but the accuracy of this technique is not sufficient to be entirely conclusive.
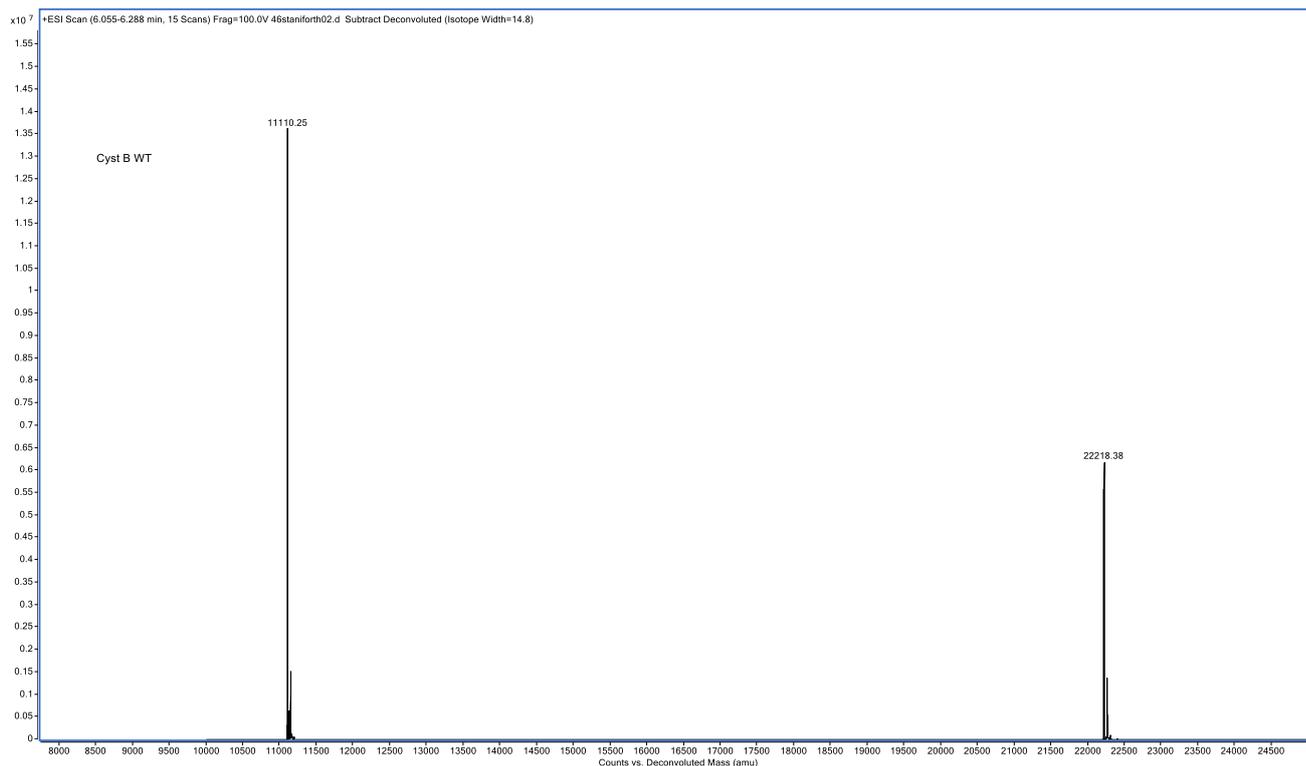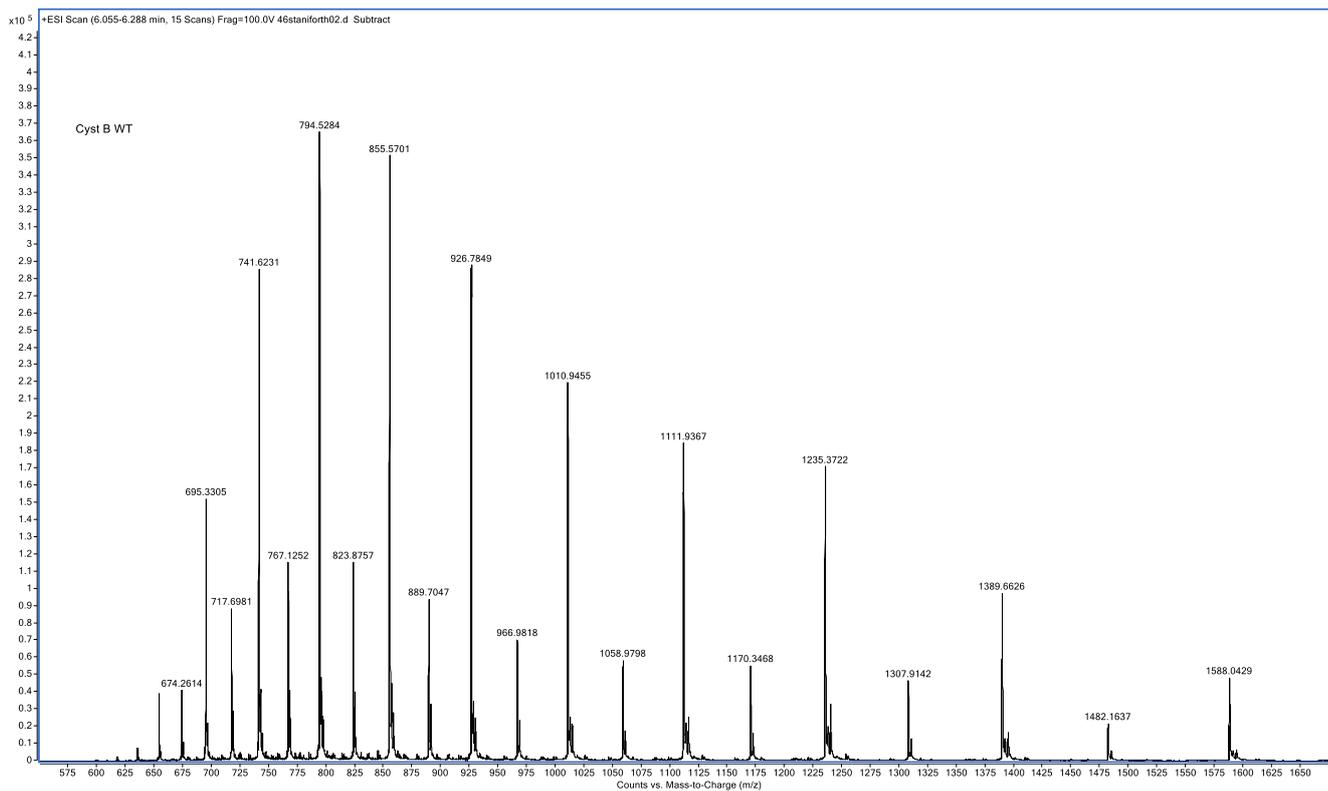
Figure 3.4: Mass spectrometry of purified cystatin B WT. *The cystatin B peak eluted between 6.055-6.228 minutes. The raw detected ion masses are shown at the top. The de-convoluted spectrum is shown below. A peak at 11110.25 corresponds to a monomer or Cystatin B WT. The peak at 22218.38 corresponds to Cystatin B dimer.*
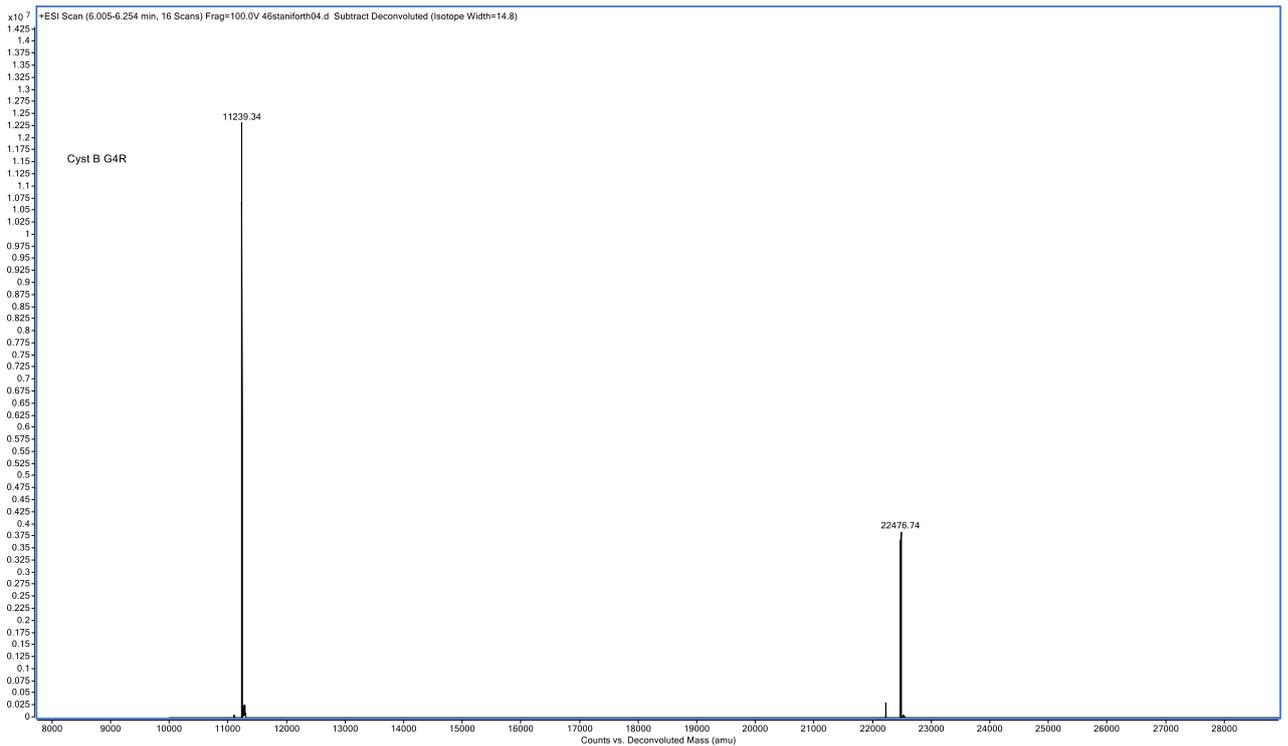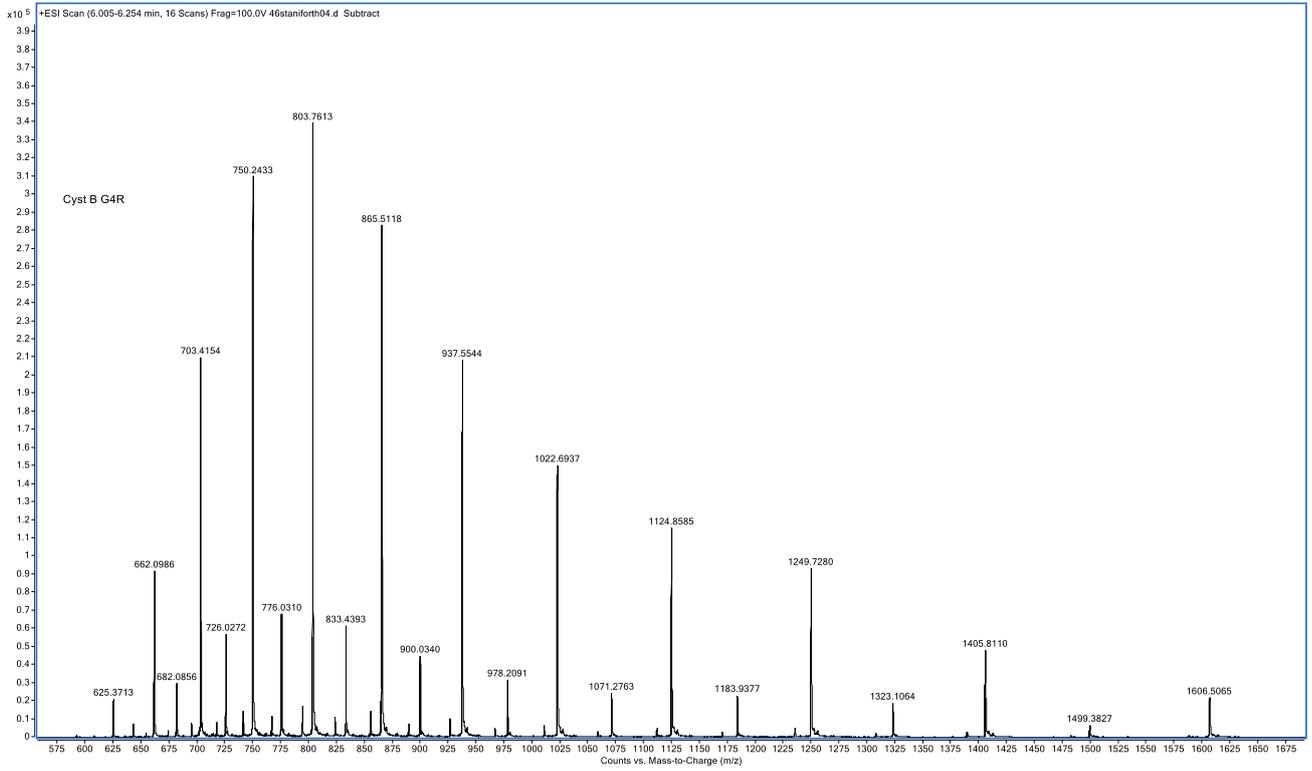
Figure 3.5: Mass spectrometry of purified cystatin B G4R. *The cystatin B peak eluted between 6.005-6.254 minutes. The raw detected ion masses are shown at the top. The de-convoluted spectrum is shown below. A peak at 11239.34 corresponds to a monomer or cystatin B G4R. The peak at 22476.74 corresponds to cystatin B G4R dimer.*

3.3.2 Distribution of species in the WT and G4R (S3C) cystatin B

It is interesting that compared with the C3S constructs, the monomer species was promoted in the purification of cystatin B, particularly the G4R construct, as can be seen in Figure 3.1. This leads one to assume that the presence of a cysteine in the protein and the resulting potential for disulphide bonding is not leading to oligomerisation *per se*.

Purifications of cystatin B C3S yielded more dimer (Figure 3.3) and indeed the protein reverts to dimer from monomer or tetramer species in the usual buffer conditions of pH 6 and no salt.

3.3.3 Fibrillisation Kinetics of Cystatin B Mutants

To identify any differences in the aggregation properties of cystatin B proteins with cysteine in position 3, a ThT fibrillisation experiment was carried out (Figure 3.6). One can see that the C3S cystatin B (previous "WT" construct) takes far longer to form fibrils than the other three cystatin B proteins and exhibits a lag phase of 900 minutes. Cystatin B C3S/G4R has a lag phase of 500 minutes as previously characterised by Paramore (2010). The WT and G4R with the cysteine re-instated have a further shortened lag phase of around 400 minutes.
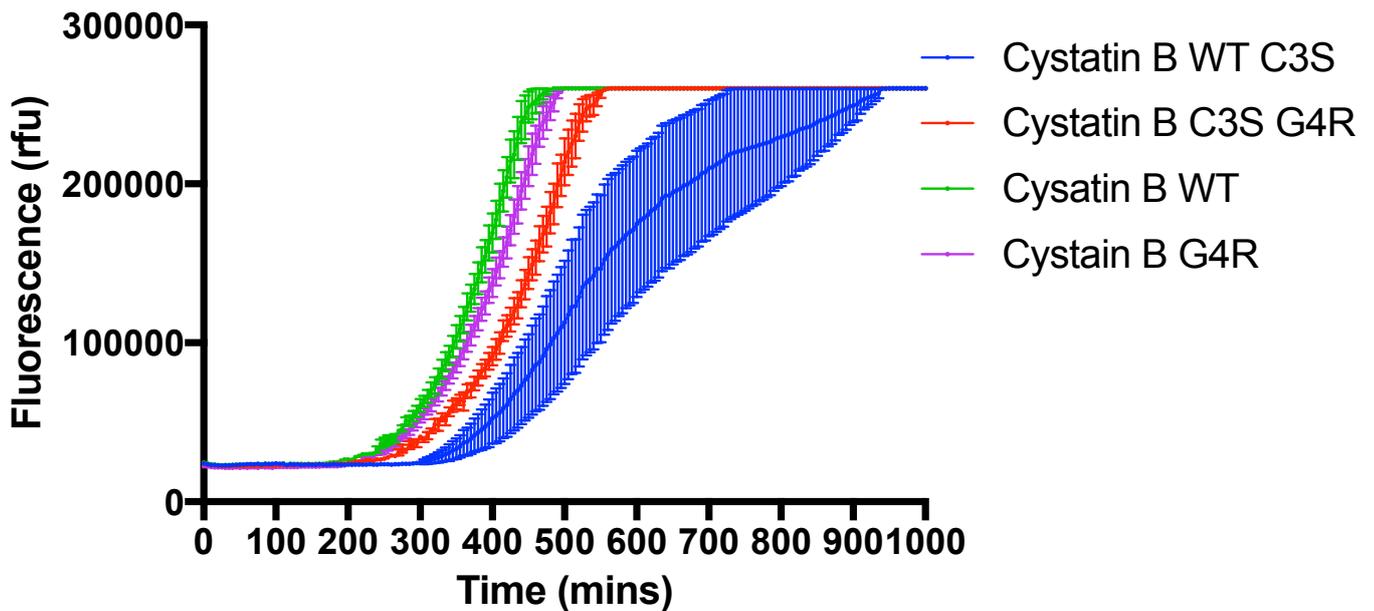
Figure 3.6: Fibrillisation curves of 4 different cystatin B mutants. *Blue and red are cystatin B C3S and C3S/G4R prior to reinstating cysteine at position 3. Green and purple are WT and G4R, both with cysteine at position 3. Each fibrillisation was replicated 5 times. The time course truncates at 260,000 rfu as this is the maximum fluorescence that the plate reader can detect.*

This potentially lends further support to the idea that the N-terminus of cystatin B, despite being unstructured in both the native and fibrillary forms of the protein, makes an important contribution to the polymerisation of cystatin B. Indeed, a truncation introduced to remove two N-terminal methionines in positions 1 and 2 also resulted in a protein with a signicantly decreased fibrillisation lag time with respect to the C3S construct (Sharma, 2009). While it may seem counter-intuitive that mutations in unstructured regions of a protein may lead to increased polymerization behaviour, this is not without precedent. Disordered regions of proteins may in fact contribute to the assembly reaction as suggested by the above results.

3.4 Conclusion

Cysteine was successfully re-instated at position 3 of the B constructs for WT and G4R. Basic characterization in this chapter showed that the protein was successfully purified under the same protocol as the C3S variant. As with previously characterised mutations at the N-terminal of the molecule, the

presence of cysteine leads to an increased tendency to assemble into amyloid. Intriguingly, the presence of cysteine favours the monomeric form over the dimer (albeit marginally). Mass spectrometry reinforces this view and shows no evidence of disulphide formation in our recombinant protein preparations.

Chapter 4: Cystatin B Oligomer Production

4.1 Introduction

As discussed in the introduction to this thesis, the oligomeric species of amyloid proteins are thought to be toxic and are, therefore, of the utmost interest to those looking at amyloid disease therapeutics. The Zerovnik group have been able to produce cystatin B oligomers composed of 6-, 8-, 12- and 16-mers (Ceru et al. 2008). However, oligomeric species are transient in nature and difficult to isolate in large quantities from protein preparations. Whilst our group has had some success producing oligomers using the G4R EPM1 related mutant (figure 1.14), WT oligomers have proved far more elusive. The reasons for this may well be physiological: while amyloidogenic proteins associated with pathology form oligomers very readily, non-pathological amyloidogenic proteins (functional amyloids) or synthetic peptides rarely form stable "oligomeric" species (Fowler et al, 2007).

Another reason could be the use of the C3S variant of WT cystatin B by our group. Work to date in the Staniforth group on cystatin B has been conducted solely using the C3S variant of both WT and G4R cystatin B because this was the original construct designed for protein crystallization. This was not thought to have a major impact on amyloid formation because the mutation is within an unstructured region of the protein. However a paper published by the Melli group in 2013 highlighted the importance of a cysteine residue at position 3 for cystatin B oligomerisation (Rispoli et al. 2013). This paper showed that cystatin B oligomerisation occurred in a similar way in a number of cell types including human and bacterial cell lines. They went on to isolate the *E.coli* Hsp70, DnaK, as the "polymerising factor" responsible for cystatin B oligomerisation *in vivo*. Given the ubiquitous nature of this chaperone, the implication is that similar processes are likely to be occurring in human cells.

In their polymerisation experiments, Rispoli et al. (2013) used cystatin B monomers electro-eluted from SDS-PAGE gels. However, they found that DnaK alone was not enough to produce oligomers; copper is also required *in vivo* unless the cysatin B is destabilised by another method. In section 1.7.1 of

this thesis, there is a full account of DnaK and its interaction with co-chaperones DnaJ and GrpE, and Mg-ATP. Rispoli et al. showed that Mg-ATP is only required for cystatin B oligomerisation by DnaK at molar ratios below 1:6. Co-chaperones are not required for this oligomerisation even at sub-stoichiometric concentrations of DnaK and cystatin B.

It was, therefore, hypothesized in this project that large quantities of WT cystatin B oligomers could be produced by adding DnaK and Cu^{2+} to purified monomeric WT and G4R cystatin B containing a cysteine at position 3. The aim of this chapter was therefore to investigate this and characterise the resulting oligomers in solution, beyond the SDS-PAGE analysis proposed by the Melli group. The novelty of this work lies in characterizing the involvement of chaperones in the formation rather than dissolution of non-native oligomeric forms of proteins.

Unlike amyloid fibrils for which there are well characterised fluorescent dyes such as Thioflavin T and Congo red, there are no specific probes for looking at oligomers. Therefore, those working in this area are limited to working with the following techniques, all of which have serious limitations when dealing with large, disordered and highly heterogeneous aggregate samples. Light scattering and sedimentation analysis is dominated by very large aggregates which populate oligomer preparations making it hard to detect and quantify the full range of oligomeric species. Gel filtration has often been used in this field but the solid phase of chromatography columns can interfere with the process of oligomer formation and certain species can be lost due to adherence to the column. EM has proved useful for visualising structural elements of these species but is not sufficiently quantitative for kinetic work. Furthermore, EM can only view species above 100 kDa. A few groups have attempted fluorescent tagging to detect the coming together of two monomers (Lee et al, 2011; Garai and Frieden, 2013) but the tags are bulky and likely interfere with the assembly reaction. Since cystatin B is mainly dimer under the experimental conditions used in this project, the use of this technique would be very limited in this study and indeed in all studies attempting to look at something bigger than dimer. Finally, SDS-PAGE along with western

blotting analysis can provide evidence for protein assembly but cannot give an accurate report on the size or structure of the species formed.

The strategy here was, therefore, to purify oligomers of cystatin B using size exclusion chromatography in order to further analyse their structure using a combination of techniques which could include EM, limited proteolysis and hydrogen-deuterium exchange in combination with either mass spectrometry or NMR. In addition, kinetic time courses for the reaction were planned in the presence of different chaperone/ATP combinations. As evident from the above discussion, oligomeric aggregates are notoriously difficult to handle which explains the lack of biophysical characterisation in the literature. In a similar way, the plan here may have been over ambitious. However, the qualitative characterization detailed in this chapter does describe the morphology of cystatin B oligomers which resemble inclusions or bodies such as the Bunina or Marinesco bodies discussed in section 1.6. The role of chaperones in the formation of such species has never been identified previously and the qualitative description of their activity presented here is of great interest to an emerging field (Jain et al, 2016; Rabouille & Alberti, 2017). The parallels between the species observed here and that isolated in cell culture by Rispoli et al make this of particular interest as such "bodies" have not previously been prepared *in vitro*.

It should also be noted that the "oligomers" or "bodies" described in this chapter could be distinct from the oligomers associated with amyloid formation. There is now a growing interest in the area of phase separated bodies or granules. Such granules are also linked to neurodegenerative disease; for example, mRNP stress granules which are formed when protein translation is limited. Whilst their link to neurodegenerative disease has been established (e.g. mutations which cause ALS can increase stress granule formation) little is known about their structure or physical properties (Jain et al. 2016, Li et al. 2013). Much research has been undertaken to observe such granules *in vivo* but they have not been prepared *in vitro* (Jain et al. 2016).

4.2 Materials and Methods

4.2.1 DnaK Purification

The DnaK plasmid was kindly provided by Dr Steven Burston from the School of Biochemistry, University of Bristol.

2 µl of TOPO pET151-D plasmid expressing the DnaK protein construct was added to *E.coli* XL-10 blue cells (see chapter 2). Single colonies were picked and used to inoculate 100 ml LB-broth with 100 µg/ml ampicillin. 4 x 25 ml cultures were incubated in a shaking incubator for approximately 16 hours at 37°C and 220 r.p.m. Overnight cultures were used to inoculate 4 x 2 L flasks, each containing 1 L LB-Broth and 100 µg/ml ampicillin and shaken at 37°C. When the cultures had reached an OD of 0.6, expression was induced with 1 mM IPTG. 3 hours after induction, the cells were pelleted at 4 ^{o}C, 4000 r.p.m. for 20 min, before re-suspending in 60 ml of 50 mM Tris-HCl pH 7.5, 100 mM KCl, 20 mM Imidazole and 10% glycerol. The cell paste was freeze thawed at -20°C prior to sonication. The cell debris were then removed by centrifugation at 20,000 r.p.m, 4°C for 30 minutes.

The cytosolic supernatant fraction was passed down a Ni-Sepharose column pre-equilibrated in 50 mM Tris, pH 7.5, 20 mM Imidazole, 10 % Glycerol and 100 mM KCl. The N-terminally His-tagged DnaK protein that bound to the column was eluted after extensive washing using an imidazole gradient of 20 mM to 300 mM (50 mM Tris, pH 7.5, 10 % Glycerol and 100 mM KCl). The peak fractions at 280 nm were pooled and dialysed against 50 mM Tris, pH 7.5, 10 % Glycerol and 150 mM KCl, 20 mM MgCl$_2$ for storage and to remove the imidazole.

A typical purification protocol yields 200-300 mg from 4 litres, which is then aliquoted and frozen in liquid nitrogen at ~150 µM for storage at -80 ^{o}C. To calculate the concentration of DnaK, an extinction coefficient at 280nm of 14,500 cm^{-1} M^{-1} was used.

DnaJ and GrpE were supplied as purified proteins by the same group.

4.2.2 Oligomer formation

Before addition of DnaK to cystatin B, both the cystatin B and DnaK samples were buffer exchanged into 50 mM Tris, 150 mM KCl and 20 mM MgCl pH 6 using a 20 ml 10 KDa MWCO Vivaspin at 4000 r.p.m. If copper was used, 50 µM $CuCl_2$ was added to the cystatin B 10 minutes before the addition of other components. The final reaction volume was always 1 ml. When Mg-ATP was used it was used at a concentration of 5 mM.

4.2.3 Analytical size exclusion chromatography

Protein samples were tested for the presence of oligomers at specific time points using size exclusion high-pressure liquid chromatography (SEC-HPLC). Either a Shodex KW803 (with a KW-G guard column) (Shodex, Japan) or an analytical Superdex 200 HR 10/30 column (GE Healthcare) were used attached to a Perkin Elmer 200 HPLC system equipped with UV-visible absorbance detector. The column was run in the same buffer used for oligomer formation and absorbance was measured at 280 nm.

4.2.4 Circular Dichroism

Circular Dichroism (CD) was performed using a Jasco-J810 spectropolarimeter. The pathlength was 0.1cm and a wavelength range of 190-300 nm was used. Spectra were acquired at room temperature with a data pitch of 1nm and a rate of 20-50 nm/min. 10 spectra were acquired for each sample and averaged. Mean residue ellipticity ([θ]), measured in deg·cm^2 $dmol^{-1}$, was calculated using the following equation:

$$[\Theta] = \frac{(\Theta * 100 * Mr)}{(c * d * N_A)}$$

Where Θ is the measured ellipticity in degrees, Mr is molecular weight in KDa, c is the protein concentration in mg/ml, d is the pathlength in cm and N_A is the number of amino acids in the protein.

4.2.5 Limited proteolysis and Mass Spectrometry

A protocol for limited proteolysis of oligomers using proteinase K (Sigma Aldrich) was obtained from Davis et al (2015). The protease:cystatin B mass ratio used was 1:50. The reaction was carried out at pH 8 and 1 mM $CaCl_2$ was added to the sample. After addition of the protease, a time 0 sample was removed immediately and then quenched using a final phenymethanesulfonylfluoride (PMSF) concentration of 5 mM and frozen at -20°C. Further time point samples were removed from the reaction solution and treated in the same way.

The samples were defrosted and centrifuged at 14,000 r.p.m. for 10 minutes before analysis by mass spectrometry (MS). The supernatant was retained and the pellet was washed with 40% acetonitrile, 1% β-mercaptoethanol. Samples were run on a Grace Vydac Everest C18 reverse-phase column using a Waters Alliance 2695 HPLC machine over a linear 5-50% acetonitrile gradient for 40 minutes and 50-95% acetonitrile gradient for 5 minutes at 2 ml/min. Micromass LCT electrospray-ionisation time-of-flight (Waters Corporation, Manchester) was used for mass determination.

4.2.6 Ultracentrifugation

A 10-30% glycerol gradient was produced using a gradient mixer and dispensed into a 12 ml centrifuge tube using a fine capillary tube. 500 µl of protein sample was then applied to the top of this tube with a pipette. An SW41 rotor (Beckman) was used in a Beckman Optima LE 80K Ultracentrifuge and samples were spun at 36K rpm at 4°C for 24 hrs. Layered samples were removed in 18 x 0.7 ml aliquots from each tube and the contents analysed by western blot.

4.2.7 SDS-PAGE

Oligomer protein samples were either run on a 10% gel (stacking gel as in 2.6.3) or a RunBlue precast 4-20% gradient gel (Expedeon, UK). The gels were stained with Instant Blue (Expedeon, UK).

4.2.8 Western Blotting

Gels were transferred to a nitrocellulose membrane using a BioRad Trans-Blot Turbo machine. The membrane was blotted with blotting buffer (5% milk, 0.1% Tween-20 in PBS) for 2 hrs. Blotting buffer was removed and the membrane was incubated in the primary antibody overnight at 4 °C. The membrane was washed 3 times with 0.1% Tween-20 in PBS for 5 minutes each time then incubated in the secondary antibody for 1 hour at room temperature. To visualise the blot, the membrane was incubated in clarity western ECL blotting substrate (BioRad, UK) and viewed using a ChemDoc MP Docking System (BioRad, UK).

Primary antibodies were goat anti-cystatin B C-16 and goat anti-cystatin B A-12 (Santa Cruz Biotechnology, Germany). Both primary antibodies were diluted 1:250 in buffer. The secondary antibody used was donkey anti-goat-HRP IgG diluted 1:4000 in buffer.

4.2.9 Expression and Purification of α-synculein

α-synuclein was expressed and purified as described as in section 2.1.2.

ε_{280nm} for α-synuclein is 5120 cm^{-1} M^{-1}.

4.3 Results

4.3.1 Cystatin B oligomer formation by DnaK does not require Mg-ATP or co-chaperones

The purification of different forms of WT and G4R cystatin B including oligomers from *E. coli* presented in Chapter 3 suggests that size exclusion chromatography would be a useful tool to separate and quantify the oligomeric species produced in the presence of cystatin B and chaperone. The first part of this study involved screening for the presence of oligomers in the presence of different ratios of chaperone to cystatin B and in the presence of Mg-ATP and / or co-chaperones.

Figure 4.1 A shows a SEC-HPLC elution profile of 50 μM cystatin B incubated 1:1 with DnaK in the presence of Mg-ATP and copper. The buffer conditions

were kept at pH 6.0 in Tris buffer so as to favour the monomeric form of cystatin B, which is suggested by Rispoli et al (2013) to be the form of cystatin B necessary for assembly. Samples were injected at the intervals shown to observe any assembly reaction as a function of time. "Time 0" corresponds to injection immediately after mix. An analytical superdex-200 column was used in this experiment meaning the total elution time is 60 minutes. Control runs (Figure 4.1 B-D) were used to assign elution times for DnaK (25 min), cystatin B monomer (35 min), dimer (32 min) and tetramer (28 min). These correspond to peaks B, D and C in figure 4.1 A and occur at the expected retention times from our calibration (Figure 4.1D).

Figure 4.1 A shows that cystatin B elutes in this mixture principally as dimer (C) with only a small peak for the monomer (D). One can see a small peak at about 17 minutes which corresponds to a very large species (A). This is very close to the void volume of the column, meaning these oligomers have a high molecular weight (greater than 600KDa). The large peak at 38 minutes is the Mg-ATP which elutes with the sample solvent.

Figure 4.1 can be used to estimate the ratio in peak height between the DnaK peak (B) and the total cystatin B dimer and monomer peaks (C+D respectively) before any oligomerisation occurs, which is expected to be 3.2 ($\varepsilon_{280\ (DnaK)}$ / $\varepsilon_{280\ (CysB)}$ = 14,500 / 4470) even though they are at equimolar concentrations (50µM), due to their differing aromatic content. However in control runs with pure DnaK or cystatin B, the ratio is 2.45 ± 0.2. It is therefore likely that some DnaK is lost either through aggregation or through adsorption to the column matrix. This ratio is independent of concentration and the presence of Mg-ATP. The time course presented in figure 4.1. shows that this ratio remains unchanged for the duration of the experiment (4 hours).

To look at oligomer production, it is useful to look at the reduction of monomer (since this is converted to the oligomers). The monomer peak (D) has been enlarged in Figure 4.2. One can see that the monomer peak starts at about 0.03 but is reduced to about 0.015 by the end of the first hour of the

experiment (a reduction of about half). There does not seem to be any further reduction in the height of the monomer peak even after 24 hours (data not shown). This result suggests a significant population of the monomeric cystatin B is lost.

Figure 4.3 is an enlarged view of the void volume peak (A). One can see that oligomers have been produced by the end of the first run (0 hrs) while they are absent from the control runs containing cystatin B or DnaK alone (Figure 4.1.B & C). Any potential increase in the height of this peak is within the noise of the experiment. It is likely that some species are not resolved by the column; perhaps with time the oligomers increase further in size to that of a species that is filtered out by the online filters. It also became clear after further experimentation that the population of oligomers is heterogeneous and so their elution on SEC may occur at different times and be difficult to detect.
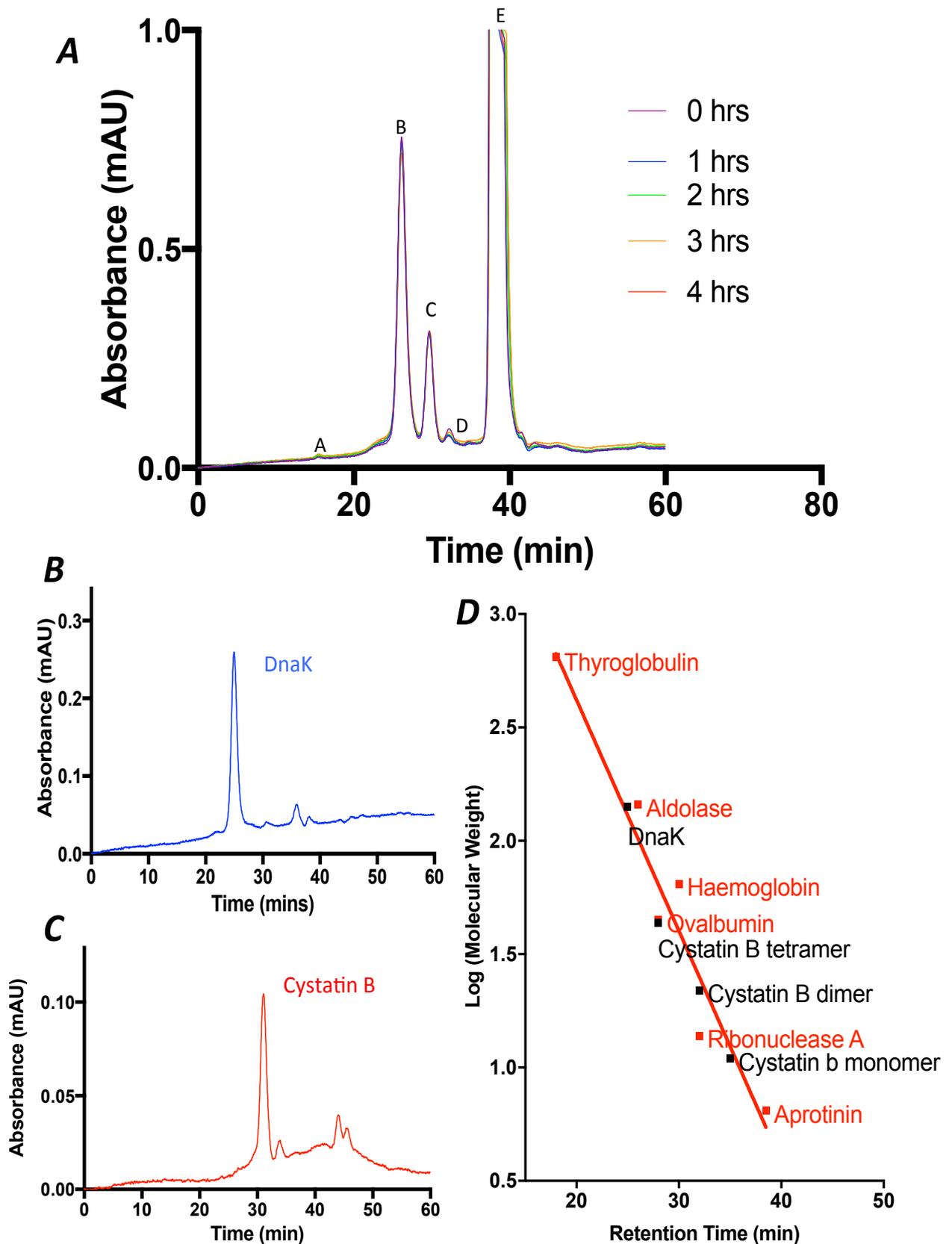
Figure 4.1: Time course of Cystatin B incubated with DnaK and Mg-ATP. *A: Time dependent elution profile of 50 μM Cystatin B WT incubated 1:1 with DnaK and 5mM Mg-ATP. 50 μM CuCl₂ was also present in the sample. Peak A is the void volume peak, B is DnaK, C is Cystatin B dimer, D is cystatin B monomer and E is ATP. B: Elution profile of 15 μM DnaK. C: Elution profile of 15 μM Cystatin B. D: Calibration curve of proteins run on the HPLC superdex-200 column for comparison with different species of cystatin B and DnaK.*
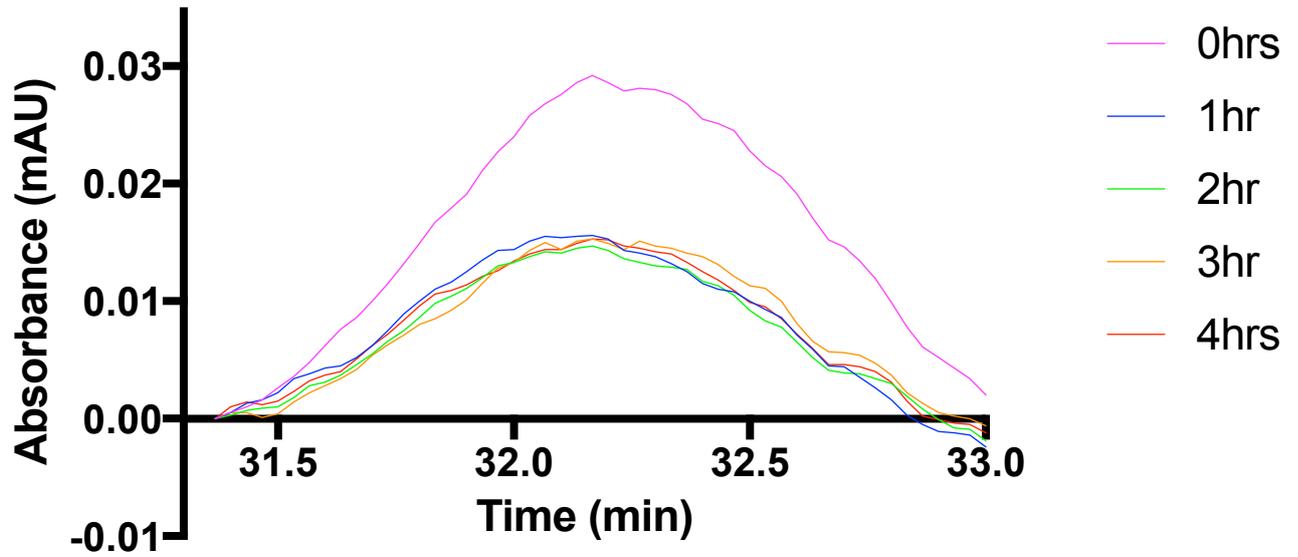
Figure 4.2: Cystatin B monomer peak *(D) from SEC-HPLC profile shown in Figure 4.1 as a function of incubation time with DnaK and Mg-ATP*
.
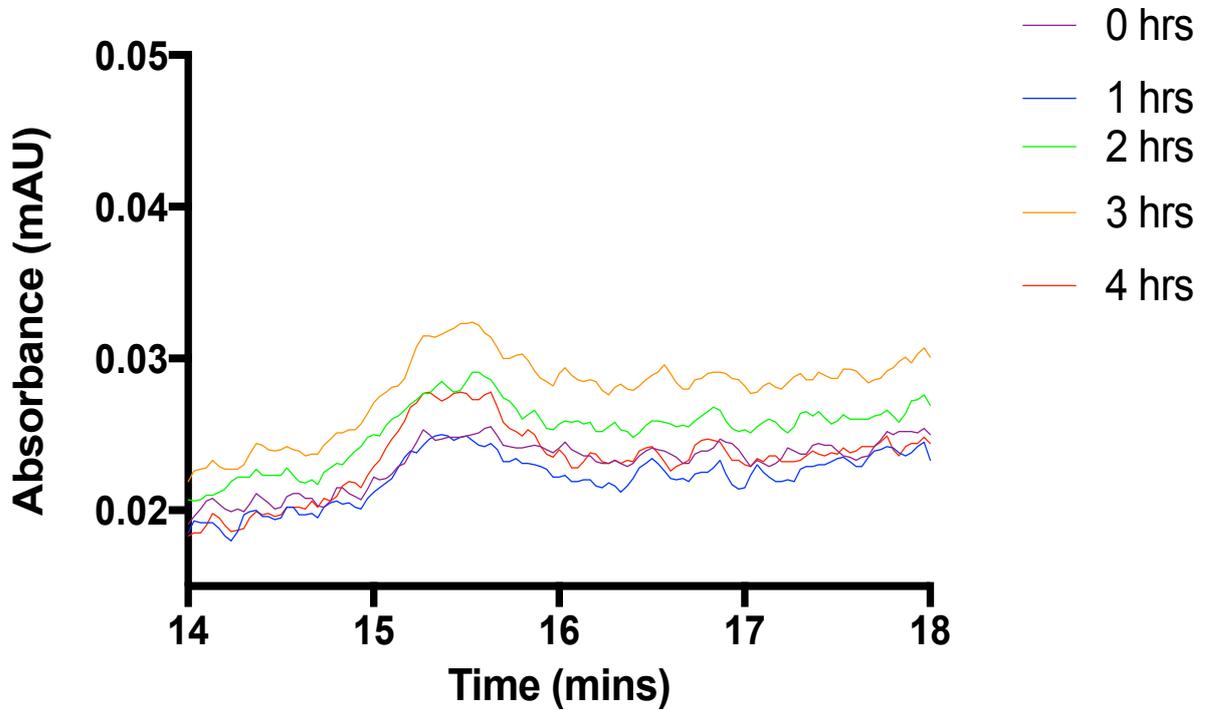
Figure 4.3: Void volume peak (A) *from SEC-HPLC profile in Figure 4.1 as a function of reaction time*

To examine the concentration dependence of the oligomerisation of cystatin B, and to remove nucleotides from the data, the experiment was repeated with 2 µM cystatin B and DnaK without Mg-ATP present. A Shodex SEC column was also used as this has a shorter elution time (20 minutes) which would allow for better resolution of the first hour of the experiment. It was also thought that the different chemistry of the column could allow for better resolution of the oligomers. Both wild-type (Figure 4.4) and the G4R mutant (Figure 4.5) were tested. In addition to the DnaK (9.8 min) peak, dimeric (11.2 min) and monomeric (11.9 min) cystatin B peaks, a clear peak can be seen at 15 minutes which cannot be seen in the cystatin B and DnaK only controls. This was therefore assumed to be oligomers. When using the Shodex column, cystatin B oligomers seem to be eluted after the non-aggregated species, even though they are at a higher molecular weight. This is consistent with previous findings of the Staniforth lab (Davis, 2013). It may also be that at these concentrations of cystatin B, 25-fold less than in the previous experiment, the oligomers formed stick to the column suggesting a more hydrophobic exterior. It is symptomatic of aggregates and misfolded proteins that elution times on size exclusion are disturbed due to interactions with the column.

In all of these 2 µM elution profiles, as well as the formation of a 15 minute peak, there is a striking increase in the apparent DnaK peak (9.8 min) height over time (Figure 4.7 A). This could indicate that the oligomer peak is overlapped with that of the DnaK under these experimental conditions or that the conformation of the DnaK structure is changing significantly. This seems less likely as there is no nucleotide (Mg-ATP) in this reaction.

The experiment was repeated with wild type cystatin B at 20 µM to see if more oligomers could be produced (Figure 4.6). Samples were run every 5 minutes to allow for even better time resolution at the start of the experiment. As with the 2µM samples, very little is observed in the void volume but instead changes can be seen at both 9.8 and 15 minutes. Compared with the 2 µM data, the 9.8 min DnaK peak is better resolved and a clear shoulder appears on the DnaK peak at 9.1min. This suggests the presence of a significantly

different molecular weight species, likely to be larger than a simple complex of DnaK and cystatin B monomer.

The 15 min peak remains fairly stable throughout the experiment (Figure 4.7 B). Therefore these oligomers are formed before the HPLC equipment can make its first reading (time 0). However, it should also be noted that it is only small fraction of the total cystatin B which is converted into this oligomeric form.

Figure 4.7 C & D compare the populations of monomeric and dimeric cystatin B in these time courses. Whilst not completely clear from the data, it seems that the dimeric species is converted more readily to oligomers because as the concentration of cystatin B is increased, the proportion of monomeric cystatin B that is converted decreases more than that of the dimer. This agrees with Melli and co-worker's hypothesis (Cipollini et al, 2008).
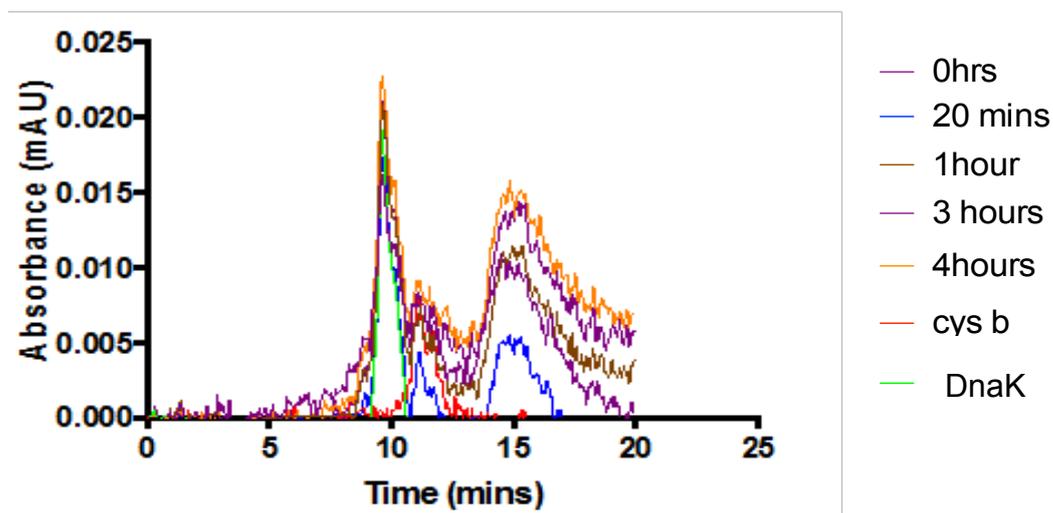

Figure 4.4: SEC-HPLC profile of 2 μM cystatin B (S3C) WT incubated 1:1 with DnaK over 4 hrs. CuCl₂ was also present in the sample
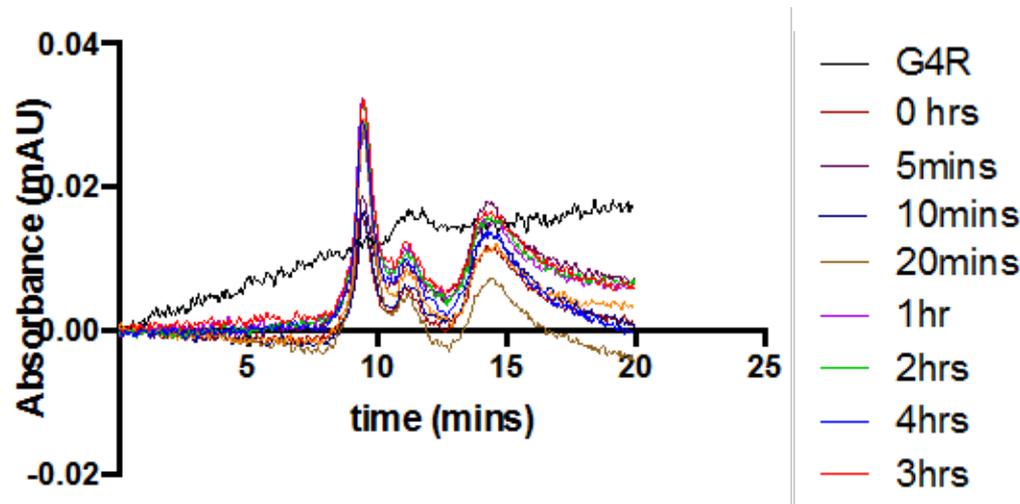
Figure 4.5: *SEC HPLC profile of 2 µM cystatin B (S3C) G4R* incubated 1:1 with DnaK over 4 hours. $CuCl_2$ was also present in the sample
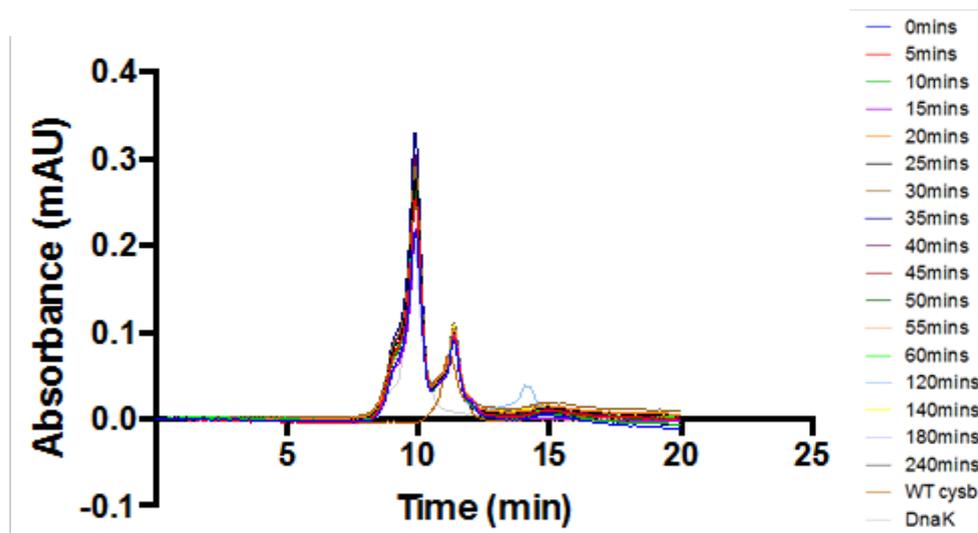

Figure 4.6: *SEC HPLC elution profile of 20 µM cystatin B (S3C WT) incubated with DnaK over 4 hrs*. Control profiles of both cystatin B and DnaK can be seen in orange and grey. $CuCl_2$ was also present in the sample
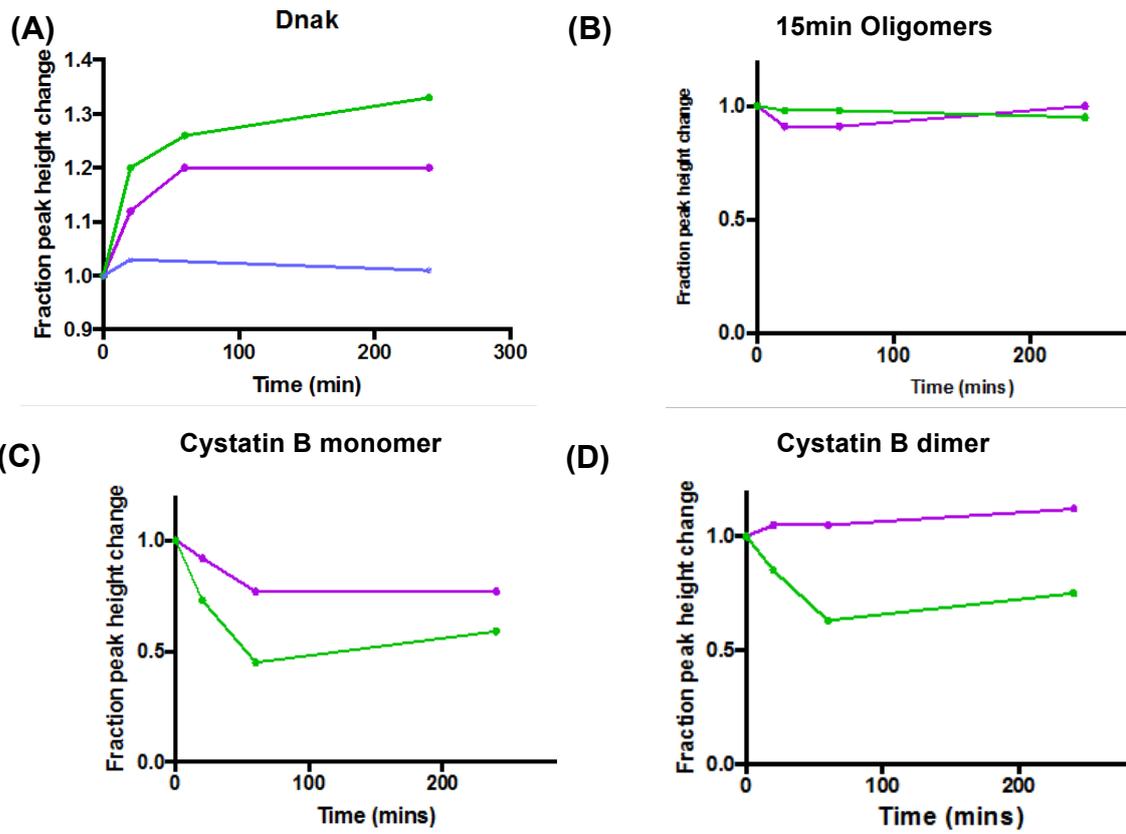
Figure 4.7: Change in protein peak heights over 4hrs. *(A) change in DnaK peak height, (B) change in the 15 minute cystatin B oligomer peak height, (C) change in 11.9 min (cystatin B (S3C) WT monomer) peak height and (D) change in cystatin B 11.2 min (dimer) peak height over time. Green is an experiment in which DnaK and cystatin B were both 2 µM, purple is for the experiment in which both proteins were 20 µM and blue is a control sample in which cystatin B was not present.*

Oligomers formed at low ratios of DnaK to cystatin B

To ascertain whether these oligomers could be made *in vivo*, where the availability of DnaK may be limiting, different ratios of DnaK to cystatin B were tested in the presence of 5 mM Mg-ATP (Figure 4.8). A constant concentration of 10µm cystatin B was used in this experiment. The following ratios of cystatin B:Dnak were used; 1:1, 1:10, 1:100, and 1:1000. Potential oligomer peaks can be seen before 20 minutes for the 1:1 sample. However, potential oligomer peaks for the 1:10, 1:100, 1:1000 experiments were not clear.
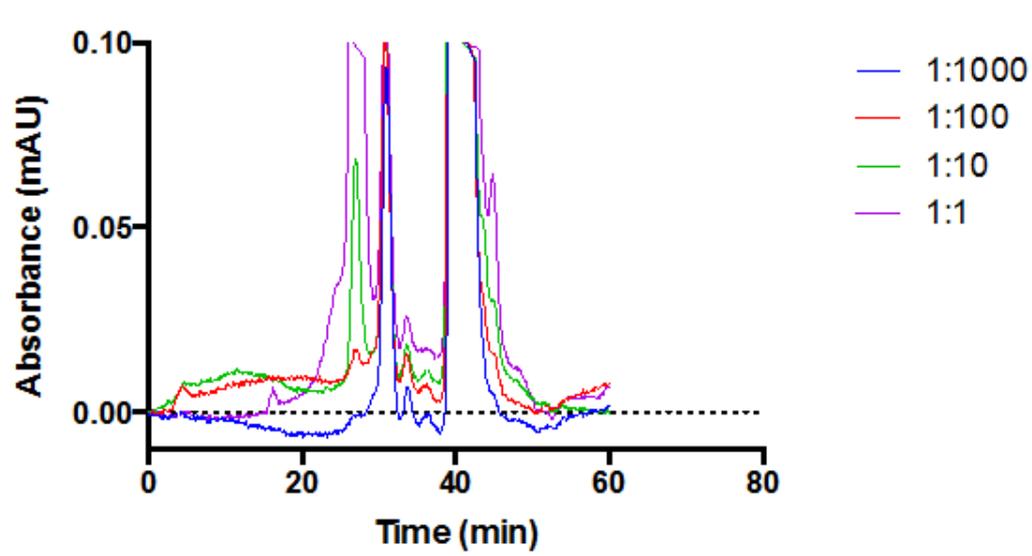
Figure 4.8: SEC-HPLC elution profile of Cystatin B (S3C) WT *incubated at different ratios with DnaK. CuCl$_2$ and Mg-ATP were also present in the sample*

In conclusion, the HPLC results in this section suggest that the monomeric form of cystatin B is crucial to the assembly of oligomers, in agreement with Melli and co-workers. The elution behaviour of the oligomers makes these species difficult to quantify because they appear to have different retention times. The increase in a peak at 9.1 min on the Shodex column, which overlaps with the elution time for DnaK seems the most likely candidate. The lower ratio of absorbance observed on SEC between DnaK and cystatin B is not resolved here, but is addressed in section 4.3.2, which describes further analysis using electron microscopy. This validates the idea that the oligomeric species observed in the presence of cystatin B do not occur in DnaK only controls. The next step, therefore, was to validate the presence of oligomers in these samples using electron microscopy. This is a well used technique in the literature for the visualization of oligomers and allows for comparison of the oligomers studied in this project with others found in the literature.

## 4.3.2 Morphology and Validation of Cystatin B Oligomers by TEM

It should be noted here that oligomers of cystatin B have never been seen in any fibrillar preparations of the protein by our group and is, therefore, not naturally pathological. On the other hand, cystatin C preparations are always full of oligomeric species when examined by EM. EM is therefore a very powerful technique for validating the presence of oligomeric species as well as characterizing them.

We examined the morphology of the cystatin B oligomers formed in the presence of DnaK without Mg-ATP (Figure 4.9), with the co-chaperones DnaJ, GrpE and Mg-ATP (Figure 4.10) and with DnaK and just Mg-ATP (Figure 4.11). Oligomers varied in size and morphology but were generally observed to be circular species which could be described as spherical rather than annular in appearance. While most of the observed species were droplet-like in the absence of Mg-ATP (Figure 4.9), in the presence of Mg-ATP, the oligomers looked more consistently granular and similar in size (Figure 4.11). In the presence of co-chaperones or in the absence of nucleotide, the oligomers took on a "beads on a string" appearance, sometimes appearing like bracelets. The size of these beads varied more on the grids prepared with co-chaperones. Very large spherical structures, a little like imploded vesicles, can be seen (Figure 4.10) None of these structures could be seen on the control grids with only the chaperones (Figure 4.12) where only the odd amorphous aggregate is observed.

Remarkably, all these structures resembled oligomeric structures co-purified along with G4R C3S cystatin B from *E. coli* over-expressing this protein (Davis, 2013). Control grids of the cystatin B preparation in the absence of chaperones show no oligomeric structures (data not shown): indeed, our lab has been trying to isolate such structures for many years with very little success!

Prior work by Davis (2013) and work presented in 4.3.7 shows that such oligomers are resistant to being broken down by a number of solvents and

proteases. They are also resistant to lipase degradation indicating that they are not lipid and are, therefore, protein inclusions. Whilst Davis's oligomers were purified from *E. Coli*, the oligomers presented here were produced using purified protein, meaning the only other protein these oligomeric species could contain is DnaK. However, whilst it cannot be ruled out that these are oligomers of DnaK, given the chaperoning nature of DnaK and the unknown chaperoning activity of cystatin B it would seem unlikely that cystatin B is creating aggregates of DnaK. However, the presence of DnaK in the aggregates is plausible. This could be probed directly using an antibody to the DnaK His-tag followed by gold labeling under the TEM. This could also add detail to inferences made about the difference in morphology observed when Mg-ATP is present in the sample. Indeed Mg-ATP lowers the affinity of the chaperone for its substrate (1.7). The data presented here indicates that the presence of Mg-ATP yields a more regular and ordered oligomeric species (Figures 4.10- 4.13).
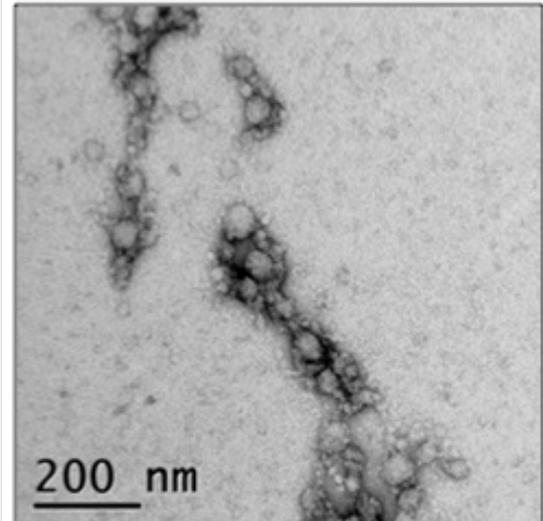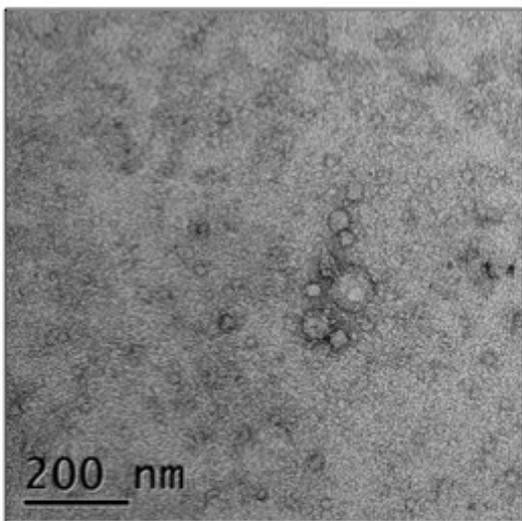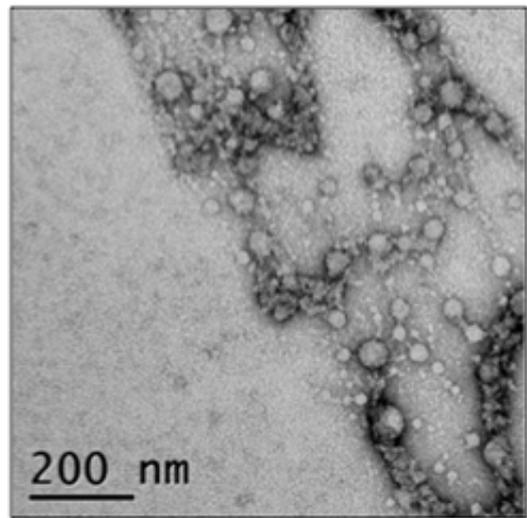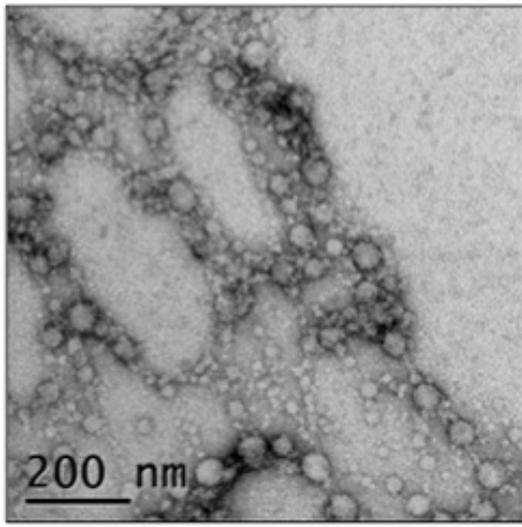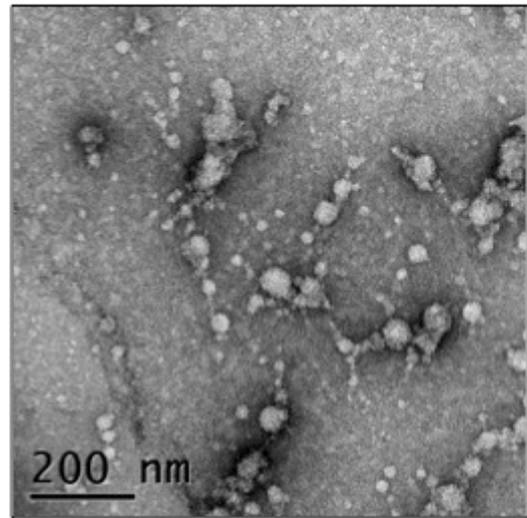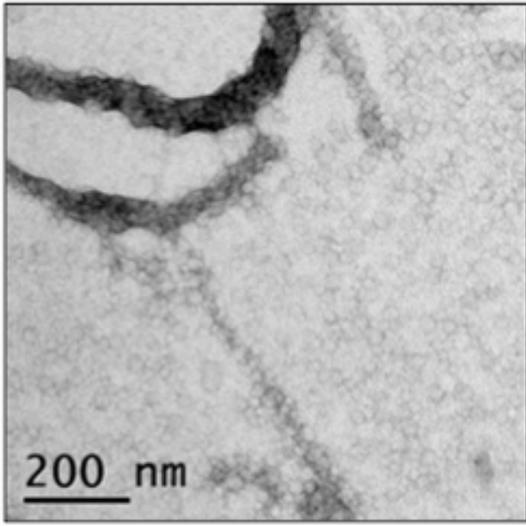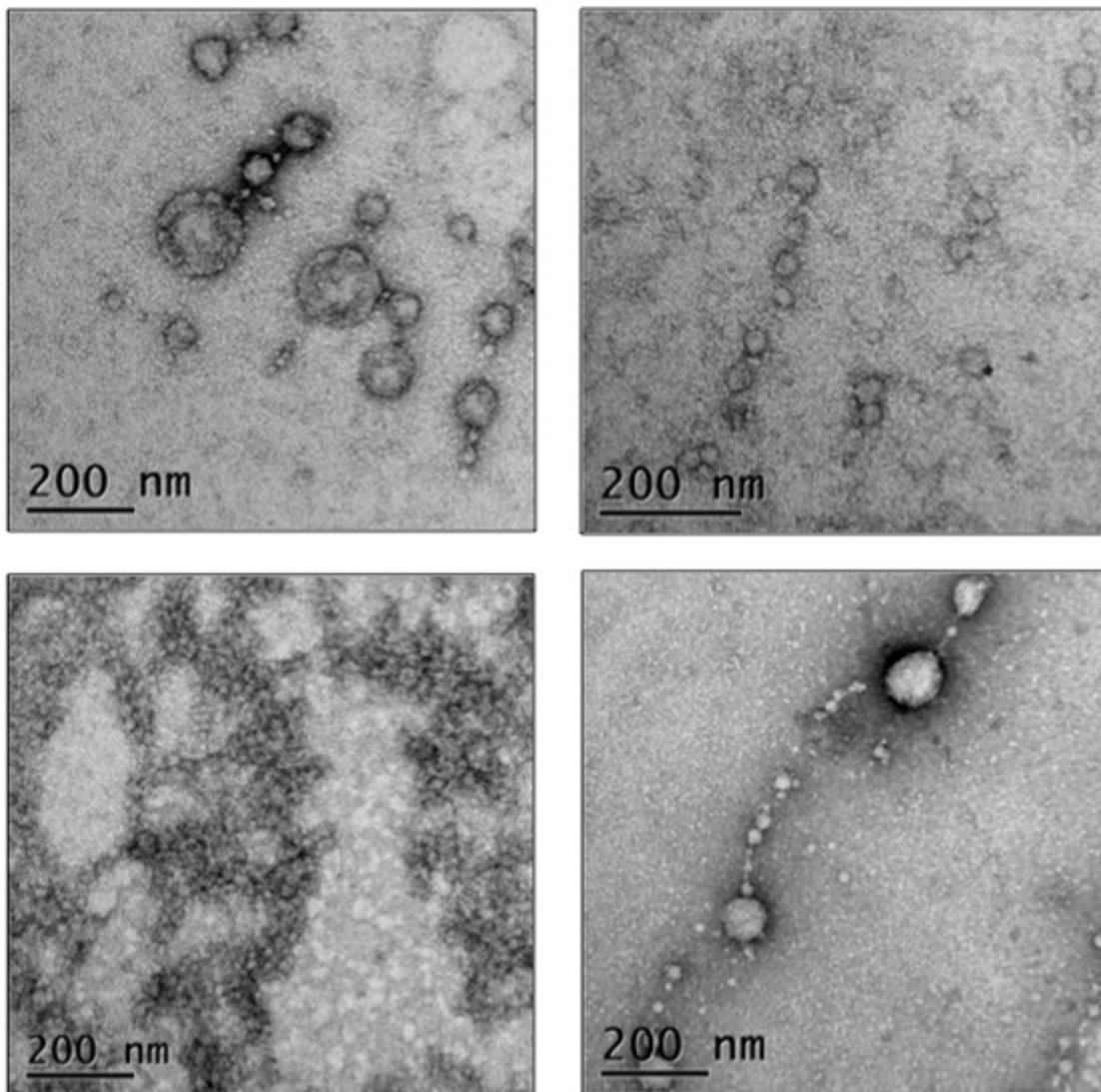
Figure 4.9: Electron micrographs of cystatin B (S3C) WT Oligomers formed with DnaK but without ATP or co-chaperones. The cystatin B and DnaK concentration was 10µm. $CuCl_2$ was also present in the sample. Micrographs are at 21000x magnification.
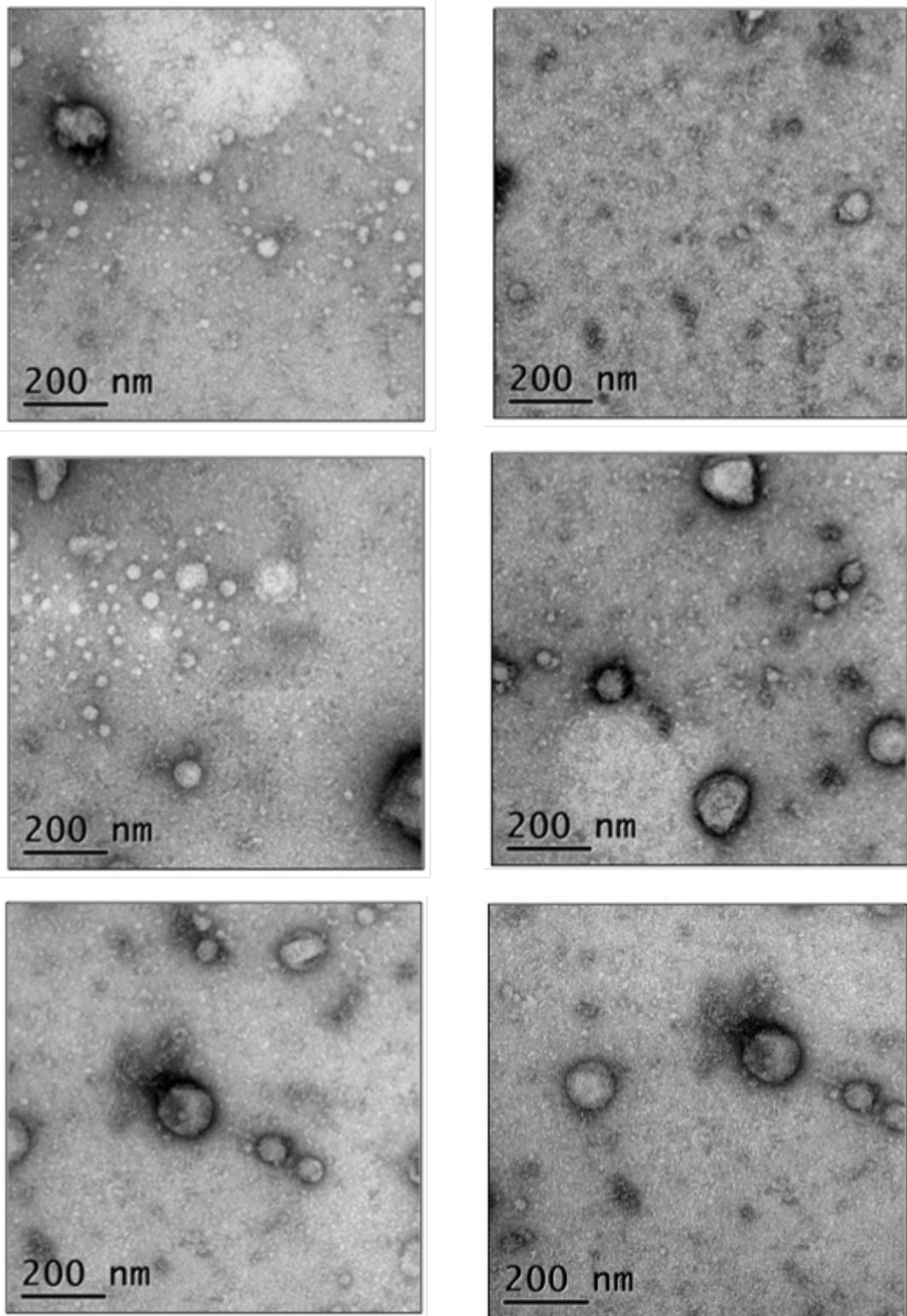
Figure 4.10: Electron micrographs of cystatin B (S3C) WT oligomers formed in the presence of ATP and co-chaperones. *The cystatin B and DnaK concentration was 10µM. CuCl$_2$ was also present in the sample Micrographs are at 21000x magnification.*
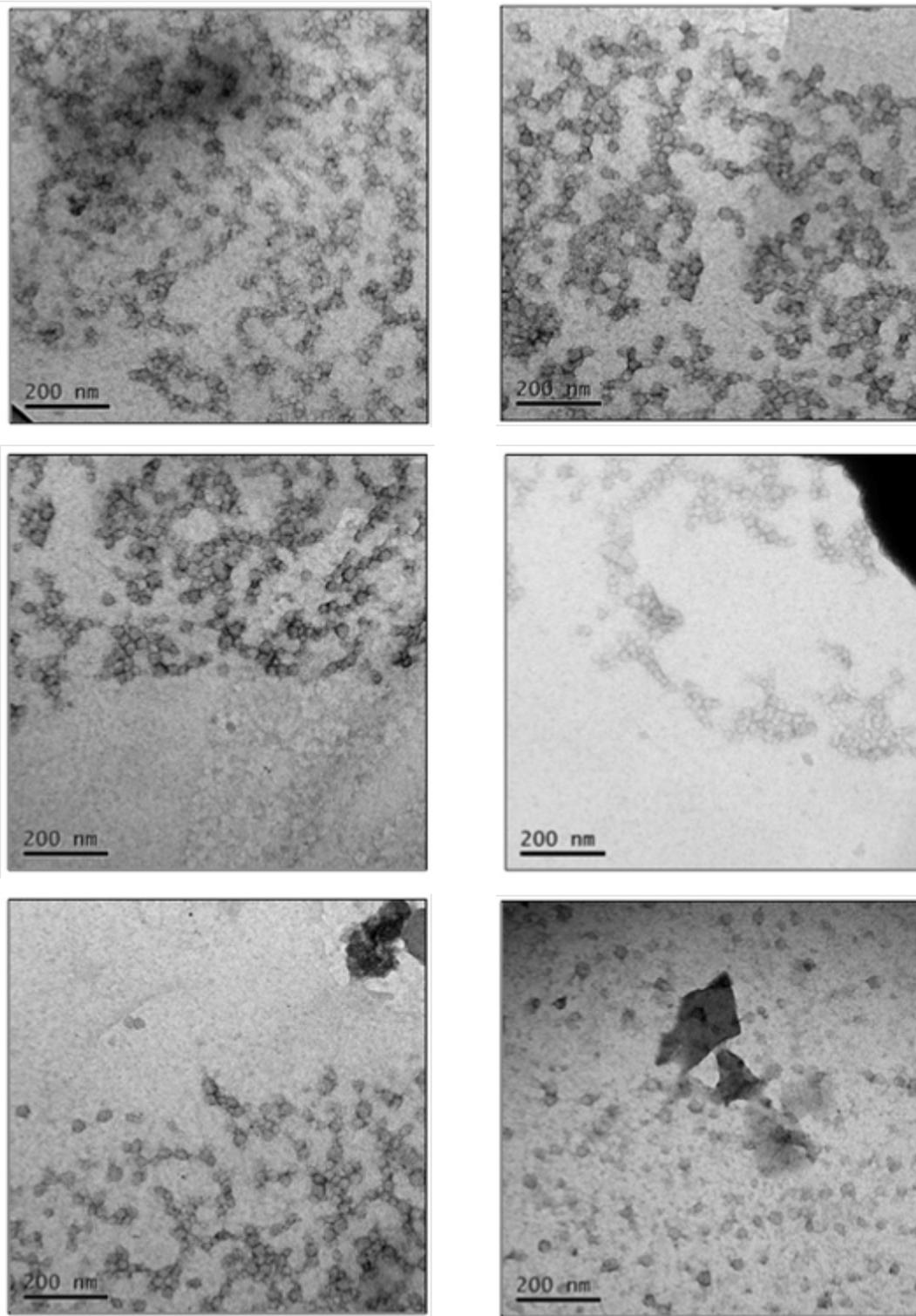
Figure 4.11: Electron micrographs of cystatin B (S3C) WT oligomers formed in the presence of ATP. *The cystatin B and DnaK concentration was 10µm. CuCl$_2$ was also present in the sample. Micrographs were taken at 21000x magnification.*
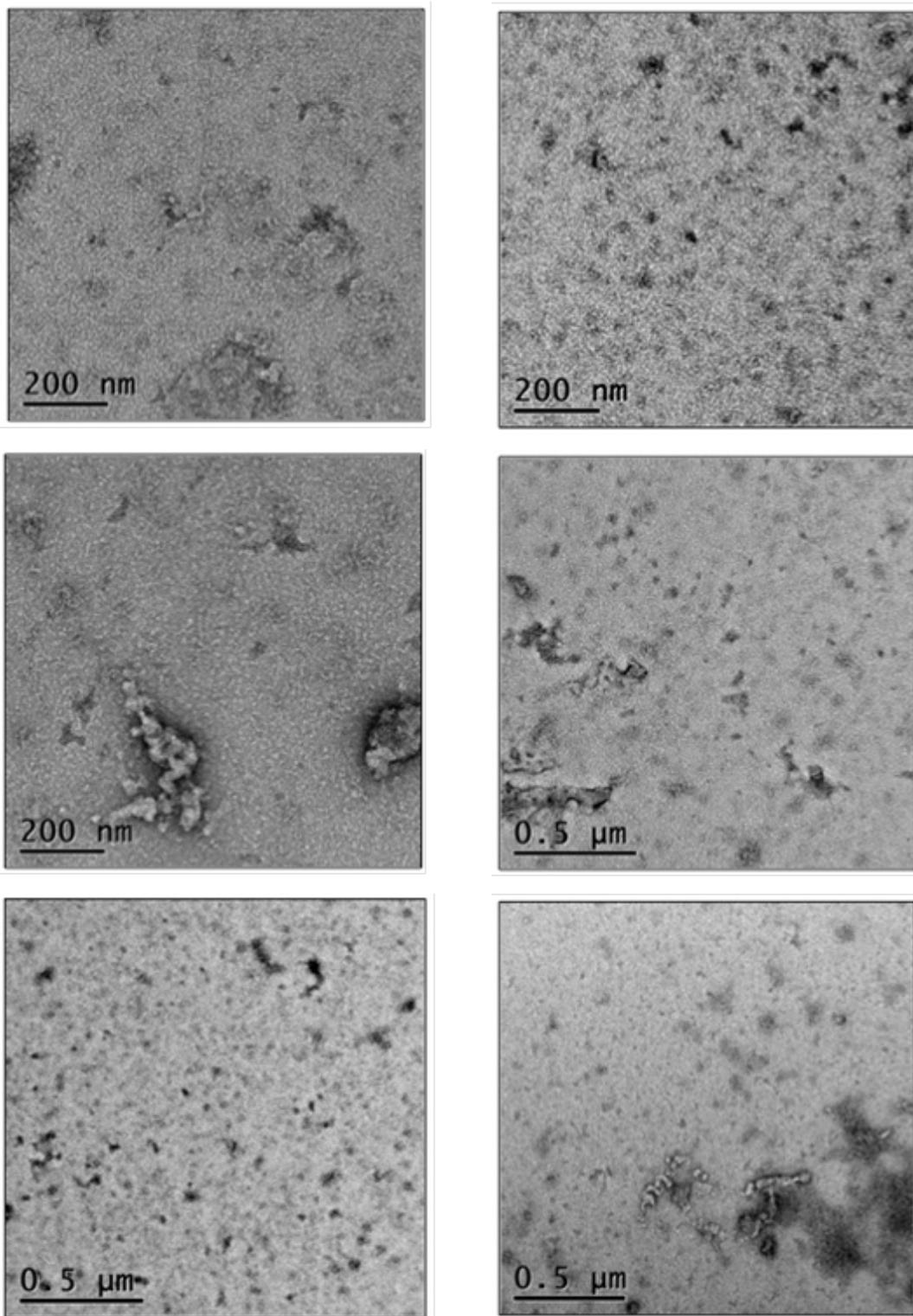
**Figure 4.12: Electron micrographs of DnaK without Cystatin B.** *The DnaK concentration was 10µm. $CuCl_2$ was also present in the sample. Micrographs were taken at 21000x magnification.*

An analysis of the size distribution of these species is shown in figure 4.13. While the range of particle sizes varies hugely in the absence of nucleotide or in the presence of co-chaperones (where potentially the Mg-ATP is hydrolysed faster), the species observed in the presence of Mg-ATP is more regular and is 33.7 ± 5.1 nm. In the absence of the nucleotide, rather than discrete species, a continuum of sizes is observed where it is difficult to pick out particular species. For this reason, and because the species observed are not seen in isolation but instead are clumped together with each other, further analysis by image averaging was not attempted.
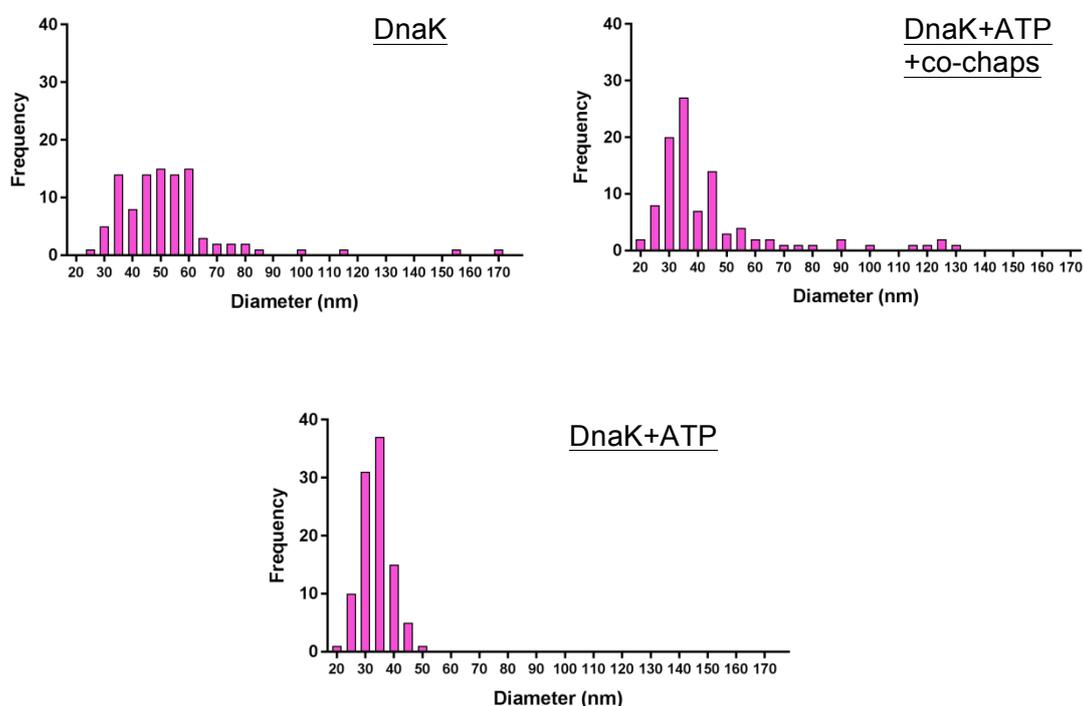
Conditions	Average Width (nm)	Maximum Width (nm)	Minimum Width (nm)
DnaK	53.02 ± 21.5	171.3	25
DnaK + ATP + co-chaperones	44.6 ± 23.3	131.1	20.17
DnaK + ATP	33.7 ± 5.1	48.4	21.7

Figure 4.13: Size distribution analysis of Cystatin B oligomers prepared under the conditions in Figures 4.9-4.11. *Oligomers were measured using Digital Micrograph 3 (Gatan). 100 oligomers were measured under each condition. The average width is shown with the standard deviation.*

Western blotting

The initial work (Cipollini et al., 2007) on the oligomerisation of cystatin B in cell lines used western blots of SDS-PAGE gels as a method for measuring the formation of oligomers. Once they had verified that the oligomers were only produced as a result of the addition of specific cellular components and were not an artifact of their experiment, the authors could use the pattern of bands observed to compare different cellular conditions.

In this work, western blotting was used to validate that oligomers produced were similar to those reported by the Melli group. Figure 4.14A shows western blots of gels run with various oligomer experiment samples using the C16 antibody to the C-terminus (top) or the A12 antibody to the N-terminus (bottom) of cystatin B. All oligomer samples were produced without Mg-ATP. Figure 4.14B shows a positive control using the C16 and A12 antibody to soluble cystatin B. The SDS-PAGE gels used in these western blots were 10% gels. This meant that the monomeric cystatin B band at around 11 KDa cannot be seen as the gel was run until the dye front had run off the gel in order to visualise the oligomer bands at the top of the gel. While the antibody to the C-terminus (C-16) was able to detect oligomers in the preparations done at higher concentrations (50µM and 20µM proteins), the antibody to the N-terminus proved very poor suggesting that the N-terminus may be hidden from the antibody even on the blot. It is clear that the oligomers maintain some structure or they would not be running as high molecular weight assemblies on this gel. The position of the DnaK chaperone is visible on the top gel as a white band with no background staining. No band(s) can be seen for 2 µM WT or G4R cystatin B oligomers in lanes 5 and 6 respectively; suggesting the concentration of oligomers in these protein preparations is too low for detection by this method.

If it is true that the N-terminus is hidden from accessing the antibody in the larger aggregates, it suggests that this part of the protein is somehow buried. Furthermore, if the N-terminus behaves as in the cystatin amyloid structure and remains unstructured, it could be that these oligomers are forming micelle-like structures with the unfolded N-terminus on the inside and the

potentially more ordered C-terminus on the outside. Such N-terminal driven formation of "aggregate compartments" has recently been shown by Franzmann et al. (2018). Their research indicates that the intrinsically disordered N-terminal prion like domain of Sup-35 (a yeast translation terminating factor) provides the interactions needed for phase separation and the formation of stress-induced membrane-less compartments, which they term "bimolecular condensates". Such formation of "compartments" or "bodies" by phase separation is discussed further in the conclusion (4.3.9) to this chapter.
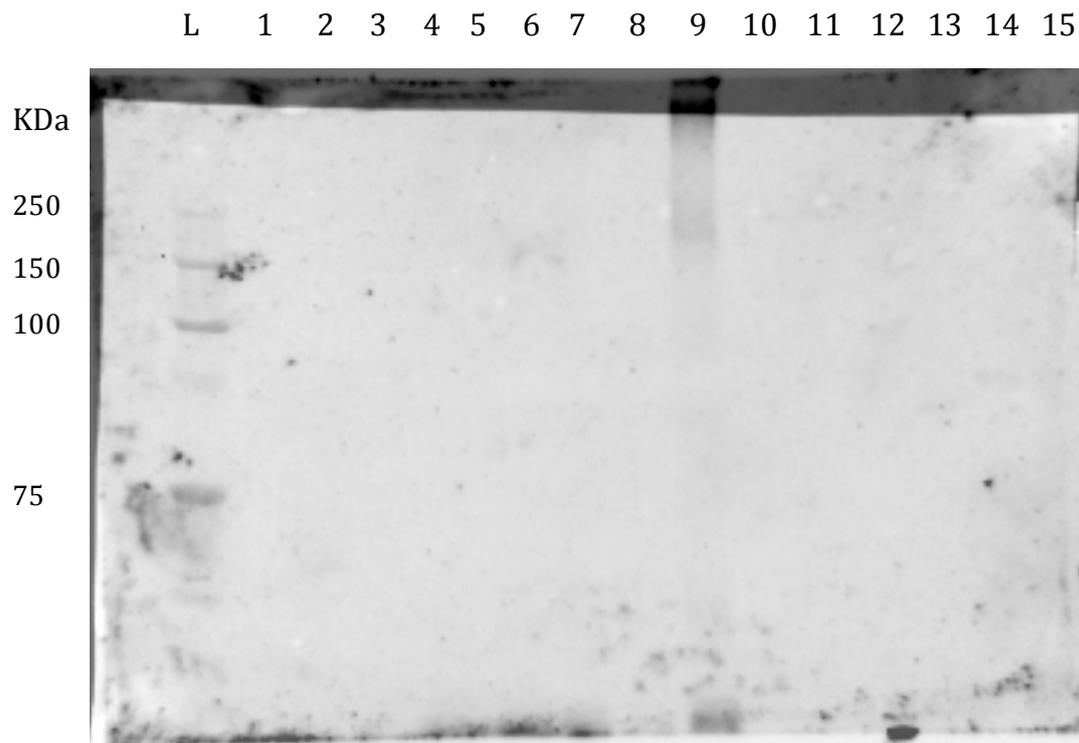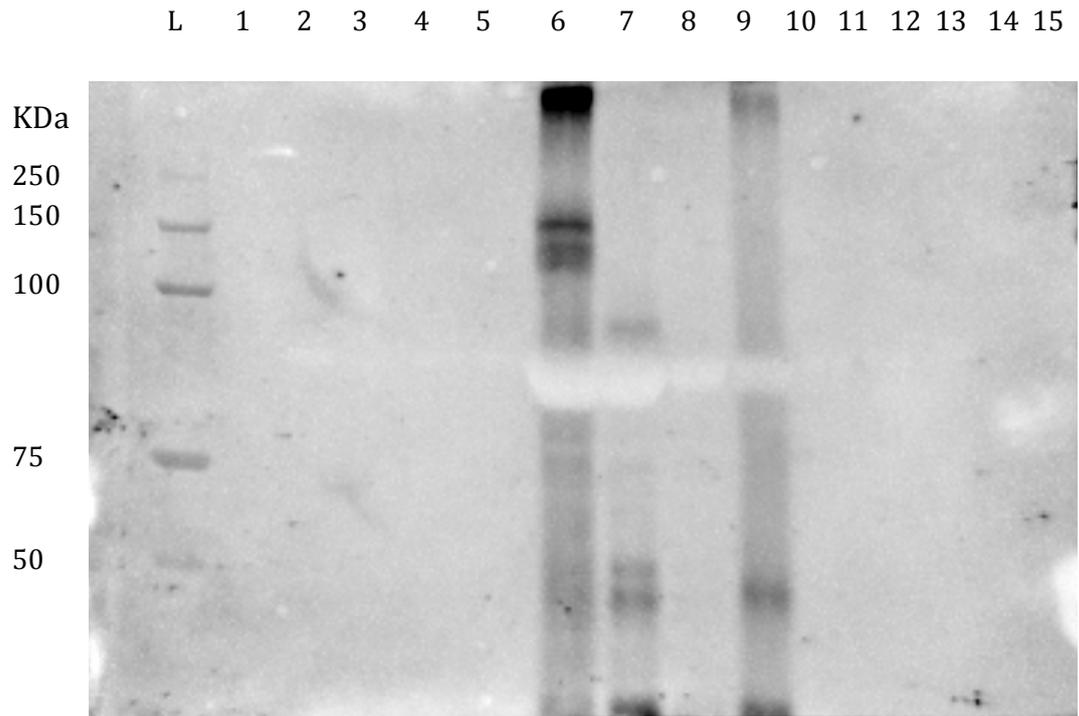
Figure 4.14A: Western Blots of cystatin B oligomer samples run on 10% SDS PAGE gels. Western blots incubated with C16 (top) and A12 (bottom) antibody. Lanes: 1=Cystatin B (S3C) WT, 2=Cystatin B (S3C) G4R, 3=DnaK, 4= 2µM WT oligomers 5= 2µM G4R oligomers, 6=50 µM WT oligomers, 7=50 µM G4R oligomers, 8=20 µM WT oligomers, 9=20 µM G4R oligomers, 10=10 µM WT oligomers, 11=10 µM G4R oligomers, 12=1:10 WT oligomers, 13: 1:100 WT oligomers, 14: 1:1000 WT oligomers.
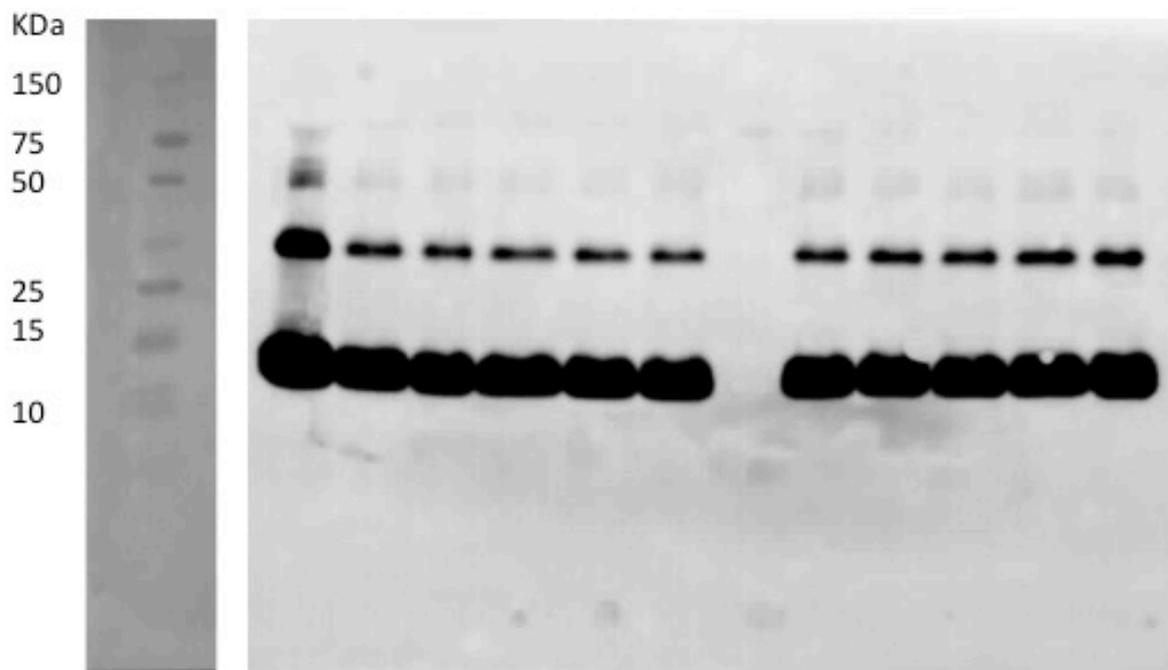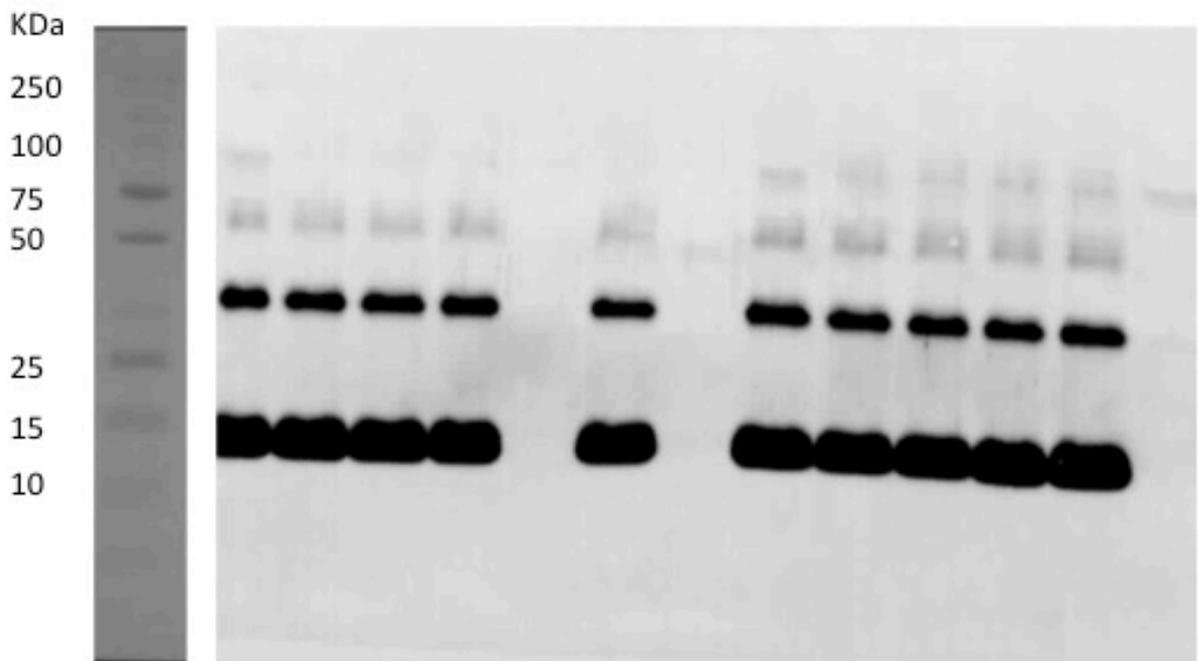
***Figure 4.14B: Control western blots of cystatin B WT samples run on 10% SDS PAGE gels.*** *Western blots were incubated with C16 (top) and A12 (bottom) antibody. 50 µM cystatin B was loaded into each lane. .*

4.3.2 The importance of copper in the formation of cystatin B oligomers

Ultracentrifugation and western blotting

Oligomer samples containing either copper or EDTA were produced as in table 4.1. These samples were then purified by gradient ultracentrifugation to separate the cystatin B oligomer species from the rest of the soluble protein species, and indeed the DnaK. After centrifugation, the total gradient was carefully aliquoted, fraction 1 coming from the top of the centrifuge tube and fraction 17 or 18 coming from the bottom of the tube. Larger protein species with larger molecular weights (i.e. oligomers) should be in the fractions near the bottom of the centrifuge tube. These fractions were analysed by SDS-PAGE using a gradient gel (RunBlue precast 4-20%) and then western blotted using the C-16 antibody to cystatin B. The results of this can be seen in Figures 4.15 and 4.16.

Sample	Conditions
1	10µM Cystatin B, Cu^{2+}, 10 µM DnaK, ATP
2	10µM Cystatin B, Cu^{2+}, 10 µM DnaK,
3	10 µM Cystatin B + 10 µM DnaK + EDTA + ATP
4	10 µM Cystatin B+10 µM DnaK + EDTA

Table 4.1: Sample conditions for ultracentrifugation

Sample 1 (Figure 4.15A), which contains copper and ATP, does not show much protein in fractions 1-9. These are fractions from the top of the centrifuge tube so should contain protein which has not been converted to a higher molecular weight species. There are some small bands in these fractions at around 11 KDa and 22 KDa showing monomer and dimer species of cystatin B. The lack of protein in these fractions could indicate that protein in this sample has been converted to oligomer. However, sample 1 does not appear to have any bands on the western blot for fractions near the bottom of the ultracentrifuge tube (10-17). This could be because the oligomers were too big to make their way into the gel and or are spread out of a wide range of molecular weights (see EM data presented in figure 4.13). It could also be

because the concentration of oligomers is too low, as 500 µl of each 10 µM sample is dissolved in a 12ml glycerol gradient for ultracentrifugation.

Sample 2 (Figure 4.15B) which contained copper but no ATP has a few bands corresponding to monomer/dimer cystatin B from fractions at the top of the ultracentrifuge tube (1-5). There are no detectable bands on the western for fractions 6-8. However, there are large bands in the lanes corresponding to fractions 9-10 and 15-18. This could indicate that some oligomers of cystatin B had formed but were broken down in the denaturing conditions of the gel and loading buffer. Some smudged, unresolved oligomers can be seen higher on the gel. This poor resolution is due to low concentrations and the range of molecular weights.

Samples 3 and 4 (Figure 4.16) which contain EDTA and no copper have much larger bands in the fractions from the top of the ultracentrifuge tube. There are no bands seen in fractions taken from the bottom of the ultracentrifuge tube (fractions 14-17). This indicates that much of the cystatin B remained as monomer and dimer and did not form oligomeric species. This confirms the importance of copper in the formation of cystatin B oligomers.
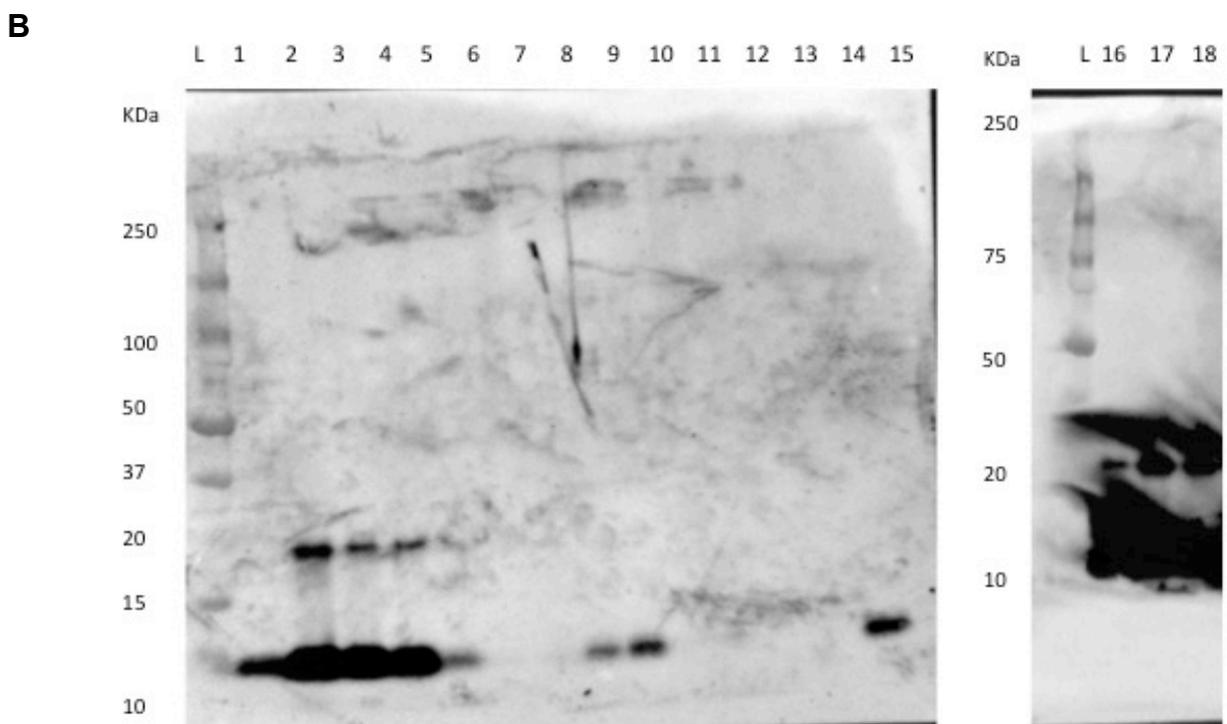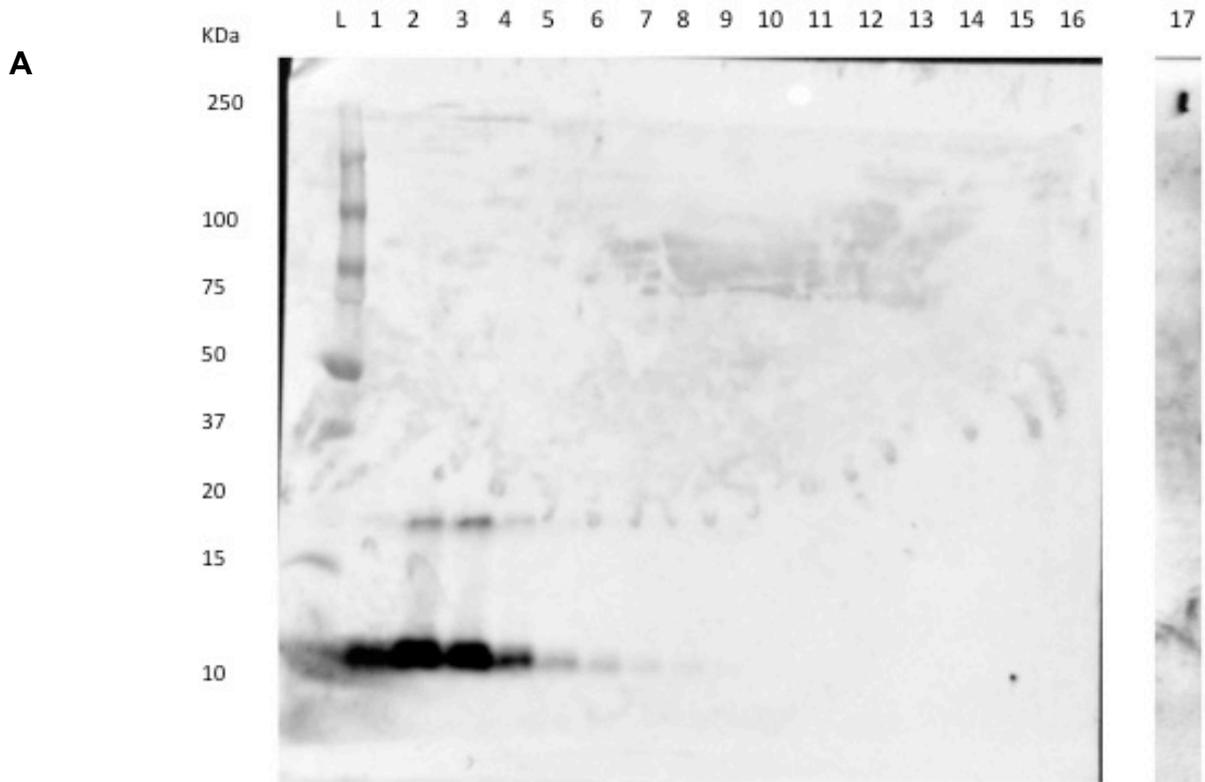
Figure 4.15: Western Blots of ultracentrifuge oligomer samples. *(A) Sample 1 fractions (B) Sample 2 fractions.*

A

B
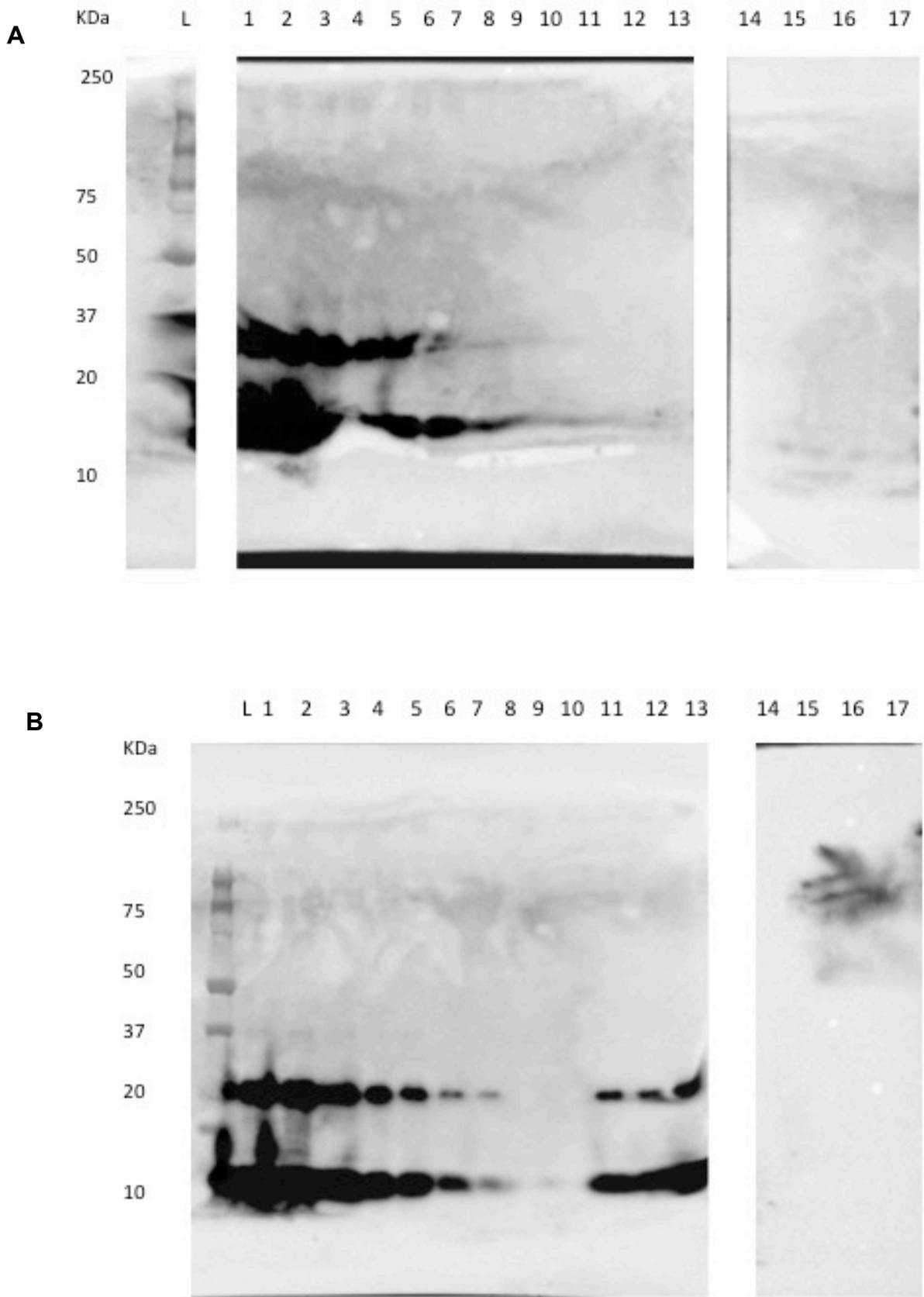
Figure 4.16: Western Blots of ultracentrifuge oligomer samples. *(A) Sample 3 fractions. (B) Sample 4 fractions*

TEM of ultracentrifuged samples

The purified oligomers were also analysed by TEM. However, images in Figure 4.17 do not show any visible oligomers. This could be because, under the conditions of this experiment, the oligomers are at such a low concentration after dilution in the 12 ml of gradient buffer needed for ultracentrifugation (see 4.2.6).
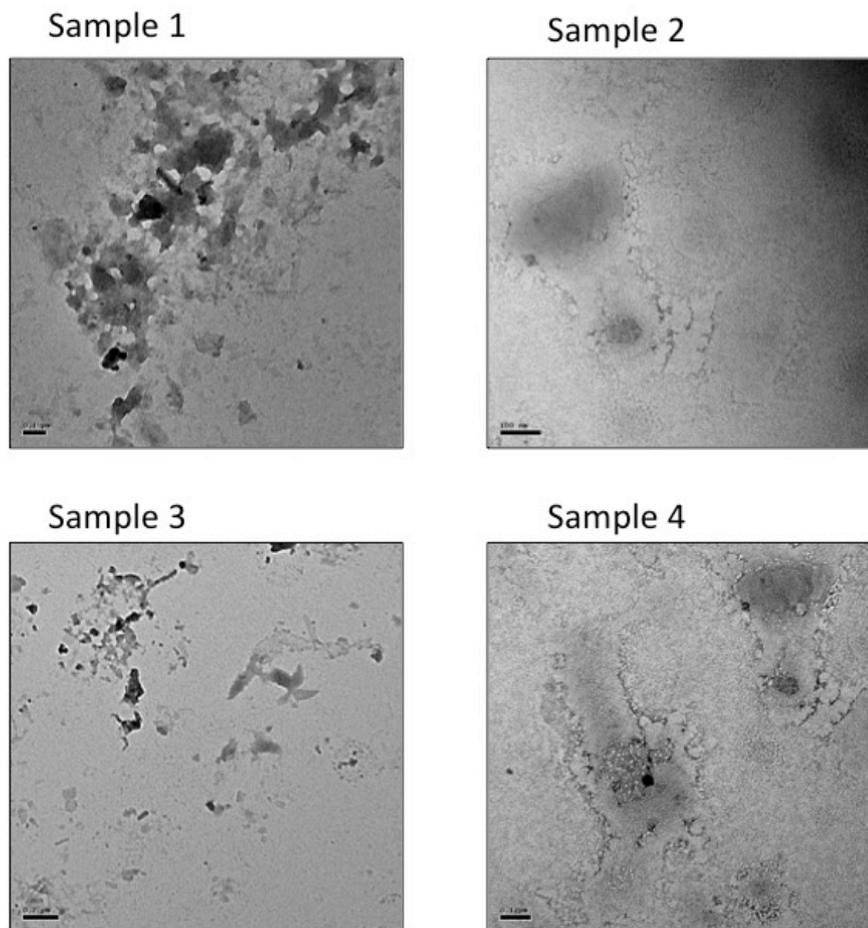
Figure 4.17: Micrographs of ultracentrifuged samples 1-4. *Samples for EM were taken from fraction 17 of the ultracentrifuged samples.*

4.3.3 Separation of oligomers from DnaK

From the EM and HPLC experiments, DnaK appears to form some sort of transitory complex with the oligomers formed. In order to view the oligomers by TEM without DnaK present and for further analysis of the oligomers by mass spectrometry, a vivaspin (Sartorius, UK) with a molecular weight cutoff of 1 million Daltons was used to filter the chaperones from the sample. The flow-through and retentate were kept and analysed by EM. The flow-through was analysed by TEM and this showed that no oligomers were present. However, the retentate after successive washes with buffer only yielded amorphous aggregates which can be seen in the TEM images in Figure 4.18.There are two possible reasons for this. Firstly, it could imply that DnaK is somehow involved in the maintenance of the oligomer structures viewed. Its removal from the complex by purification results in a loss of oligomeric structure and the formation of large amorphous aggregates. Secondly, the vivaspins could be causing the formation of the amorphous aggregates due to the "sticky" membrane surface – something which has been reported in the Staniforth lab previously when working with oligomeric species. This particular separation technique was unsuccessful since the flow-through contained no protein according to the absorbance at 280nm.
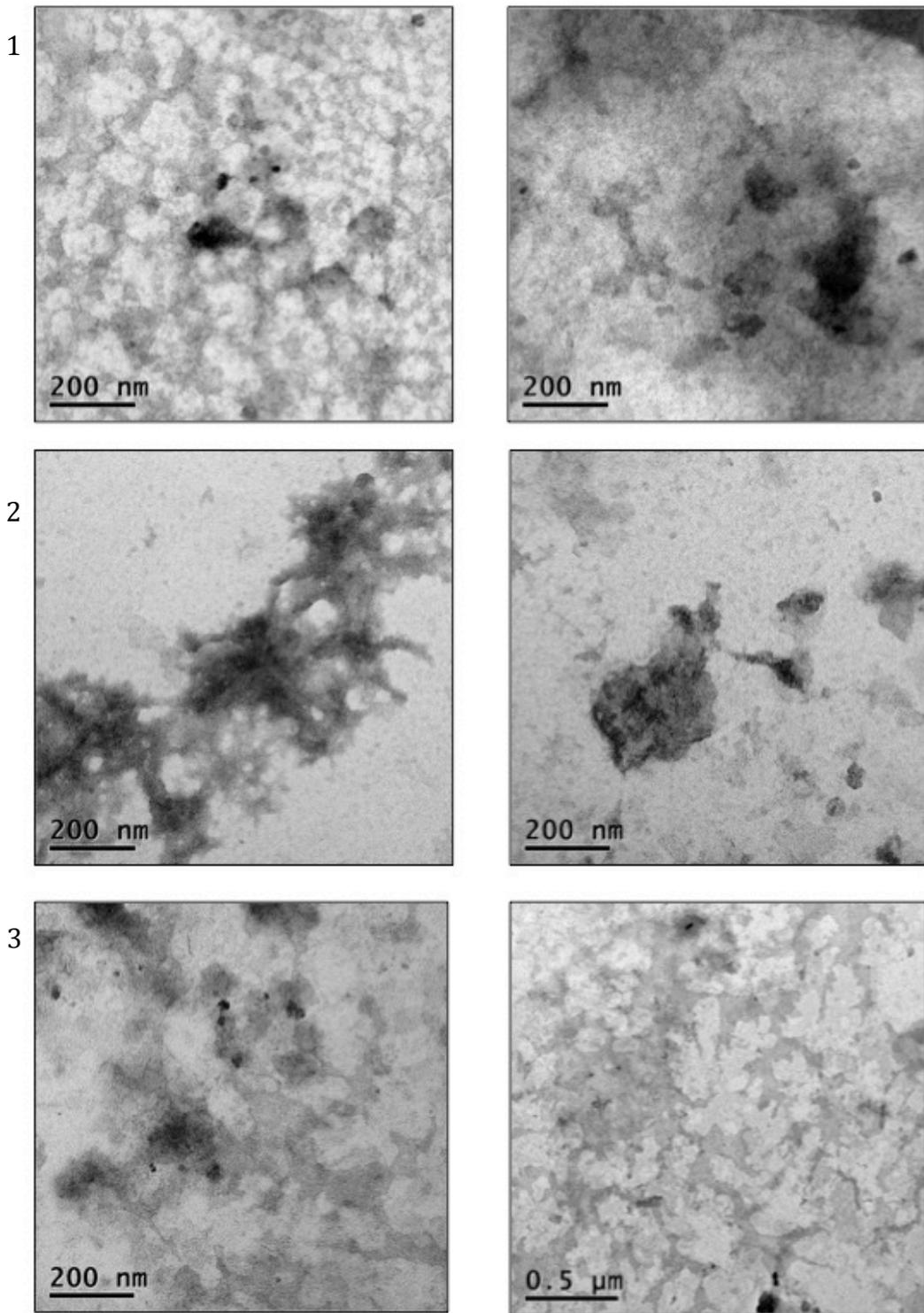
Figure 4.18: Samples of oligomer from vivaspin filtering devices (Sartorius, UK). Washes 1, 2 and 3 are labeled.

4.3.4 Is oligomer formation by DnaK specific to Cystatin B?

To test whether DnaK was able to chaperone oligomer formation from other proteins, another human protein, α-synuclein, was used. As mentioned in chapter 1 of this thesis, α-synuclein is also an amyloidogenic protein and is able to form oligomers *in vivo* (section 1.4.3)*. The same conditions were used as for the Cystatin B experiments. Figure 4.19 shows the analysis of different α-synuclein species during the time course of the experiment. Four peaks were identified on the HLPC traces as originating solely from α-synuclein (A-D). To observe possible aggregation over time, changes in these peak heights were measured over 4 hours.
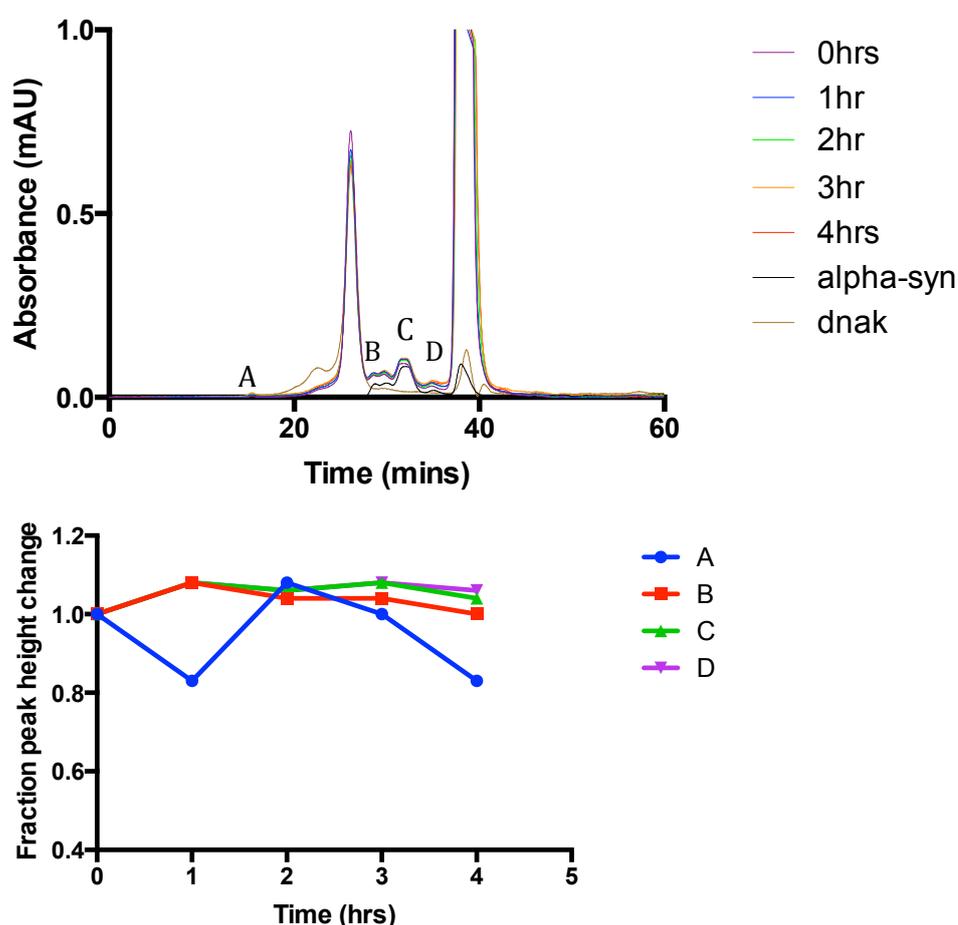
Figure 4.19: SEC-HPLC of 50µM α-synuclein incubated with Mg-ATP and DnaK. *The peaks corresponding solely to α-synuclein species are labelled in the elution profile as A-D. Control elution profiles for α-synuclein (black) and DnaK (brown) alone are also shown. The change in peak height is plotted below for each of these peaks. The error on species "A" is highest as the signal is lowest. This error is about 10% for peak A as estimated from the signal to noise. The large peak at 25 minutes is from DnaK and the large peak at 38 minutes is from Mg-ATP.*

No changes in the population of soluble α-synuclein are detectable here and together with the TEM data in figure 4.20, where only the odd patch of stain could be seen, it seems that the observed cystatin B oligomeric species are indeed likely to be specific to this protein.
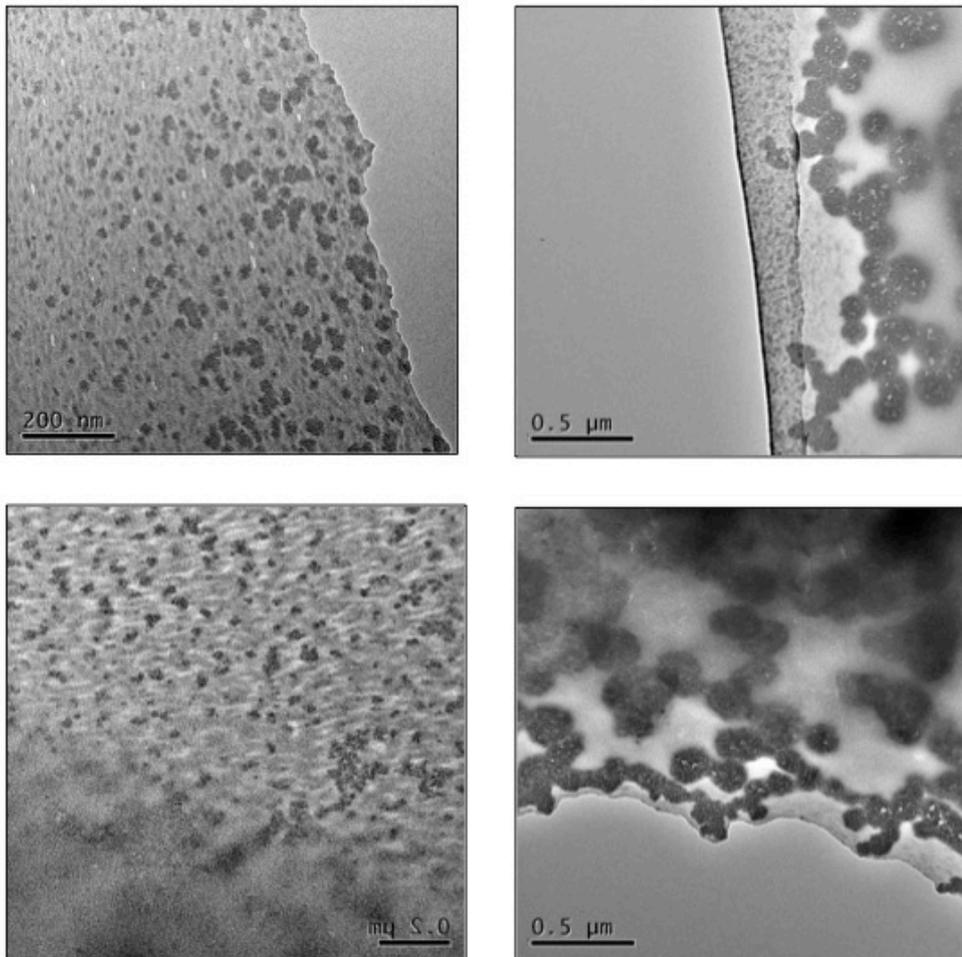
Figure 4.20: TEM of 50µM α-synuclein incubated 1:1 with DnaK in the presence of Mg-ATP. Due to the presence of large patches of stain it was difficult to establish whether the above features represent true proteinaceous species rather than artefactual stain. The species most likely to be protein are shown here.

4.3.5 Cystatin B oligomers can be purified from *E. coli*

When the WTS3C or G4RS3C cystatin B constructs were expressed in BL21 DE3 *E. coli* cells grown in minimal media (section 2.5.2), purification of these proteins by size exclusion chromatography revealed a peak corresponding to oligomeric forms of the proteins. Figure 4.21 (A) shows a slight peak and shoulder (labeled oligomer) which includes fraction 18-23. This corresponds to high molecular weight species larger than the tetramer. This was of great interest since oligomers of WT cystatin B have never been purified straight from an *E. coli* growth by the Staniforth group.

The same proteins purified from LB broth by size exclusion chromatography can be seen in figure 3.1. In the chromatograms in Figure 3.1 there is no evidence for oligomers in the WT cystatin B and only a small peak covering fractions 16-18 is observed for oligomer species in the G4R. The tetramer peak is also small compared to the monomer and dimer peaks. Some oligomers of G4R cystatin B purified from *E.coli* grown in LB broth were observed by EM but no WT oligomers were observed (Figure 3.2). The *E.coli* grown in minimal media produced more high molecular weight species of cystatin B (Figure 4.21). The tetramer and dimer species seem to be promoted in minimal media as their peaks are much larger for the WT and G4R than that in figure 3.1. There is also an oligomer peak in both the WT and G4R chromatograms. Further evidence of the presence of oligomers in the fractions was collected using EM (Figure 4.22 and 4.23)

Figure 4.21 B shows a chromatogram for purified Cystatin B G4R grown in minimal media. Similar to figure 4.21A there is a peak (A) corresponding to oligomeric species of G4R. Whilst oligomers of cystatin B have been successfully purified from *E. coli* in past work (Davis, 2013) and in chapter 3 of this thesis , in those conditions the observed peak is very small. An estimate of the fraction of cystatin B which is oligomeric grown in minimal media condition is ≈ 5% for the WT and ≈ 15% for G4R in these S3C constructs, while the proportion purified by Peter Davis for G4R in the S3 construct had been closer to 3%.

It is notable that these oligomers were made by the *E. coli* when grown in minimal media. Under these conditions the *E.coli* will be producing more heat shock proteins, including DnaK. It is possible, therefore, that the same process is going on *in vivo* that I had been trying to replicate *in vitro.*

The oligomeric fractions from SEC were then analysed by TEM. As can be seen in figures 4.22 (G4R) and 4.23 (WT), these look very similar to the oligomers in figure 1.15 by Peter Davis using the C3S construct. Further to this, one can also see the similarity to the morphologies observed in Figure 4.10 which are cystatin B oligomers prepared *in vitro* (in the presence of DnaK, ATP and co-chaperones) where there are no potential cell membrane or content contaminations. One could therefore determine that an therefore confirm that these could beare oligomers of Cystatin B. Previous work by the Staniforth group (Davis. 2016) on G4R oligomers (see chapter 1) showed that they were lipase resistant indicating that they are indeed protein oligomers and not anything cell membrane related. In addition, when *E. coli* express WT Cystatin B very few oligomeric species are observed eluting from the gel filtration column; whereas purification of G4R cystatin B does yield an observed peak corresponding to oligomeric species. This indicates that these oligomers are either of the protein itself or are something which is a result of the protein being expressed. Gold labeling by TEM could also validate this. Either cystatin B is chaperoning the formation of these inclusions or as previously stated above the more likely explanation is that a chaperone is causing the cystatin B to become inclusions.
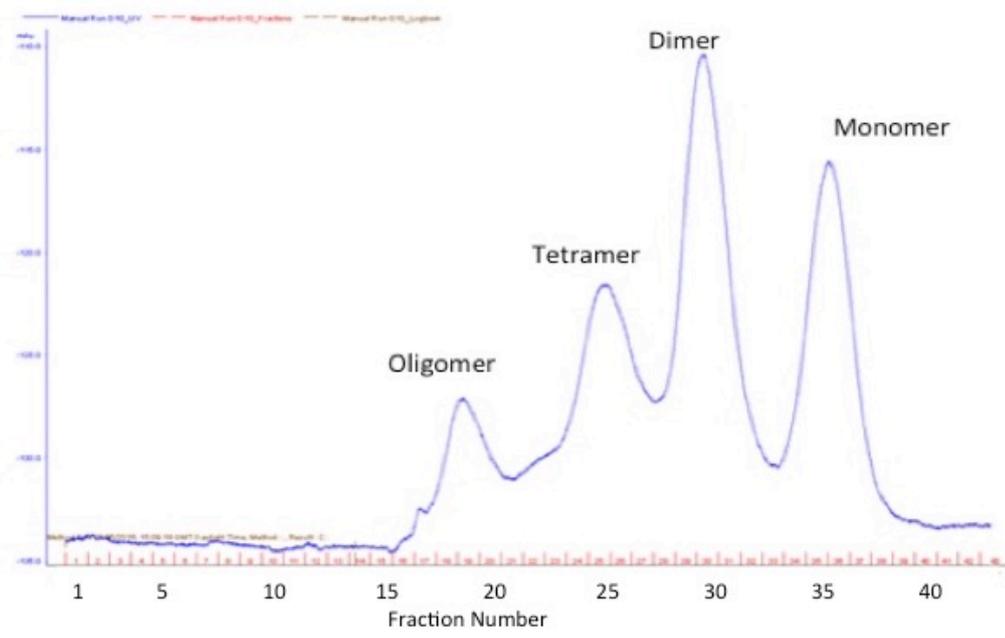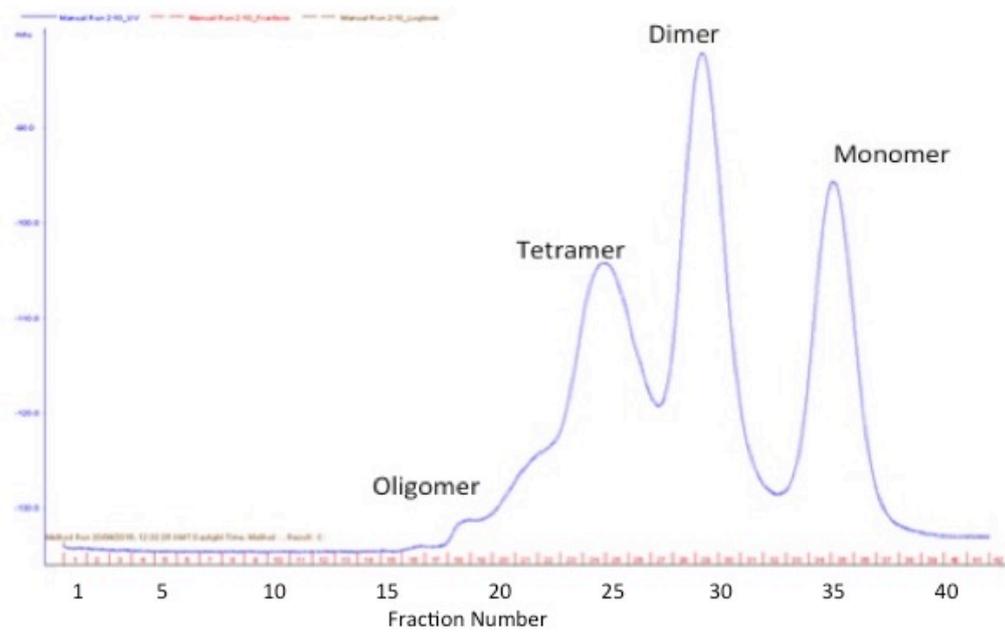
Figure 4.21: Chromatograms for the last step in the purification of cystatin B from E. coli extracts. Top: Cystatin B WT, Bottom: Cystatin B G4R.
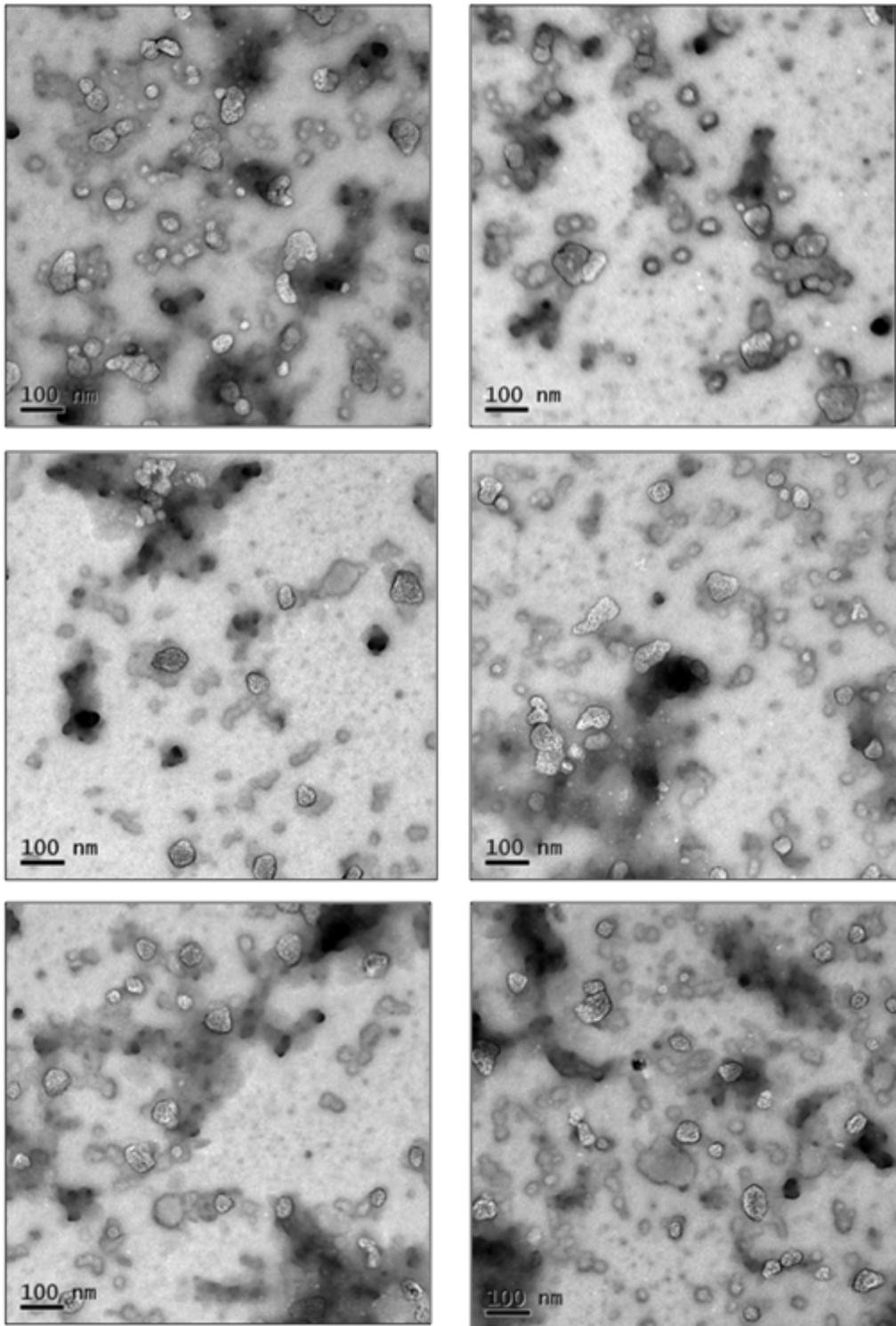
Figure 4.22: TEM of cystatin B S3C G4R oligomers purified from E. coli (Fraction 19). *All images were taken using a magnification of 21,000.*
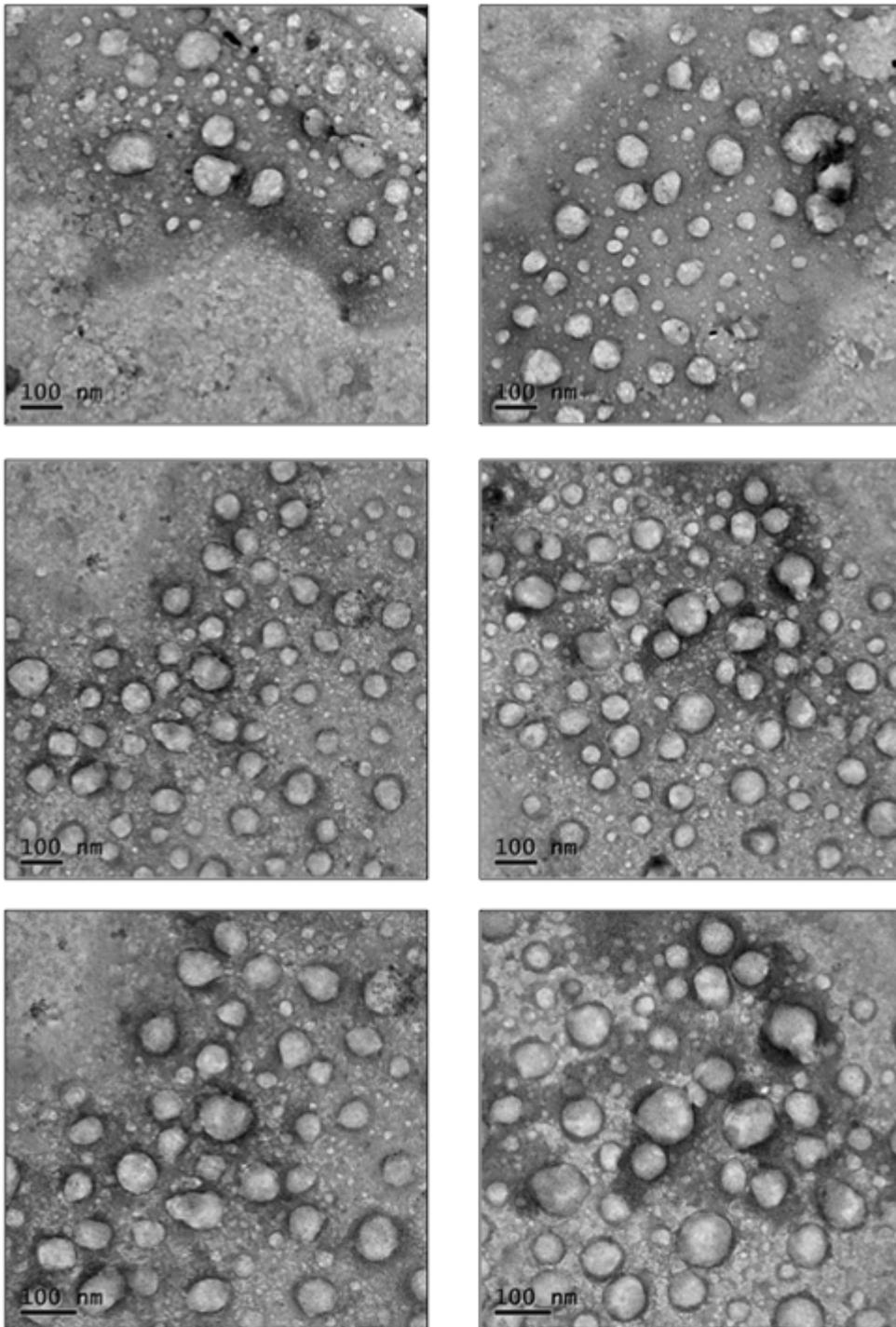
Figure 4.23: TEM of WT S3C oligomers (Fractions 18-23) purified from E. coli.
All images were taken using a magnification of 21,000.

4.3.6. Defining the size of the oligomers by HPLC

The oligomers (fraction 19 from SEC in Figure 4.21) purified from *E. coli* were analysed further using analytical SEC-HPLC to estimate their molecular weight (Figure 4.24). Although the concentration (3.35 µm) and absorbance of this oligomer fraction is low the figure suggests that oligomers remain stable and elute at the void volume of the analytical superdex 200 HR10-30 column. The WT oligomers were too dilute to detect using this method. As can be seen from the data presented in Figure 4.24, the oligomers elute at the void volume of the column at around 15 minutes. It is, therefore, impossible to determine their exact size using this method.
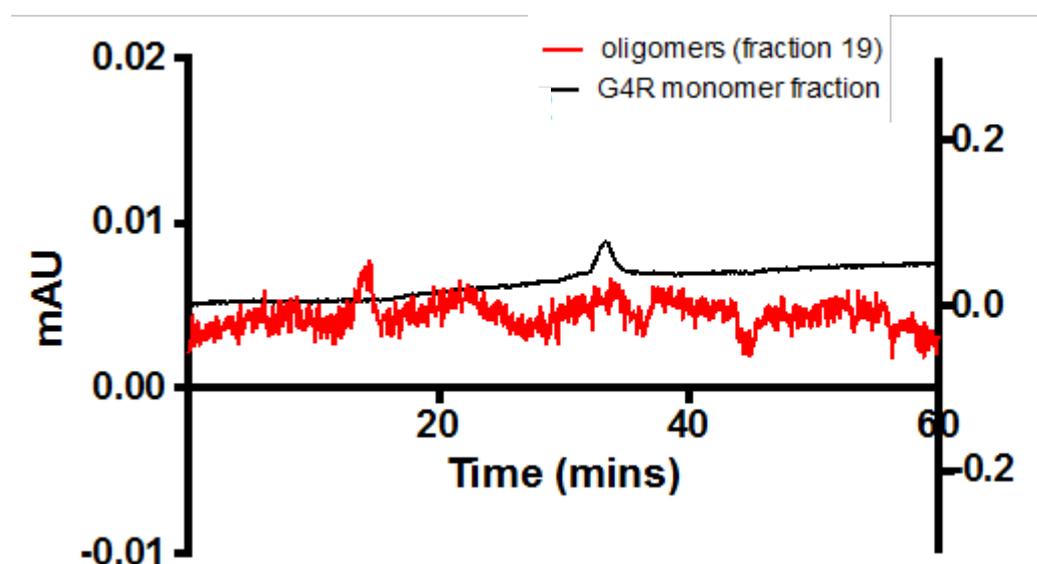
Figure 4.24: Characterisation of oligomers purified from E. coli by SEC-HPLC. *The y-scale on the left is for the oligomers while the y-scale on the right is for the G4R monomer fraction.*

4.3.7. Stability of the oligomers

The stability of the G4R oligomers was also explored using acetonitrile solvents. If a suitable diluent could be found, then we would be able to use this to characterise the components using mass spectrometry. As shown in figure 4.25, 40% acetonitrile was the optimal condition for this. Unfortunately, even under optimized conditions, the protein concentration is very low due to either incomplete dissolution or low initial protein mass. Thus, no mass spectrometry data were obtained from this sample. In future, the purification of

greater quantities of this species would allow not only verification of its identity by mass spectrometry but also potentially a limited proteolysis experiment in which we would have added proteases to the oligomers then compared their breakdown products at different times after the addition of protease. This would then allow direct structural comparison with cystatin B amyloid fibrils.

The absence of a monomeric peak in the apparently dissolved sample in 40% acetonitrile suggests that dissolution may not have been successful and this would also explain the lack of mass spectrometry data.
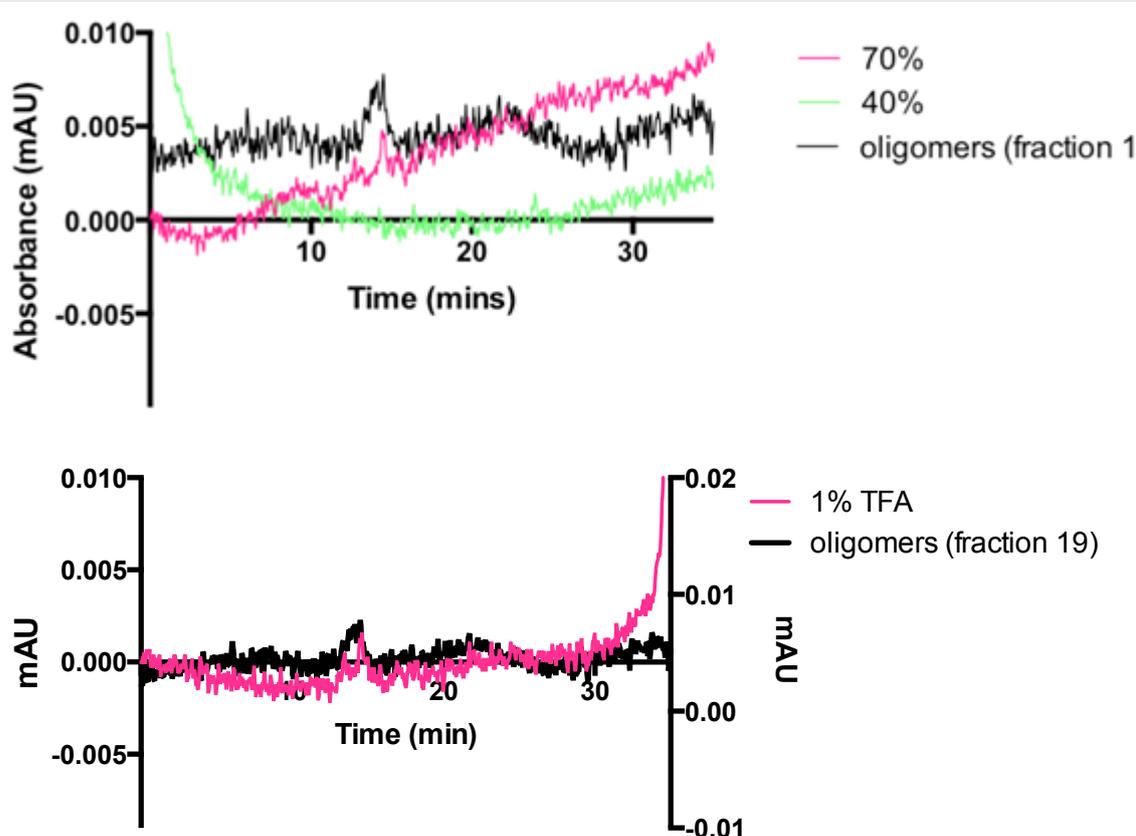
Figure 4.25: Stability of G4R oligomers purified from E. coli. *Above is the SEC-HPLC of the protein dissolved in PBS (black), 70%acetonitrile (0.1% TFA) – pink - and 40% acetonitrile (0.1 % TFA) - green. Below is the SEC-HPLC of the protein dissolved in 1% TFA. Monomeric cystatin B should elute at 30 minutes.*

4.3.8. Structural analysis of Cystatin B oligomers

Figure 4.26 shows the far-UV CD spectrum of the G4R oligomers (Fraction 19 from the fractions collected by SEC shown in Figure 4.21) compared with the monomeric fractions (34-38). Not only does the resulting spectrum show the sample to be protein, but one can see that the oligomer peak has shifted to the left compared to the monomer peak. This shape change indicates a change in protein secondary structure from mostly β-sheet (as is the case in monomeric Cystatin B) to a less structured or more α-helical structure. Analysis of the peaks showed that the oligomers are only 5% β-sheet and are 28% α-helical. While the presence of fraction 19 depends on the overexpression of G4R cystatin B and is most likely therefore this protein, given the work of Melli and co-workers, it is plausible that G4R cystatin B induces the formation of inclusions that are heterogeneous in protein content. This represents an alternative explanation to the CD data.
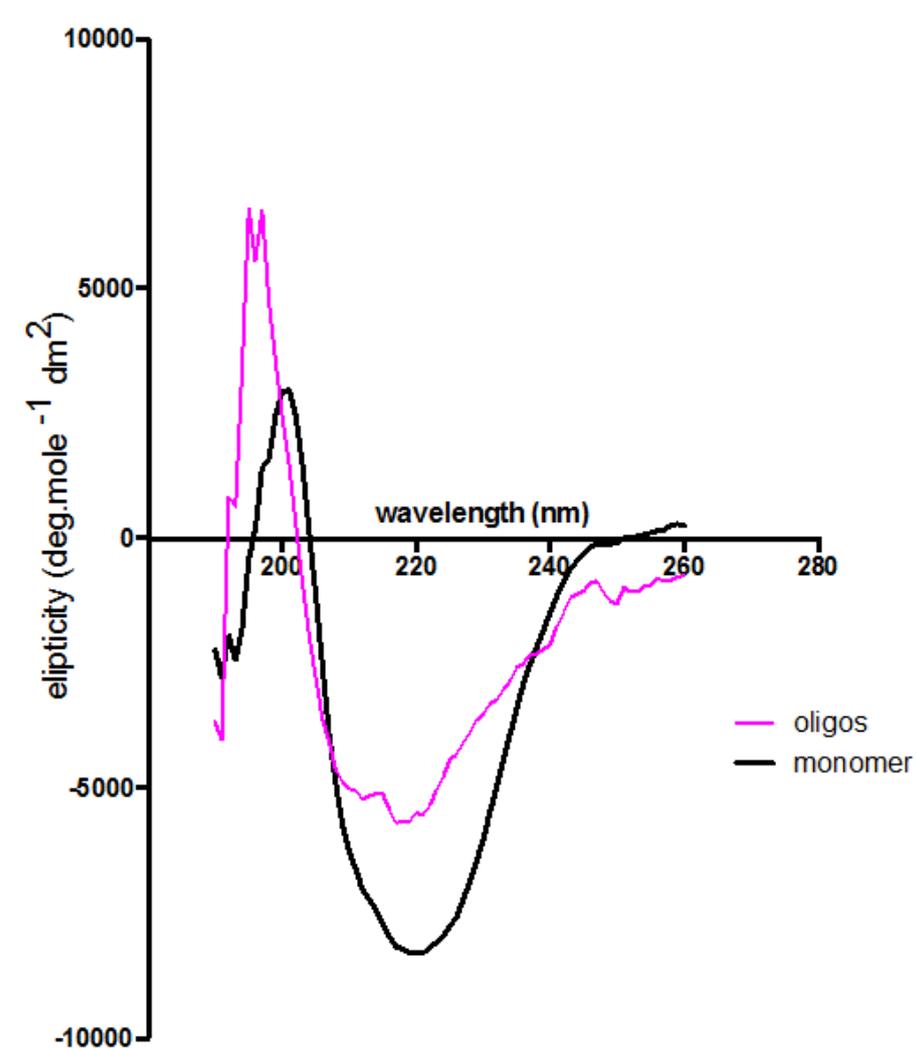
Figure 4.26: Far-UV CD of cystatin B oligomers purified from E. coli.

Despite the failure to dissolve oligomers using acetonitrile, in order to further analyse the structure of the oligomers by mass spectrometry, a sample of the G4R oligomers was digested using Proteinase K at a ratio of 1:50 Cystatin B to DnaK. It was hoped that the addition of protease would render the resulting species less stable and allow their analysis. Aliquots were removed from the whole sample at 0mins, 30 mins, 1hr, 4hrs and 24hrs. These were immediately frozen to halt the reaction. The resulting digested samples were dissolved in 40% acetonitrile (1% β-mercaptoethanol) due to earlier data on the stability of the oligomers under different conditions (see 4.3.7). However, after the samples were run, first down a reverse column and then electrospray mass spectrometry-no masses were found. This could be due to a very low

concentration of protein or imperfect dissolution of the oligomers meaning the mass is still too big for mass spectrometry resolution.

4.3.9 Conclusion

It is important here to put the potential oligomers produced in the work described in this chapter into the context of the wider research literature in this area. Since these potential oligomers were either produced from purified protein or in *E.coli,* it is essential to address whether they are comparable to other such structures found in human cells, and, therefore, of physiological significance. In the introduction to this thesis (section 1.6), I looked at other examples of proteins which form "oligomers" or inclusions which are not always pathogenic e.g. Marinesco bodies. It is possible that the potential oligomers observed in this chapter are not true amyloidogenic "oligomers" but could be more homologous to the bodies, granules or compartments discussed below.

Work by Alberti group (Alberti & Hyman, 2016) refers to membrane-less compartmentalization in the cytoplasm of cells by a process called phase separation. These compartments are thought to be liquid-liquid phase separate from the cytoplasm, leading to the formation of liquid droplets in the cytoplasm. There has been much work on the molecular mechanisms of phase separation. Intrinsically disordered proteins (IDPs) have been the most studied drivers of phase separation. One example is the RNA-containing compartments found in ALS patients. It is thought that two IDPs, TDP-43 and FUS, are responsible for their formation (Patel et al. 2015). In ALS, these proteins form pathological inclusions later in the disease.

Such cellular compartments are associated with ageing and disease and therefore, this phase separation must be sensitive to changes in the cellular environment such as heat shock, changes in macro-molecular concentration of the phase-separating proteins and changes in the concentration of ions.
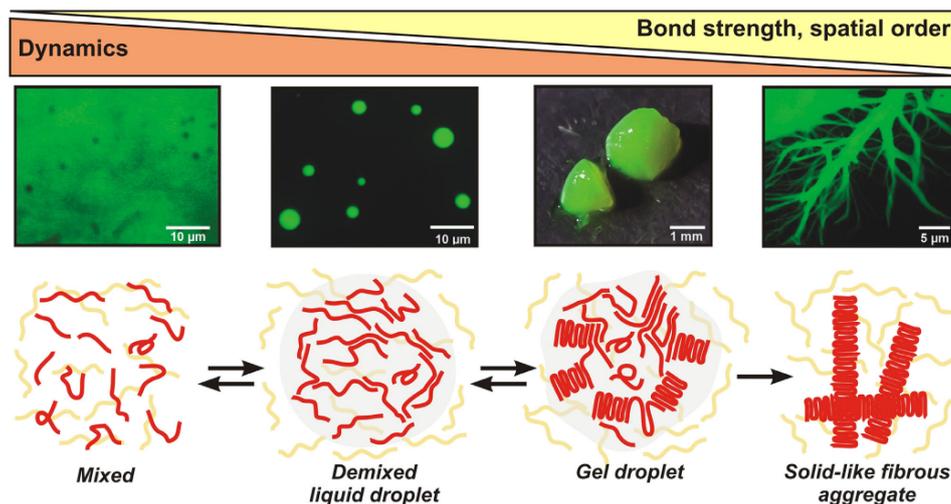
Figure 4.27: A model of phase separation. A protein (red) undergoes a phase transition into a liquid droplet by liquid–liquid demixing. The droplet changes structure over time. The above images on the top show purified FUS protein forming liquid droplets, a gel, and fibrous aggregate (from Alberti & Hyman, 2016).

These liquid compartments can convert into more solid-like structures with different physical properties and morphologies. It is thought that there may be a "hydrogel" type intermediate state between liquid and solid compartments and that the solid compartments may contain highly ordered fibrils. The proteins FUS (Patel et al. 2015, Han et al. 2012, Kato et al. 2012) and hnRNPA1 (Molliex et al. 2015, Kim et al. 2013) have been shown to do this.

There seems to be a driving force for proteins in liquid-like compartments to form solids with time (Alberti & Hyman, 2016). One reason why proteins may form solid structures is that these solid-like structures have important physiological functions. For example thr human mitochondrial antiviral signaling (MAVS) protein can change into a fibrous state on the surface of mitochondria. In its fibrous form MAVS interacts with tumor necrosis factor (TNF) receptor-associated factors (TRAFs) and propagates a signal that results in the induction of type I interferons and other antiviral molecules (Hou et al. 2011).
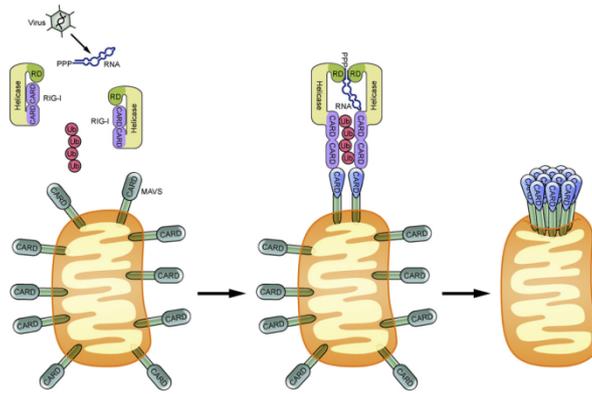
Figure 4.28: A Model of MAVS Activation Involving a Prion-like Conformational Switch. *Binding of RIG-I to viral RNA and ubiquitin allows the CARD domains of RIG-I to interact with the CARD domain of MAVS. This interaction induces a conformational change of the MAVS on the mitochondrial outer membrane into prion-like aggregates (from Hou et al. 2011).*

The liquid-like compartments could also allow for concentrated bio-chemical reactions, and then the solid-like compartments could be used to inactivate or store macromolecules. In the case of cystatin B, this phase separation could be occurring and perhaps these "oligomers" should be referred to as compartments or inclusions.

In order to assess the most likely "granule" type we can assign to the cystatin B assemblies observed here, it is useful to consider the physical properties of the different granules reported in the literature.

Size: the range of sizes of granules reported in the literature varies significantly and may be a distinguishing feature of the different assembly type. For example, membrane-less compartments reported by Alberti and others are 1-10 µm, RNA containing stress granules in both human and yeast cells have dimensions of 250nm while synthetic haemoglobin S droplets produced by concentrating the protein to >3 mM are 1-10 µM in size. The Marinesco bodies presented in the introduction are also of similar size (Yuen & Baxter, 1963)

Density: the density of intracellular inclusions is one of the key characteristics reported on in the literature. Methods of choice include STORM where the rate of diffusion of fluorescently tagged protein is observed to change over time in liquid droplets as they undergo a phase separation often associated with pathology (Jain et al. 2016). Another method which does not require tagging includes light scattering (combination of static and dynamic).

Shape: While liquid droplets are amorphous spheres, stress granules have a more granular, cluster-like morphology with a range of shapes (Buchan & Parker, 2009; Jain et al. 2016). Bunina bodies are roughly spherical, clear in the centre and contain filaments (Figure 1.19). They are often seen to form chain-like structures (Figure 1.19).

Content: While some intracellular inclusions are relatively pure, as methods to characterise them become more sophisticated, it is apparent that a number of these are heterogeneous. Stress granules contain RNA and RNA binding proteins which include a wide range of species associated with translation and its control, as well as ribosomal units and factors involved in cell signaling (Buchan & Parker, 2009).

While the size of the granules observed here is consistent with those observed in the literature, the presence of liquid compartments, hydrogel-like compartments and solid-like compartments could account for the variation in morphologies seen by EM (Figures 4.9-13). It is interesting that copper is required for their formation since this has been highlighted as important in other amyloid studies and an increase in copper concentration is associated with ageing (Matheou et al. 2015). It could also be that these Cystatin B inclusions are copper storage compartments which act as a useful sink when copper is in excess but equally acts as a source for physiological functions when it is scarce.

While the density of the granules is currently unknown, the remarkable change in morphology in the presence of Mg-ATP suggests that the absence of this co-factor leads to a change in the ordering of the protein within the

inclusions. This is particularly interesting in the light of the recent discovery of the role of Mg-ATP in stress granule formation *in vivo* (Jain et al. 2016). Levels of Mg-ATP are also known to decrease with age, suggesting that this may contribute to an increase in stress granule formation. It may be that we have discovered a route to the formation of such species in the brain, something which has not been reported on previously. Indeed, cystatin B is known to localise to the nucleus in human cell lines (Riccio et al. 2001) and plays a key role in neurogenesis (Polajnar et al. 2014). Cystatin B containing inclusions have been reported in one EPM1 patient, lack of further research makes it unclear whether this is a general feature of the disease (Cohen et al 2011 and Polajnar et al. 2012).

4.3.10 Future work

Ongoing work in the Staniforth laboratory includes the use of asymmetric field flow fractionation (AF4), a new state-of-the-art fractionation technique allowing for the separation of a range of oligomer sizes and characterisation of different species quantitatively using online UV and MALS. This would contribute greatly to our understanding of the yield of cystatin B assemblies produced using DnaK. While current analysis is far from perfect, the phase separation that occurs in solutions of the enzyme lumasine synthase yields a % mass of 10^{-4} to 10^{-6} (Gliko et al, 2007). This indicates that a low yield is potentially a result of an existing equilibrium between different phases, with the transition catalyzed, in this case, by DnaK.

Given the importance of RNA in stress granules, the role of RNA in the production of cystatin B granules may be a missing piece in the puzzle. Adding RNA to our purified cystatin B and/or DnaK mixtures would be a logical next step in this study, which may impact on the observed equilibrium and allow more in depth characterization of the granules.

It would be useful to test these cystatin B oligomers/compartments/inclusions for their pathogenicity. While small molecular weight species have been

tested by Zerovnik and co-workers, these larger inclusions may represent non-pathogenic assemblies. It would be particularly significant to understand the difference between Mg-ATP and Mg-ATP free assemblies in this context. This could be done firstly using a dye leakage assay as in section 5.3.4.

Single molecule analysis, perhaps using Cryo-EM would be useful to gain further structural information. Cryo-EM could also report on density which could give insight into the molecular dynamics of the compartments or inclusions.

Chapter 5: A Novel therapeutic from *Salvia sclareoides*

5.1 Introduction

As discussed in section 1.8 of this thesis, the development of novel therapeutics to treat amyloid diseases is a research priority. *Salvia* (sage) plant species have been studied to this end due to their reported medicinal properties, having been regularly used in European and Chinese folk medicine. As natural products, compounds from *Salvia* plant species are excellent candidates in the search for a safe and effective treatment for amyloid-related diseases.

Salvia sclareoides is an aromatic herb related to common sage that is native to Portugal. Preliminary studies on *Salvia sclareoides* n-butanol extract (SD) showed interactions with human prion protein (huPrP$_{91-231}$) (Rauter et al. 2012). In a ^{1}H ^{15}N HSQC-NMR experiment, amide resonances corresponding to residues 93-112, 130-187 and 205-225 were attenuated. These residues are in the unstructured N-terminal region, two strands of the β-sheet and the three α-helices indicating a potential for extensive binding across the prion protein. Attenuation of resonances is typically associated with ligand exchange dynamics, and is usually seen when ligands have dissociation constants in the μM range (Rauter et al. 2012).

Preliminary work on *Salvia* extracts also included testing in an *in vivo* model (Fig 5.1.). Screening was carried out on SMB cells, mouse brain cells of non-neuronal origin persistently infected with Scrapie (an infectious form of prion protein and commonly designated PrP^{sc}) so they consistently produce PrP^{Sc} (Reddy et al, 2006 and Rudy et al, 2000). Cells were dosed for 5 days with different extracts and then analysed using a dot blot protocol optimised for blotting PrP^{Sc}. Cell viability and total protein concentration were also established after cell lysis using MTT and Bradford assays respectively (data provided by Jenny Louth and Beining Chen, Chemistry Dept., University of Sheffield). Data was analysed using labworks software to determine the density of each dot. This is presented as '% control'. The signal from cells dosed with DMSO was used to represent the signal from untreated cells;

anything around 70% of the average blank value was classed as non-active. The MTT data is also presented in this format, with anything above 70% of the average blank classed as non-toxic. Good activity is represented by low results showing reduced levels of PrP^{Sc}.

The *Salvia* water extract (SE) was the most effective at reducing the concentration of PrP^{SC}. As this extract represents a practical form of the plant, which could be manufactured as a dietary supplement, and it contains water soluble components, it became the main therapeutic focus of this project. Another key point of investigation in this project was the use of *Salvia* as a general anti-amyloid agent. In the studies reported in this chapter, the use of *Salvia* extracts was therefore investigated for use against cystatin B, amyloid β and α-synuclein.
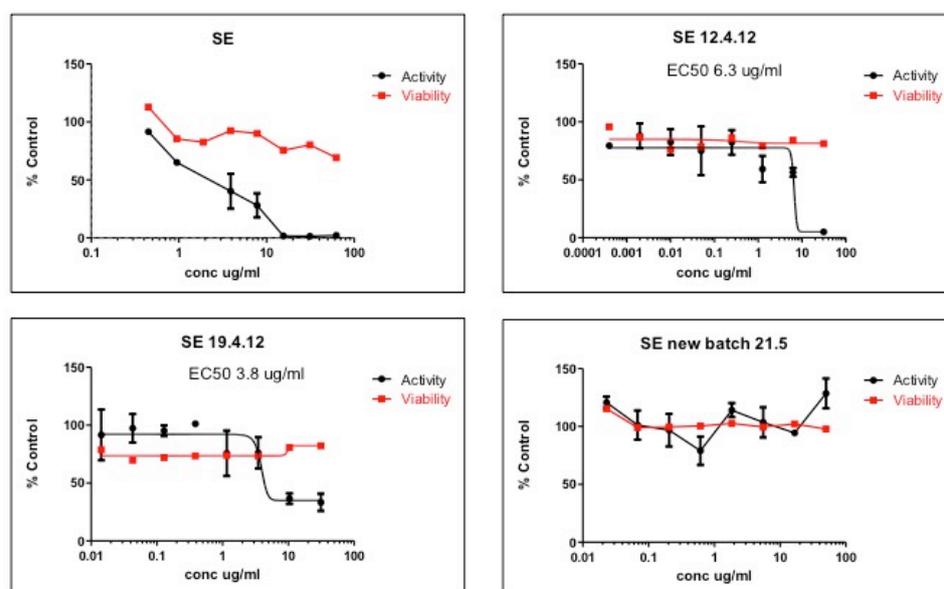
Figure 5.1: SE extract attenuates PrP^{sc} concentration in scrapie mouse SMB cells. *Method: Cells (Birkett et al. 2001) were plated out in 96 well plates at 12,000 cells per well and left overnight to attach. The extracts were diluted to the correct concentration in DMSO, diluted 1:10 in HBSS (Hank's balanced salt solution, Gibco) and then diluted 1:20 into the culture medium. After 5 days the cells were lysed with lysis buffer and benzonase, and an MTT viability assay was used to determine toxicity. A Bradford assay was also carried out to determine total protein concentration. Dot blots were carried out the day after lysing to determine the presence of PrP^{sc}. 8H4 (Liu et al, 2001) was used as the primary antibody and a HRP-tagged IgG was the secondary antibody. Images were detected via chemiluminescence. Each graph is a different batch of SE extract. Results: All batches except 21.5 showed activity in the μg/mL range. Extracts are not homogenous and as such it is difficult to get repeatable results from them. The 21.5 stock solution was a lighter colour than the other samples. The extracts were also very hard to solubilise so experiments were done with the soluble fraction. As samples were only partly dissolved in the cell medium, it was hard to determine exact concentrations. Figure provided by Jennifer Louth (dept. Chemistry, University of Sheffield).*

5.2 Materials and Methods

5.2.1 *Salvia sclareoides* Extracts: Extraction Procedures

The *Salvia sclareoides* extracts used in this study were obtained from Professor Amelia Pilar Rauter and Professor Jorge Justino (University of Lisbon). Figure 5.2 illustrates the extraction processes and highlights that all the extracts have had the extraction solvent removed by evaporation. 10% DMSO buffered aqueous solvent was used to re-suspend the majority of the extracts and act as a general organic solvent to solvate organic active compounds, while infusion and water extract (SE) were suspended in aqueous buffer.
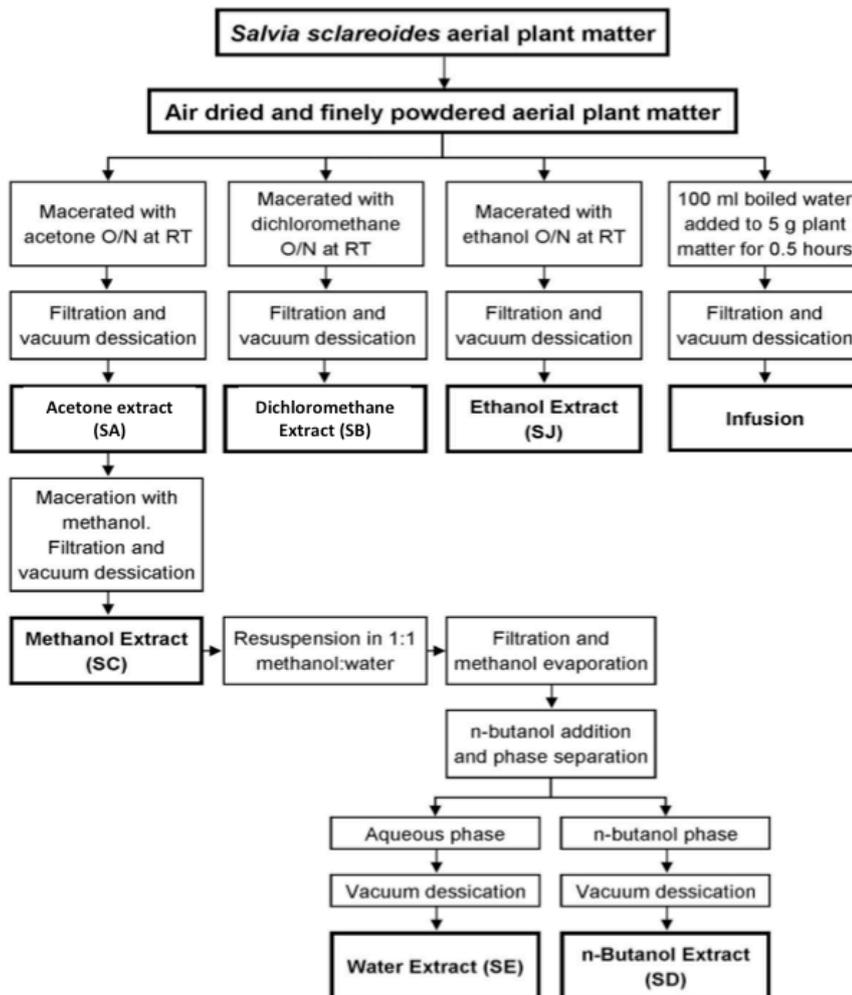
Figure 5.2: Extraction procedure for Salvia Sclaeroides. *The extraction procedure was devised by Catarina Dias (University of Lisbon).*

5.2.2 ThT defibrilisation assays

Cystatin B fibrils (produced as in section 2.4.1) were incubated with *Salvia* extracts at 25°C, in 15 mM sodium acetate 150 mM NaCl pH 4.7 with constant stirring of the samples. Defibrillisation was monitored continuously using thioflavin T (ThT) fluorescence. Specifically, 100 μl of DMSO was added to 900 μl of 30 μM cystatin B fibrils (10% DMSO) if using extracts suspended in DMSO (no DMSO was required for SE). Thioflavin T was added to this fibril solution to a final concentration of 10 μM. 1 ml of this solution was quickly transferred to a quartz cuvette with a path length of 1 cm and a small magnetic stirrer bar (5x2 mm) placed in the bottom of the cuvette. A Varian Cary Eclipse spectrofluorimeter was used to record the fluorescence spectra at different time points. An excitation wavelength (λ_{ex}) of 442 nm was used and emission spectra were recorded from 400-600 nm. After the first few readings had been taken, 10 μl of 20 mg/ml *Salvia* extract was quickly added to the 1 ml sample in the cuvette (final concentration 200 μg/mL). Emission values at 482 nm were plotted against time to follow fibril kinetics.

5.2.3 EM timecourse

EM grids were prepared and visualized as in section 2.5. For the defibrillisation time courses, SE extract was added to fibrils at a concentration of 1mg/ml (to mirror the NMR experiments) and 2 μl aliquots were taken and placed on EM grids at specific time points.

5.2.3 NMR

For all NMR experiments, extracts were used at 1mg/ml.

Preparation of $A\beta_{1-42}$ ADDLs for NMR

$A\beta_{1-42}$ ADDLs were produced using an adaptation of methods from the literature (Klein 2002; Ryan et al. 2010). This method is designed to produce a homogeneous sample of small $A\beta_{1-42}$ oligomers which are termed ADDLs. A 0.1mg aliquot of freshly HFIP treated and lyophilised $A\beta_{1-42}$ was first re-suspended in 8μl of DMSO and sonicated for 10 minutes. The peptide was

then diluted in 333μl of cold 15 mM deuterated sodium phosphate, pH 7.5, 0.15 M NaCl, 1 mM NaN$_3$. The final volume was made up to 500 μl with cold D$_2$O to give a final Aβ$_{1-42}$ concentration of 72 μM in 10 mM phosphate buffer, pH 7.5, 0.1 M NaCl. The sample was incubated at 4ºC for 24 hrs. Before using, the sample was spun for 10 minutes at 4ºC and the supernatant withdrawn (no residue was observed in the bottom of eppendorf). EM was used to confirm the presence of ADDLs.

Preparation of Aβ$_{1-42}$ oligomers for NMR

Aβ$_{1-42}$ was also prepared for NMR using the method of Airoldi et al. (2013). Lyophilized Aβ$_{1-42}$ was dissolved in 10 mM NaOD in D$_2$O at a concentration of 160 μM and then diluted 1:1 with 10 mM phosphate buffer (pH 7.4 and made in D$_2$O) containing 100 mM NaCl (PBS) and SE extract of *Salvia sclareoides* or rosmarinic acid. The final concentrations or quantities of Aβ$_{1-42}$, rosmarinic Acid and the SE extract of *Salvia sclareoides* in the samples were 80 μM, 1 mM and 1 mg/ml respectively. The final concentration of the buffer components was therefore 5 mM phosphate buffer (pH 7.4) containing 50mM NaCl. The pH of each sample was adjusted to pH 7.5 with NaOD and/or DCl.

STD NMR

This type of NMR experiment is used to characterize ligand-receptor interactions. The experiment is based on the Nuclear Overhauser Effect (NOE) and the observation of the ligand resonance signals. It can be used as a screening technique in the identification of lead structures, but it is also a useful tool for identifying ligands within a mixture (such as the *Salvia* extracts) which bind to a receptor. An STD-NMR experiment relies on the fact that, for a weak binding ligand (K$_D$ ranging from 10^{-8} M to 10^{-3} M), there is exchange between the bound and the free ligand state. Briefly, an STD experiment involves subtracting a spectrum in which the protein was selectively saturated (on-resonance spectrum obtained by irradiating at a region of the spectrum that contains only resonances of the receptor (0 ppm to 1 ppm), from one recorded without protein saturation (off-resonance spectrum). The difference spectrum should contain only signals from the ligand(s) that receive saturation

transfer from the protein via spin diffusion through the Nuclear Overhauser Effect. Other compounds that may be present but do not bind to the receptor will not receive any saturation transfer. Their signals will be of equal intensity in the on-resonance and off-resonance spectra.

Saturation transfer difference (STD) NMR experiments were completed using the same parameters as detailed in Airoldi et al. (2013). Briefly, the pulse program used was from the standard Bruker library (stddiffesgp.3). This uses a shaped pulse train for saturation which consists of 50ms gaussian pulses for 2s. It also includes a spinlock to decrease signals arising from protein (Mayer & Meyer, 1999).

NOESY NMR

The Nuclear Overhauser Effect (NOE) in NOESY NMR is used to observe binding events. The NOE is a phenomenon that occurs when one proton resonance in an NMR spectrum is saturated or inverted and proton resonances which are spatially close experience a change in intensity (Neuhaus and Williamson, 2000). NOEs are partly determined by molecular correlation times which are inversely related to molecular tumbling rates. Molecules with a large molecular weight have a larger correlation time (and slower rate of tumbling). NOEs are positive for smaller molecules (< 600 Da) and are negative for larger molecules (> 1200 Da) (Decatur, 2007). One can therefore look at binding as free small molecule ligands should have positive NOE cross peaks, whereas bound ligands should have negative cross peaks.

DOSY NMR

Diffusion Ordered Spectroscopy (DOSY) NMR experiments can be used to identify molecules in a mixture based on their diffusion coefficients (D), and, therefore, their size and shape. Modulation of NMR signals during a pulse field gradient experiment (radio frequency pulses combined with magnetic field gradients) is used to measure diffusion. The degree of modulation is a function of the magnetic gradient pulse amplitude and is proportional to the diffusion coefficient (D) of the molecule (Johnson Jr. 1999). The 2D spectra plots chemical shift against logD. The logD values of a ligand or ligands can

be measured in the presence or absence of the protein. Each measured logD value is an average of the ligands' bound and free states. Ligands with NMR signals which show an increase in logD and, therefore, molecular weight, signify a bound population.

5.3.4 Dye Leakage assays

Preparation of carboxyfluorescein containing vesicles (LUVs)

Using a glass pipette, 1 ml of 80% DOPC 20% DOPG lipid solution (in chloroform) was dispensed into a round bottomed flask and a stream of nitrogen gas was used to evaporate the chloroform and leave a film of lipid. 1 ml of 50 mM carboxyfluorescein solution (50mM HEPES pH 7.4 with NaCl added to 440 µS) was then added and the round bottomed flask was vortexed until the lipid film was fully re-suspended. The resulting vesicle solution was passed through an Avanti mini-extruder with a 400 nm PC membrane and a 200 nm PC membrane in order to ensure large unilamellar vesicles of uniform size (Avanti Polar Lipids, Alabama, USA). The LUVs were then filtered through a PD10 desalting column (GE healthcare, UK) to remove any excess carboxyfluorescein solution.

Dye leakage assay

The resulting vesicle solution was serially diluted to 10 µg/ml into 50 mM HEPES pH 7.4 (NaCl was added to 440 µS) and incubated at room temperature for 48 hours in quartz cuvettes in the presence of 2 µM $A\beta_{1-42}$, 2 µM $A\beta_{1-42}$ and 10 µg/mL *Salvia* extract together, 10 µg/mL *Salvia* extract alone and in the absence of anything else. Fluorescence measurements (λ_{ex} = 485nm and λ_{em} = 517nm) were taken every 5 minutes using a Varian Cary Eclipse spectrofluorimeter (Agilent, UK).

5.2.5 Mass spectrometry of Fibrils and *Salvia* extract

Figure 5.3. outlines the sample preparation method. Briefly, a sample of 25 µl 80 µM $A\beta_{1-42}$ fibrils was incubated for 1 minute with 25 µl SE extract at 20 mg/ml and then centrifuged for 10 minutes at 14, 00124700 xg 0 rpm to produce a pellet. The supernatant was removed and sent for mass

spectrometry analysis. The pellet was washed with water and the supernatant removed. This process was repeated 4 times with the wash/supernatant being sent for mass spec analysis. The pellet was finally solubilised in HFIP, lyophilised and then re-suspended in 40% acetonitrile, 0.1% TFA. This sample was also sent for mass spec analysis. Control samples containing 10mg/ml SE extract in the absence of $A\beta_{1-42}$ and a number of compounds identified by the Rauter group as being present in the extract (Catarina Dias, personal communication) were also sent for analysis. These included luteolin, luteolin-7-o-glucoside, glycoside A, glycoside B and glycoside S.

Samples were applied directly into an electrospray time-of-flight mass spectrometer (agilent Q-TOF). Masslynx 3.5 software (Waters Corp.) was used to determine the masses present.
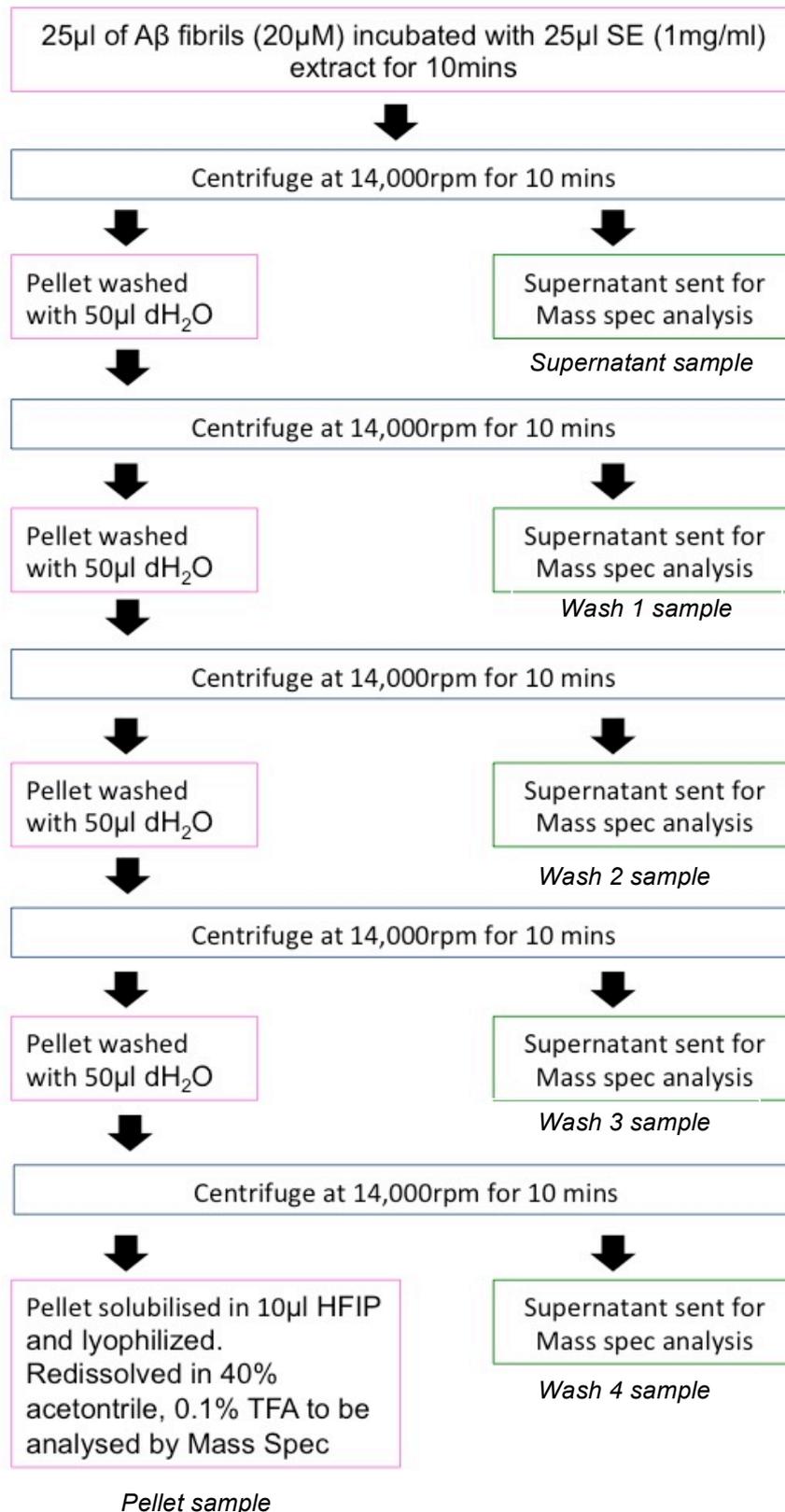
Figure 5.3: Outline of method for preparing samples of Aβ_{1-42} incubated with SE extract for analysis by mass spectrometry.

5.2.6 Cell toxicity assays

The CytoTox-ONE assay kit (Promega) was used for all cell assays. This is a fluorescent assay which measures the release of lactate dehydrogenase (LDH) from cells with a damaged membrane. LDH released into the culture medium is measured in the kit by supplying lactate, NAD^+, and resazurin as substrates in the presence of diaphorase, resulting in the conversion of resazurin into resorufin. The generation of the fluorescent resorufin product is proportional to the amount of LDH released and therefore dead cells.

LDH assay with SH-SY5Y cells

Human neuroblastoma cells (SH-SY5Y) in media containing F-12 Ham's nutrient mixture supplemented with 10% fetal bovine serum (FBS), 1% L-glutamine (L-Q), 1% penicillin/streptomycin antibiotics (P/S) and 1% nonessential amino acids (n-aa) (Invitrogen) were grown in a 5% CO_2 atmosphere at 37°C in a 175 cm^2 flask. Confluent cells were removed from the flask by trypsinisation. The cells were counted and plated on a 96-well polystyrene plate with approximately 10 000 cells per well. The plate was incubated overnight at 37°C to allow cells to adhere to the plastic.

Cell media was removed from the wells and replaced with 100 µl of fresh media containing either test compounds or DMSO. The plate was then incubated at 37°C for 24 hrs.

After incubation, the plate was equilibrated to room temperature for 30 minutes. Some wells containing just cells in media were used as dead cell (positive) controls. 2 µl of lysis solution was added to these cells.

100 µL of CytoTox-ONE solution was added to the wells followed by 10 min incubation at room temperature. 50 µL of stop solution was then added to each well. The fluorescence was measured at an excitation frequency of 545 ± 20 nm and an emission frequency of 620 ± 7.5 nm. It is also important to measure the fluorescence of the cell medium incubated with CytoTox-ONE solution. There were 3 repeats for each condition.

Results are calculated using this equation:

$$\% \; cytoxicty = \frac{(experimental - cell \; media \; background)}{(dead \; cell \; control - cell \; media \; background)}$$

LDH assay with mouse primary neurons

When using primary neurons, a 12 well plate with 100,000 cells per well was used. Cells were cultured in phenol red free neurobasal media (with B27 supplement) (Invitrogen).

5.3 Results

5.3.1 *Salvia* extracts do not work by simple monomer binding

Cystatin B has been used in our lab as a model for the study of amyloid formation; indeed a study of cystatin B oligomeric inclusions is included in chapter 4 of this thesis. Here we used soluble cystatin B to determine the general propensity of salvia extracts to bind to protein. As discussed in chapter 3, soluble cystatin B naturally populates at least 3 different forms under most experimental concentrations: tetramer, dimer and monomer where only the latter is relevant physiologically but where dimer dominates under most laboratory experimental conditions (approx. 70% of samples used here, as established by SEC).

^{1}H ^{15}N HSQC NMR of soluble cystatin incubated with SE Extracts

The binding of *Salvia* extracts to soluble cystatin B was tested using ^{1}H ^{15}N HSQC NMR by Peter Davis. As shown in Figure 5.4, the following dimer peaks are greatly reduced on addition of the SE extract: V47, V49, G50, T51, E62, V69, and F98. Peaks S7, Q10 N52 D63 S72, E76, T81 and S83 are also somewhat reduced upon addition of the extract. The attenuated residues are also shown on the structure of both the monomer and dimer of cystatin B. The attenuated residues are mainly found at the dimer interface. The disappearance or decrease in intensity of peaks can be interpreted in a number of ways. It suggests that addition of the extract has led to the formation of a new "bound" species or catalyzed the formation of a different species which is either in slow exchange with the previously observed species or is exchanging with a larger protein species which cannot be detected using solution NMR due to a slow tumbling speed. In the first instance, one would expect the concomitant appearance of new resonances with different chemical shifts whereas in the latter case, this would not occur.

Our data therefore support a model where *Salvia* extracts destabilise cystatin B dimers to form a species undetectable by NMR, most likely an aggregated species. The specificity of this effect for the non-physiological dimer is

intriguing. It suggests that the species that the extracts bind to is in equilibrium with dimeric but not monomeric cystatin B.
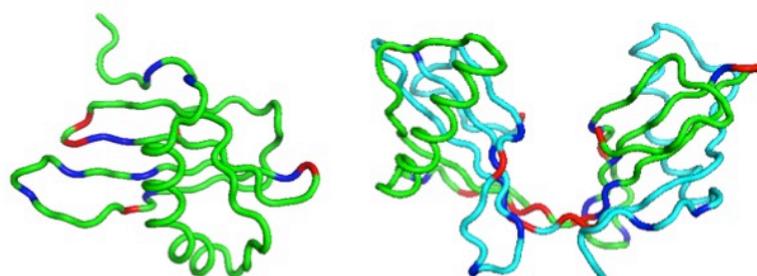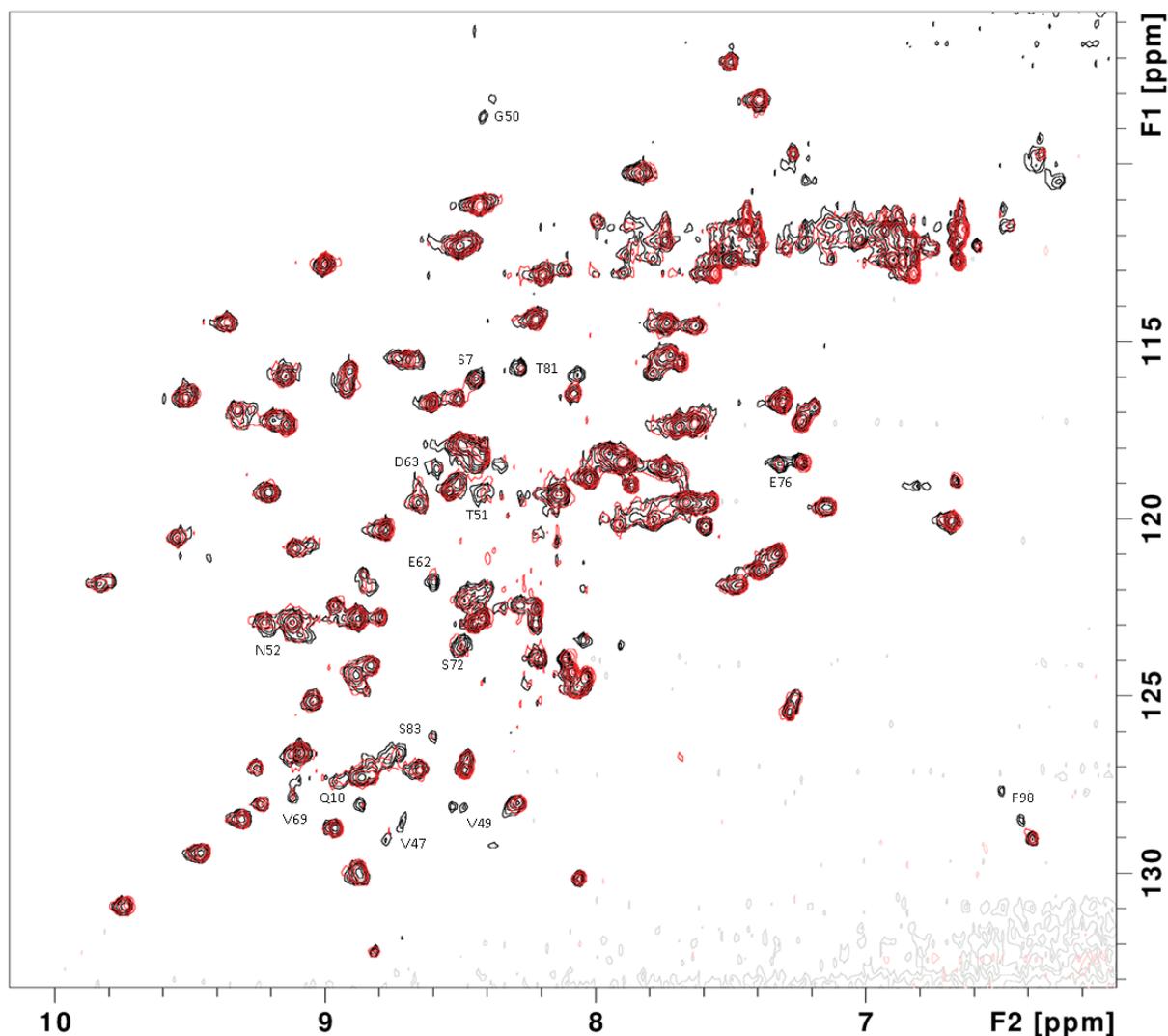
*Figure 5.4: Top ^1H ^{15}N HSQC NMR spectra of cystatin B and SE extract.* The spectrum of 30 µM cystatin B is shown in Black, that of 30 µM cystatin B with 1 mg/mL SE extract is overlaid in red. Peaks corresponding to attenuated dimer peaks are labelled. Bottom: cystatin B monomer and dimer with greatly attenuated residues shown in red and peaks which show some attenuation shown in dark blue.

146

The impact of SE extract on soluble Aβ$_{1-42}$ assemblies

We then proceeded to analyse the effect of the extracts on 80µM solubilised Aβ$_{1-42}$ peptide, freshly prepared in PBS. According to previous work by Airoldi et al (2013) on the SD extract, a preparation of this sort rapidly assembles into a solution rich in soluble oligomers (sections 5.2.3 and 5.3.4.), however in our hands this solution retained a similar 1D ^{1}H-NMR spectrum over 24 hours (Figure 5.5). The intensities of the NMR peaks decrease by only 20%, suggesting up to 80% of the sample remains monomeric or of a small molecular weight. Our experiment was to resuspend our Aβ$_{1-42}$ prepared as in section 5.2.3 in either PBS alone, PBS containing SE extract or PBS containing the anti-amyloid compound rosmarinic acid. In the presence of SE, the Aβ$_{1-42}$ peptide forms no fibrils (Figure 5.6), and a significant proportion remains soluble as evidenced by NMR. The reduction in monomer Aβ$_{1-42}$ signal over 24 hours is less when either SE extract or rosmarinic acid (a typical anti-amyloid agent) are present but is still significant. The ratio of intensity of the monomer Aβ$_{1-42}$ peak is 0.79 when there is no extract present, 0.88 when 80µM rosmarinic acid is present and 0.86 when the soluble Aβ$_{1-42}$ ADDLs are incubated with SE extract. The difference between these three conditions does not appear significant.

The resulting solution was examined by electron microscopy (Figure 5.6). No evidence of fibrillary species was seen although small worm-like oligomers are present on some grids. Most of the visible species are very small, with diameters less than 10nm, suggesting a species with a small number of Aβ$_{1-42}$ molecules, in the range of 10 molecules. In comparison, the control sample contains small fibrils and some amorphous aggregate.
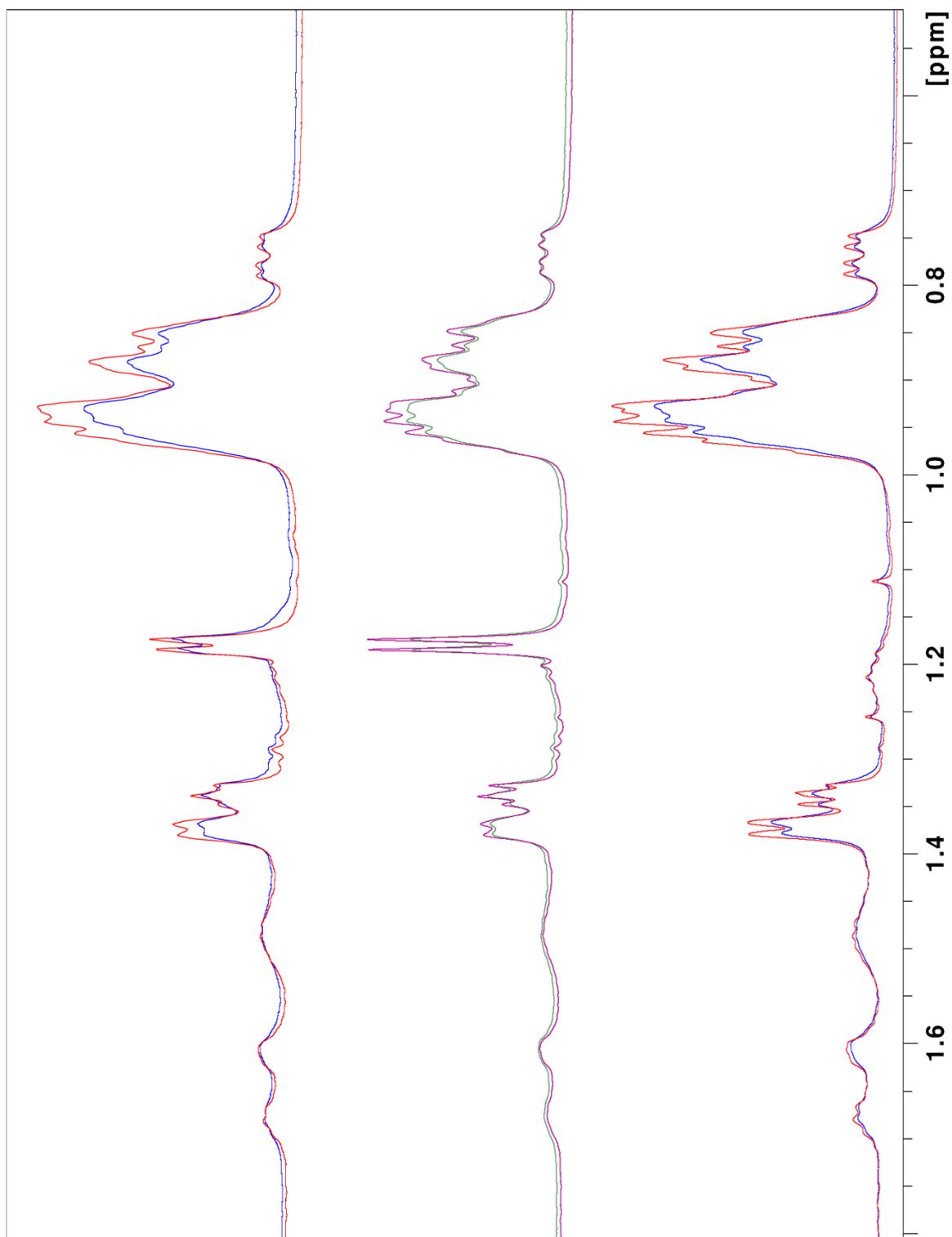
Figure 5. 5: The relative efficiency of the SE extract on the population of soluble Aβ$_{1-42}$ as detected by 1D ^{1}H NMR spectroscopy. *80 µM freshly solubilised Aβ$_{1-42}$ samples incubated in 5mM phosphate pH 7.5, 50mM NaCl and 25ºC, on their own (top), with rosmarinic acid (middle) and with SE extract (bottom): initial spectra are shown in red (top and bottom) or purple (middle); at 24 hours the spectra are shown as blue (top and bottom) or green (middle).*
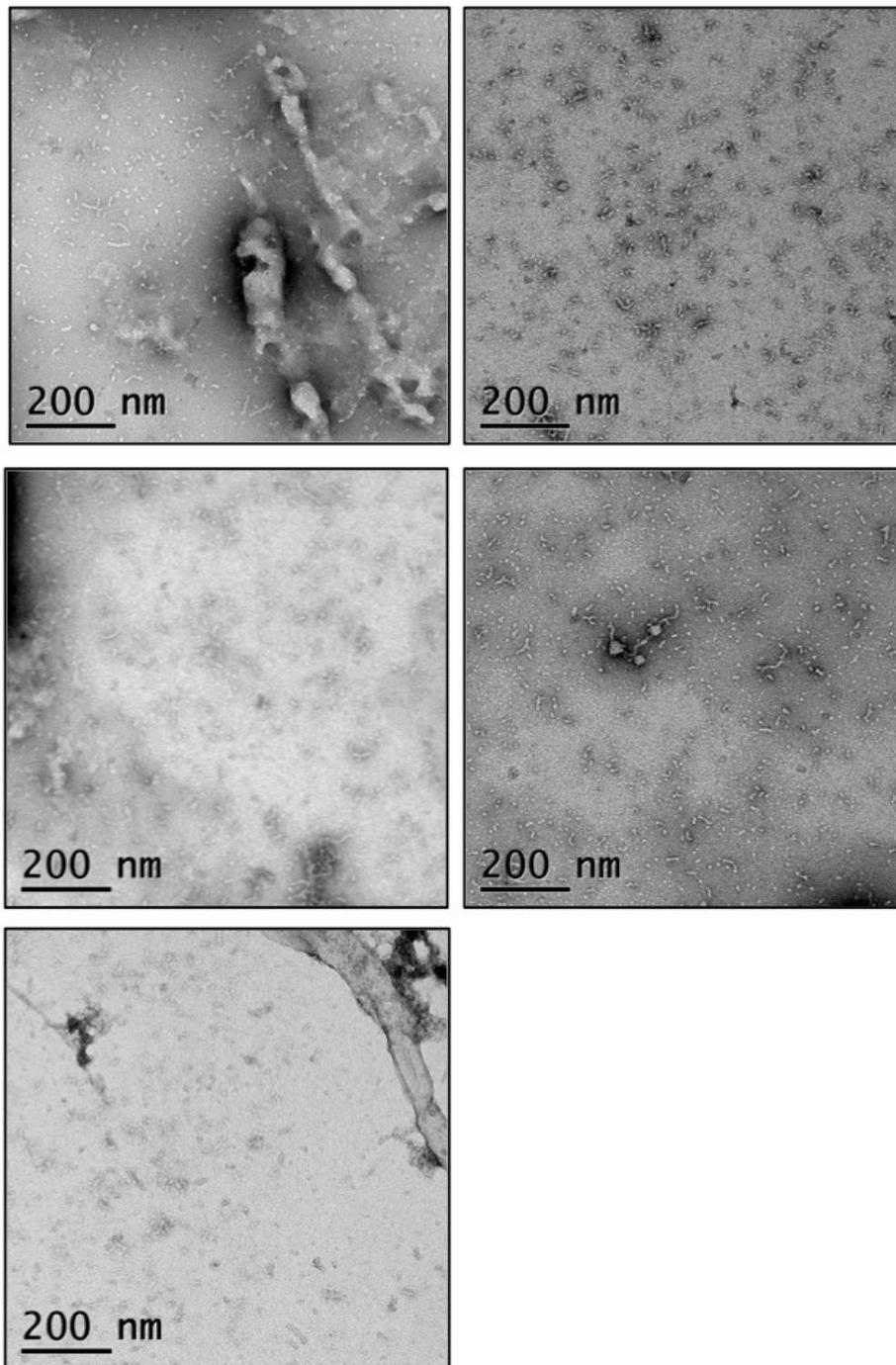
Figure 5.6A: Initially monomeric Aβ₁₋₄₂ incubated with SE extract during 24 hour NMR experiment. *80μM Aβ₁₋₄₂ was prepared freshly and incubated with SE extract in 10mM PO4, 100mM NaCl pH 7.4 for 24 hours at 25ºC, then the resultant solution visualized using TEM.. Size bars are shown*
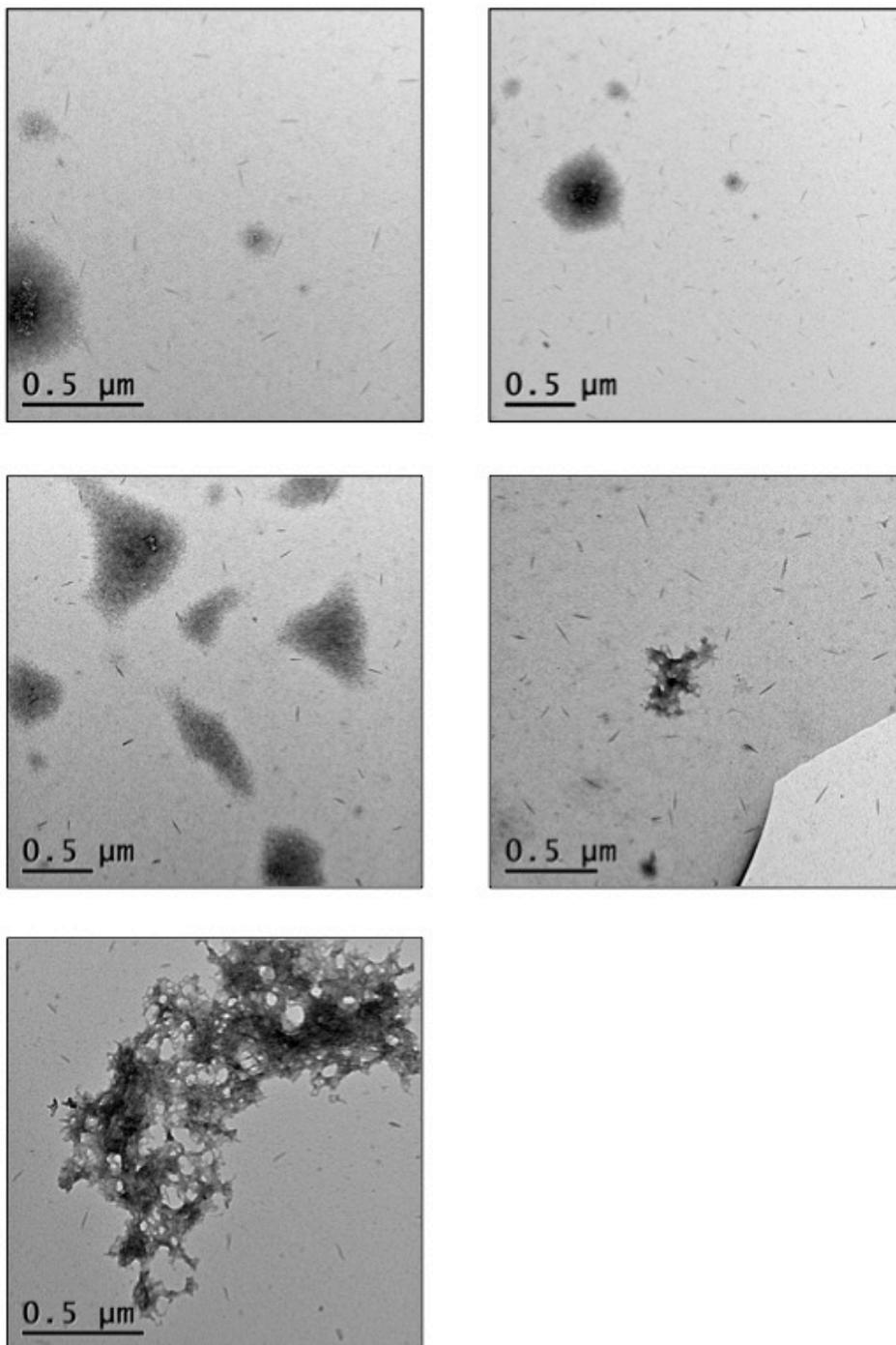
Figure 5.6B: A control reaction *(Aβ$_{1-42}$ incubated in 10mM PO$_4$, 100mM NaCl pH 7.4 for 24 hours at 25°C). Size bars are shown. Images of the SE extract on its own are shown in Figure 5.13.*

In conclusion, both the ^{1}H ^{15}N HSQC NMR of soluble cystatin B and the EM of soluble Aβ_{1-42} incubated with SE extract show that protein is not kept soluble by the extract. Cystatin B, which exists mainly as a dimer when in solution, appears to form larger protein species when incubated with SE and the initially soluble Aβ_{1-42} can be seen to form small oligomeric species. These results are of interest because it was originally hypothesised that the extract could be working by stabilising monomeric species. This is obviously not the case and more importantly, the role of aggregated species in the prevention of toxicity as well as in its causation needs to be understood further. Characterisation and quantification of these species would be a desirable next step with the impending arrival of fractionation (asymmetric field flow fractionation – AF4) and light scattering equipment to Sheffield.

5.3.2. Toxicity of aggregate species in the presence of SE extract

Dye Leakage

Figure 5.7 shows the protective effect of SE extract on a lipid bilayer in the presence of Aβ_{1-42}. Dye leakage from large unilamellar vesicles (LUVS) was similar when SE and Aβ were both present and for the SE and LUV controls. The rate of dye leakage is far higher when the LUVs are incubated with Aβ_{1-42} alone. This indicates that membrane damage by Aβ is reduced in the presence of SE extract. This experiment was only completed once and further repeats are required to confirm this conclusion.
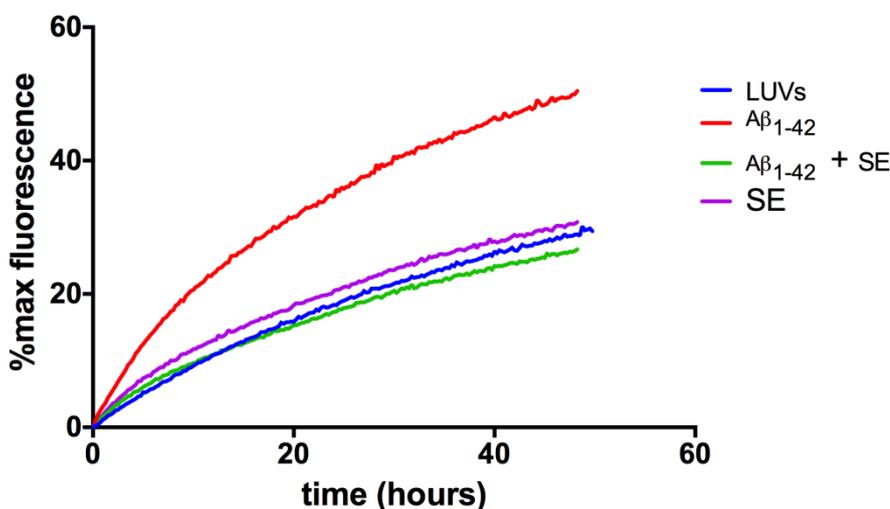
Figure 5.7: Dye leakage from LUVs in the presence of Aβ$_{1-42}$ and SE extract. *Fluorescence due to dye leakage from LUVs is shown in the presence of Aβ$_{1-42}$ alone (red), SE extract alone (purple) and in the presence of both Aβ$_{1-42}$ and SE extract (green). A control showing dye release from LUVs alone is shown in blue.*

Aβ$_{1-42}$ Cell toxicity assays

The SE extract was tested for its ability to inhibit the toxicity of Aβ$_{1-42}$ to mouse primary neurons. This data is shown in Figure 5.8. Whilst the data indicates that cells incubated with SE extract showed increased cell death, there was in fact only one well (out of 3 repeats under those conditions) which showed a real increase in cell death. It could have been that the cells in this well were more "sickly" than the rest of the plate.

There was also no significant difference in cell death between the DMSO control cells, cells incubated with Aβ and the cells co-incubated with Aβ and SE. This could be because the assay itself needs optimization and more repeats need to be done. Aβ does not always induce cell death consistently and batch testing of Aβ may need to take place. The cells may also need to be incubated with the Aβ for longer (48hrs).

SE extract (as well as SD and Infusion) were also tested for their toxicity to SHS-5Y cells at different concentrations. As shown in Figure 5.9, SE was not toxic to the cells at any of the concentrations used.
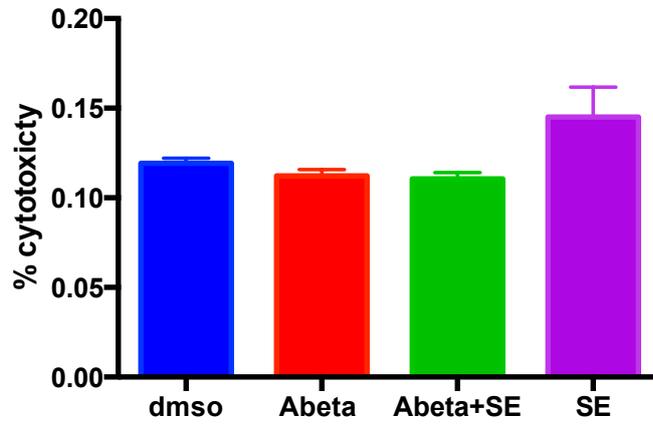
Figure 5.8: % cytotoxicity of mouse primary neurons incubated for 24hrs under 4 different conditions.
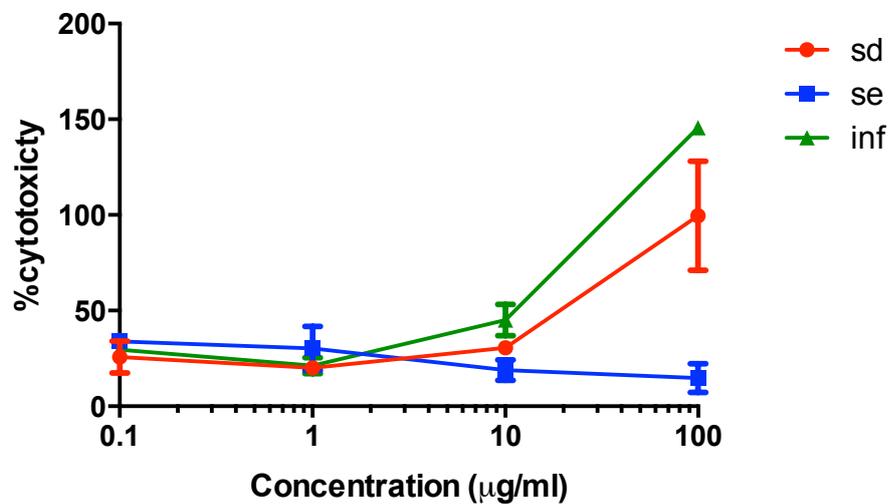
Figure 5.9: % cytotoxicity of SHS-5Y cells incubated for 24hrs with Salvia extracts. SD(red), SE(blue) and Infusions (green). Each experiment was replicated 5 times and variability between replicates is shown as error bars.

5.3.3. SE extract remodels amyloid fibrils into amorphous aggregate

In order to look at the kinetics of defibrillisation by the *Salvia* SE extract, a continuous Thioflavin T (ThT) fluorescence assay was employed. This technique is used conventionally in this field to quantify the levels of amyloid fibril-like species. Cystatin B amyloid fibrils are most stable at pH 4.7 and so the experiments presented in figures 5.10-5.11 were done at this pH. If the *Salvia* extracts are able to destabilise the fibrils at this pH, this would support their application as a therapeutic.

As shown in Figure 5.10, Thioflavin T loss (ThT) is rapid and occurs within 20 seconds of the addition of 0.2mg/ml SE extract. Thioflavin T in the control sample remains constant. This rate of fluorescence loss is extremely fast, although not uncommon in the literature (Bieschke *et al*., 2010). Time courses were therefore done with diluted *Salvia* extracts to see if the time over which the fluorescence drop was observed could be increased in order to produce more highly resolved data.

Even with a 10 fold dilution, SE extract still appears to break down the fibrils extremely quickly (figure 5.11A). A time course with a 50 fold dilution of SE extract was also completed to see if this would produce better data (figure 5.11B). It appears that the extract at this low concentration has no effect on the fibrils. This could be because the ratio of extract to fibril is very important and no effect is seen as soon as there are not enough molecules of active compound to interact with the fibril.

Although it is tempting to interpret this data as directly reporting on the fibrillary state of cystatin B, a more likely interpretation is that at higher concentrations of extract, an active compound or compounds in the extract is displacing the ThT dye from the fibril. This is a well reported issue with ThT assays (see section 1.3.1) but does have the advantage that it does instead report on the affinity of the extract for amyloid fibrils, in that it competes well for the thioflavin T binding site at very low concentrations. The extracts are not directly quenching the fluorescence at these wavelengths: the extracts do not absorb light at the wavelengths used for excitation and emission of thioflavin T (420-500nm).
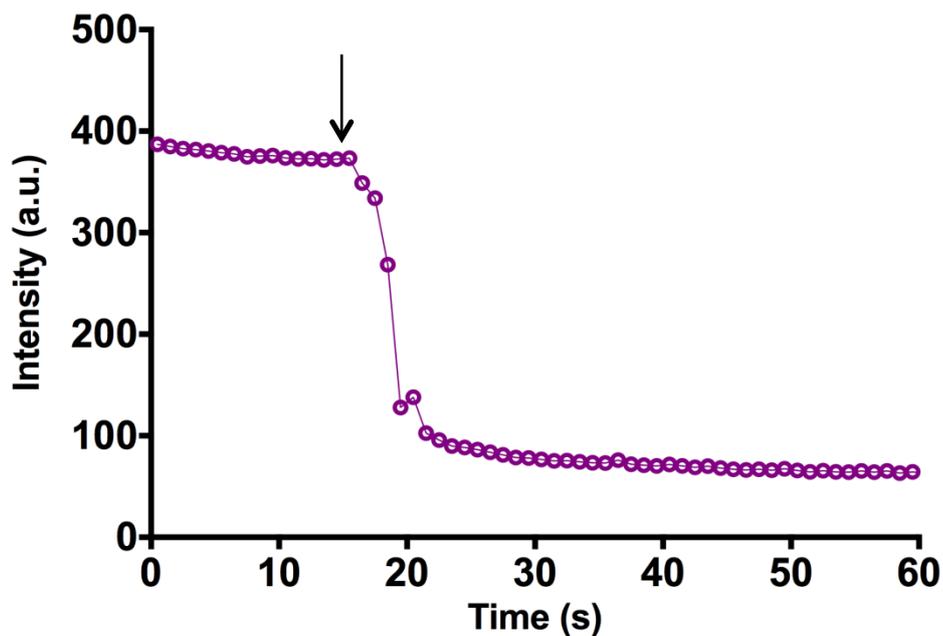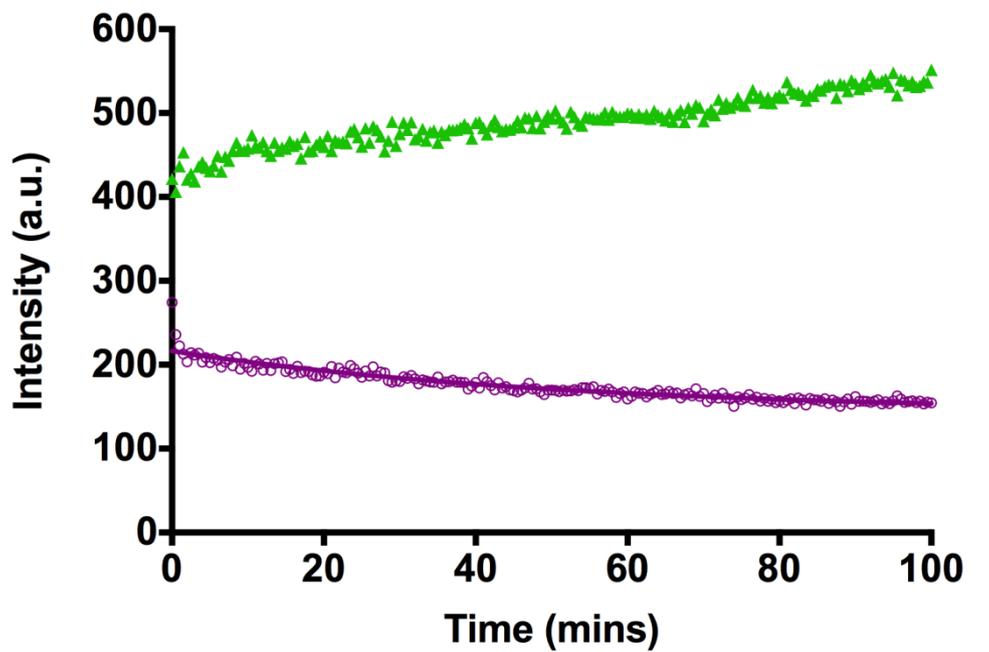
Figure 5.10: The effect of SE extract on the Thioflavin T fluorescence of cystatin B fibrils at pH 4.7. *The extract leads to a considerable drop in fluorescence when added at 0.2mg/ml. Top is a time course monitored over a longer time (100 minutes) to observe any long term effects. A control of cystatin B fibrils without addition of SE extract is shown in green. The bottom time course shows the rapid decrease in ThT fluorescence within the first few seconds when SE extract was added at 20 seconds to cystatin B fibrils (arrow).*
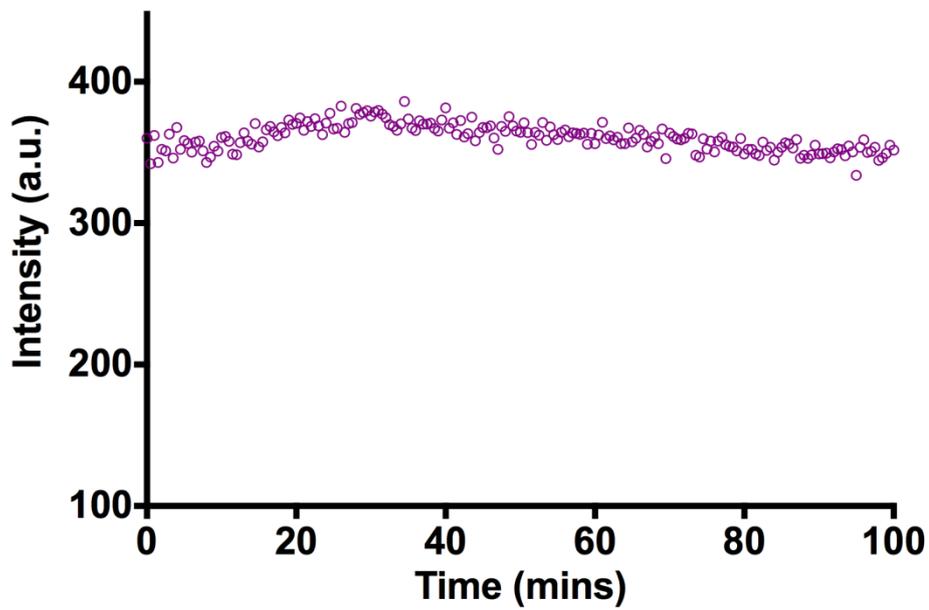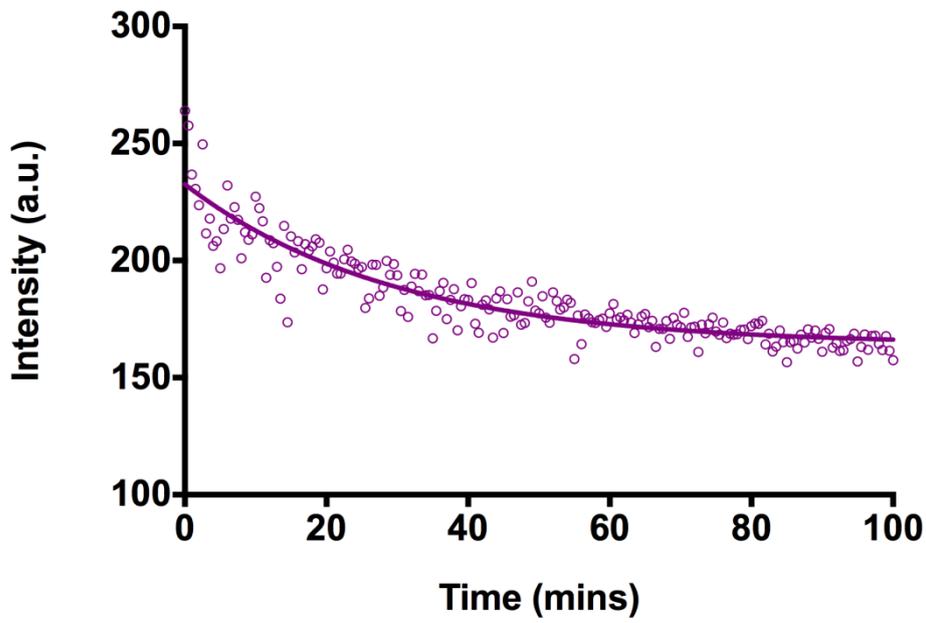
Figure 5.11: Dilutions of SE extract show varying levels of activity. *SE extracts remains active at 10x dilution (top) Further dilution of SE to 50x renders it ineffective on 30µM cystatin B fibrils.*

EM Time Courses of Amyloid fibrils incubated with SE extract

Due to the potentially misleading and inconclusive data from the ThT time courses, it was decided that an electron microscopy time course would be a good alternative. A new sample of cystatin B fibrils was treated in the same way as for the ThT timecourse where 1mg/ml SE extract was added to a 30µM fibril sample. 2µl aliquots of this reaction were taken at time points and put on a grid. Each time point is defined as the time at which the EM grid was placed in the stain after the extract was added.

Cystatin B Fibril Time Course

As one can see in figure 5.12, the time course does show that cystatin B fibrils incubated with SE *Salvia* extract are remodeled over time to form amorphous aggregates. Distinctive amyloid fibrils are still seen after 40s and indeed fibrils can still be seen after 1hr although many are noticeably shorter. After 2 hours, however, there are only small fibrils and the grid is covered in amorphous aggregate. After 4 hours there is almost no fibril to be seen, and almost all protein which can be seen on the grid is amorphous. It is noticeable that small droplet-like species are seen to crowd around the fibrils after 10 minutes. The identity of these species, whether extract or protein, is unclear.

0 s (DMSO control)

1 µm

0 s (DMSO control)

0.5 µm

40 s

1 µm

40 s

0.5 µm

10 min

0.5 µm

10 min

1 µm
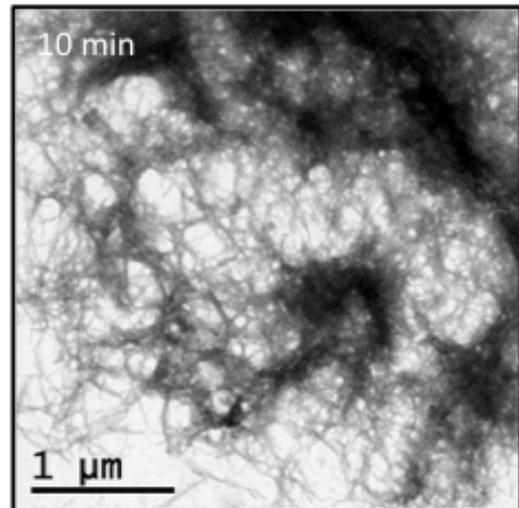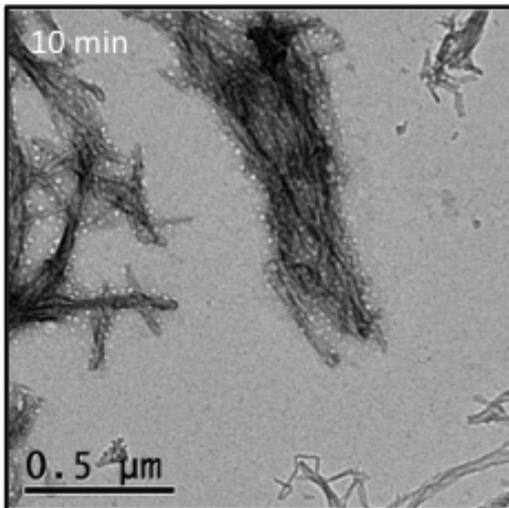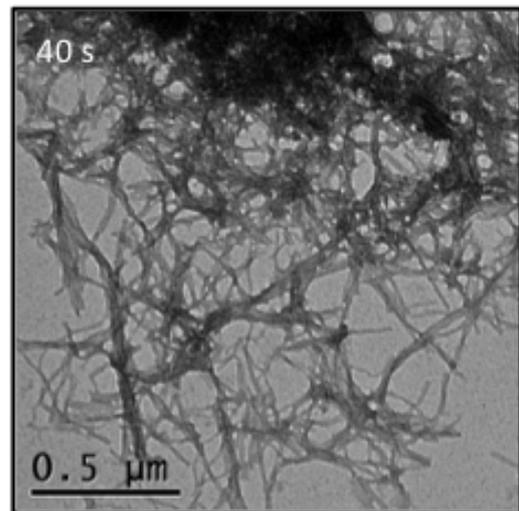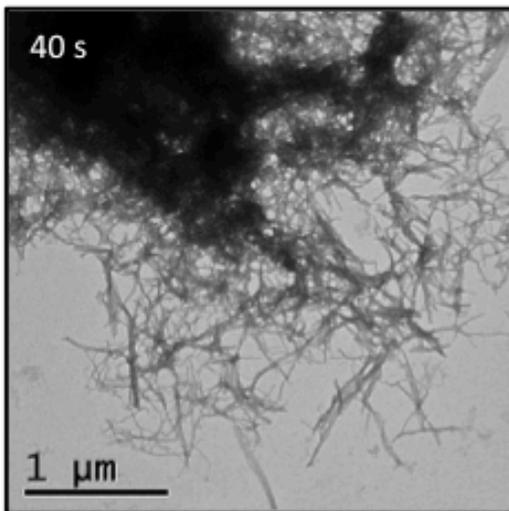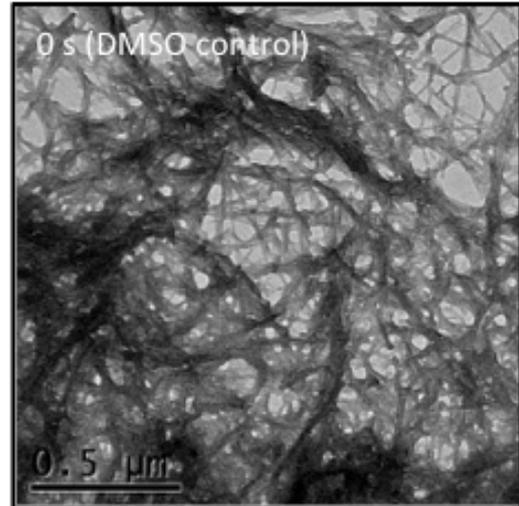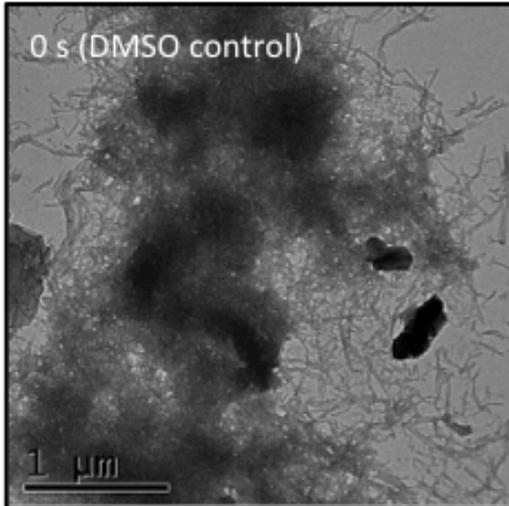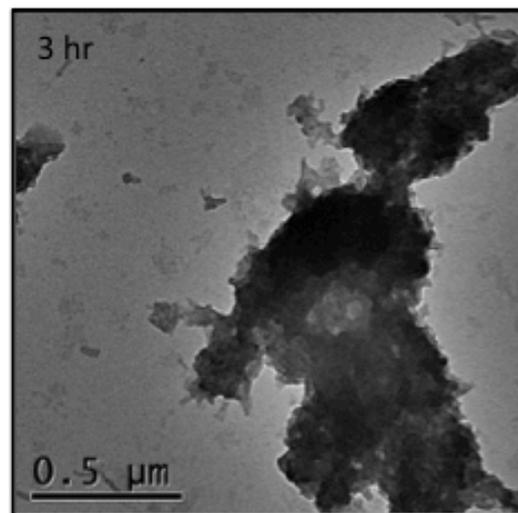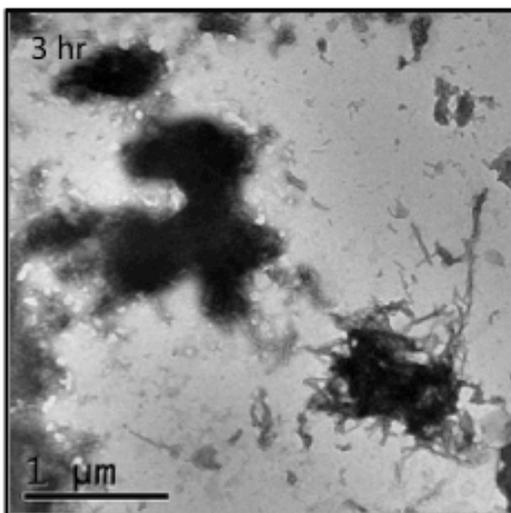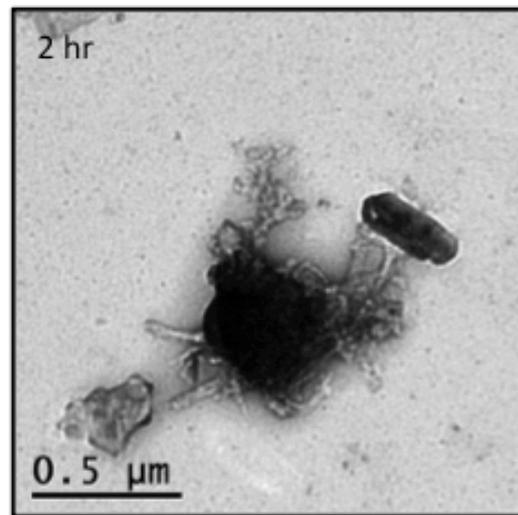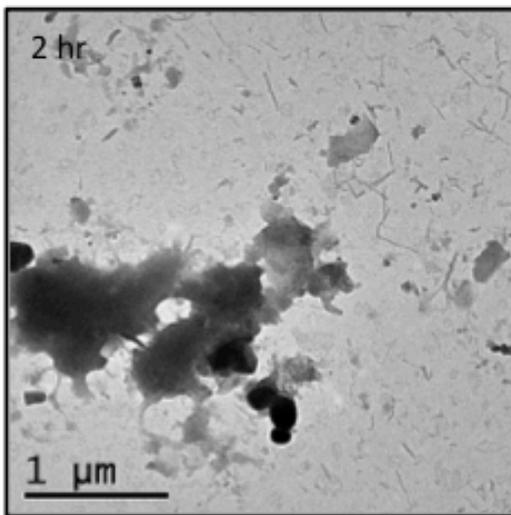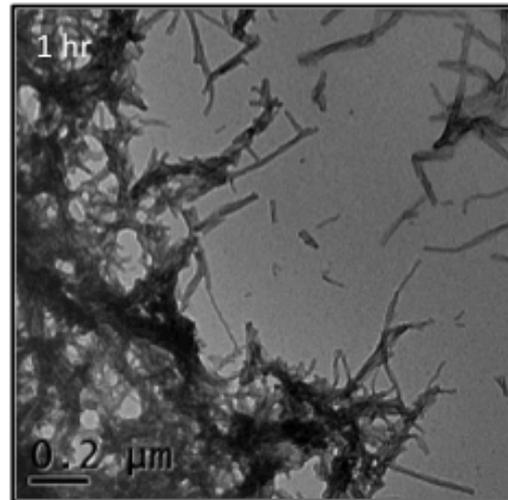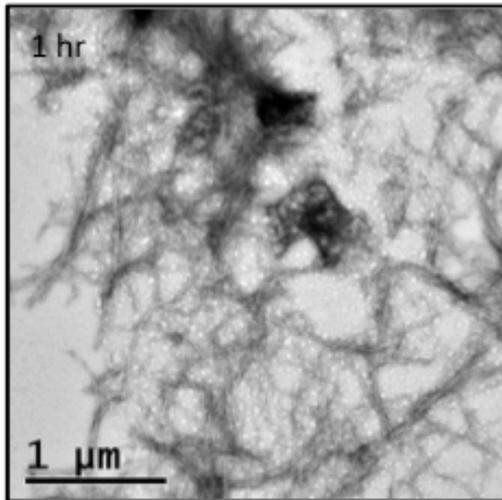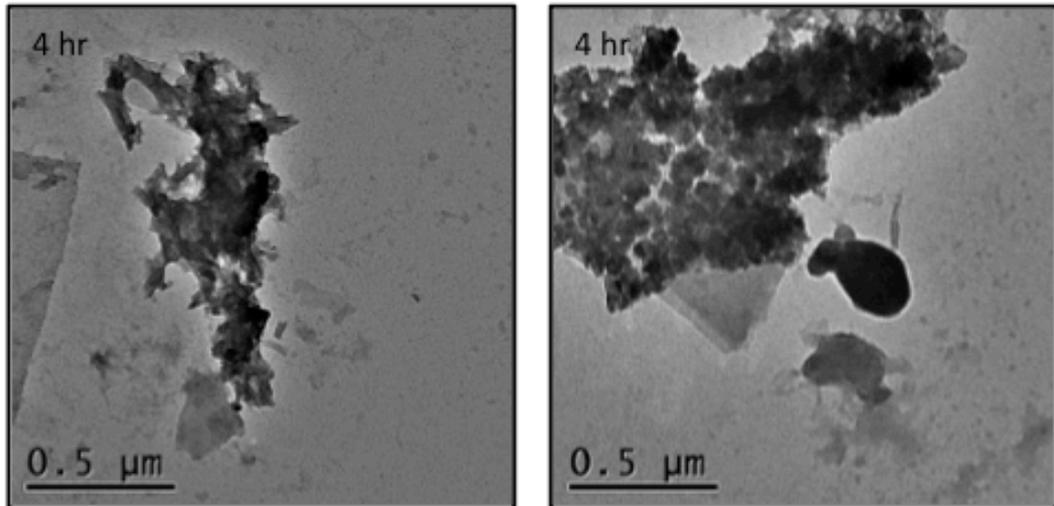
Figure 5.12. EM Timecourse of WT cystatin B fibrils incubated with SE extract.
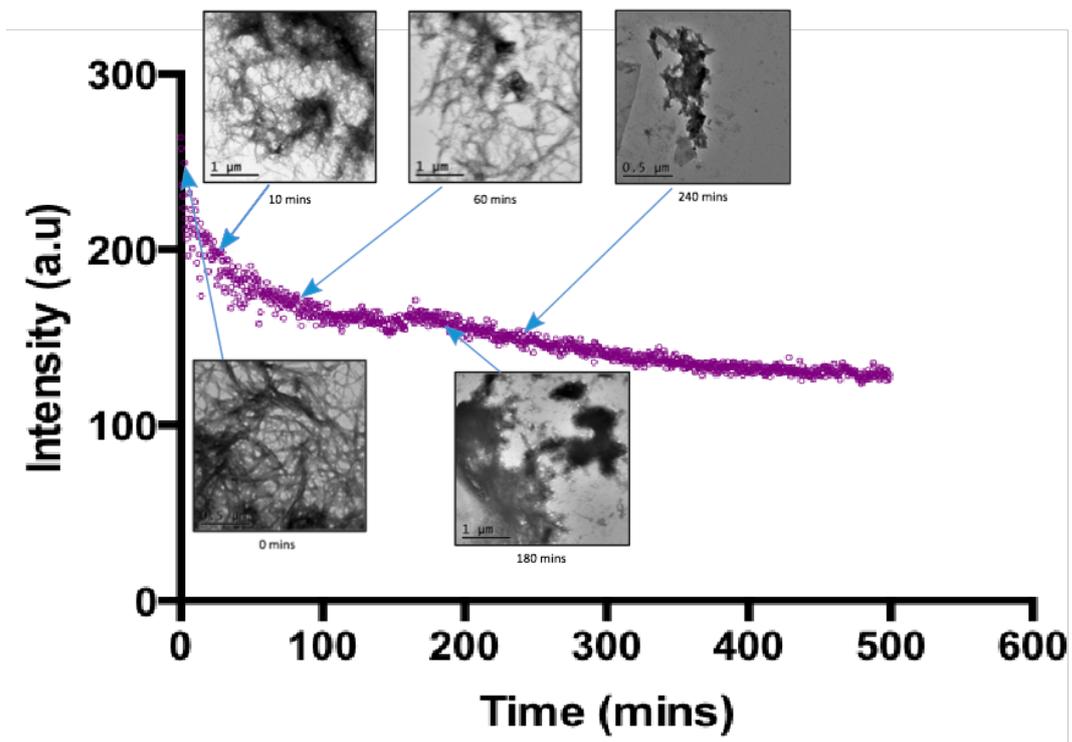
Figure 5.13. The discrepancy between the observed drop in ThT fluorescence and the change in morphology of the cystatin B fibrils.

Figure 5.13 shows the EM time course images superimposed on a ThT defibrillisation experiment. This clearly shows that the ThT data does not match up with the EM time-course data. Whilst SE extract does remodel the fibrils, this happens over hours-not over 20 seconds. The ThT data suggests that binding to the amyloid is likely to be rapid (~20s) while re-modelling is slow.

A-synuclein Fibril Time Course

To ascertain whether this effect on amyloid fibrils was limited to cystatin B fibrils, fibrils made from α-synuclein were incubated with SE extract. Figure 5.14 shows that the SE extract also remodeled the α-synuclein fibrils into amorphous aggregate. Again, droplet-like species are seen surrounding the amyloid. In this time course, the dissolution occurs more rapidly, with clearly modified morphologies apparent after 10 minutes. The active compound(s) within the extract are clearly not protein specific and instead must bind to general structural features of amyloid fibrils.
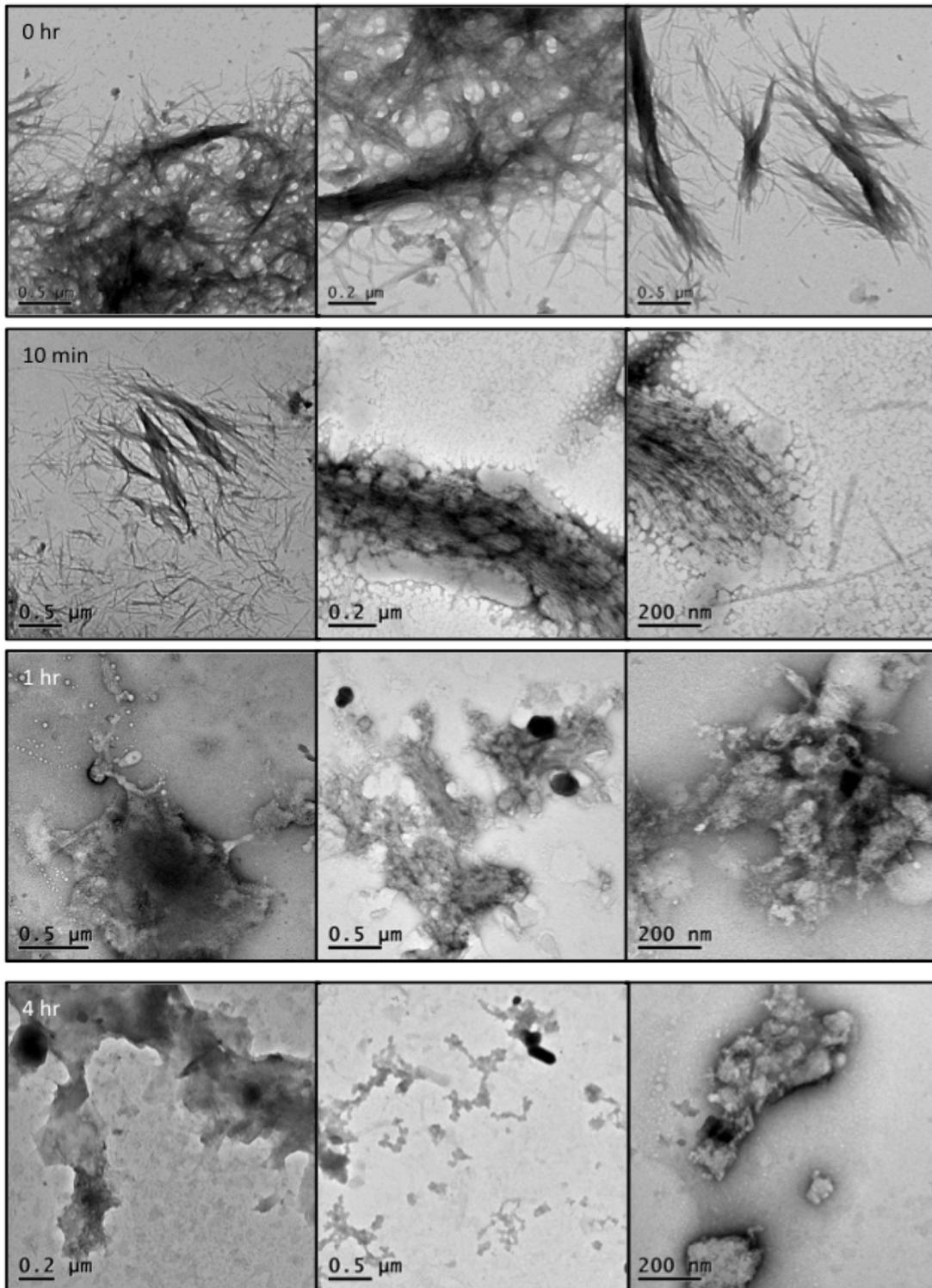
Figure 5.14. EM Time Course of α-synuclein fibrils incubated with SE extract.

Aβ₁₋₄₀ Fibril Time Course

Finally, SE extract was tested against Aβ$_{1-40}$ fibrils, prepared as detailed in section 2.4.2. Again, dissolution is evident and apparent very rapidly, within the first minute of incubation.
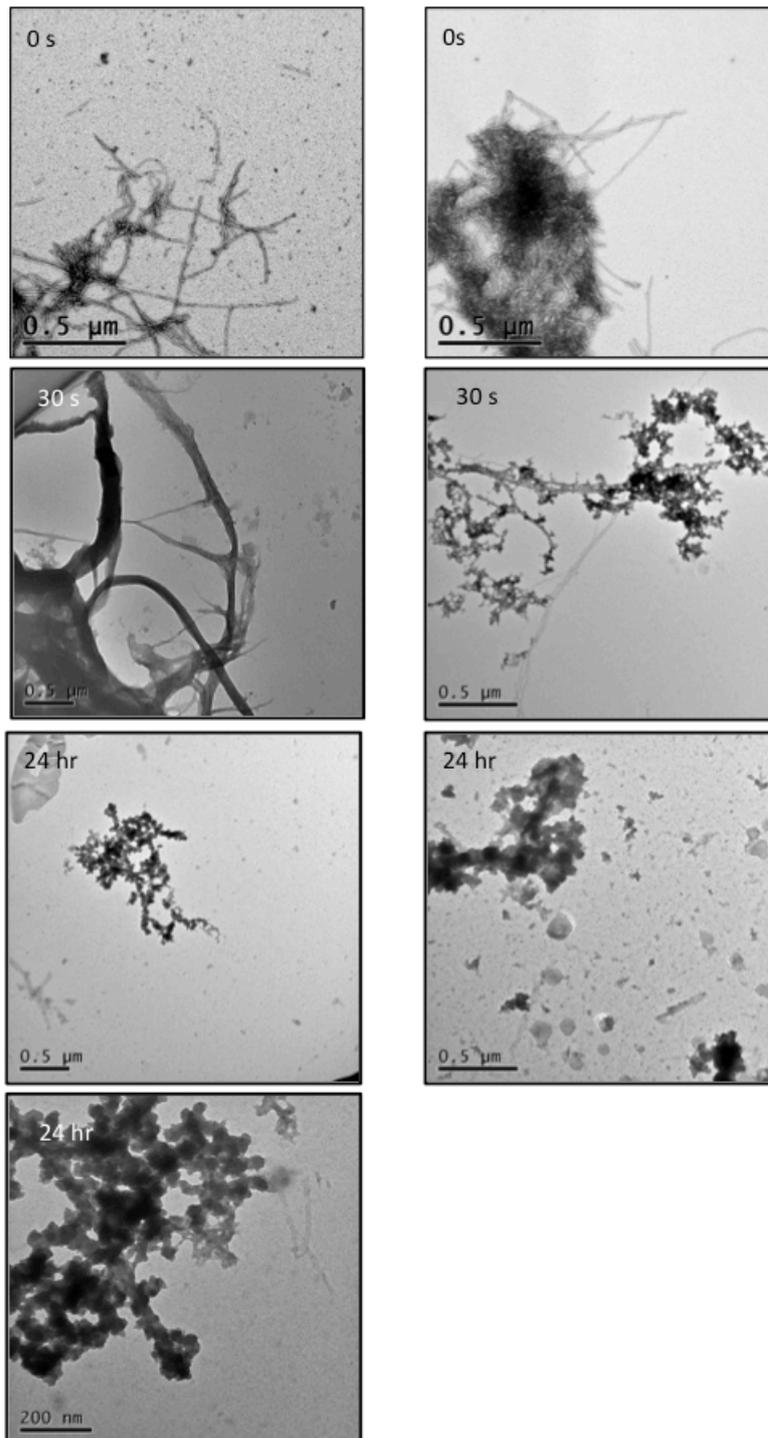
Figure 5.15. EM Time course of Aβ$_{1-40}$ fibrils incubated with SE extract

EM of SE extract without fibrils

To investigate the nature of the droplet-like species, control grids were prepared with only SE extract in the absence of any protein. Figure 5.13. suggests these droplets are indeed a component of the extract although they are present only in small patches of the grids. The localization of these species to the amyloids on the protein containing grids suggests an affinity for these species. Their organization into droplets lends further support to existing literature on the mechanism of compounds such as EGCG – the current hypothesis is that this compound forms colloidal arrays surrounding the amyloid aggregate (Palhano et al. 2013).
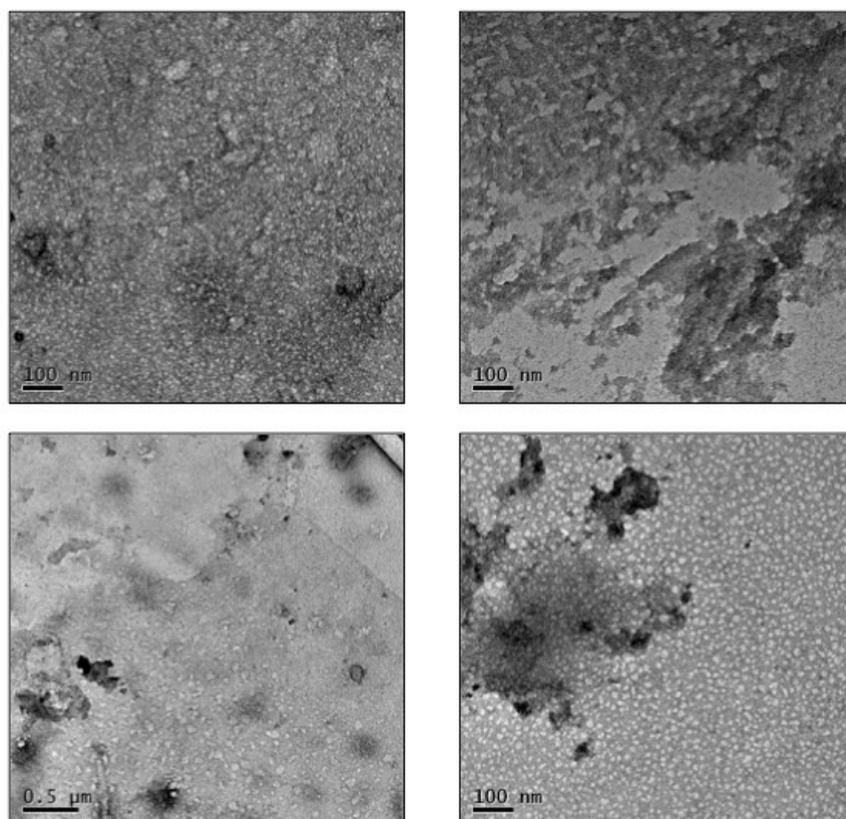
Figure 5.13. EM micrographs of 1mg/ml SE extract incubated in the absence of protein.

5.3.4 Exploring the mechanism of the *Salvia* extracts anti-amyloid activity

Does SE extract stabilize Aβ ADDLs and oligomers?

STD NMR

STD NMR was originally proposed by Airoldi et al (2013) as a valid method for the identification of compounds that can bind A$\beta_{1\text{-}42}$ oligomeric species. In their study, they identified rosmarinic acid as an active component of the SD or butanol extract from *Salvia sclareoides*. The 1D ^{1}H NMR spectrum of the SE extract was compared with rosmarinic acid and shown to lack this compound in any significant quantity. Its active ingredient is therefore likely to be something else given its similar anti-amyloid activity.

Due to the lack of homogeneity in "oligomeric" Aβ samples it was thought that ADDLs would be a better species of A$\beta_{1\text{-}42}$ to use to assess binding. One of the difficulties of using A$\beta_{1\text{-}42}$ for these sorts of studies is that A$\beta_{1\text{-}42}$ is able to form a vast number of different species when incubated at room temperature in PBS. Therefore, a model for A$\beta_{1\text{-}42}$ is an important requirement.

Two different protocols were used to prepare ADDLs. The first was a standard protocol adopted by our lab and produced oligomers of similar size as probed by EM (Figure 5.14A). We also attempted to reproduce previous work by Airoldi et al (2013) on *Salvia sclareoides* extracts: the preparation of A$\beta_{1\text{-}42}$ species produced using their protocol (section 5.2.3) is shown in Figure 5.14B. In their protocol whilst ADDLs are present, other oligomeric species of A$\beta_{1\text{-}42}$ are present as well.
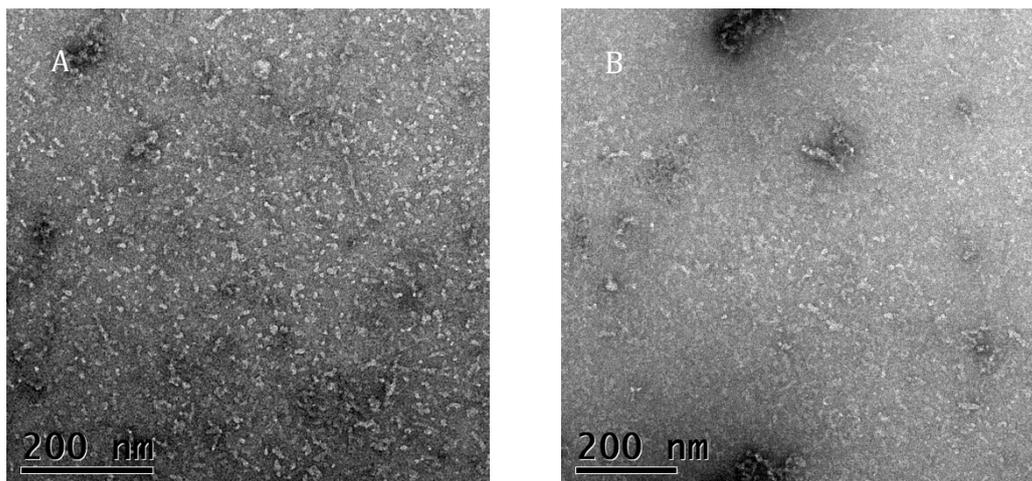
Figure 5.14. ADDLs prepared using two different protocols. *In (A), methods adapted for NMR spectroscopy by Klein et al. (2002) and Ryan et al. (2010). In (B), the method adopted by the Rauter group (Airoldi et al., 2013).*

The principal difference between these two protocols is that, while the former technique involved the addition of relatively mature, stable ADDLs incubated for 24 hours and shown previously to remain stable at room temperature for at least 5 days, the latter preparation involves co-incubation of all soluble species, when freshly prepared from the monomeric $A\beta_{1-42}$ peptide. As shown in section 5.3.1, under the latter conditions, the SE extract stabilizes oligomeric species: here we aimed to identify the compounds responsible.

The 1D ^{1}H NMR spectra of ADDLs in the presence and absence of SE extract are dominated by the presence of soluble $A\beta_{1-42}$ species. It was envisaged that these species would not disturb the interaction of oligomeric "ADDL" $A\beta_{1-42}$ species with the small molecular weight compounds present in the SE extract. However, upon selective saturation of upfield frequencies (on-resonance and off-resonance), a difference spectrum showed very little signal, suggesting few if any compound(s) within SE were binding $A\beta$ ADDLs, or rather that the STD experiment performed here was not sensitive enough (Figure 5.15).

A problem further compounding this experiment was the presence of relatively large molecular weight species in the SE extract. This would add to the lack of specificity in the experiment as compounds binding to these species would also be identified. A control STD experiment was performed to rule out the possibility of saturation transfer within the extract constituents (Figure 5.16). The STD revealed no signals outside the noise.

The SE extract was ultracentrifuged to remove insoluble plant matter and the resulting NMR spectrum revealed a considerable loss in signals (Figure 5.17). This clarified SE extract was just as effective as judged by EM defibrillisation assays but had fewer components to complicate STD.
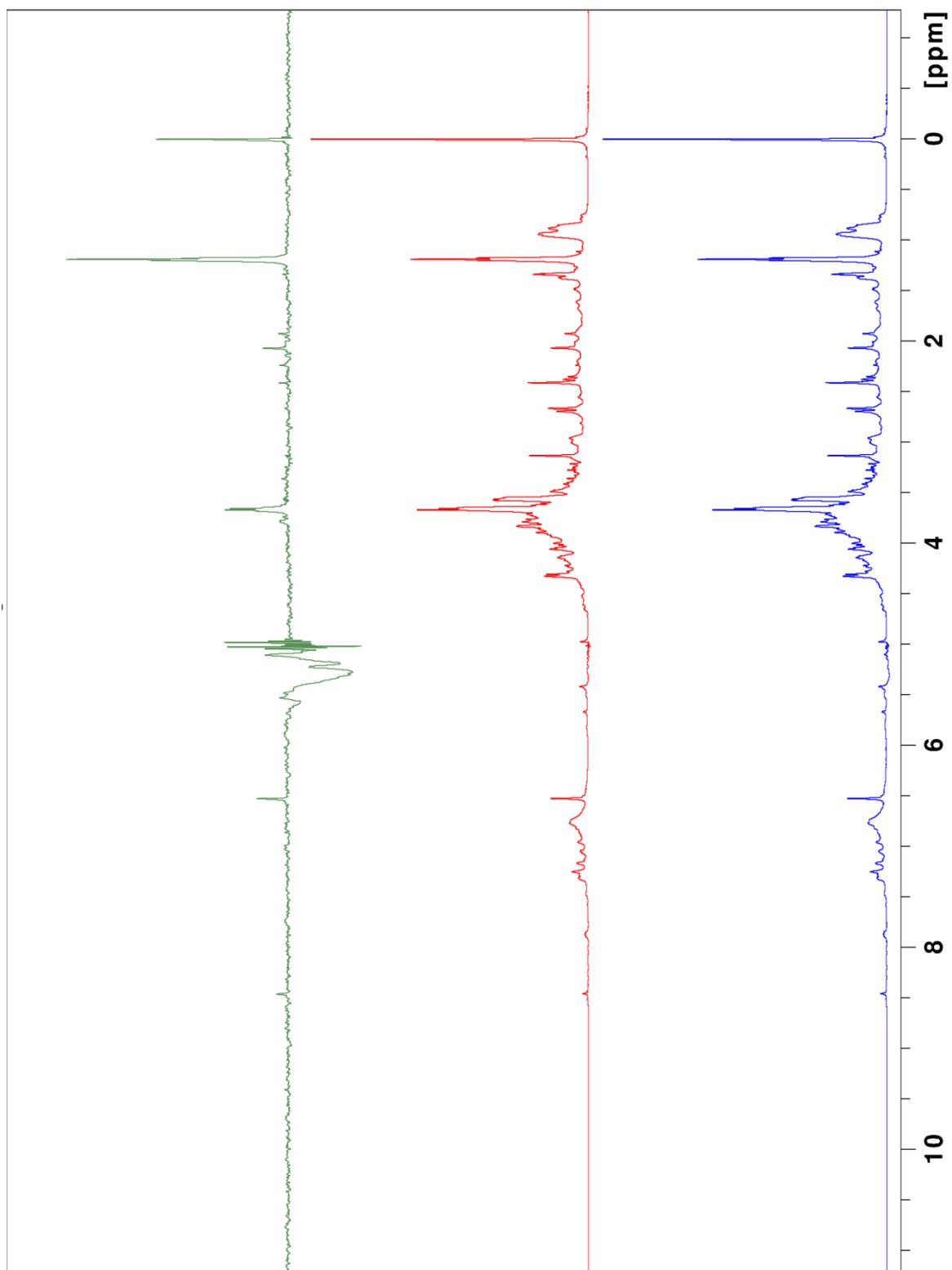
Figure 5.15. STD experiment of Aβ₁₋₄₂ ADDLs incubated with SE extract*. The off-resonance 1D ¹H NMR spectrum of the ADDL&SE sample (blue) and the on-resonance spectrum of ADDLs and SE extract (red) show very few differences. The difference spectrum or STD spectrum is shown in green.*
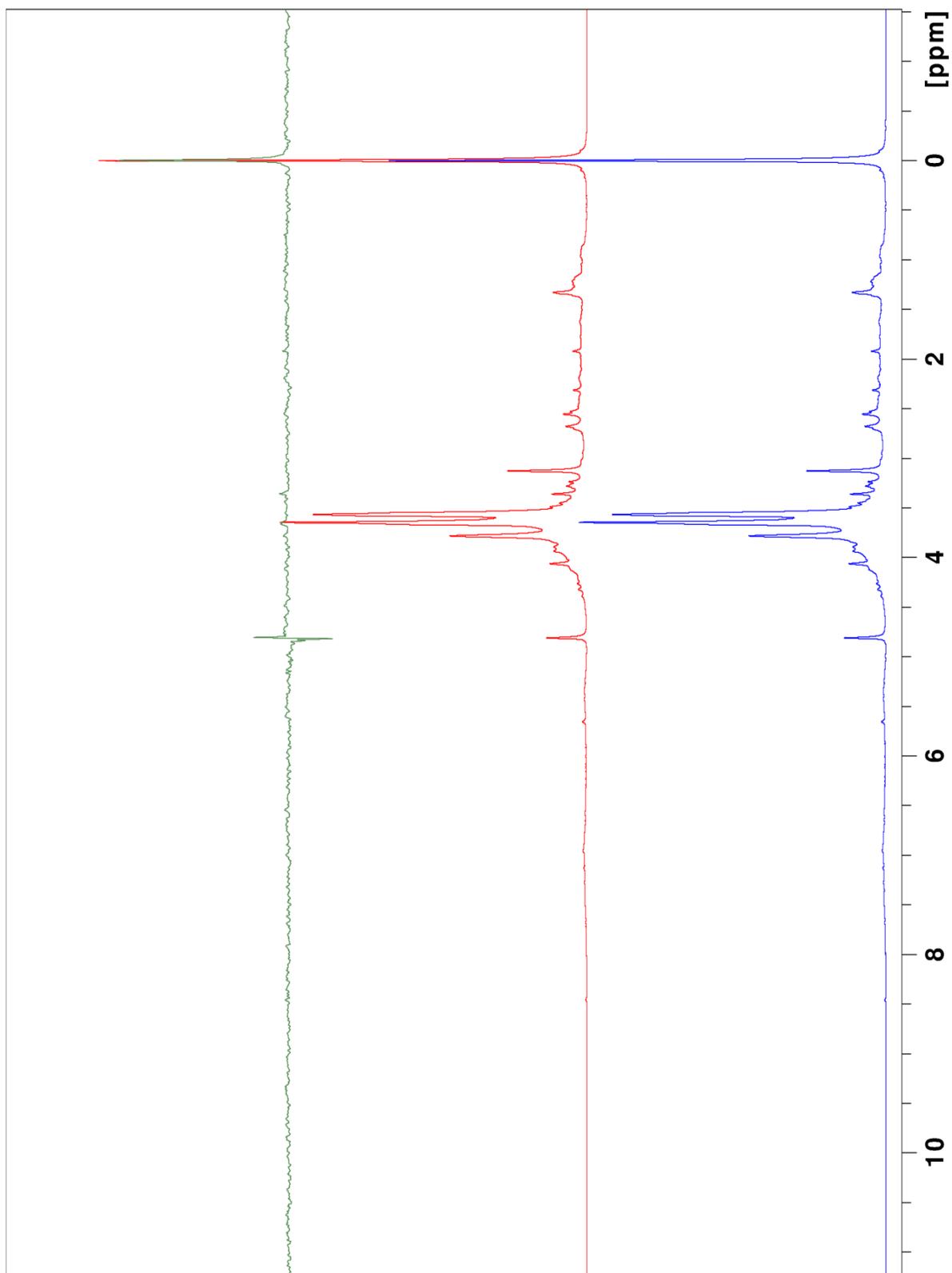
Figure 5.16. Control STD experiment of SE extract. *In blue, off-resonance spectrum, in red the on-resonance spectrum and in green the STD spectrum.*
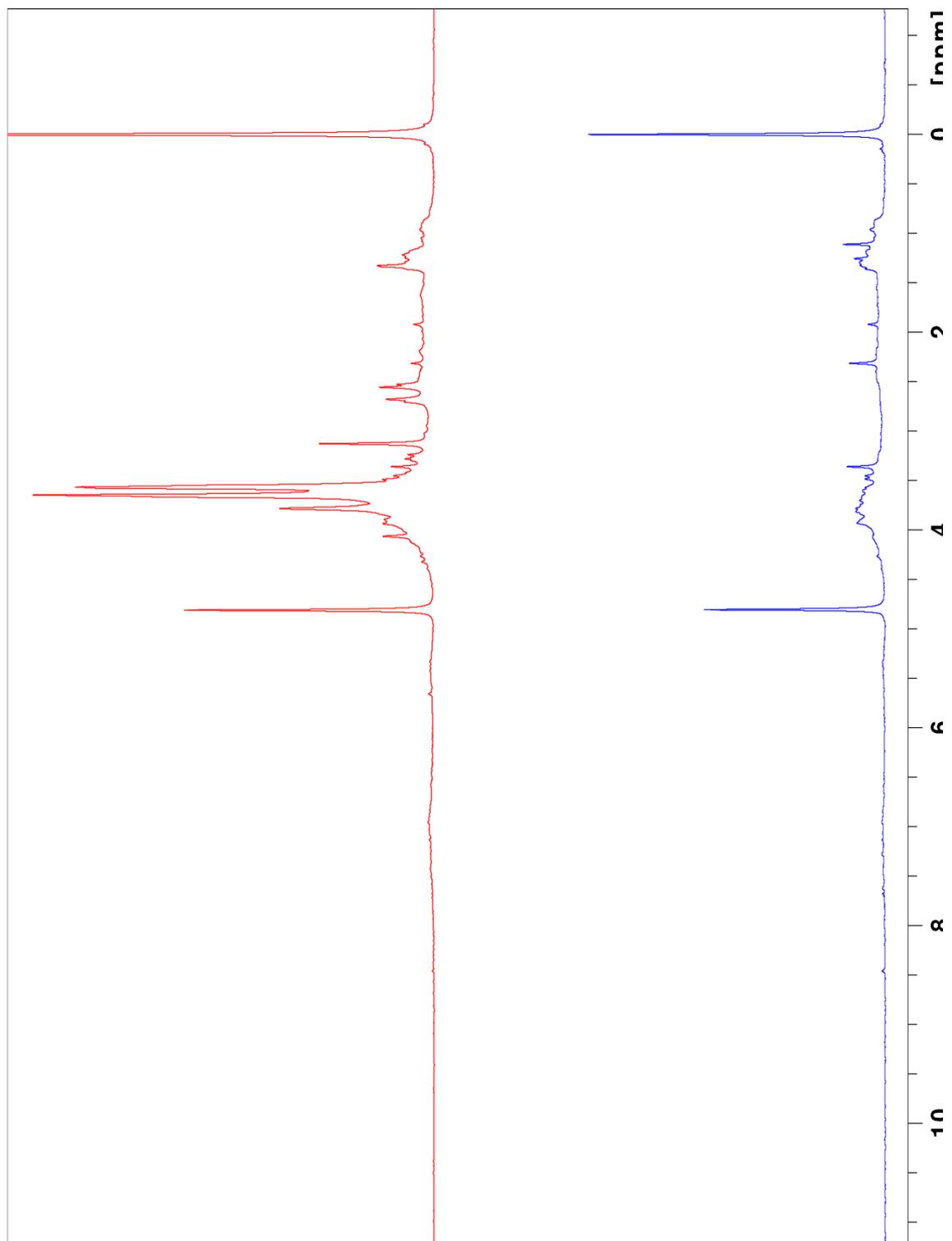
Figure 5.17. 1D ^{1}H NMR spectra of SE extracts before (red) and after (blue) clarification.

The experiment was repeated under the conditions of Airoldi et al. (2013) who had successfully identified rosmarinic acid as an active compound in a different extract. We therefore repeated our experiment in their conditions, adding either SE extract (Figure 5.18) or rosmarinic acid as a control (Figure 5.19).

Although some evidence of saturation transfer is present in the rosmarinic acid control, the lack of strong signals in the STD experiments with SE extract suggested that the concentration of bound species was insufficient to create a large enough signal or the rate of transfer between the free and bound species was too slow. It could also be that the species that the active compound binds to is present at too low a concentration. Furthermore, it is possible that there is a complete lack of interaction between compounds in the extract and oligomeric $A\beta_{1-42}$. Analysis by electron microscopy of the species observed before and after incubation with SE extracts or rosmarinic acid is shown in figure 5.20 and shows remarkably little morphological change. This could be explained by the ADDLs not being the correct species model for observing any interaction between SE extract and amyloid.
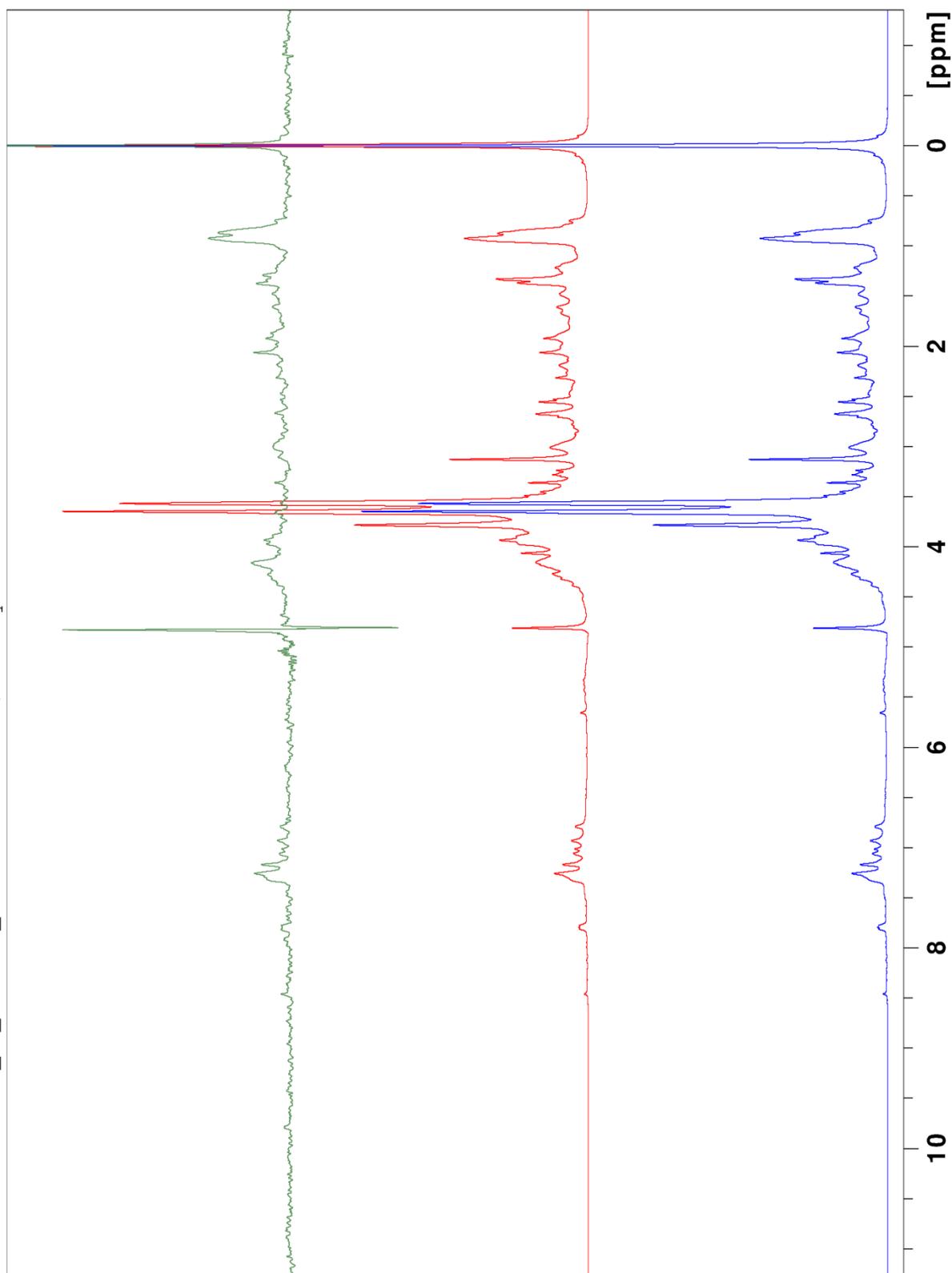
Figure 5.18. STD experiment of "soluble" Aβ₁₋₄₂ incubated with clarified SE extract according to Airoldi et al (2013). *Off-resonance spectrum (blue), on-resonance spectrum (red). In green, the STD spectrum shows essentially no signal.*
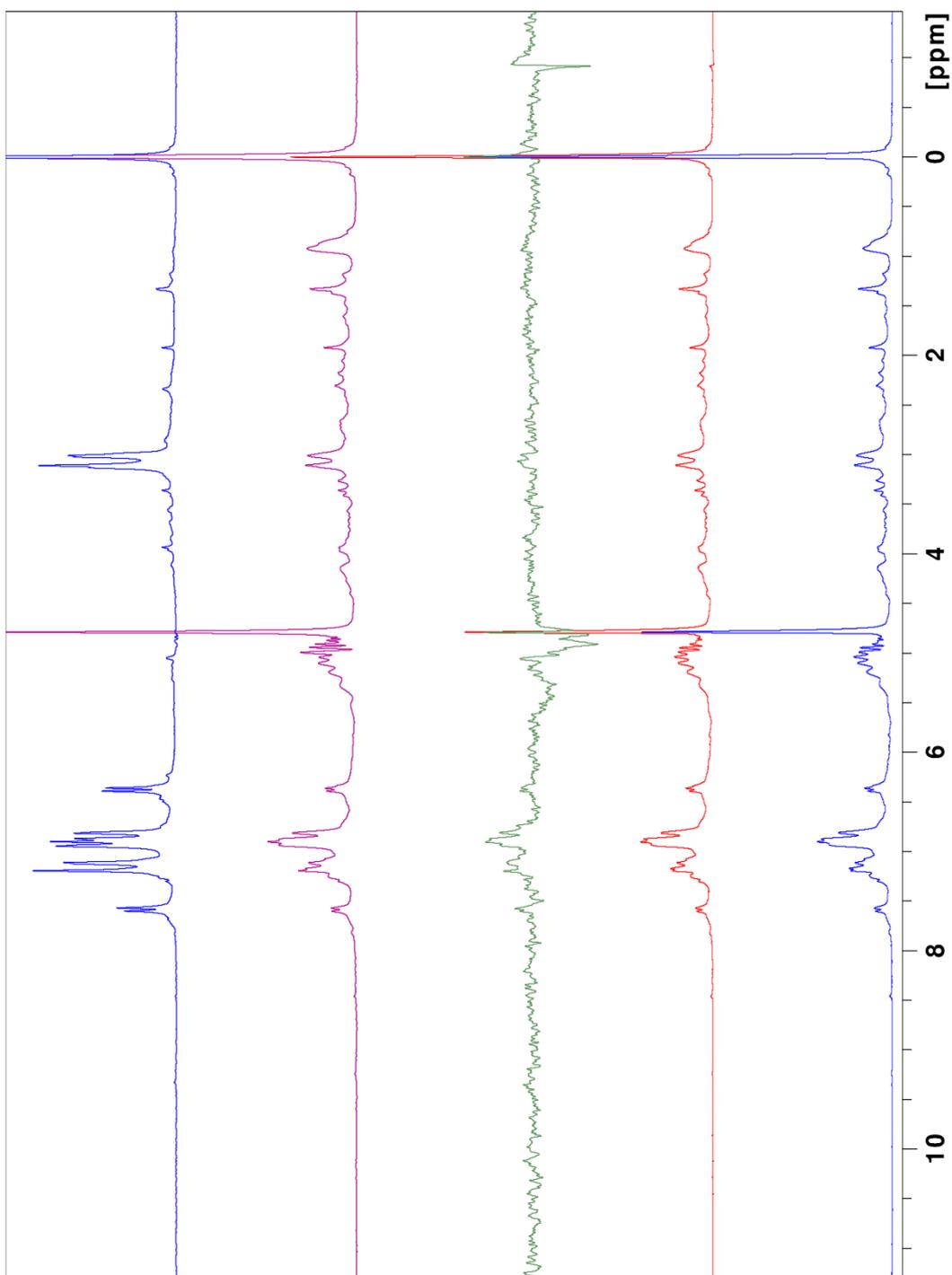
Figure 5.19. STD experiment of "soluble" Aβ$_{1-42}$ incubated with rosmarinic acid according to Airoldi et al (2013). *1D 1H NMR spectra of rosmarinic acid (top blue) and Aβ$_{1-42}$ with rosmarinic acid (purple) are shown for comparison to the STD difference spectra in green. The STD off resonance spectra for Aβ$_{1-42}$ is shown in red and the on resonance spectra is shown in blue at the bottom of the figure.*
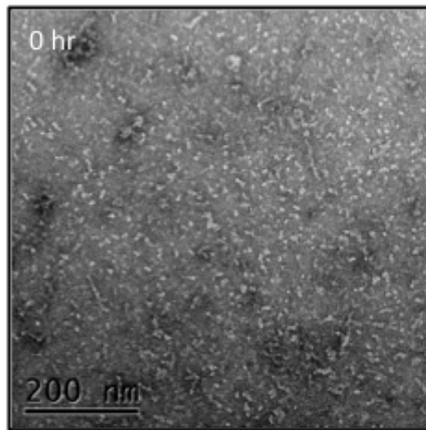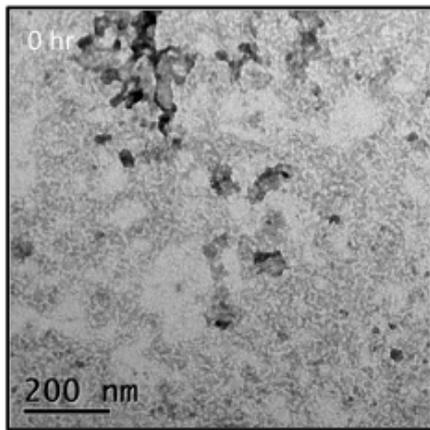
SE 1mg/ml
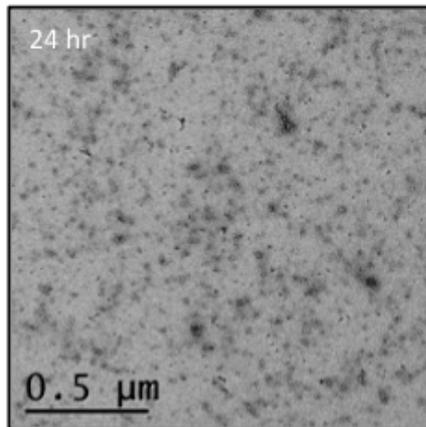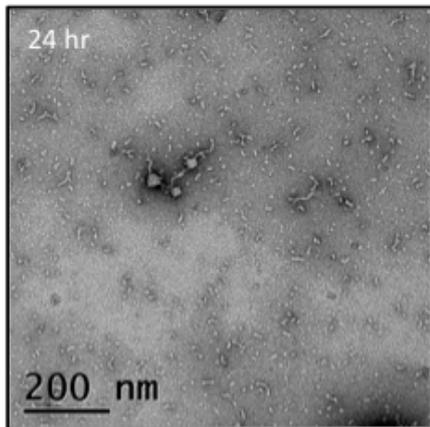
Rosmarinic Acid 1mM
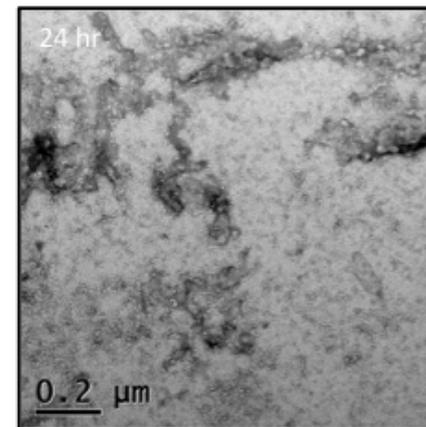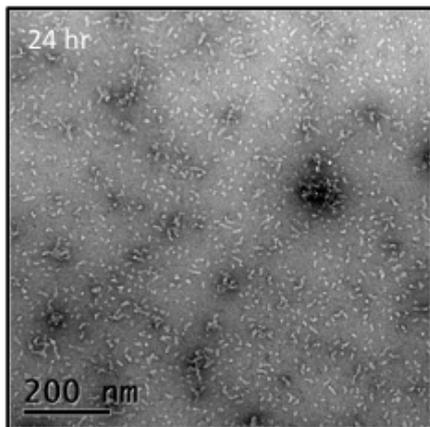
Figure 5.20. Aβ ADDLs before NMR and after 24 hour NMR experiment. *Top micrographs show freshly prepared Aβ ADDLs before addition of extract. Middle micrographs show ADDLs after 24 hour incubation with SE extract. Bottom micrographs show ADDLs after 24 hours incubation with rosmarinic acid.*

174

STD is not a valid method for observing interaction of extracts with Aβ$_{1-42}$ oligomers

A number of control experiments were performed which helped explain the observations of Airoldi et al. but also discounted their protocol as a valid route to identification of the active compound in our conditions. Given the mixture of large and low molecular weight species in the Aβ$_{1-42}$ sample, saturation transfer is occurring both between the extracts and the oligomers and between the soluble Aβ$_{1-42}$ species and the oligomers, meaning that the frequencies observed in the STD spectrum not only overlapped with Aβ$_{1-42}$ signals but were Aβ$_{1-42}$ signals. This was verified in a control not containing the SE extract (Figure 5.21). While one possible solution to this problem could be to subtract the control spectrum from that with the SE extract, thereby removing the spectrum of any soluble Aβ$_{1-42}$ species able to interact with the oligomers. However, as shown in figure 5.22 this is not possible since the spectra observed for Aβ incubated with SE extract is remarkably different from that of Aβ alone. This suggests that the nature of the species present in the control experiment was, perhaps unsurprisingly, different to that observed in the presence of the SE extract.
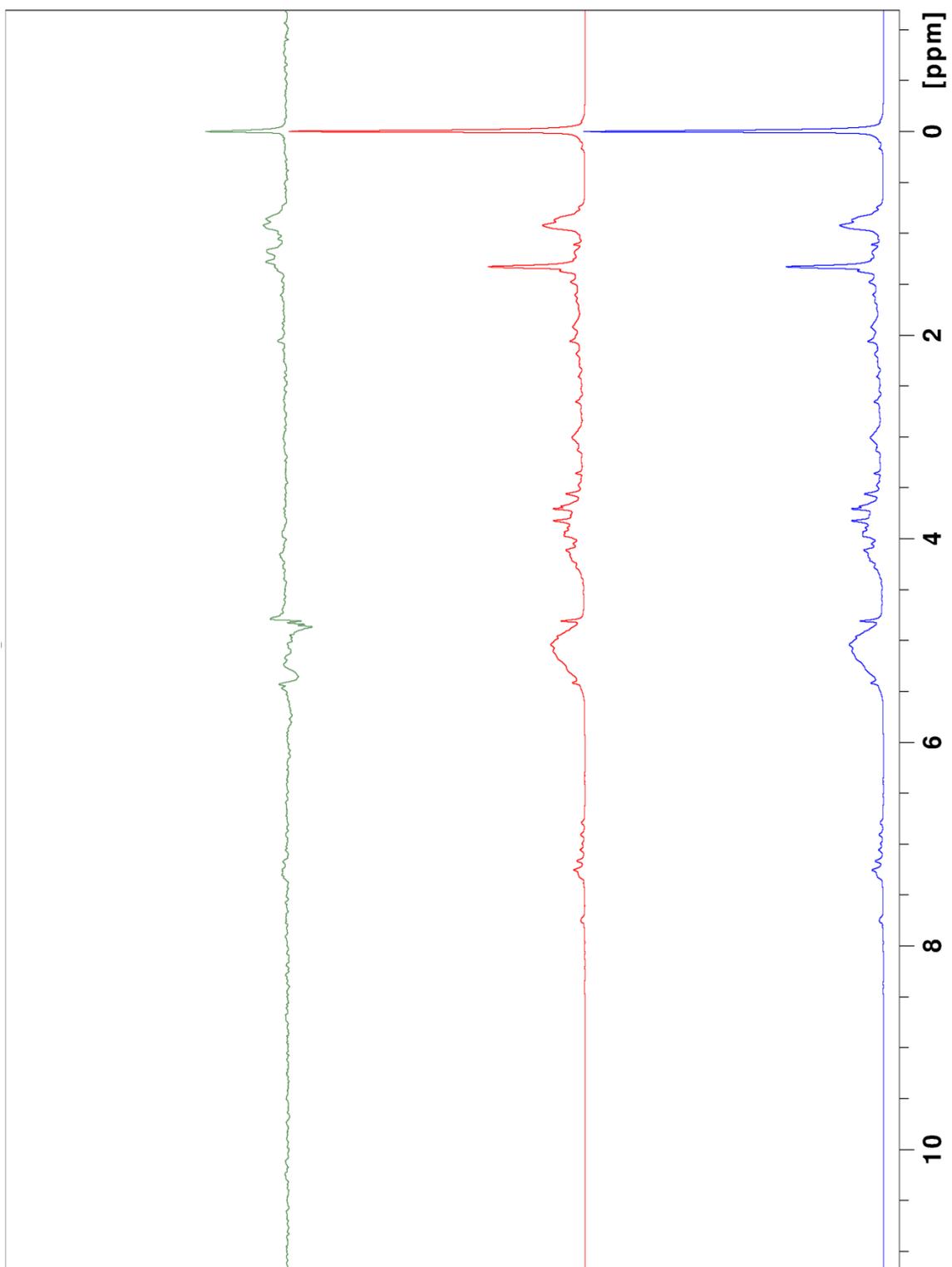
Figure 5.21: Control STD experiment of Aβ₁₋₄₂ alone. *The off resonance spectrum is shown in blue, on resonance in red and the difference spectrum is shown in green.*

.
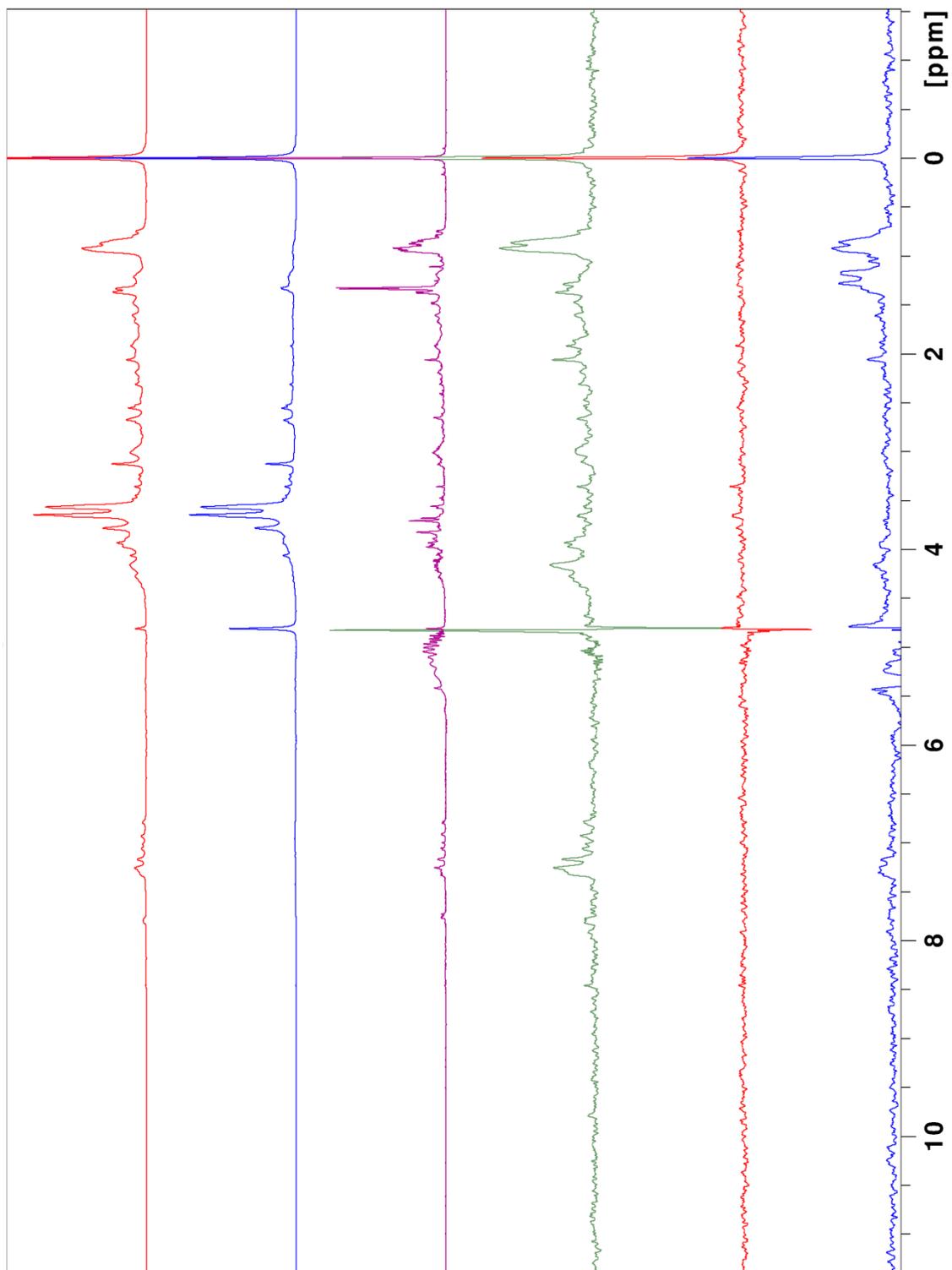
Figure 5.22: *From the top: 1D 1H NMR spectrum of Aβ$_{1-42}$ incubated with SE extract (red), 1D 1H NMR spectrum of SE extract (blue), 1D 1H NMR spectrum of Aβ$_{1-42}$ (purple), STD difference spectrum of Aβ$_{1-42}$ incubated with SE extract (green) STD difference spectrum of SE extract (red) and STD difference spectrum of Aβ$_{1-42}$.*

A NOESY experiment comparing SE extract alone with Aβ mixed with SE extracts was carried out to see if NOEs could be detected between species in the Aβ sample and the SE extract (Figure 5.23). Very small peaks may be detectable but it was unclear whether these were outside the noise of the experiment. A more concentrated sample of SE extract and a sample of Aβ with more "binding partner" would be needed to examine this further using this technique.

DOSY measures the diffusion coefficient of different species in solution and when bound, a shift is expected to a lower value (towards the top of the spectrum in Figure 5.24). Although some shifts are seen, it is difficult to dissect those which are solely due to binding between Aβ and compounds in the SE extract as interactions with any other Aβ species would result in the same shifts. This is because the chemical shifts of Aβ overlap with those of the compounds in the SE extract.
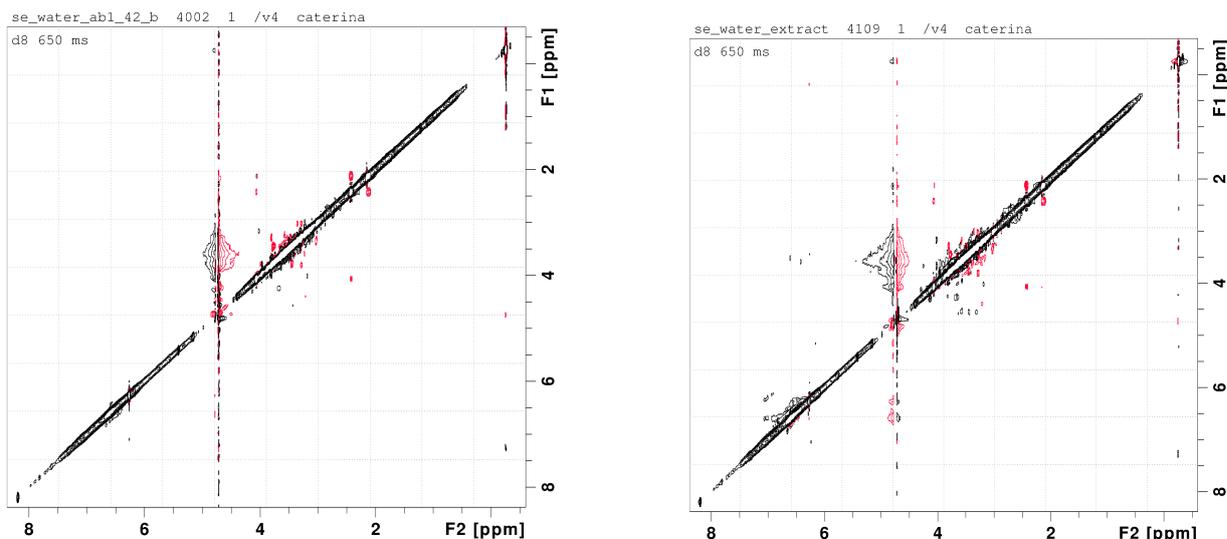
Figure 5.23: NOESY spectrum of SE extract incubated with Aβ ADDLs. *Left hand spectrum shows SE extract incubated with Aβ. Small ligands display a different sign when in solution (positive) to when they are bound to a receptor protein (negative). There are small changes in the spectrum when Aβ is not present (right hand spectrum).*
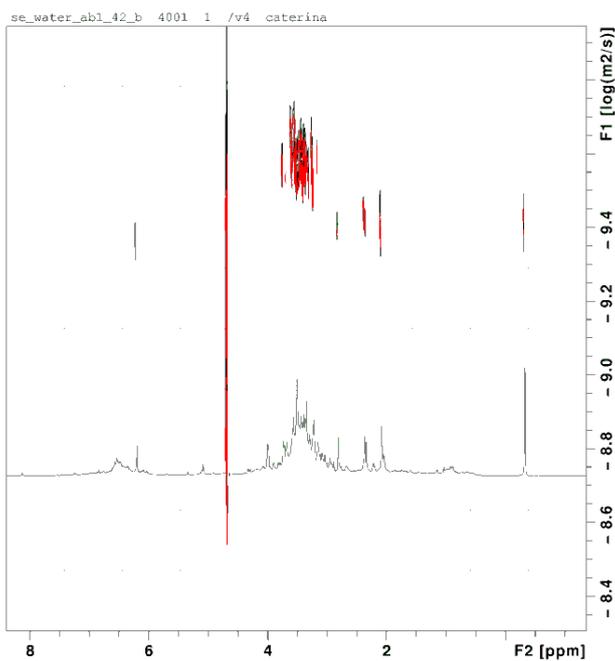
Figure 5.24: DOSY spectrum of SE extract incubated with Aβ ADDLs. *Black is SE extract and Aβ. Red is SE extract alone. 1D 1H NMR spectrum of the sample is shown in green. The experiment was inconclusive due to an overlap between the spectra.*

5.4.5 What is the active compound(s) in SE extract responsible for anti-amyloid activity?

Due to the difficulties encountered with NMR such as the lack of a homogeneous $A\beta_{1-42}$ sample and the possibility of protein being present in the extracts, a protocol was devised whereby bound ligands to $A\beta_{1-42}$ fibrils could be analysed by mass spectrometry. 80µM $A\beta_{1-42}$ fibrils were incubated with high concentrations (10mg/ml) SE extract for 10 minutes before five repeated rounds of centrifugation were used to separate the compounds bound to the fibrils from those remaining in solution. Four washes, a supernatant and a final solubilised pellet sample were collected and analysed directly by mass spectrometry. A full method can be found in section 5.2.5. A control sample of SE extract spun down on its own in the absence of $A\beta_{1-42}$ was also analysed.

Table 5.1 shows the molecular weights identified in different samples analysed by mass spectrometry. Masses present in both the control pellet and the $A\beta$ containing samples were discounted. Only the solubilised pellet samples contained masses which were also present in the control. The experiment seemed to distinguish very well between weakly bound species and higher affinity binders because the compound masses present in washes 1 & 2 were generally distinct from those found in washes 3 & 4. The full mass spectra and tables of masses for all samples can be found in the appendix. The analysis therefore focused on compound masses in washes 3 & 4 and the solubilised pellet since these represented the ligands with the highest affinity for the $A\beta$ fibrils. The human metabolome database was searched for matches (http://www.hmdb.ca/, last accessed August 2016). The reasoning for this is the ease of use of this library and its previous application to searches for plant phenolics in strawberries, grains and olive oil (Rohloff, 2015).

Likely candidates for some of the identified masses are listed in Table 5.1. It is notable that rosmarinic acid is absent from this list. For a number of masses, there may be more than one possibility even within this library. However, given the similarity of the compounds, it is just as likely that both compounds

exist in the mixture. The phenolic nature of the proposed compounds and in a number of cases, their known plant origin, validated the analysis further.

Potential constituents include molecules that resemble known anti-amyloidogenic compounds but also include a number of new substances. For example, oleacein, which is also found in olive oil is found in this analysis and has been reported previously to have anti-amyloid properties (Rigacci et al, 2010). Oxidised camphor was also found here but, to our knowledge has not been directly reported as having anti-amyloid activity although it is used in a number of existing medicinal products such as "vaporubs". At least 2 of the compounds are easy to source from chemical suppliers such as Sigma-Aldrich and so a next step in this analysis would be to validate their individual activities. These include β-Sitosterol β-D-glucoside (similar in structure and functional groups to β-Sitosterol 3-O-β -D-galactopyranoside) and Camphoric acid.

In addition to the Q-tof mass spectrometry presented here, gas phase mass spectrometry would allow for further analysis of these samples as it would enable more accurate identification of the components by analysing their fragmentation products: different compounds yield different and predictable patterns of breakdown products.

Name of Compound	Chemical Formula	Structure	Average MW	Description
β-Sitosterol 3-O-β-D-galactopyranoside	$C_{35}H_{60}O_6$		576.8473	Found in many herbs and spices. Has been identified as an anti-oxidant and anti-inflammatory (Naressi et al. 2015, Cakir et al. 2003).
Schottenol 3-glucoside	$C_{35}H_{60}O_6$		576.8473	Has been identified as an anti-cancer agent from *Baccharis coridifolia* and *Ipomopsis aggregate* (plants native to South America) (Arisawa et al. 1985).
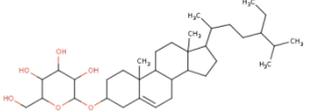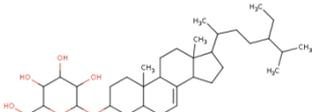
Table 5.1 Possible constituents of Aβ pellet wash as determined by analysis of masses using the Human Metabolome Database

Name of Compound	Chemical Formula	Structure	Average MW	Description
(S)-Oleuropeic acid	$C_{10}H_{16}O_3$		184.2322	Component of fats and oils, including olive oil. Has been previously studied due to its antioxidant activity (Perez-Bonilla et al. 2014)
(1'R)-Nepetalic acid	$C_{10}H_{16}O_3$		184.2322	Found in many herbs and spices, including *Nepeta cataria* (Catnip), an ancient chinese remedy. Extracts from this plant have been used in cancer studies (Emami et al. 2016) and antimicrobial/antioxidant studies (Adiguzal et al. 2009)
(±)-Camphoric acid	$C_{10}H_{16}O_4$		200.2316	Oxidised form of camphor. Camphor has been studied as a dietary agent in the prevention and therapy of cancer (Aggarwal & Shishodia, 2006). It is already in medicinal use as a constituent of Vicks VapoRub.
Hesperaline	$C_{14}H_{22}NO_4$		268.3288	Known constituent of plants in the of *Brassica* family which includes broccoli, cabbage and kale.
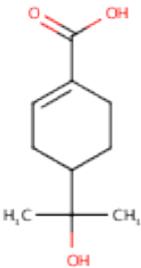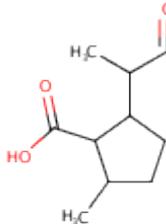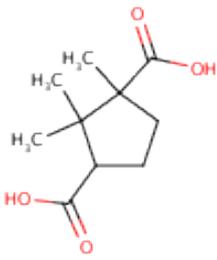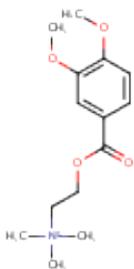
Niazirin	$C_{14}H_{17}NO_5$		279.2885	Is found in *Brassicas.* Is also a known constituent of the leaves of the horseradish tree (*Moringa oleifera*) which has been studied as a cancer therapeutic (Dayal et al. 2013).
Helipyrone	$C_{17}H_{20}O_6$		320.3371	Helipyrone is found in many herbs and spices but is a well known constituent of *Helichrysum italicum* (curry plant). It has been studied for its antioxidant activity (Rosa et al. 2007), as an anti-inflammatory and a HIV therapeutic (Appendino et al. 2007).
Oleacein	$C_{17}H_{20}O_6$		320.3371	Oleacein is a known constituent of olive oil. It has been studied as an anti-amyloid thereapeutic (see chapter 1).
(R)-Pronuciferine	$C_{19}H_{21}NO_3$		311.3749	(R)-Pronuciferine is a plant alkaloid which has been studied for its anticholinesterase inhibitory activity (Dong et al. 2015) and as a cancer therapeutic (Wang et al. 2004).
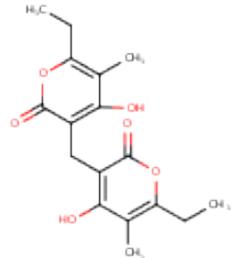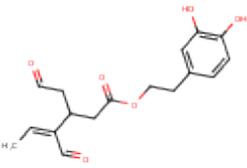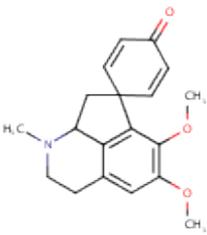
Piperettine	$C_{19}H_{21}NO_3$		311.3749	Piperettine is a natural plant alkaloid. It has been studied as a cancer therapeutic (Reshmi et al. 2010).
N-[2-Methoxy-2-(4-methoxyphenyl)ethyl] cinnamide	$C_{19}H_{21}NO_3$		311.3749	A known constituent of *Aegle marmelos,* a plant used for its medicinal properties in parts of Asia. Extracts from this plant have been used in anti-diabetes, anti-malaria, anti-fungal, anti-venom and anti-bacterial studies (Chakthong et al. 2012).
8-Methyldihydrocheler ythrine	$C_{22}H_{21}NO_4$		363.4064	Found in plants and fruits. Has been studied for its affect on breast cancer cell lines (Chen et al. 1994).
Di-4 coumaroylputrescine	$C_{22}H_{24}N_2O_4$		380.437	Is a known constituent of many herbs and plants incuding (sunflower), *Pyrus communis* (pear), *Rubus idaeus* (raspberry) and *Vicia faba*. It has been studied as an acetylcholinesterase inhibitor (Matochko et al. 2010).
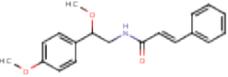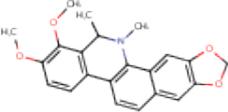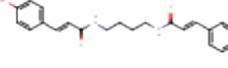
Table 5.2 Possible constituents of Wash 4 as determined by analysis of masses using the Human Metabolome Database

Name of Compound	Chemical Formula	Structure	Average MW	Description
Graveolone	$C_{14}H_{12}O_4$		244.2427	Found in many herbs and spices and has been previously extracted from Parsley (Beier et al. 1994)
Suberone	$C_{14}H_{12}O_4$		244.2427	Found in herbs and spices. It belongs to the Coumarin family which have been well studied for their therapeutic use in cancer, oedema, and as an anti-inflammatory (Jain & Joshi, 2012). Coumarin analogs have also been found to inhibit Aβ aggregation (Soto-Ortega et al. 2011
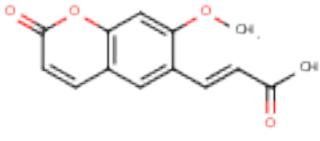
(R)-Apiumetin	$C_{14}H_{12}O_4$		244.2427	Also a member of the coumarin family.
3,3',4'5-Tetrahydroxystilbene (Piceatannol)	$C_{14}H_{12}O_4$			Is a metabolite of resverterol and has also been studied for its anti-amyloidogenic activity. This polyphenol has been shown to inhibit the aggregation and prevent the cytotoxicty of Aβ and α-synuclein (Riviere et al. 2007, Temsamani, 2016)
4'-Methoxychalcone	$C_{16}H_{14}O_2$		238.2812	Has been shown to have anti-angiogenic and anti-tumour properties (Lee et al. 2006).
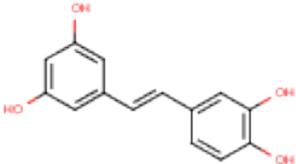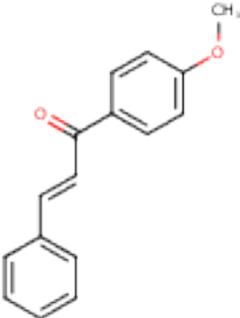
Benzyl cinnamate	$C_{16}H_{14}O_2$		238.2812	Benzyl cinnamate has been isolated from various plant species. It has been shown to be an inhibitor of angiotension II induced hypertension (Ohno et al. 2008).
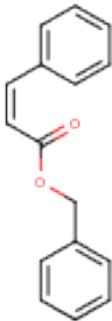
Table 5.3 Possible constituents of Wash 3 as determined by analysis of masses using the Human Metabolome Database

5.4.6 Conclusion

Salvia sclareoides plant extracts contain a number of active compounds which act on a variety of protein amyloids, from prions to Aβ, α-synuclein and cystatin B. The work presented here highlights its use as a general anti-amyloid and furthermore proposes that it exerts its activity using more than one mechanism. While components of *Salvia sclareoides* do indeed bind soluble protein, the selectivity of this activity is intriguing and warrants further research. The data presented here suggest that this activity does not, as previously thought, stabilise soluble forms directly, but instead can lead to segregation of amyloidogenic forms into higher aggregates. At the same time, while no one ingredient was identified as binding specifically to soluble oligomers, another strong activity of these plant extracts was to dissolve existing amyloids of many types, resulting not in soluble monomers but instead in amorphous aggregates. Mass spectrometry analysis was most powerful at providing a clue to possible active amyloid-binding components, a number of which had no previous association with anti-amyloidogenic activities. This project is now well underway to isolating new active compounds from these plants as a route to increasing our understanding of how to regulate toxic amyloidogenic processes.

5.4.7 Future Work

Although not strictly saturation transfer 'difference' NMR, the Clore group has used saturation transfer NMR to look at the mechanism of Aβ protofibrils formation from Aβ monomers. They used saturation transfer from the large NMR invisible aggregates to the binding monomer state and then instead of looking at relative saturation transfer, measuring ^{15}N spin–spin R2 relaxation of the monomer residues. They call this dark-state exchange saturation transfer (DEST) and used this to identify regions of the Aβ monomers that remained in close contact with the protofibril and, therefore, develop their three-state model of Aβ aggregation (Fawzi et al. 2011). A variation on this technique could perhaps be used in the future to look at binding of *Salvia* compounds to Aβ oligomers and more importantly, fibrils.

As mentioned in 5.4.5 at least two of the compounds listed in tables 5.1-3 are available to purchase from Sigma Aldrich. These pure compounds could be tested for their anti-amyloid activity using both the *in vitro* and cell-based techniques discussed in this chapter.

Chapter 6: Conclusion

6.1 Cystatin B mutation and characterisation

Cystatin B WT and G4R constructs were successfully mutated to reinstate cysteine at position 3 and were purified using the same protocol as the original C3S variant used by the Staniforth lab. The N-terminus of the molecule is important to amyloid assembly since the presence of the cysteine leads to an increased tendency for the cystatin B protein to form amyloids. The presence of cysteine also adjusts the ratio of cystatin B species purified from *E.coli* as the monomeric form seems to be marginally favoured over the dimer. Mass spectrometry confirmed this and also showed no evidence for disulphide formation in protein preparations.

6.2. Chaperone catalysed cystatin B inclusion formation

Chapter 4 presents a study of the oligomeric species of cystatin B. Uniquely, this work has revealed information about the structure of this oligomers. Further to showing that Hsp70/DnaK does indeed promote the formation of these oligomers, this research has shown the Mg-ATP dependence of the oligomeric structures by electron microscopy. When Mg-ATP is present, the oligomers are more homogeneous and ordered. When DnaK, ATP and co-chaperones are present (DnaJ and GrpE) larger, more amorphous oligomers are formed. Under these conditions, due to the presence of co-chaperones, Mg-ATP would be converted to Mg-ADP more rapidly such that the state of the chaperones on the grids is actually Mg-ADP bound rather than Mg-ATP. The oligomers formed in the presence of DnaK alone can also adopt a range of structures and there are also large, amorphous species present. This could indicate that DnaK is included in the structure of oligomers formed without Mg-ATP and that DnaK recycling is important in the formation of these structures. One could use a technique such as gold labeling of the DnaK and analysis by electron microscopy to ascertain whether DnaK remains within the oligomers after their formation.

SEC-HPLC data also revealed that a range of oligomeric structures are formed. Figure 4.7 shows that a decrease in monomer is linked to an apparent increase in the DnaK elution peak. This indicates that oligomers are forming but they elute as a range of sizes underneath the DnaK peak. This DnaK peak also gains a shoulder (Fig 4.6) indicating the presence of significantly different molecular weight species, larger than a simple DnaK and cystatin B monomer complex.

Another important factor in the formation of these oligomers is the presence of copper. Previous work by our group has shown that metal ions such as copper are able to destabilize the N-terminal of cystatin B (Paramore et al, 2012). The N-terminal is important in the formation of these oligomers, since WT oligomers were only produced once cystatin B had been mutated to have a cysteine residue at position 3 (previously mutated to a serine for crystallographic purposes). It is also of note that the N-terminal antibody was not as successful as the C-terminal antibody at highlighting the oligomers by western blotting. This again indicates that the N-terminal is modified during oligomer formation, either by becoming hidden or being involved in some structural transition such as copper binding. It would be interesting to explore this interaction between copper and the N-terminus of WT S3C Cystatin B further.

It is also important to consider a physiological function for these structures, since oligomers similar to those formed in the DnaK, Mg-ATP and co-chaperone conditions could be purified straight from *E. coli.* It is interesting that the presence of copper is important in their formation. It may be that these structures are not oligomers as studied in other amyloid diseases. They could instead be seen as cellular inclusions or compartments more similar to the Bunina or Marinesco bodies discussed in section 1.6 of this thesis. One physiological function for these structures could be as copper storage compartments. The Alberti group (Alberti & Hyman, 2016) has linked such compartmentalisation of proteins to an increase in cellular metal ion concentration. Such metal ion storage compartments have also been found in bacteria. Recently, it has been shown that bacteria do have organelles which

are surrounded by a protein shell rather than a membrane. One such organelle, Encapsulin, is an iron storage compartment (McHugh et al. 2014).

It also interesting that the formation of these structures by Hsp70 is specific to cystatin B, since Hsp70 was not successful at producing oligomers or inclusions of α-synuclein. This could also indicate another physiological role for such structures as a way of compartmentalising excess cystatin B. Cystatin B, due to its many functions, needs to be well regulated and its compartmentalisation by Hsp70 could be an important part of this regulation. The proposal here would be that Hsp70 functions by reversibly binding to and stabilising structure in the external shell of these inclusions which, according to the above, is likely to expose a more structured C-terminal end. The core of these inclusions may be disordered as evidenced by the loss of secondary structure observed by CD.

In future studies, it would be useful to explore the toxicity of these different cystatin B structures (+/- Mg-ATP) as a lack of toxicity to cells or to our vesicle model could indicate that they do indeed have a physiological function and they are not the toxic oligomers seen in amyloid disease.

6.3. Oligomeric species as a drug target – the mechanism of action of natural compounds from *Salvia sclareoides.*

Chapter 5 studied the role of compounds from *Salvia sclareoides* as novel amyloid therapeutics and revealed some key findings about the therapeutic target for such compounds. Previously, it had been hypothesised that such compounds may work by stabilising oligomeric forms of amyloid proteins such as Aβ. However, the data presented here shows that this is not the case. Electron microscopy showed no morphological changes to Aβ ADDLs after 24hr incubation with SE extract from *Salvia*. There was also no evidence of binding of compounds from this extract with ADDLs or Aβ oligomers by NMR.

However, electron microscopy data did show that SE extract is able to remodel amyloid fibrils into non-toxic amorphous aggregates. The fibrils, themselves, may therefore be a good therapeutic target for these natural therapeutic compounds from *Salvia*. Whilst the fibrils themselves are often seen as a non-toxic species, they are in equilibrium with toxic oligomer species and smaller species and therefore their removal may reduce the overall toxic protein load.

It has also been shown that SE extract is able to reduce Aβ disruption of membranes using a lipid vesicle model and that the extract itself is not toxic to cells at therapeutic concentrations (Fig 5.7 and 5.9).

Further to this, a number of compounds within the SE extract have been identified which may be the active component responsible for its activity. The next stage in this work would be to purchase some of these intriguing compounds (e.g. hesperaline) and repeat the above experiments.

To answer the original question posed at the start of this thesis, "Are the oligomeric species a good therapeutic target?" evidence points to other species such as the fibrils also being a good target, especially when looking at natural therapeutics such as the polyphenols discussed in Chapter 1 and the compounds in *Salvia* discussed in Chapter 5. Chapter 4 also highlights that oligomeric species may inhabit a range of different structures and that such polymerisation of protein may also have a physiological non-toxic function.

References

Abrahamson, M. 1996. Molecular basis for amyloidosis related to hereditary brain hemorrhage. *Scandinavian Journal of Clinical & Laboratory Investigation,* 56:47-56.

Adiguzel, A., Ozer, H., Sokmen, M., Gulluce, M., Sokmen, A., Kilic, H., Sahin, F. & Baris, O. 2009. Antimicrobial and Antioxidant Activity of the Essential Oil and Methanol Extract of *Nepeta cataria. Polish Journal of Microbiology,* 58(1):69-76.

Agarraberes, F.A. & Dice, J.F. 2001. A molecular chaperone complex at the lysosomal membrane is required for protein translocation. *Journal of Cell Science,* 114(13):2491-2499.

Aggarwal, B.B. & Shishodia, S. 2006. Molecular targets of dietary agents for prevention and therapy of cancer. *Biochemical Pharmacology,* 71(10):1397-1421.

Aggarwal, B.B., Sundaram, C., Malani, N. & Ichikawa, H. 2007. Curcumin: The Indian solid gold. *Molecular Targets and Therapeutic Uses of Curcumin in Health and Disease,* 595:1.

Airoldi, C., Sironi, E., Dias, C., Marcelo, F., Martins, A., Rauter, A.P., Nicotra, F. & Jimenez-Barbero, J. 2013. Natural Compounds against Alzheimer's Disease: Molecular Recognition of A β 1-42 Peptide by *sclareoides* Extract and its Major Component, Rosmarinic Acid, as Investigated by NMR. *Chemistry-an Asian Journal,* 8(3):596-602.

Alberti, S. & Hyman, A.A. 2016. Are aberrant phase transitions a driver of cellular aging? Bioessays, 38(10):959-968.
Alves-Rodrigues, A., Gregori, L. & Figueiredo-Pereira, M.E. 1998. Ubiquitin, cellular inclusions and their role in neurodegeneration. *Trends in Neurosciences,* 21(12):516-520.

Andrich, K. & Bieschke, J. 2015. The Effect of (-)-Epigallo-catechin-(3)-gallate on Amyloidogenic Proteins Suggests a Common Mechanism. In: Vassallo, N. (ed.). *Natural Compounds as Therapeutic Agents for Amyloidogenic Diseases.* Berlin: Springer-Verlag Berlin.

Appendino, G., Ottino, M., Marquez, N., Bianchi, F., Giana, A., Ballero, M., Sterner, O., Fiebich, B.L. & Munoz, E. 2007. Arzanol, an anti-inflammatory and anti-HIV-1 phloroglucinol α-pyrone from *Helichrysum italicum ssp microphyllum. Journal of Natural Products,* 70(4):608-612.

Arisawa, M., Kinghorn, A.D., Cordell, G.A., Phoebe, C.H. & Fansworth, N.R. 1985. Plant anticancer agents .36. Schottenol glucoside from baccharis-coridifolia and ipomopsis-aggregata. *Planta Medica,* 51(6):544-545.

Auluck, P.K., Chan, H.Y.E., Trojanowski, J.Q., Lee, V.M.Y. & Bonini, N.M. 2002. Chaperone suppression of α-synuclein toxicity in a Drosophila model

for Parkinson's disease. *Science,* 295(5556):865-868.

Bazoti, F.N., Bergquist, J., Markides, K. & Tsarbopoulos, A. 2008. Localization of the noncovalent binding site between amyloid-β -peptide and oleuropein using electrospray ionization FT-ICR mass spectrometry. *Journal of the American Society for Mass Spectrometry,* 19(8):1078-1085.

Beach, T.G., Walker, D.G., Sue, L.I., Newell, A., Adler, C.C. & Joyce, J.N. 2004. Substantia nigra Marinesco bodies are associated with decreased striatal expression of dopaminergic markers. *Journal of Neuropathology and Experimental Neurology,* 63(4):329-337.

Beecher, G.R. 2003. Overview of dietary flavonoids: Nomenclature, occurrence and intake. *Journal of Nutrition,* 133(10):3248S-3254S.

Beier, R.C., Ivie, G.W. & Oertli, E.H. 1994. Linear furanocoumarins and graveolone from the common herb parsley. *Phytochemistry,* 36(4):869-872.

Benilova, I., Karran, E. & De Strooper, B. 2012. The toxic A β oligomer and Alzheimer's disease: an emperor in need of clothes. *Nature Neuroscience,* 15(3):349-357.

Bieschke, J., Russ, J., Friedrich, R.P., Ehrnhoefer, D.E., Wobst, H., Neugebauer, K. & Wanker, E.E. 2010. EGCG remodels mature α-synuclein and amyloid-β fibrils and reduces cellular toxicity. *Proceedings of the National Academy of Sciences of the United States of America,* 107(17):7710-7715.

Birkett, C.R., Hennion, R.M., Bembridge, D.A., Clarke, M.C., Chree, A., Bruce, M.E. & Bostock, C.J. 2001. Scrapie strains maintain biological phenotypes on propagation in a cell line in culture. Embo Journal, 20(13):3351-3358.
Buchan, J.R. & Parker, R. 2009. Eukaryotic Stress Granules: The Ins and Outs of Translation. Molecular Cell, 36(6):932-941.

Cakir, A., Mavi, A., Yildirim, A., Duru, M.E., Harmandar, H. & Kazaz, C. 2003. Isolation and characterization of antioxidant phenolic compounds from the aerial parts of *Hypericum hyssopifolium L.* by activity-guided fractionation. *Journal of Ethnopharmacology,* 87(1):73-83.

Caruana, M. & Vassallo, N. 2015. Tea Polyphenols in Parkinson's Disease. In: Vassallo, N. (ed.). *Natural Compounds as Therapeutic Agents for Amyloidogenic Diseases*. Berlin: Springer-Verlag Berlin.

Caughey, B. & Lansbury, P.T. 2003. Protofibrils, pores, fibrils, and neurodegeneration: Separating the responsible protein aggregates from the innocent bystanders. *Annual Review of Neuroscience,* 26:267-298.

Chakthong, S., Weaaryee, P., Puangphet, P., Mahabusarakam, W., Plodpai, P., Voravuthikunchai, S.P. & Kanjana-Opas, A. 2012. Alkaloid and coumarins from the green fruits of *Aegle marmelos*. *Phytochemistry,* 75:108-113.

Chan, M.M.Y., Huang, H.I., Fenton, M.R. & Fong, D. 1998. In vivo inhibition of nitric oxide synthase gene expression by curcumin, a cancer preventive natural product with anti-inflammatory properties. *Biochemical Pharmacology,* 55(12):1955-1962.

Chen, I.S., Wu, S.J., Tsai, I.L., Wu, T.S., Pezzuto, J.M., Lu, M.C., Chai, H., Suh, N. & Teng, C.M. 1994. Chemical and bioactive constituents from *Zanthoxylum simulans*. *Journal of Natural Products,* 57(9):1206-1211.

Chernoff, Y.O., Lindquist, S.L., Ono, B., Ingevechtomov, S.G. & Liebman, S.W. 1995. Role of the chaperone protein hsp104 in propagation of the yeast prion-like factor psi. *Science,* 268(5212):880-884.

Chiti, F. & Dobson, C.M. 2006. Protein misfolding, functional amyloid, and human disease. *Annual Review of Biochemistry*. Palo Alto: Annual Reviews. 75:333-366.

Choi, Y.T., Jung, C.H., Lee, S.R., Bae, J.H., Baek, W.K., Suh, M.H., Park, J., Park, C.W. & Suh, S.I. 2001. The green tea polyphenol (-)-epigallocatechin gallate attenuates β-amyloid-induced neurotoxicity in cultured hippocampal neurons. *Life Sciences,* 70(5):603-614.

Cipollini, E., Riccio, M., Di Giaimo, R., Dal Piaz, F., Pulice, G., Catania, S., Caldarelli, I., Dembic, M., Santi, S. & Melli, M. 2008. Cystatin B and its EPM1 mutants are polymeric and aggregate prone *in vivo*. *Biochimica Et Biophysica Acta-Molecular Cell Research,* 1783(2):312-322.

Cohen, S.I.A., Vendruscolo, M., Dobson, C.M. & Knowles, T.P.J. 2012. From Macroscopic Measurements to Microscopic Mechanisms of Protein Aggregation. *Journal of Molecular Biology,* 421(2-3):160-171.

Cremades, N., Cohen, S.I.A., Deas, E., Abramov, A.Y., Chen, A.Y., Orte, A., Sandal, M., Clarke, R.W., Dunne, P., Aprile, F.A., Bertoncini, C.W., Wood, N.W., Knowles, T.P.J., Dobson, C.M. & Klenerman, D. 2012. Direct Observation of the Interconversion of Normal and Toxic Forms of α-synuclein. *Cell,* 149(5):1048-1059.

Cummings, J.L., Vinters, H.V., Cole, G.M. & Khachaturian, Z.S. 1998. Alzheimer's disease - Etiologies, pathophysiology, cognitive reserve, and treatment opportunities. *Neurology,* 51(1):S2-S17.

Davis, P. 2016. *Structural Studies of Cystatin B Amyloid Fibre and Oligomer.* University of Sheffield.

Davis, P.J., Holmes, D., Waltho, J.P. & Staniforth, R.A. 2015. Limited Proteolysis Reveals That Amyloids from the 3D Domain-Swapping Cystatin B Have a Non-Native β-Sheet Topology. *Journal of Molecular Biology,* 427(15):2418-2434.

Dayal, B., Yannamreddy, V.R., Amin, R., Lea, M.A. & Attygalle, A.B. 2013. Bioactive Compounds in *Moringa oleifera:* Isolation, Structure Elucidation, and

Their Antiproliferative Properties. *Tropical and Subtropical Fruits: Flavors, Color, and Health Benefits,* 1129:203-219.

De Strooper, B. & Annaert, W. 2000. Proteolytic processing and cell biological functions of the amyloid precursor protein. *Journal of Cell Science,* 113(11):1857-1870.

Decatur, J. (2007) NOESY on the 400 and 500 Using Topspin http://www.columbia.edu/cu/chemistry/groups/nmr/noesy.pdf (accessed March 2017)

Dedmon, M.M., Christodoulou, J., Wilson, M.R. & Dobson, C.M. 2005. Heat shock protein 70 inhibits α-synuclein fibril formation via preferential binding to prefibrillar species. *Journal of Biological Chemistry,* 280(15):14733-14740.

Del Mar, C., Greenbaum, E.A., Mayne, L., Englander, S.W. & Woods, V.L. 2005. Structure and properties of α-synuclein and other amyloids determined at the amino acid level. *Proceedings of the National Academy of Sciences of the United States of America,* 102(43):15477-15482.

Delrieu, J., Ousset, P.J., Caillaud, C. & Vellas, B. 2012. Clinical trials in Alzheimer's disease': immunotherapy approaches. *Journal of Neurochemistry,* 120:186-193.

Diez-Espino, J., Buil-Cosiales, P., Serrano-Martinez, M., Toledo, E., Salas-Salvado, J. & Martinez-Gonzalez, M.A. 2011. Adherence to the Mediterranean Diet in Patients with Type 2 Diabetes Mellitus and HbA1c Level. *Annals of Nutrition and Metabolism,* 58(1):74-78.

Diomede, L., Rigacci, S., Romeo, M., Stefani, M. & Salmona, M. 2013. Oleuropein Aglycone Protects Transgenic C. elegans Strains Expressing A β 42 by Reducing Plaque Load and Motor Deficit. *Plos One,* 8(3):9.

Dobson, C.M. 2003. Protein folding and misfolding. *Nature,* 426(6968):884-890.

Dong, J.W., Cai, L., Fang, Y.S., Xiao, H., Li, Z.J. & Ding, Z.T. 2015b. Proaporphine and aporphine alkaloids with acetylcholinesterase inhibitory activity from *Stephania epigaea. Fitoterapia,* 104:102-107.

Doyle, S.M., Genest, O. & Wickner, S. 2013. Protein rescue from aggregates by powerful molecular chaperone machines. *Nature Reviews Molecular Cell Biology,* 14(10):617-629.

Ehrnhoefer, D.E., Bieschke, J., Boeddrich, A., Herbst, M., Masino, L., Lurz, R., Engemann, S., Pastore, A. & Wanker, E.E. 2008. EGCG redirects amyloidogenic polypeptides into unstructured, off-pathway oligomers. *Nature Structural & Molecular Biology,* 15(6):558-566.

Ehrnhoefer, D.E., Duennwald, M., Markovic, P., Wacker, J.L., Engemann, S., Roark, M., Legleiter, J., Marsh, J.L., Thompson, L.M., Lindquist, S.,

Muchowski, P.J. & Wanker, E.E. 2006. Green tea (-)-epigallocatechin-gallate modulates early events in huntingtin misfolding and reduces toxicity in Huntington's disease models. *Human Molecular Genetics,* 15(18):2743-2751.

Ekiel, I. & Abrahamson, M. 1996. Folding-related dimerization of human cystatin C. *Journal of Biological Chemistry,* 271(3):1314-1321.

Ekiel, I., Abrahamson, M., Fulton, D.B., Lindahl, P., Storer, A.C., Levadoux, W., Lafrance, M., Labelle, S., Pomerleau, Y., Groleau, D., LeSauteur, L. & Gehring, K. 1997. NMR structural studies of human cystatin C dimers and monomers. *Journal of Molecular Biology,* 271(2):266-277.

Ellis, R.J. 1991. Chaperone function - cracking the 2nd-half of the genetic-code. *Plant Journal,* 1(1):9-13.

Emami, S.A., Asili, J., Hossein Nia, S., Yazdian-Robati, R., Sahranavard, M. & Tayarani-Najaran, Z. 2016. Growth Inhibition and Apoptosis Induction of Essential Oils and Extracts of Nepeta cataria L. on Human Prostatic and Breast Cancer Cell Lines. *Asian Pacific journal of cancer prevention :* 17, No.125-130.

Fandrich, M. & Dobson, C.M. 2001. Protein folding aspects of amyloid fibril formation. *Amyloid-Journal of Protein Folding Disorders,* 8:26-26.

Fandrich, M. 2012. Oligomeric Intermediates in Amyloid Formation: Structure Determination and Mechanisms of Toxicity. *Journal of Molecular Biology,* 421(4-5):427-440.

Fandrich, M., Fletcher, M.A. & Dobson, C.M. 2001. Amyloid fibrils from muscle myoglobin - Even an ordinary globular protein can assume a rogue guise if conditions are right. *Nature,* 410(6825):165-166.

Fawzi, N.L., Ying, J.F., Ghirlando, R., Torchia, D.A. & Clore, G.M. 2011. Atomic-resolution dynamics on the surface of amyloid-β protofibrils probed by solution NMR. *Nature,* 480(7376):268-U161.

Franzmann, T.M., Jahnel, M., Pozniakovsky, A., Mahamid, J., Holehouse, A.S., Nuske, E., Richter, D., Baumeister, W., Grill, S.W., Pappu, R.V., Hyman, A.A. & Alberti, S. 2018. Phase separation of a yeast prion protein promotes cellular fitness. Science, 359(6371):47

Galanakis, P.A., Bazoti, F.N., Bergquist, J., Markides, K., Spyroulias, G.A. & Tsarbopoulos, A. 2011. Study of the Interaction Between the Amyloid β Peptide (1-40) and Antioxidant Compounds by Nuclear Magnetic Resonance Spectroscopy. *Biopolymers,* 96(3):316-327.

Ganguli, M., Chandra, V., Kamboh, M.I., Johnston, J.M., Dodge, H.H., Thelma, B.K., Juyal, R.C., Pandav, R., Belle, S.H. & DeKosky, S.T. 2000. Apolipoprotein E polymorphism and Alzheimer disease - The Indo-US cross-national dementia study. *Archives of Neurology,* 57(6):824-830.

Garai, K. & Frieden, C. 2013. Quantitative analysis of the time course of Aβ oligomerization and subsequent growth steps using tetramethylrhodamine-labelled Aβ. Proceedings of the National Academy of Sciences of the United States of America, 110(9):3321-3326.

Gasteiger E., Hoogland C., Gattiker A., Duvaud S., Wilkins M.R., Appel R.D., Bairoch A. 2005 Protein Identification and Analysis Tools on the ExPASy Server; (In) John M. Walker (ed): The Proteomics Protocols Handbook, Humana Press (2005). pp. 571-607

Genton, P. 2010. Unverricht-Lundborg disease (EPM1). *Epilepsia,* 51:37-39.

Ghosh, A.K., Brindisi, M. & Tang, J. 2012. Developing ss-secretase inhibitors for treatment of Alzheimer's disease. *Journal of Neurochemistry,* 120:71-83.

Ghosh, A.K., Rao, K.V., Yadav, N.D., Anderson, D.D., Gavande, N., Huang, X.P., Terzyan, S. & Tang, J. 2012. Structure-Based Design of Highly Selective β -Secretase Inhibitors: Synthesis, Biological Evaluation, and Protein-Ligand X-ray Crystal Structure. *Journal of Medicinal Chemistry,* 55(21):9195-9207.

Gliko, O., Pan, W., Katsonis, P., Neumaier, N., Galkin, O., Weinkauf, S. & Vekilov, P.G. 2007. Metastable liquid clusters in super- and undersaturated protein solutions. *Journal of Physical Chemistry B,* 111(12):3106-3114.

Glover, J.R. & Lindquist, S. 1998. Hsp104, Hsp70, and Hsp40: A novel chaperone system that rescues previously aggregated proteins. *Cell,* 94(1):73-82.

Graham, H.N. 1992. Green tea composition, consumption, and polyphenol chemistry. *Preventive Medicine,* 21(3):334-350.

Gravitz, L. 2011. DRUGS A tangled web of targets. *Nature,* 475(7355):S9-S11.

Grelle, G., Otto, A., Lorenz, M., Frank, R.F., Wanker, E.E. & Bieschke, J. 2011. Black Tea Theaflavins Inhibit Formation of Toxic Amyloid-β and α-synuclein Fibrils. *Biochemistry,* 50(49):10624-10636.

Grossi, C., Rigacci, S., Ambrosini, S., Dami, T.E., Luccarini, I., Traini, C., Failli, P., Berti, A., Casamenti, F. & Stefani, M. 2013. The Polyphenol Oleuropein Aglycone Protects TgCRND8 Mice against Aβ Plaque Pathology. *Plos One,* 8(8):13.

Haass, C. & Selkoe, D.J. 2007. Soluble protein oligomers in neurodegeneration: lessons from the Alzheimer's amyloid β-peptide. *Nature Reviews Molecular Cell Biology,* 8(2):101-112.

Han, T.N.W., Kato, M., Xie, S.H., Wu, L.C., Mirzaei, H., Pei, J.M., Chen, M., Xie, Y., Allen, J., Xiao, G.H. & McKnight, S.L. 2012. Cell-free Formation of RNA Granules: Bound RNAs Identify Features and Components of Cellular Assemblies. *Cell,* 149(4):768-779.

Härd T. 2011. Protein engineering to stabilize soluble amyloid β -protein aggregates for structural and functional studies. *Febs Journal,* 278(20):3884-3892.

Hatcher, H., Planalp, R., Cho, J., Tortia, F.M. & Torti, S.V. 2008. Curcumin: From ancient medicine to current clinical trials. *Cellular and Molecular Life Sciences,* 65(11):1631-1652.

Hodson, S., Marshall, J.J.T. & Burston, S.G. 2012. Mapping the road to recovery: The ClpB/Hsp104 molecular chaperone. *Journal of Structural Biology,* 179(2):161-171.

Hou, F.J., Sun, L.J., Zheng, H., Skaug, B., Jiang, Q.X. & Chen, Z.J.J. 2011. MAVS Forms Functional Prion-like Aggregates to Activate and Propagate Antiviral Innate Immune Response. *Cell,* 146(3):448-461.

Ii, K., Ito, H., Kominami, E. & Hirano, A. 1993. Abnormal distribution of cathepsin proteinases and endogenous inhibitors (cystatins) in the hippocampus of patients with alzheimers disease, parkinsonism-dementia complex on guam, and senile dementia and in the aged. *Virchows Archiv a-Pathological Anatomy and Histopathology,* 423(3):185-194.

Jacomelli, M., Pitozzi, V., Zaid, M., Larrosa, M., Tonini, G., Martini, A., Urbani, S., Taticchi, A., Servili, M., Dolara, P. & Giovannelli, L. 2010. Dietary extra-virgin olive oil rich in phenolic antioxidants and the aging process: long-term effects in the rat. *Journal of Nutritional Biochemistry,* 21(4):290-296.

Jahn, T.R., Parker, M.J., Homans, S.W. & Radford, S.E. 2006. Amyloid formation under physiological conditions proceeds via a native-like folding intermediate. *Nature Structural & Molecular Biology,* 13(3):195-201.

Jain, S., Wheeler, J.R., Walters, R.W., Agrawal, A., Barsic, A. & Parker, R. 2016. ATPase-Modulated Stress Granules Contain a Diverse Proteome and Substructure. *Cell,* 164(3):487-498.

Jain, P.K, & Joshi, H. 2012. Coumarin: Chemical and Pharmacological Profile. *Journal of Applied Pharmaceutical Science,* 2(06):236-240.

Janowski, R., Kozak, M., Jankowska, E., Grzonka, Z., Grubb, A., Abrahamson, M. & Jaskolski, M. 2001. Human cystatin C, an amyloidogenic protein, dimerizes through three-dimensional domain swapping. *Nature Structural Biology,* 8(4):316-320.

Jerala, R. & Zerovnik, E. 1999. Accessing the global minimum conformation of stefin A dimer by annealing under partially denaturing conditions. *Journal of Molecular Biology,* 291(5):1079-1089.

Jobin, C., Bradham, C.A., Russo, M.P., Juma, B., Narula, A.S., Brenner, D.A. & Sartor, R.B. 1999. Curcumin blocks cytokine-mediated NF-kB activation and proinflammatory gene expression by inhibiting inhibitory factor I-kB kinase activity. *Journal of Immunology,* 163(6):3474-3483.

Johnson Jr. C.S 1999 Diffusion ordered nuclear magnetic resonance spectroscopy: principles and applications. *Progress in Nuclear Magnetic Resonance Spectroscopy* 34 203–256

Kato, M., Han, T.N.W., Xie, S.H., Shi, K., Du, X.L., Wu, L.C., Mirzaei, H., Goldsmith, E.J., Longgood, J., Pei, J.M., Grishin, N.V., Frantz, D.E., Schneider, J.W., Chen, S., Li, L., Sawaya, M.R., Eisenberg, D., Tycko, R. & McKnight, S.L. 2012. Cell-free Formation of RNA Granules: Low Complexity Sequence Domains Form Dynamic Fibers within Hydrogels. *Cell,* 149(4):753-767.

Keller, B. O, Sui, J. Young, A.B, Whittal R. M. 2008 Interferences and contaminants encountered in modern mass spectrometry *Analytica Chimica Acta* 627 (1) 71-81

Knowles, T.P.J., Vendruscolo, M. & Dobson, C.M. 2014. The amyloid state and its association with protein misfolding diseases. *Nature Reviews Molecular Cell Biology,* 15(6):384-396.

Kumada, S., Uchihara, T., Hayashi, M., Nakamura, A., Kikuchi, E., Mizutani, T. & Oda, M. 2002. Promyelocytic leukemia protein is redistributed during the formation of intranuclear inclusions independent of polyglutamine expansion: An immunohistochemical study on Marinesco bodies. *Journal of Neuropathology and Experimental Neurology,* 61(11):984-991.

Lafreniere, R.G., Rochefort, D.L., Chretien, N., Rommens, J.M., Cochius, J.I., Kalviainen, R., Nousiainen, U., Patry, G., Farrell, K., Soderfeldt, B., Federico, A., Hale, B.R., Cossio, O.H., Sorensen, T., Pouliot, M.A., Kmiec, T., Uldall, P., Janszky, J., Pranzatelli, M.R., Andermann, F., Andermann, E. & Rouleau, G.A. 1997. Unstable insertion in the 5' flanking region of the cystatin B gene is the most common mutation in progressive myoclonus epilepsy type 1, EPM1. *Nature Genetics,* 15(3):298-302.

Lahiri, D.K., Maloney, B., Long, J.M. & Greig, N.H. 2014. Lessons from a BACE1 inhibitor trial: Off-site but not off base. *Alzheimers & Dementia,* 10(5):S411-S419.

Lashuel, H.A., Petre, B.M., Wall, J., Simon, M., Nowak, R.J., Walz, T. & Lansbury, P.T. 2002. α-synuclein, especially the Parkinson's disease-associated mutants, forms pore-like annular and tubular protofibrils. *Journal of Molecular Biology,* 322(5):1089-1102.

Lee, J., Culyba, E.K., Powers, E.T. & Kelly, J.W. 2011. Amyloid β forms fibrils by nucleated conformational conversion of oligomers. *Nature Chemical Biology*, 7(9):602-609.

Lee, Y.S., Lim, S.S., Shin, K.H., Kim, Y.S., Ohuchi, K. & Jung, S.H. 2006. Anti-angiogenic and anti-tumor activities of 2 '-hydroxy-4 '-methoxychalcone. *Biological & Pharmaceutical Bulletin,* 29(5):1028-1031.

Levites, Y., Amit, T., Mandel, S. & Youdim, M.B.H. 2003. Neuroprotection and

neurorescue against Aβ toxicity and PKC-dependent release of non-amyloidogenic soluble precursor protein by green tea polyphenol (-)-epigallocatechin-3-gallate. *Faseb Journal,* 17(3):952

Li, Y.R., King, O.D., Shorter, J. & Gitler, A.D. 2013. Stress granules as crucibles of ALS pathogenesis. *Journal of Cell Biology,* 201(3):361-372.

Liu, T., Zwingman, T., Li, R.L., Pan, T., Wong, B.S., Petersen, R.B., Gambetti, P., Herrup, K. & Sy, M.S. 2001. Differential expression of cellular prion protein in mouse brain as detected with multiple anti-PrP monoclonal antibodies. *Brain Research*, 896(1-2):118-129.

Lopez del Amo, J.M., Fink, U., Dasari, M., Grelle, G., Wanker, E.E., Bieschke, J. & Reif, B. 2012. Structural Properties of EGCG-Induced, Nontoxic Alzheimer's Disease Aβ Oligomers. *Journal of Molecular Biology,* 421(4-5):517-524.

Lu, J.X., Qiang, W., Yau, W.M., Schwieters, C.D., Meredith, S.C. & Tycko, R. 2013. Molecular Structure of β-Amyloid Fibrils in Alzheimer's Disease Brain Tissue. *Cell,* 154(6):1257-1268.

Luhrs, T., Ritter, C., Adrian, M., Riek-Loher, D., Bohrmann, B., Doeli, H., Schubert, D. & Riek, R. 2005. 3D structure of Alzheimer's amyloidβ (1-42) fibrils. *Proceedings of the National Academy of Sciences of the United States of America,* 102(48):17342-17347.

Mandel, S.A., Amit, T., Kalfon, L., Reznichenko, L., Weinreb, O. & Youdim, M.B.H. 2008. Cell Signaling Pathways and Iron Chelation in the Neurorestorative Activity of Green Tea Polyphenols: Special Reference to Epigallocatechin Gallate (EGCG). *Journal of Alzheimers Disease,* 15(2):211-222.

Matheou, C.J., Younan, N.D. & Viles, J.H. 2015. Cu^{2+} accentuates distinct misfolding of Aβ(1-40) and Aβ(1-42) peptides, and potentiates membrane disruption. *Biochemical Journal,* 466:233-242.

Matochko, W.L., James, A., Lam, C.W., Kozera, D.J., Ata, A. & Gengan, R.M. 2010. Triterpenoidal Alkaloids from Buxus natalensis and Their Acetylcholinesterase Inhibitory Activity. *Journal of Natural Products,* 73(11):1858-1862.

McHugh, C.A., Fontana, J., Nemecek, D., Cheng, N.Q., Aksyuk, A.A., Heymann, J.B., Winkler, D.C., Lam, A.S., Wall, J.S., Steven, A.C. & Hoiczyk, E. 2014. A virus capsid-like nanocompartment that stores iron and protects bacteria from oxidative stress. *Embo Journal*, 33(17):1896-1911.

Meimaridou, E., Gooljar, S.B. & Chapple, J.P. 2009. From hatching to dispatching: the multiple cellular roles of the Hsp70 molecular chaperone machinery. *Journal of Molecular Endocrinology,* 42(1-2):1-9.

Meng, F.L., Abedini, A., Plesner, A., Verchere, C.B. & Raleigh, D.P. 2010.

The Flavanol (-)-Epigallocatechin 3-Gallate Inhibits Amyloid Formation by Islet Amyloid Polypeptide, Disaggregates Amyloid Fibrils, and Protects Cultured Cells against IAPP-Induced Toxicity. *Biochemistry,* 49(37):8127-8133.

Mizuno, Y., Amari, M., Takatama, M., Aizawa, H., Mihara, B. & Okamoto, K. 2006. Transferrin localizes in Bunina bodies in amyotrophic lateral sclerosis. *Acta Neuropathologica,* 112(5):597-603.

Molliex, A., Temirov, J., Lee, J., Coughlin, M., Kanagaraj, A.P., Kim, H.J., Mittag, T. & Taylor, J.P. 2015. Phase Separation by Low Complexity Domains Promotes Stress Granule Assembly and Drives Pathological Fibrillization. *Cell,* 163(1):123-133.

Morgan, G.J., Giannini, S., Hounslow, A.M., Craven, C.J., Zerovnik, E., Turk, V., Waltho, J.P. & Staniforth, R.A. 2008. Exclusion of the native α-helix from the amyloid fibrils of a mixed α/β protein. *Journal of Molecular Biology,* 375(2):487-498.

Mori, F., Kakita, A., Takahashi, H. & Wakabayashi, K. 2014. Co-localization of Bunina bodies and TDP-43 inclusions in lower motor neurons in amyotrophic lateral sclerosis. *Neuropathology,* 34(1):71-76.

Mori, F., Tanji, K., Miki, Y. & Wakabayashi, K. 2009. Decreased Cystatin C Immunoreactivity in Spinal Motor Neurons and Astrocytes in Amyotrophic Lateral Sclerosis. *Journal of Neuropathology and Experimental Neurology,* 68(11):1200-1206.

Mori, F., Tanji, K., Miki, Y., Kakita, A., Takahashi, H. & Wakabayashi, K. 2010. Relationship between Bunina bodies and TDP-43 inclusions in spinal anterior horn in amyotrophic lateral sclerosis. *Brain Pathology,* 20:32-33.

Morten, I.J., Gosal, W.S., Radford, S.E. & Hewitt, E.W. 2007. Investigation into the role of macrophages in the formation and degradation of β2-microglobulin amyloid fibrils. *Journal of Biological Chemistry,* 282(40):29691-29700.

Muchowski, P.J. & Wacker, J.L. 2005. Modulation of neurodegeneration by molecular chaperones. *Nature Reviews Neuroscience,* 6(1):11-22.

Naressi, M.A., Manholer, D.D., Ames, F.Q., Bersani-Amado, C.A., Formagio, A.S.N., Pereira, Z.V., da Costa, W.F., Baldoqui, D.C. & Sarragiotto, M.H. 2015. Chemical constituents, anti-inflammatory, and free-radical scavenging activities of *guettarda viburnoides cham. & schltdl. (rubiaceae). Quimica Nova,* 38(7):932-936.

Neuhaus, D., Williamson, M.P. The Nuclear Overhauser Effect in Structural and Conformational Analysis. 2nd ed. Wiley-VCH

Ohno, O., Ye, M., Koyama, T., Yazawa, K., Mura, E., Matsumoto, H., Ichino, T., Yamada, K., Nakamura, K., Ohno, T., Yamaguchi, K., Ishida, J., Fukamizu, A. & Uemura, D. 2008. Inhibitory effects of benzyl benzoate and its derivatives

on angiotensin II-induced hypertension. *Bioorganic & Medicinal Chemistry,* 16(16):7843-7852.

Okamoto, K., Hirai, S., Amari, M., Iizuka, T., Watanabe, M., Murakami, N. & Takatama, M. 1993. Oculomotor nuclear pathology in amyotrophic-lateral-sclerosis. *Acta Neuropathologica,* 85(5):458-462.

Okamoto, K., Hirai, S., Amari, M., Watanabe, M. & Sakurai, A. 1993. Bunina bodies in amyotrophic-lateral-sclerosis immunostained with rabbit anti-cystatin-c serum. *Neuroscience Letters,* 162(1-2):125-128.

Ono, K., Hasegawa, K., Naiki, H. & Yamada, M. 2004. Curcumin has potent anti-amyloidogenic effects for Alzheimer's β-amyloid fibrils *in vitro*. *Journal of Neuroscience Research,* 75(6):742-750.

Paramore, R., Morgan, GJ., Davis, PJ., Sharma, CA., Hounslow, A., Taler-Vercic., A Zerovnik., E Waltho, JP., Cliff, MJ., Staniforth, RA. 2012. Mapping local structural perturbations in the native state of stefin B (cystatin B) under amyloid forming conditions. *Frontiers in molecular neuroscience*, 5: 94

Palhano, F.L., Lee, J., Grimster, N.P. & Kelly, J.W. 2013. Toward the Molecular Mechanism(s) by Which EGCG Treatment Remodels Mature Amyloid Fibrils. *Journal of the American Chemical Society,* 135(20):7503-7510.

Paslawski, W., Andreasen, M., Nielsen, S.B., Lorenzen, N., Thomsen, K., Kaspersen, J.D., Pedersen, J.S. & Otzen, D.E. 2014. High Stability and Cooperative Unfolding of α-Synuclein Oligomers. *Biochemistry,* 53(39):6252-6263.

Paslawski, W., Lorenzen, N. & Otzen, D.E. 2016. Formation and Characterization of α-Synuclein Oligomers. In: Eliezer, D. (ed.). *Protein Amyloid Aggregation: Methods and Protocols*. Totowa: Humana Press Inc.

Patel, A., Lee, H.O., Jawerth, L., Maharana, S., Jahnel, M., Hein, M.Y., Stoynov, S., Mahamid, J., Saha, S., Franzmann, T.M., Pozniakovski, A., Poser, I., Maghelli, N., Royer, L.A., Weigert, M., Myers, E.W., Grill, S., Drechsel, D., Hyman, A.A. & Alberti, S. 2015. A Liquid-to-Solid Phase Transition of the ALS Protein FUS Accelerated by Disease Mutation. *Cell,* 162(5):1066-1077.

Perez-Bonilla, M., Salido, S., van Beek, T.A. & Altarejos, J. 2014. Radical-Scavenging Compounds from Olive Tree (Olea europaea L.) Wood. *Journal of Agricultural and Food Chemistry,* 62(1):144-151.

Perez, R.G., Zheng, H., VanderPloeg, L.H.T. & Koo, E.H. 1997. The β -amyloid precursor protein of Alzheimer's disease enhances neuron viability and modulates neuronal polarity. *Journal of Neuroscience,* 17(24):9407-9414.

Polajnar, M., Zavasnik-Bergant, T., Kopitar-Jerala, N., Tusek-Znidaric, M. & Zerovnik, E. 2014. Gain in toxic function of stefin B EPM1 mutants

aggregates: Correlation between cell death, aggregate number/size and oxidative stress. *Biochimica Et Biophysica Acta-Molecular Cell Research,* 1843(9):2089-2099.

Polajnar, M., Zavasnik-Bergant, T., Skerget, K., Vizovisek, M., Vidmar, R., Fonovic, M., Kopitar-Jerala, N., Petrovic, U., Navarro, S., Ventura, S. & Zerovnik, E. 2014. Human Stefin B Role in Cell's Response to Misfolded Proteins and Autophagy. *Plos One,* 9(7):15.

Rabouille, C. & Alberti, S. 2017a. Cell adaptation upon stress: the emerging role of membrane-less compartments. *Current Opinion in Cell Biology*, 47:34-42.

Rauter, A.P., Dias, C., Martins, A., Branco, I., Neng, N.R., Nogueira, J.M., Goulart, M., Silva, F.V.M., Justino, J., Trevitt, C. & Waltho, J.P. 2012. Non-toxic *Salvia* sclareoides Brot. extracts as a source of functional food ingredients: Phenolic profile, antioxidant activity and prion binding properties. *Food Chemistry,* 132(4):1930-1935.

Reddy, T.R.K., Mutter, R., Heal, W., Guo, K., Gillet, V.J., Pratt, S. & Chen, B. 2006. Library design, synthesis, and screening: Pyridine dicarbonitriles as potential prion disease therapeutics. *Journal of Medicinal Chemistry,* 49(2):607-615.

Reshmi, S.K., Sathya, E. & Devi, P.S. 2010. Isolation of piperidine from *Piper nigrum* and its antiproliferative activity. *African Journal of Pharmacy and Pharmacology,* 4(8):562-573.

Rezai-Zadeh, K., Shytle, D., Sun, N., Mori, T., Hou, H.Y., Jeanniton, D., Ehrhart, J., Townsend, K., Zeng, J., Morgan, D., Hardy, J., Town, T. & Tan, J. 2005. Green tea epigallocatechin-3-gallate (EGCG) modulates amyloid precursor protein cleavage and reduces cerebral amyloidosis in Alzheimer transgenic mice. *Journal of Neuroscience,* 25(38):8807-8814.

Riccio, M., Di Giaimo, R., Pianetti, S., Palmieri, PP., Melli, M., Santi, S. 2001 Nuclear localization of cystatin B, the cathepsin inhibitor implicated in myoclonus epilepsy (EPM1) *Experimental Cell Research* 262, 2, 84-94

Rigacci, S., Guidotti, V., Bucciantini, M., Parri, M., Nediani, C., Cerbai, E., Stefani, M. & Berti, A. 2010. Oleuropein aglycon prevents cytotoxic amyloid aggregation of human amylin. *Journal of Nutritional Biochemistry,* 21(8):726-735.

Rispoli, A., Cipollini, E., Catania, S., Di Giaimo, R., Pulice, G., van Houte, S., Sparla, F., Dal Piaz, F., Roncarati, D., Trost, P. & Melli, M. 2013. Insights in progressive myoclonus epilepsy: Hsp70 promotes cystatin B polymerization. *Biochimica Et Biophysica Acta-Proteins and Proteomics*, 1834(12):2591-2599.

Riviere, C., Richard, T., Quentin, L., Krisa, S., Merillon, J.M. & Monti, J.P. 2007. Inhibitory activity of stilbenes on Alzheimer's β -amyloid fibrils *in vitro*. *Bioorganic & Medicinal Chemistry,* 15(2):1160-1167.

Rohloff, J. 2015. Analysis of Phenolic and Cyclic Compounds in Plants Using Derivatization Techniques in Combination with GC-MS-Based Metabolite Profiling. *Molecules,* 20(2):3431-3462.

Rosa, A., Deiana, M., Atzeri, A., Corona, G., Incani, A., Melis, M.P., Appendino, G. & Dessi, M.A. 2007. Evaluation of the antioxidant and cytotoxic activity of arzanol, a prenylated α-pyrone-phloroglucinol etherodimer from *Helichrysum italicum subsp microphyllum. Chemico-Biological Interactions,* 165(2):117-126.

Rudyk, H., Vasiljevic, S., Hennion, R.M., Birkett, C.R., Hope, J. & Gilbert, I.H. 2000. Screening Congo Red and its analogues for their ability to prevent the formation of PrP-res in scrapie-infected cells. *Journal of General Virology,* 81:1155-1164.

Sanders, A., Craven, C.J., Higgins, L.D., Giannini, S., Conroy, M.J., Hounslow, A.M., Waltho, J.P. & Staniforth, R.A. 2004. Cystatin forms a tetramer through structural rearrangement of domain-swapped dimers prior to amyloidogenesis. *Journal of Molecular Biology,* 336(1):165-178.

Sasaki, S., Komori, T. & Iwata, M. 2006. Neuronal inclusions in sporadic motor neuron disease are negative for α-synuclein. *Neuroscience Letters,* 397(1-2):15-19.

Schmidt, M., Sachse, C., Richter, W., Xu, C., Fandrich, M. & Grigorieff, N. 2009. Comparison of Alzheimer A β (1-40) and A β (1-42) amyloid fibrils reveals similar protofilament structures. *Proceedings of the National Academy of Sciences of the United States of America,* 106(47):19813-19818.

Schnabel, J. 2011a. AMYLOID Little proteins, big clues. *Nature,* 475(7355):S12-S14.

Schnabel, J. 2011b. VACCINES Chasing the dream. *Nature,* 475(7355):S18-S19.

Selkoe, D.J. 2003. Folding proteins in fatal ways. *Nature,* 426(6968):900-904.

Serpell, L.C. & Makin, S. 2002. Using cryo-electron microscopy and fibre diffraction to examine amyloid fibril structure. *Abstracts of Papers of the American Chemical Society,* 223:C28-C28.

Serpell, L.C. 2000. Alzheimer's amyloid fibrils: structure and assembly. *Biochimica Et Biophysica Acta-Molecular Basis of Disease,* 1502(1):16-30.

Serpell, L.C., Fraser, P.E. & Sunde, M. 1999. X-ray fiber diffraction of amyloid fibrils. *Amyloid, Prions, and Other Protein Aggregates,* 309:526-536.

Simon, A. & Anthony, H.A. 2016. Are aberrant phase transitions a driver of cellular ageing? *Bioessays,* 38: (10) 959-968

Soto-Ortega, D.D., Murphy, B.P., Gonzalez-Velasquez, F.J., Wilson, K.A., Xie, F., Wang, Q.A. & Moss, M.A. 2011. Inhibition of amyloid-β aggregation

by coumarin analogs can be manipulated by functionalization of the aromatic center. *Bioorganic & Medicinal Chemistry,* 19(8):2596-2602.

Spillantini, M.G., Schmidt, M.L., Lee, V.M.Y., Trojanowski, J.Q., Jakes, R. & Goedert, M. 1997. α-synuclein in Lewy bodies. *Nature,* 388(6645):839-840.

Staniforth, R.A., Giannini, S., Higgins, L.D., Conroy, M.J., Hounslow, A.M., Jerala, R., Craven, C.J. & Waltho, J.P. 2001. Three-dimensional domain swapping in the folded and molten-globule states of cystatins, an amyloid-forming structural superfamily. *Embo Journal,* 20(17):4774-4781.

Stefani, M. & Rigacci, S. 2013. Protein Folding and Aggregation into Amyloid: The Interference by Natural Phenolic Compounds. *International Journal of Molecular Sciences,* 14(6):12411-12457.

Stefani, M. 2012. Structural features and cytotoxicity of amyloid oligomers: Implications in Alzheimer's disease and other diseases with amyloid deposits. *Progress in Neurobiology,* 99(3):226-245.

Stromer, T. & Serpell, L.C. 2005. Structure and morphology of the Alzheimer's amyloid fibril. *Microscopy Research and Technique,* 67(3-4):210-217.

Sunde, M. & Blake, C. 1997. The structure of amyloid fibrils by electron microscopy and X-ray diffraction. *Advances in Protein Chemistry, Vol 50: Protein Misassembly,* 50:123-159.

Temsamani, H., Krisa, S., Decossas-Mendoza, M., Lambert, O., Merillon, J.M. & Richard, T. 2016. Piceatannol and Other Wine Stilbenes: A Pool of Inhibitors against α-Synuclein Aggregation and Cytotoxicity. *Nutrients,* 8(6):12.

Thapa, A. & Chi, E.Y. 2015. Biflavonoids as Potential Small Molecule Therapeutics for Alzheimer's Disease. In: Vassallo, N. (ed.). *Natural Compounds as Therapeutic Agents for Amyloidogenic Diseases.* Berlin: Springer-Verlag Berlin.

Tipping, K.W., Karamanos, T.K., Jakhria, T., Iadanza, M.G., Goodchild, S.C., Tuma, R., Ranson, N.A., Hewitt, E.W. & Radford, S.E. 2015. pH-induced molecular shedding drives the formation of amyloid fibril-derived oligomers. *Proceedings of the National Academy of Sciences of the United States of America,* 112(18):5691-5696.

Trevitt, C.R. & Collinge, J. 2006. A systematic review of prion therapeutics in experimental models. *Brain,* 129:2241-2265.

Turk, V. & Bode, W. 1991. The cystatins - protein inhibitors of cysteine proteinases. *Febs Letters,* 285(2):213-219.

Tyan, S.H., Shih, A.Y.J., Walsh, J.J., Maruyama, H., Sarsoza, F., Ku, L., Eggert, S., Hof, P.R., Koo, E.H. & Dickstein, D.L. 2012. Amyloid precursor protein (APP) regulates synaptic structure and function. *Molecular and Cellular Neuroscience,* 51(1-2):43-52.

Valls-Pedret, C., Lamuela-Raventos, R.M., Medina-Remon, A., Quintana, M., Corella, D., Pinto, X., Martinez-Gonzalez, M.A., Estruch, R. & Ros, E. 2012. Polyphenol-Rich Foods in the Mediterranean Diet are Associated with Better Cognitive Function in Elderly Subjects at High Cardiovascular Risk. *Journal of Alzheimers Disease,* 29(4):773-782.

Vilar, M., Chou, H.T., Luhrs, T., Maji, S.K., Riek-Loher, D., Verel, R., Manning, G., Stahlberg, H. & Riek, R. 2008. The fold of α-synuclein fibrils. *Proceedings of the National Academy of Sciences of the United States of America,* 105(25):8637-8642.

Virtaneva, K., Damato, E., Miao, I.M., Koskiniemi, M., Norio, R., Avanzini, G., Franceschetti, S., Michelucci, R., Tassinari, C.A., Omer, S., Pennacchio, L.A., Myers, R.M., DieguezLucena, J.L., Krahe, R., delaChapelle, A. & Lehesjoki, A.E. 1997. Unstable minisatellite expansion causing recessively inherited myoclonus epilepsy, EPM1. *Nature Genetics,* 15(4):393-396.

Walsh, D.M. & Selkoe, D.J. 2007. A β Oligomers - a decade of discovery. *Journal of Neurochemistry,* 101(5):1172-1184.

Wang, P., Liao, W., Fang, J., Liu, Q., Yao, J., Hu, M. & Ding, K. 2014. A glucan isolated from flowers of Lonicera japonica Thunb. inhibits aggregation and neurotoxicity of Aβ 42. *Carbohydrate polymers,* 110:142-147.

Wang, S.H., Dong, X.Y. & Sun, Y. 2012. Effect of (-)-epigallocatechin-3-gallate on human insulin fibrillation/aggregation kinetics. *Biochemical Engineering Journal,* 63:38-49.

Wang, W.-Y., Liu, C.-P., Kuo, Y.-C. & Lin, Y.-L. 2004. Anti-lymphoproliferative alkaloids from *Plumula nelumbinis*. *Chinese Pharmaceutical Journal (Taipei),* 56(1):25-30.

Wegrzyn, R.D., Bapat, K., Newnam, G.P., Zink, A.D. & Chernoff, Y.O. 2001. Mechanism of prion loss after Hsp104 inactivation in yeast. *Molecular and Cellular Biology,* 21(14):4656-4669.

Wetzel, R. 2002. Ideas of order for amyloid fibril structure. *Structure,* 10(8):1031-1036.

Witt, S.N. 2009. The Fink Blueprint for Hsp70/Hsc70 Molecular Chaperones. *Current Protein & Peptide Science,* 10(5):424-431.

Wolfe, M.S. 2006. Shutting down Alzheimer's. *Scientific American,* 294(5):72-79.

Woulfe, J., Gray, D., Prichett-Pejic, W., Munoz, D.G. & Chretien, M. 2004. Intranuclear rodlets in the substantia nigra: Interactions with marinesco bodies, ubiquitin, and promyelocytic leukemia protein. *Journal of Neuropathology and Experimental Neurology,* 63(11):1200-1207.

Xue, W.F. 2015. Nucleation: The Birth of a New Protein Phase. *Biophysical*

Journal, 109(10):1999-2000.

Yamada, M., Ono, K., Hamaguchi, T. & Noguchi-Shinohara, M. 2015. Natural Phenolic Compounds as Therapeutic and Preventive Agents for Cerebral Amyloidosis. In: Vassallo, N. (ed.). *Natural Compounds as Therapeutic Agents for Amyloidogenic Diseases.* Berlin: Springer-Verlag Berlin.

Yang, F.S., Begum, A., Lim, G., Ambegaokar, S., Ubeda, O., Chen, P.P., Frautschy, S.A. & Cole, G.M. 2004. Curcumin binds A β , inhibits A β aggregation and fibril formation *in vitro* and crosses the BBB to label plaques and reduces A β accumulation in aged APPSW transgenic mice. *Neurobiology of Aging,* 25:S158-S158.

Yu, L.P., Edalji, R., Harlan, J.E., Holzman, T.F., Lopez, A.P., Labkovsky, B., Hillen, H., Barghorn, S., Ebert, U., Richardson, P.L., Miesbauer, L., Solomon, L., Bartley, D., Walter, K., Johnson, R.W., Hajduk, P.J. & Olejniczak, E.T. 2009. Structural Characterization of a Soluble Amyloid β -Peptide Oligomer. *Biochemistry,* 48(9):1870-1877.

Yuen, P. & Baxter, D.W. 1963. Morphology of marinesco bodies (paranucleolar corpuscles) in melanin-pigmented nuclei of brain-stem. *Journal of Neurology Neurosurgery and Psychiatry,* 26(2):178-&.

Zahn, R., Buckle, A.M., Perrett, S., Johnson, C.M., Corrales, F.J., Golbik, R. & Fersht, A.R. 1996. Chaperone activity and structure of monomeric polypeptide binding domains of GroEL. *Proceedings of the National Academy of Sciences of the United States of America,* 93(26):15024-15029.

Zecca, L., Youdim, M.B.H., Riederer, P., Connor, J.R. & Crichton, R.R. 2004. Iron, brain ageing and neurodegenerative disorders. *Nature Reviews Neuroscience,* 5(11):863-873.

Zerovnik, E., Cimerman, N., Kos, J., Turk, V. & Lohner, K. 1997. Thermal denaturation of human cystatin C and two of its variants; Comparison to chicken cystatin. *Biological Chemistry,* 378(10):1199-1203.

Zerovnik, E., Pompe-Novak, M., Skarabot, M., Ravnikar, M., Musevic, I. & Turk, V. 2002. Human stefin B readily forms amyloid fibrils *in vitro. Biochimica Et Biophysica Acta-Protein Structure and Molecular Enzymology,* 1594(1):1-5.

Zerovnik, E., Turk, V. & Waltho, J.P. 2002. Amyloid fibril formation by human stefin B: influence of the initial pH-induced intermediate state. *Biochemical Society Transactions,* 30:543-547.

Zimmermann, R. 1998. The role of molecular chaperones in protein transport into the mammalian endoplasmic reticulum. *Biological Chemistry,* 379(3):275-282.

Appendix- Mass spectrometry of Aβ$_{1-42}$ fibrils incubated with SE extract

The full mass spectra and a table of masses are presented for each sample prepared for analysis (see 5.2.5). The mass spectra are cut off at 600 Da as above this mass compounds would not be classed as small molecules. While all the masses are presented in the tables, none of the higher masses above 600 Da were identified in the human metabolome database (see section 5.4.5). The origin of these higher masses is likely to be peptide breakdown products from the *Salvia* (SE) extract. Masses present in both the sample and the control are highlighted in yellow as these were discounted from further analysis.

1. Mass spectrometry of the solubilised pellet
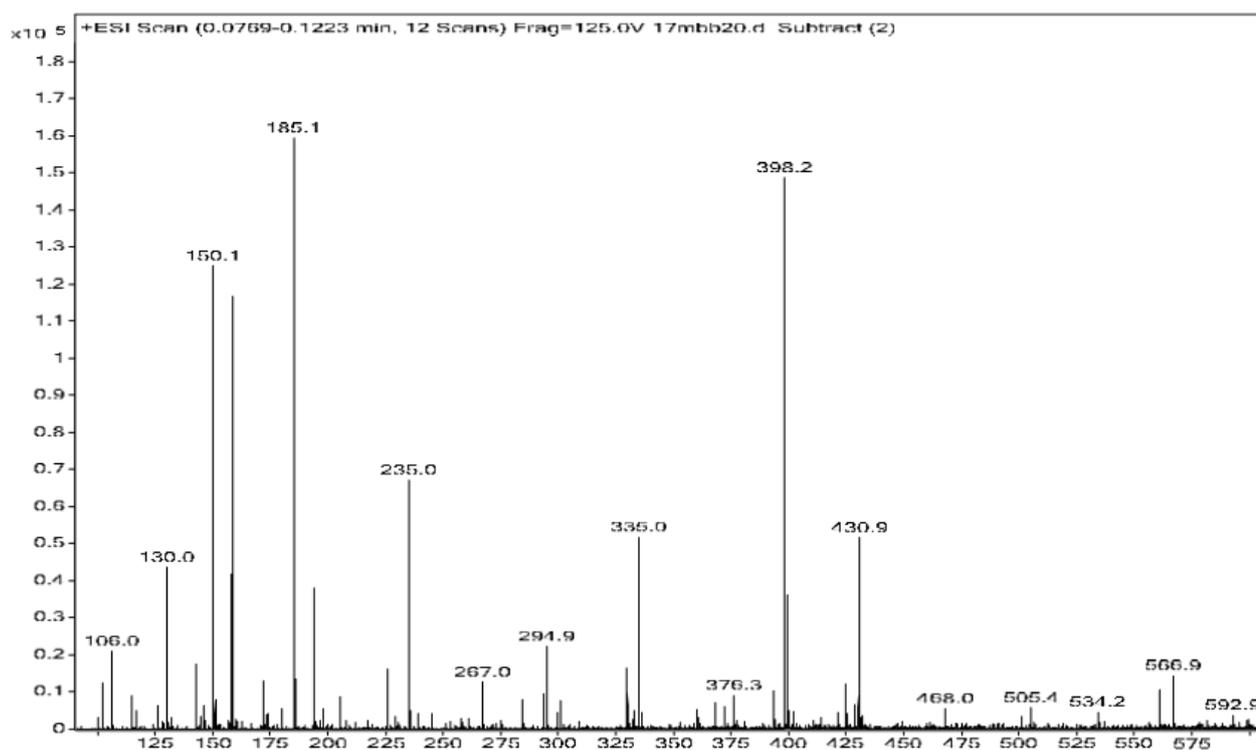
m/z	Abund
99.9878	3660.03
102.0136	10564.4
106.005	19079.74
115.0371	12000.72
125.9875	2960.39
130.0086	18142.93

130.1597	7082.4
143.04	14470.75
145.0313	2929.15
146.0206	6345.67
149.9962	3838.28
150.1132	167089.2
151.1161	11252.92
157.0838	3175.69
158.0025	12543.4
158.9649	175315.25
159.9686	4027.67
172.095	19196.36
173.0827	5358.57
174.0155	3522.67
179.9909	4312.84
185.1158	215751.4
186.1191	18312.61
193.9746	41249.71
194.1204	6209.74
196.9556	3023.75
197.9953	5579.2
205.0692	11146.52
217.1058	3338.19
225.9912	11770.76
229.1392	4929.8
235.0013	74236.14
236.004	5326.26
239.0202	4499.48
239.1622	4132.79
244.9955	4396.94
261.1314	4177
267.0173	8795.85
274.9342	3233.44
284.3326	10442.17
293.9789	11109.33
294.9402	35677.91
299.9598	3640.65
301.1429	9481.46
329.9496	23188.12
332.3325	3557.15
332.9373	7154.99
335.0057	59245.92
336.0079	5427.02
360.3638	6657.83
360.9326	4331.6
367.9467	7348.25
372.3487	7846.27
376.2605	9875.7

393.2869	8941.23
398.2437	201141.3
399.2466	47452.65
400.2489	6632.6
400.3797	6190.31
402.3601	6158.32
410.9141	3336.05
414.2215	4636.53
421.3185	6972.38
424.8981	17971.49
425.2211	4692.04
428.9199	9401.08
430.3901	12310.21
430.9154	83280.76
431.3944	3910.54
431.9188	5674.25
449.3488	3250.79
467.9512	5576.95
500.937	3277.23
505.4124	8857.46
534.2197	6075.38
534.2875	3018.84
560.8736	16896.51
566.8898	23539.08
581.3667	3181.8
592.888	4945.45
598.8724	3251.98
599.4284	3426.26
625.393	3039.93
660.8776	14178.99
696.8491	12817.06
700.8676	3654.8
702.8658	17770.97
773.4962	8316.61
774.4985	4206.6
796.8536	11513.67
832.8243	9048.66
838.8406	13302.18
968.7994	11306.88
974.8155	8802.72
1104.7734	6826.96
1110.7901	5906.6
1234.7318	4966.64
1240.7476	5352.29
1246.7644	3710.72
1376.7229	4440.67

2. Mass spectrometry of wash 4

+ESI Scan (0.1215-0.1422 min, 6 Scans) Frag=125.0V 17mbb21.d Subtract (3)
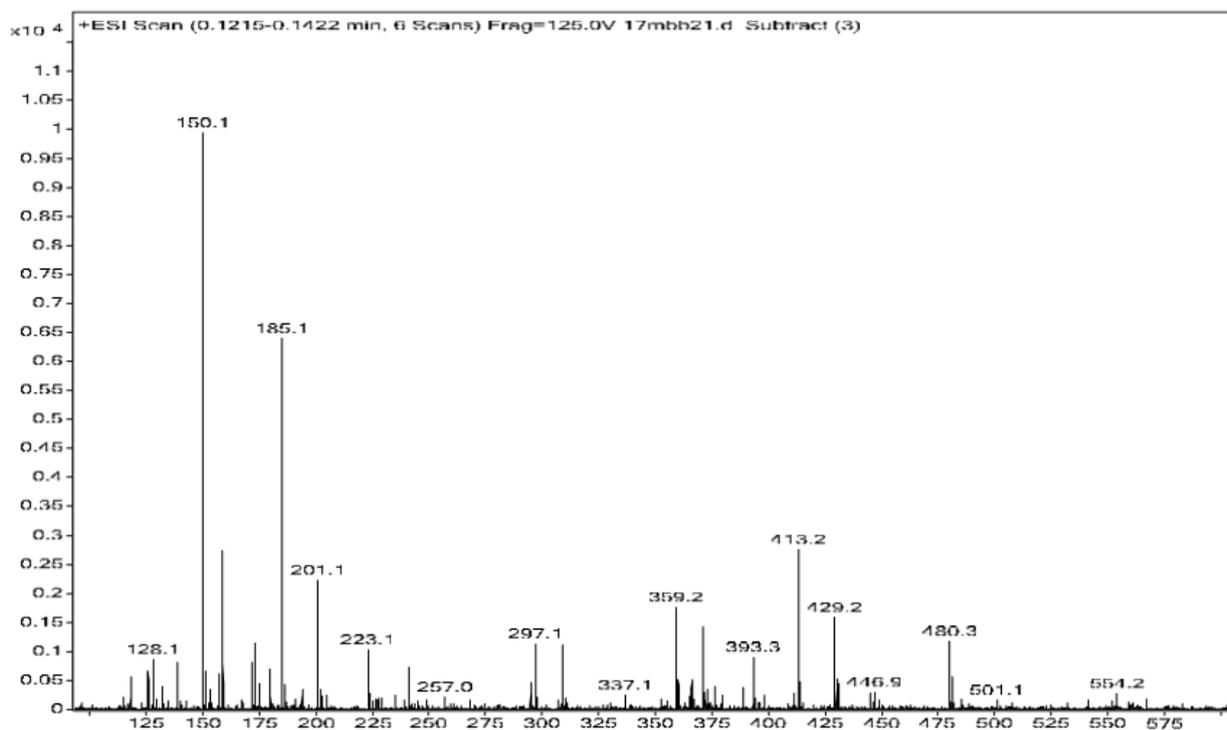
m/z	Abund
113.108	1596.97
115.0366	1881.78
118.0869	1110.91
118.1226	1480.39
128.1437	1059.05
129.0524	2839.54
130.1597	37807.75
131.1629	3396.51
132.1024	3433.86
135.0033	6870.41
139.0505	14024.71
140.0561	1119.63
150.013	882.32
150.1117	110807.16
150.9768	1245.16
151.1145	7098.22
155.1284	2281.35
156.0759	1038.06
157.0838	6766.28
158.9645	7286.89
161.0316	2466.55

171.0624	1147.35
171.0996	2374.08
172.0951	98661.48
173.0968	7092.95
175.1184	1202.66
180.0869	1363.83
185.1153	520423.46
185.2272	30548.08
186.119	44428.16
187.1194	4634.72
188.069	4234.39
198.0879	1509.63
201.0895	41350.63
202.079	5442.02
203.0809	3657.08
205.0716	918.29
207.0991	1023.19
217.1058	3143.72
223.0944	2334.86
224.0516	2282.17
225.1088	2106.57
227.1231	1037.69
229.1409	3173.26
249.1079	1147.31
251.126	8282.49
252.1319	961.49
261.1304	2804.96
265.1169	1113.44
267.1171	2626.26
272.1296	1244.64
275.1456	1080.88
277.1119	904.51
289.1535	1284.61
291.1446	919.73
295.1452	959.23
297.1442	900.55
305.1498	2803.77
307.1524	2917.02
309.1624	2398
321.1336	1798.93
323.1463	2635.6
325.1567	1694.54
329.1859	3030.43
333.1739	1388.06
335.1779	1499.65
339.1349	1176.99
349.1768	2049.19
351.1754	1732.93

363.177	939.25
365.1139	4822.34
367.1743	1152.28
373.1945	1049.2
376.2601	3412.51
377.2603	998.11
379.185	877.69
381.1807	908.06
389.1925	1199.71
391.2055	1515.42
393.209	2051.37
393.2861	13867.58
394.2888	3457.63
395.1956	885.41
398.2423	59739.37
399.2448	14174.96
400.2474	2085.98
405.1871	1326.2
407.2005	2040.25
409.2049	1723.09
414.216	9500.55
415.2182	2493.23
416.2178	1068.79
421.1844	938.6
423.1936	1535.6
425.2039	1157.17
437.2231	1121.14
505.4119	5057.56
506.4147	1717.36
773.4931	1856.38
774.4972	899.81

3. Mass spectrometry of wash 3

+ESI Scan (0.0864-0.1359 min, 13 Scans) Frag=125.0V 17mbb22.d Subtract (2)
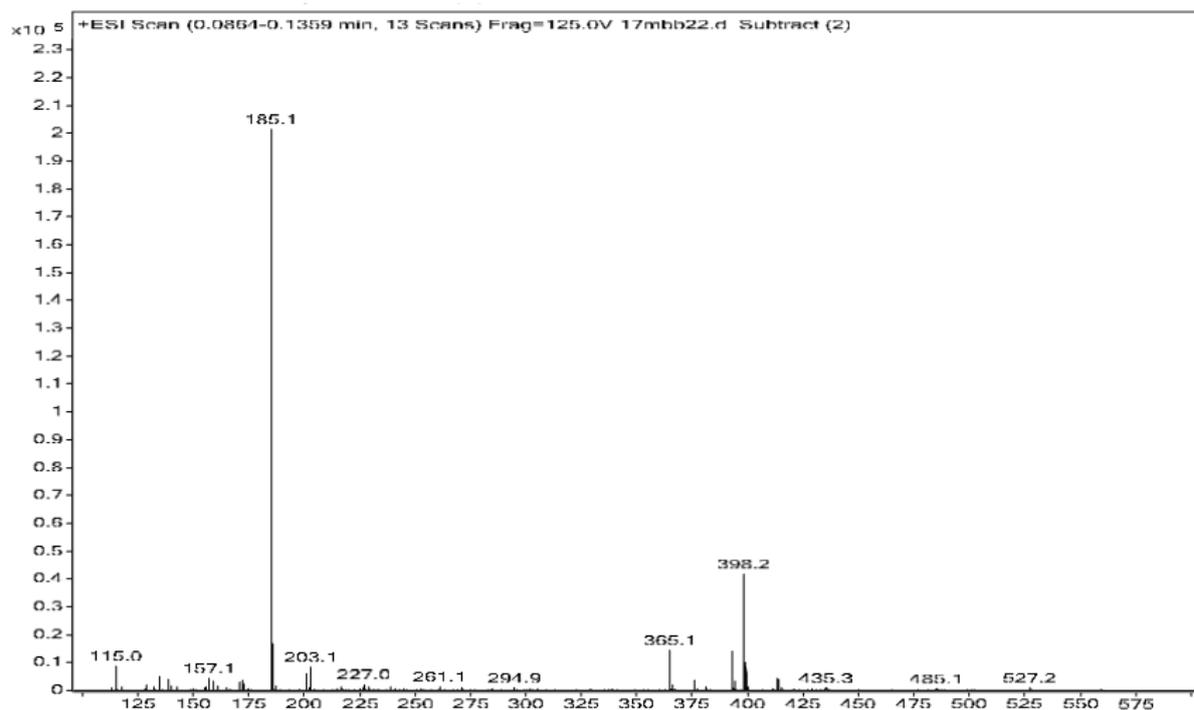
m/z	Abund
80.9482	3543.35
82.9454	1059.27
90.9769	1971.97
96.9217	500.39
113.1077	717.2
115.0367	7079.43
118.123	1053.04
128.1433	342.85
129.0519	1535.8
135.0026	896.37
138.9064	729.74
139.0496	1644.33
140.9035	489.31
142.948	6772.34
148.9352	434.53
157.0831	2583.57
158.9215	460.36
158.9643	4488.7
161.0314	891.29
164.9293	4674.04
171.0621	1299.45
171.0975	1720.11

172.0949	1593.97
173.0779	1705.11
174.1595	1089.67
180.9029	719.87
185.1152	150590.36
186.1187	12766.53
187.1182	1030.27
196.8663	523.94
198.8614	403.94
201.0887	9518.04
202.0883	786.81
202.1802	791.23
203.0512	529.8
203.0857	789.8
206.8936	872.66
208.8896	545.81
216.9225	1884.85
217.1046	1183.94
218.9194	656.67
222.8871	1409.68
224.8837	548.58
226.9516	1814.4
227.1209	341.5
229.1402	1135.02
230.0245	558.54
232.9086	598.29
234.0547	370.51
239.1675	335.48
245.0813	471.69
249.1452	949.46
254.8238	399.55
256.8202	436.32
258.8626	386.16
261.0886	531.44
261.1279	770.42
262.9063	555.8
265.1265	336.65
274.881	524.17
276.8765	339.24
278.9207	405.54
280.8457	744.43
282.8426	543.18
284.9045	859.64
294.9393	744.52
300.8999	560.56
305.1571	393.14
332.838	334.95
336.8757	344

338.8038	367.25
340.7995	393.73
342.8539	503.31
349.1831	379.66
352.8959	452.76
358.8581	481.97
365.1066	1134.75
366.1941	412
376.2591	1592.89
393.285	5399.8
394.2879	1491.7
398.2417	29413.07
399.2448	7091.04
400.2472	978.29
411.0936	473.17
414.215	5472.63
415.2182	1338.84
416.2161	585.16
420.8797	377.8
429.2034	503.04
435.3076	1541.84
480.2808	552.8
485.1113	372.43
502.2639	1167.34
503.2653	401.65
518.2406	617.8
543.2411	444.2
561.2525	411.09
959.9655	2234.12
960.9704	370.99

4. Mass spectrometry of wash 2

+ESI Scan (0.0878-0.1580 min, 18 Scans) Frag=125.0V 17mbb23.d Subtract (3)
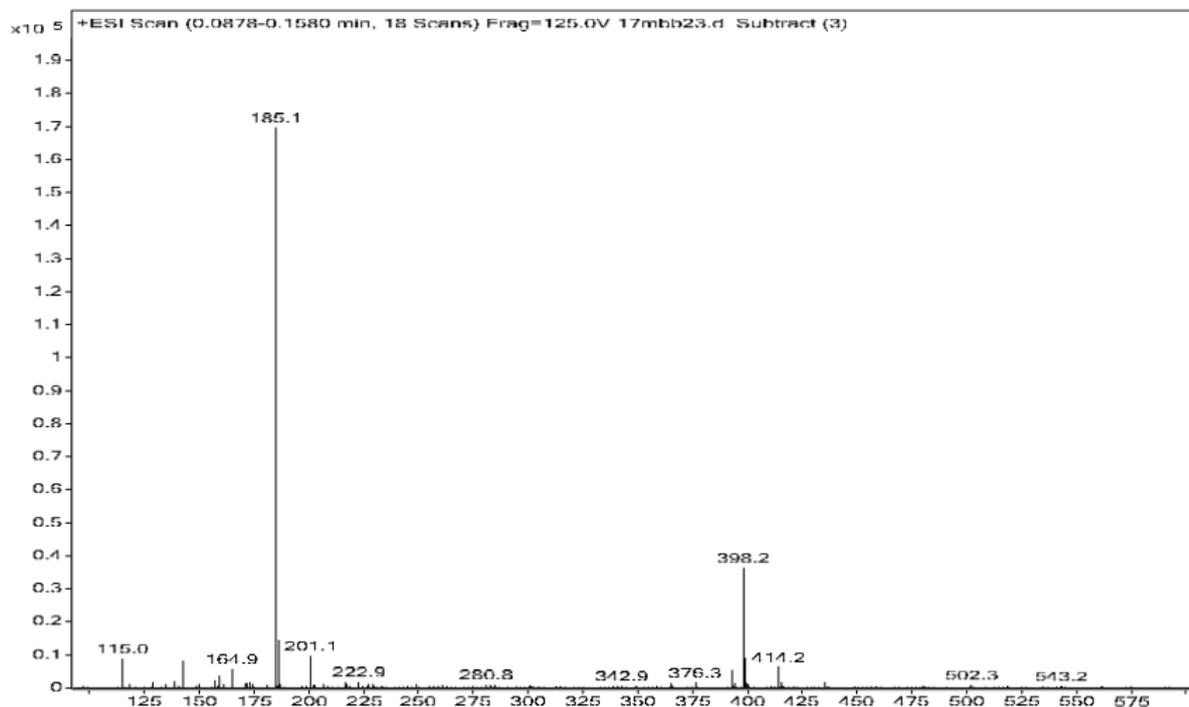
m/z	Abund
80.949	539.38
86.0969	336.76
90.977	2641.17
113.1075	1336.03
115.0366	7304.01
118.0859	1146.73
118.1219	1025.31
128.1439	475.3
129.0516	1379.31
132.0996	1049.3
135.0029	4257.73
139.0495	3552.11
140.0651	1171.74
142.9472	980.01
143.0323	421.76
150.0115	427.64
155.0526	701.7
156.0417	1086.21
156.0728	581.99
157.0834	4218.95
157.1698	456.37
158.9644	3477.85

161.0312	1538.77
164.9279	781.65
167.0072	422.6
171.0625	862.71
171.0983	3052.19
172.0947	3285.34
173.0794	1844.68
175.1186	538.01
185.1153	173369.54
186.1183	14537.93
187.1184	1500.98
198.0892	319.32
201.0892	5956.66
202.0853	552.32
202.1804	1000.77
202.225	433.46
202.9915	367.33
203.053	7077.96
203.1419	366.62
204.0555	412.54
205.063	342.72
213.1473	443.8
216.9224	1357.99
217.1052	462.99
218.9199	417.15
220.167	382.98
225.0349	624.95
226.9514	3082.57
227.1224	597.97
229.1388	1033.47
230.0248	428.13
239.1029	655.11
239.164	1129.83
241.0704	532.8
245.0808	597.42
253.0231	406.4
261.0884	1101.29
261.1229	871.18
270.9774	1184.64
271.1883	342.44
284.9097	462.58
285.1441	513.78
294.9394	1394.09
302.1956	420.17
305.1552	406.96
338.9647	388.74
349.1805	364.56
352.8962	437.68

362.9265	722.56
365.1055	12440.65
366.1091	1740.44
367.1137	351.2
376.2592	3326.76
377.2603	727.73
381.0796	1143.62
393.2856	12350.9
394.2883	3033.7
395.2912	347.03
398.2416	32581.69
399.2445	7781.06
400.2456	1121.37
411.0957	598.12
413.2334	2929.58
414.2191	3423.47
415.2215	853.64
420.8839	360.75
429.2027	430.63
430.9137	564.86
433.0908	361.44
435.3072	844.54
450.3062	390.92
480.2796	348.2
485.1128	708.19
501.0868	347.7
502.2627	482.41
527.1584	883.61
559.1307	348.72
773.4922	682.74

5. Mass spectrometry of wash 1
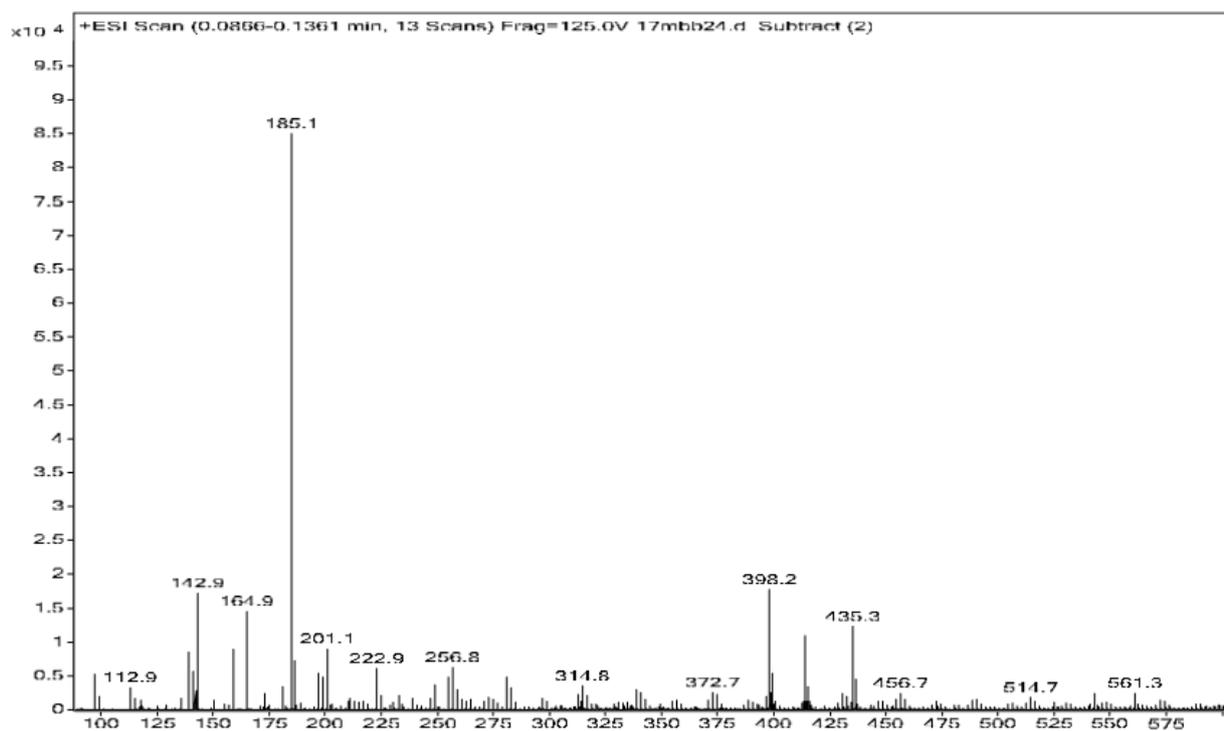
m/z	Abund
80.9486	17974.67
82.9456	5589.05
96.9223	3975.45
98.9194	1438.57
112.8963	2603.11
114.8933	1234.04
115.0366	1199.99
118.1234	1197.55
136.0754	1540.13
138.907	6422.31
140.904	4265.85
142.1095	2382.1
142.9484	16459.15
158.9221	1480.83
158.9646	7360.78
164.9296	13527.76
173.0571	1988.55
180.9031	3013.61
185.1158	90543.44
186.1193	7744.64
196.866	3934.46
198.8626	3695.89
200.8596	1192.53
200.9049	917.1

201.0892	9367.06
203.0861	993.67
206.894	1010.38
210.1353	986.85
211.0193	1585.45
212.8397	888.07
216.9226	1198.94
222.8876	5355.56
224.8842	1768.51
230.0255	1129.11
233.0638	1512.91
238.8615	1588.63
247.13	1447.04
249.1418	3322.94
254.8249	3503.26
255.0462	900.04
256.8215	4456.74
258.8193	2134.08
258.8636	1955.3
260.8623	1266.05
262.9067	1276
265.1247	1526.07
270.7983	886.7
272.796	1208.81
274.8801	1265.77
280.847	4092.49
282.8434	2664.8
284.8876	1209.35
296.82	1416.07
298.8177	985.97
312.7851	1518.35
314.0862	869.06
314.7809	2463.48
316.7781	1542.87
334.8362	886.51
338.806	2483.12
340.8023	2151.21
342.8403	1441.08
354.7788	1019.56
356.7764	1108.1
370.7435	1014.88
372.7399	1802.37
374.7396	1495.06
388.7131	947.51
396.7649	1618.22
398.2425	16989.86
398.7608	2139.59
399.2471	4819.28

400.7787	1059.66
413.1113	1008.56
414.2155	9109.54
414.7352	1051.07
415.2198	2762.94
416.2182	1027.77
430.6989	1667.69
432.6982	1418.84
435.3092	9336.86
436.3126	3288.82
446.6724	863.72
448.6697	859.3
454.7243	1198.43
456.7197	1962.26
458.727	1237.66
472.6941	951.68
488.6589	975.36
490.6552	1016.34
514.6791	1389.13
516.6798	1002.88
525.2378	1056.84
543.2424	2215.32
561.253	2377.61
572.6385	1018.35
574.6382	1003.68
630.5972	857.32
632.5941	923.61
959.9711	1213.61

6. Mass spectrometry of the supernatant

+ESI Scan (0.0728-0.1058 min, 9 Scans) Frag=125.0V 17mbb25.d Subtract (2)
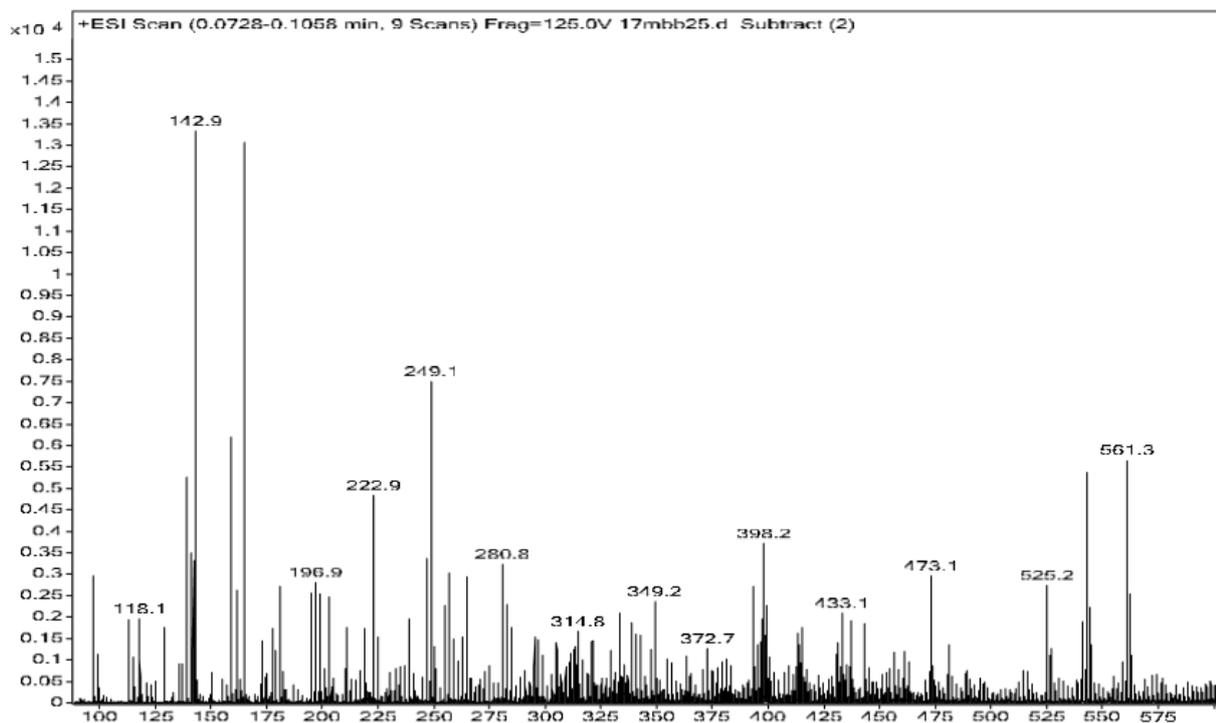
m/z	Abund
80.9487	20720.74
82.9457	6966.86
96.9226	4724.34
98.9198	1825.98
112.8964	3300.89
114.8937	1628.43
118.1235	2100.99
128.9541	2906.64
136.0746	3091.19
137.0798	1334.34
138.9073	7735.22
140.9043	4889.71
142.1093	4618.51
142.9486	11405.8
143.955	1327.35
158.9222	1017.85
158.965	9604.02
164.9294	13866.77
173.0593	1341.32
178.8998	1729.16
180.9015	3576.4
195.04	4326.62
196.867	4297.28
198.8633	3891.6

200.8604	1211.64
211.0189	1925.67
216.9234	1451.47
219.0995	1712.77
222.8879	5537.65
224.8842	1862.84
236.8596	1175.62
238.8596	2547.53
240.8571	975.94
247.1315	2960.07
249.1441	6693.35
250.1485	1616.72
254.8256	3552.6
256.8224	4460.73
258.8202	2109.36
258.8615	1481.18
262.9051	966.62
263.1143	1191.71
265.1315	2697.06
272.7961	1259.37
274.8815	1243.88
280.8466	3843.39
282.8435	2548.88
284.8867	1411.01
295.1853	1054.79
296.8184	2028.44
298.8156	1324.48
302.8308	1097.12
312.7862	1756.52
313.1798	971.6
314.7817	2427.36
316.782	1493.04
333.2053	1259.78
338.806	2248.58
340.8025	2053.65
342.8408	1420.15
349.1867	1764.76
354.7765	1456.94
356.775	1291.97
370.7457	1144.09
372.7416	1773.01
374.74	1216.46
393.2137	1761.32
396.765	1592.72
398.2442	2786.9
398.7606	1879.87
399.2569	1473.72
400.7829	971.37

412.7355	1229.47
414.2152	1579.65
414.7328	1367.3
415.1369	1029.25
415.225	1133.68
430.7009	1681.43
432.6996	1376.01
433.1467	1206.87
435.3092	1336.52
436.314	1250.81
437.2364	1307.66
443.1321	948
454.7245	1045.01
456.7204	1473.59
458.7291	990.59
472.6923	1055.29
473.145	1430.88
488.6602	1032.23
514.6806	977.06
525.2474	1766.67
527.2481	942.5
541.2311	1321.72
543.2432	3607.03
544.2484	1841.62
545.2552	1309.4
561.2528	3682.75
562.2593	2121.71
563.2642	1141.8

7. Mass spectrometry of the control sample-a solubilised pellet of the SE extract in the absence of Aβ.

+ESI Scan (0.0855-0.1062 min, 6 Scans) Frag=125.0V 17mbb26.d Subtract (2)
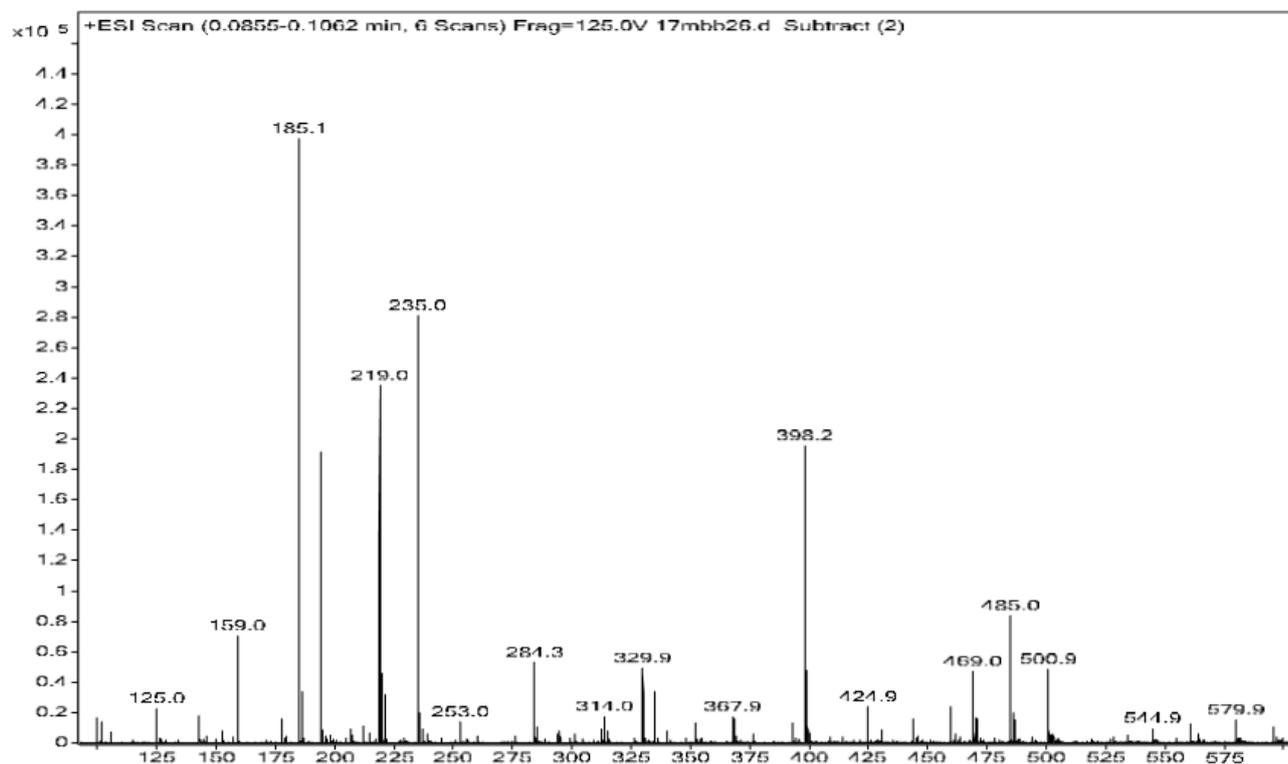
m/z	Abund
84.01	4312.07
99.9877	9832.69
102.0138	11460.51
106.005	8734.28
125.0365	9849.68
143.0408	14830.15
146.0206	5112.49
149.9947	3458.94
152.9478	4466.34
157.0837	4814.11
158.9647	95359.59
177.9967	7718.7
179.9914	3613.79
185.1154	505927.61
185.2273	29122.28
186.1191	43662.29
187.1201	4582.65
193.9748	112020.9
194.9774	4961.07
197.9926	4682.84
205.069	5638.41
206.4994	4382.47

211.9852	6393.63
214.4877	2928.88
217.1058	3033.13
219.0238	111582.26
220.0252	21712.72
221.0219	13605.44
229.1324	5173.28
235.0014	174549.16
236.0041	12247.38
237.0315	3878.81
239.0122	4446.5
239.1634	5093.14
253.0112	7956.61
276.0271	3389.09
284.3326	58398.23
285.3357	11742.35
293.9792	8059.96
294.9399	16171.21
301.142	5789.7
304.3022	3057.67
312.3638	10371.75
313.9722	9693.34
315.0745	5050.34
326.3784	3344.53
329.9497	35074.3
332.9363	2952.38
335.006	48743.66
336.0084	4381.29
340.395	8214.75
351.9689	7257.41
367.947	13199.27
368.4266	16697.7
369.4292	4714.3
376.2609	14670.11
377.2634	3554.57
393.2873	15891.08
394.2901	3965.04
398.2432	267171.51
399.2464	64521.89
400.2489	8789.65
414.2181	5464
421.3187	4173.36
424.8981	20295.98
428.9209	3908.1
430.9153	26683.6
435.309	3143.54
443.9305	7140.05
459.9081	11133.94

468.9795	20232.06
469.9809	7124.06
470.9802	7091.18
484.957	37214.19
485.9588	8997.2
486.9598	6738.95
500.9343	22754.27
534.2181	7384.77
544.8949	6645.73
560.8728	13596.49
563.9288	3006.66
566.8902	7188.98
579.9051	7602.75
595.8825	6414.14
660.8781	5458.7
674.8562	4064.52
680.8712	3467.07
690.831	3664.43
696.8489	7910.6
702.8652	4707.84
734.8999	3226.15
750.889	3329.29
773.4953	5356.66
796.8526	3743.16
832.8233	4444.07
838.8404	3051.94
869.8665	5430.78
946.804	3837.72
968.7993	4990.58
1234.7322	7387.51